

MATHEMATICAL MODELING OF WATER ALTERNATING GAS  
PROCESSES

WAGNER QUEIROZ BARROS

UNIVERSIDADE ESTADUAL DO NORTE FLUMINENSE  
LABORATÓRIO DE ENGENHARIA E EXPLORAÇÃO DE PETRÓLEO

MACAÉ - RJ  
DECEMBER - 2022

# MATHEMATICAL MODELING OF WATER ALTERNATING GAS PROCESSES

WAGNER QUEIROZ BARROS

Thesis submitted to the Science and Technology Center of Universidade Estadual do Norte Fluminense Darcy Ribeiro in partial fulfillment of the requirements for the degree of Doctor in Reservoir and Exploration Engineering.

Supervisor: Prof. Adolfo Puime Pires, D.sc.  
Co-Supervisor: Prof. Alvaro Marcello Marco Peres, Ph.D.

MACAÉ - RJ  
DECEMBER - 2022

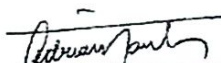
MATHEMATICAL MODELING OF WATER ALTERNATING GAS PROCESSES

WAGNER QUEIROZ BARROS

Tese apresentada ao Centro de Ciência e Tecnologia da Universidade Estadual do Norte Fluminense Darcy Ribeiro, como parte das exigências para obtenção do título de Doutor em Engenharia de Reservatório e de Exploração.

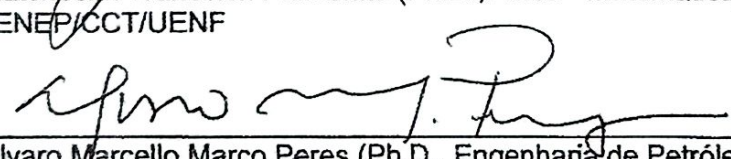
Aprovada em 21 de dezembro de 2022.

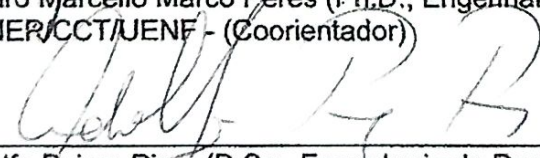
Comissão Examinadora:

  
\_\_\_\_\_  
Adriano dos Santos (D.Sc., Engenharia Civil / Geotécnica) – UFRN

  
\_\_\_\_\_  
André Duarte Bueno (D.Sc., Engenharia Mecânica) – LENE/CCT/UENF

  
\_\_\_\_\_  
Viatcheslav Ivanovich Priimenko (Ph.D., Física - Matemática) –  
LENE/CCT/UENF

  
\_\_\_\_\_  
Alvaro Marcello Marco Peres (Ph.D., Engenharia de Petróleo) –  
LENE/CCT/UENF - (Coorientador)

  
\_\_\_\_\_  
Adolfo Puime Pires (D.Sc., Engenharia de Reservatório e de Exploração) –  
LENE/CCT/UENF - (Orientador)

Dedico essa tese à minha esposa Lais de Jesus Moraes cujo apoio sempre foi incomensurável.

Primeiramente gostaria de agradecer à minha esposa Lais de Jesus Moraes cujo apoio e carinho foram fundamentais durante todo esse processo. Agradeço também aos meus pais José Roberto Frias Barros e Sueli Queiroz Barros pelo apoio e educação. Minha avó Palmira Frias Barros e tia Ana Maria Frias Barros que sempre foram as maiores incentivadoras aos meus estudos e me apresentaram o universo da pesquisa acadêmica. Agradeço também a minha irmã Gabriela Queiroz Barros e meus sobrinhos Juninho, Davi e Gabrielzinho pelo amor incondicional que sempre me proporcionaram. Tenho um carinho e agradecimento especial aos meus orientadores: prof. Adolfo Puime Pires e prof. Alvaro Marcello Marco Peres que me proporcionaram todo o conhecimento adquirido e ao longo dessa jornada e se tornaram amigos pessoais os quais eu nunca esquecerei. Também agradeço aos meus amigos Gabriel Malgaresi, Poliana Ferreira, Felipe Apolinário, Fernando Diogo, Luana Cantagesso e especialmente ao Acir Soares e sua família, pela paciência e por ouvirem quatro anos ininterruptos de reclamações a respeito dos mais variados assuntos. Agradeço também aos colegas da Enauta que além das frutíferas discussões sobre os reservatórios do pós-sal, me permitiram conciliar o final do doutorado com minhas atividades laborais. Finalmente agradeço a todos os colegas do LDSC, todos os técnicos e professores do LENEP e a CAPES pelo financiamento desta pesquisa.

*“Não atribua à maldade o que pode ser adequadamente explicado pela estupidez”,  
Navalha de Hanion.*

# *Contents*

<b>Abstract</b>	<b>vi</b>
<b>Resumo</b>	<b>vii</b>
<b>1 Introduction</b>	<b>1</b>
1.1 WAG Method Classification . . . . .	2
1.2 Mathematical Modeling and Analytical Solutions . . . . .	4
1.3 Thesis Organization . . . . .	5
<b>2 Article: Analytical Solution for One-Dimensional Three-Phase Incompressible Flow in Porous Media for Concave Relative Permeability Curves</b>	<b>7</b>
<b>3 Book Chapter: Approximate Solution for One-Dimensional Compressible Two-Phase Immiscible Flow in Porous Media for Variable Boundary Conditions</b>	<b>19</b>
<b>4 Article: Approximated Solution for Linear Step-Rate Water Injectivity Test</b>	<b>37</b>
<b>5 Book Chapter: Approximate Analytical Solutions for 1-D Immiscible Water-Alternated-Gas</b>	<b>78</b>
<b>6 Article: An Immiscible Water Alternating Gas (WAG) Analytical Solution Based in Wave Interaction Theory</b>	<b>111</b>
<b>7 Article: Analytical Solution for the Miscible Water Alternating Gas (MWAG) Recovery Method</b>	<b>164</b>
<b>8 Conclusions</b>	<b>212</b>

# ***Abstract***

The use of Water Alternating Gas (WAG) recovery technique has recently increased in the Brazilian pre-salt discoveries. This method is useful in oil fields containing large  $CO_2$  amounts, where the produced gas must be re-injected into the reservoir, achieving higher recovery factors when compared to traditional gasflooding. The alternated injection of water and gas slugs allies the good microscopic displacement efficiency of the gas phase with the mobility control provided by the water phase increasing the overall efficiency factor. Mathematical solutions are very important in the understanding of the WAG process because it brings a complete perspective of the physical phenomenon that cannot be obtained by numerical simulation only.

This document presents the development made in four years of doctoral research that improves the mathematical comprehension of the WAG recovery process. First it is discussed the immiscible simultaneous three-phase flow problem, where analytical solutions were developed using the method of characteristics considering concave relative permeability curves, common in high heterogeneous scenarios. Then the problem of step-variable boundary conditions is presented including an application to injectivity well test analysis. Finally, the mathematical solution for both immiscible and miscible WAG problem is built, where the interactions between different characteristics in the solution domain are treated by the wave interaction theory. Several examples are given throughout the thesis showing that all proposed mathematical solutions show good agreement when compared to numerical simulation results. Examples are fully discussed with a detailed explanation about the physical phenomena involved in each case.

**Keywords:** Water Alternating Gas, Method of Characteristics, Enhanced Oil Recovery, Miscible Displacement, Injectivity Test.

# Resumo

Com as recentes descobertas brasileiras do pré-sal ocorreu um aumento significativo na utilização do método de injeção alternada de água e gás (do inglês *Water Alternating Gas* - WAG). Esse processo é útil em campos com altos teores de  $CO_2$  onde o gás produzido precisa ser reinjetado no reservatório, aumentando significativamente os fatores de recuperação quando comparado com a injeção tradicional de gás (*gasflooding*). A injeção alternada de bancos de água e gás combina a boa eficiência microscópica de deslocamento do gás com o controle de mobilidade devido à água, aumentando a eficiência de recuperação média do campo. Soluções matemáticas possuem grande importância no entendimento do método WAG pois são capazes de mostrar aspectos relevantes que não poderiam ser observados a partir do uso de simulação numérica apenas.

Esse documento apresenta os resultados obtidos ao longo de quatro anos de uma pesquisa de doutorado que resultou na melhoria da compreensão física e matemática a respeito do método WAG. Primeiramente é discutido o problema do fluxo trifásico imiscível em meios porosos, onde soluções analíticas são desenvolvidas a partir do método das características considerando curvas de permeabilidade relativa côncavas, comuns em meios altamente heterogêneos. Na sequência é apresentado o problema de condições de contorno variáveis, incluindo uma aplicação em testes de injetividade. Finalmente, a solução matemática dos problemas WAG miscível e imiscível são discutidas, onde as interações entre as diferentes características no domínio são tratadas a partir da teoria da interação de ondas. Vários exemplos são apresentados ao longo da tese, mostrando uma boa concordância entre as soluções analíticas e numéricas. Os fenômenos físicos envolvidos em cada um desses exemplos são analisados em cada caso estudado.

**Palavras Chave:** Injeção Alternada de Água e Gás, Método das Características, Recuperação Avançada de Petróleo, Deslocamento Miscível, Teste de Injetividade.

# 1 Introduction

The Water Alternating Gas (WAG) method consists of the alternated injection of water and gas slugs in an oil reservoir in order to increase the recovery efficiency. This scheme is an Enhanced Oil Recovery (EOR) method that combines the high displacement efficiency of the gas injection and the mobility control provided by the water injection, increasing both vertical and horizontal sweep efficiency and stabilizing the gas injection front (CHRISTENSEN *et al.*, 2001).

The WAG scheme was first applied in the North Pembina field in Canada, operated by Mobil in 1957 (CHRISTENSEN *et al.*, 2001). Many projects are reported in literature showing an increment in oil recovery between 2 and 20% (CHRISTENSEN *et al.*, 2001). For immiscible WAG applications, the incremental recovery efficiency varies between 1 to 13% of original oil in place (OOIP), depending mainly on the oil API (HOLTZ, 2016). Recent developments are based on the combination of WAG with other recovery methods as Foam Assisted WAG (FAWAG), Polymer Alternating Gas (PAG) or Water Alternating High-Pressure Air Injection (WAHPAI), are the most common applications of  $CO_2$  and brine as injected gas and water, due to its high miscibility with oil and economical aspects (AFZALI *et al.*, 2018).

A WAG project can be divided in two main phases: screening and implementation. During the screening phase, laboratory, mathematical modeling and simulation studies are performed to evaluate rock and fluid interaction and estimating the additional oil recovery. The implementation usually starts with a pilot project, usually with a well located in a relatively isolated part of reservoir for performance evaluation (NADESON *et al.*, 2004). Awan *et al.* (2008) reviewed 19 EOR projects in the North Sea, including 7 WAG, 1 SWAG and 2 FAWAG, between 1975 and 2005 concluding that some technological restrictions such as hydrate formation, injectivity loss, availability of  $CO_2$ , high well spacing due to offshore costs; and reservoirs characteristics such as heterogeneity, thickness and anisotropy may impact the expected oil recovery.

Besides geological and fluid limitations, some operational issues can lead the project to fail during the implementation phase. Apart from equipment failed, the

main issue is the injectivity reduction after fluid cycling, controlled mainly by the rock wettability (ROGERS; GRIGG, 2001). Wettability is a parameter so important in WAG design that, for example, Zahoor *et al.* (2011) concluded that a proper WAG project requires not only a good understanding of initial rock wettability but also its variation with the injected fluid, considering adsorption phenomena and deposition of organic and inorganic components present in crude oil.

During WAG design, some uncertainty factors like heterogeneity can lead to performance forecast deviations, thus after project implementation, surveillance is the only way to determine where the technique is efficient and additional recovery will be obtained. One of the most used techniques is tracer injection, in which different molecules that are not present in reservoir fluids are injected with gas and water, and analyzed in the producer wells (YANG *et al.*, 2000). Tracer injection, combined with fluid sampling and production well logging were successfully applied in the Prudhoe Bay field, Alaska, allowing comparisons between the effects in different regions of the drainage pattern, that led to infill drilling projects to improve oil recovery in poorly swept zones (PANDA *et al.*, 2010).

## 1.1 WAG Method Classification

The WAG method can be classified according to two main attributes, fluid characteristics and injection technique (SHAHVERDI, 2012). Related to the fluid characteristics, it can be classified into one of the following groups:

### 1. Miscible WAG (MWAG):

The injected gas is miscible with the original oil in reservoir, where the decrease of interfacial tension between phases increases the displacement efficiency (SHAHVERDI, 2012; MAMANI, 2016; AFZALI *et al.*, 2018). Generation and maintenance of a stable miscible front between injected gas and reservoir oil depends mainly on four factors: oil composition, temperature, pressure and gas composition. Among them, only pressure and gas composition can be controlled for production optimization (CHRISTENSEN *et al.*, 2001);

### 2. Immiscible WAG (IWAG):

When the miscibility effect at reservoir pressure and temperature is not achieved, simultaneous flow of oil, gas and water in reservoir will take place. The surface tension between fluids decreases the displacement efficiency when compared to

the MWAG, however, this method still reaches higher recovery factors than pure gas or water injection (CHRISTENSEN *et al.*, 2001);

3. Water Alternating Steam Process (WASP):

This processes was originally developed to overcome steam injection problems, such as channeling, segregation, and fingering (AFZALI *et al.*, 2018). This method is recommended for heavy oil reservoirs in which the steam thermal energy decreases the oil viscosity and improves oil production. The WASP has advantages over the continuous steam injection due to the enhancement of both areal and vertical injection front conformance;

4. Foam Assistant WAG (FAWAG):

The main problem of the gas injection in reservoir is the mobility control, because of early breakthrough cauded by gas mobility. Even though the water controls the gas mobility in traditional WAG, in scenarios with high rock heterogeneity an additional mobility control method should be employed. The foam injection can be used in those cases, increasing the gas viscosity and improving the recovery factors when compared to traditional IWAG (AFZALI *et al.*, 2018);

5. Polymer Alternating Gas (PAG):

The addition of polymer to the water can be employed to increase its viscosity and consequently delays the water breakthrough in heavy oil reservoirs. The main advantage of PAG compared to the traditional WAG is that the same recovery factor is obtained using less gas (AFZALI *et al.*, 2018);

6. Chemically Enhanced WAG (CWAG):

This is a general term used for any chemical component added to the water phase to control the mobility, to reduce the interfacial tension between fluids and to modify the rock wettability. The most used components in industry are alkalys, surfactants and emulsifiers (AFZALI *et al.*, 2018).

Related to the injection technique, three can be cited:

1. Conventional WAG:

Alternated slugs of water an gas are injected in the reservoir, where the slug ratio and cycling frequency can be optimized to increase the oil recovery (SHAHVERDI, 2012). Usually, the most used WAG ratio is 1:1, but this parameter has low influence in oil recovery factor when compared to other, specially in mixed-wet formations (CHRISTENSEN *et al.*, 2001; AFZALI *et al.*, 2018);

## 2. Simultaneous WAG (SWAG):

In order to minimize fingering or fluid segregation in reservoirs, it has been developed the SWAG method. It consists of injecting gas and water together in the same well, maximizing the contact between phases (SHAHVERDI, 2012). The method was first tested in field scale in 1963 in Texas, during an injection project of water enriched with gas at high pressures (AFZALI *et al.*, 2018);

## 3. Hybrid WAG (HWAG):

This method is also known as Denver Unit WAG (DUWAG) due to the pilot test performed in Wasson field in Texas that started in 1983 and consists of a massive injection of  $CO_2$  (sometimes around 40% of porous volume) followed by small 1:1 cycles of gas and water (SHAHVERDI, 2012; AFZALI *et al.*, 2018). The main advantage of this technique is the increase of reservoir pressure and reduction of surface tension provided by the initial  $CO_2$  injection, followed by the increase of sweep efficiency achieved by the small WAG cycles.

## 1.2 Mathematical Modeling and Analytical Solutions

Buckley e Leverett (1942) published one of the first solutions for the two-phase flow problem in porous media. It was assumed one-dimensional transient oil displacement by an immiscible fluid (water or gas) in an homogeneous reservoir, neglecting gravitational and capillary effects. Three-phase flow solutions are more complicated, because some standard assumptions of the Buckley-Leverett equation can lead to mathematically ill-posed problems (BELL *et al.*, 1986; HOLDEN, 1990; MARCHESIN; PLOHR, 2001). Nevertheless, comparing the most common three-phase relative permeability models (STONE, 1970; BAKER, 1988; COREY *et al.*, 1956; DELSHAD; POPE, 1989) such elliptical regions are usually small and do not cause numerical instabilities during numerical simulations (SHEARER; TRANGENSTEIN, 1989) nor create physically inadmissible solutions (GUZMÁN; FAYERS, 1997a; GUZMÁN; FAYERS, 1997b).

There is no agreement in literature if the existence of elliptical regions in three-phase solutions is caused by physical reasons or is a direct consequence of the simplified relative permeability models (JUANES; PATZEK, 2003; JUANES; PATZEK, 2004a; JUANES; PATZEK, 2004b; JUANES; PATZEK, 2004c; JUANES, 2005). Jackson e Blunt (2002) investigated if elliptical regions can appear in a theoretical pore-scale model made from a bundle of cylindrical pores of different sizes, if it obeys the Darcy's law and if the relative permeability is a function of the saturations only. When gravita-

tional effects are included in this model, elliptical regions appear in a large area of the ternary saturation diagram, concluding that elliptical regions may not be created by the relative permeability models.

Another effect that impacts WAG modeling is the mass exchange between injected and displaced phases. Using a tie line construction to model miscible effects, Dindoruk (1992) solved the one-dimensional two-phase miscible case, considering up to four components system. Solutions considering the displacement of oil by a single component gas was tested experimentally using a slim-tube  $CO_2$  injection (JOHNS; ORR, 1996). Even though the minimum miscibility pressure results are consistent, the produced oil composition suggests that the dispersion free hypothesis may not be correct. The one-dimensional multi-component miscible solution was obtained by Bedrikovetsky *et al.* (2004) using a lifting technique, where the equations are divided in a new auxiliary system containing only thermodynamic variables and a single independent lifting equation that depends on both hydrodynamic and thermodynamic variables.

The hysteresis effect can be modeled creating a new variable related to the sturayon point in the relative permeability curve (BEDRIKOVETSKY *et al.*, 1996; BEDRIKOVETSKY, 1997). For three-phase solutions, it was included the effect of molecular discontinuity of the oil phase (ganglionar trapping), causing an increment of injected phase velocity, decreasing the miscible WAG recovery factor. The hysteresis due to oil ganglia effects can be evaluated for two-phase flow of oil and water, creating different solutions for imbibition and drainage processes (KATS; DUIJN, 2001). The relative permeability hysteresis of gas phase can also be modeled by this model, achieving a good agreement when compared to numerical solutions (PLOHR *et al.*, 2002).

### 1.3 Thesis Organization

The main objective of this thesis is the development of a mathematical solution for the WAG injection scheme that considers both immiscible and miscible effects. The solution is built using the method of characteristics, in which the interactions between the characteristics caused by a variable boundary condition, inherent of the WAG method, are treated using the wave interaction theory. This doctoral research resulted in six different publications, each one is a chapter of this volume.

In the next chapter we discuss the analytical solutions for one-dimensional, three-phase, incompressible flow in porous media. The next two chapters present a new method to approximate the solution of step-rate injectivity tests. The related papers

show how a variable boundary condition affects the analytical solution of oil displacement problems and how it can be applied in injectivity test analysis. The fifth chapter presents our very first results regarding the WAG method, where an approximate method is discussed for large injection cycles cases, when the breakthrough shock front has already reached the outlet of the domain.

Chapters six and seven are the main core of this thesis. First we adapt the wave interaction theory to immiscible WAG problems, where each wave interaction is treated as a Riemann problem. Then, we formulate and solve the miscible WAG scheme where the injected gas and the original oil fluid exchange mass during the flow. Examples are given throughout the thesis that show that all proposed mathematical solutions show good agreement to numerical simulation results. The examples are discussed and the physical phenomena involved in each case are analyzed.

**2     *Article: Analytical Solution for  
One-Dimensional Three-Phase  
Incompressible Flow in Porous  
Media for Concave Relative  
Permeability Curves***



# Analytical solution for one-dimensional three-phase incompressible flow in porous media for concave relative permeability curves

Wagner Q. Barros, Adolfo P. Pires\*, Alvaro M.M. Peres

Laboratório de Engenharia e Exploração de Petróleo, Universidade Estadual do Norte Fluminense Darcy Ribeiro, Rodovia Amaral Peixoto, Km 163, Imboassica, Macaé, 27925-310, Rio de Janeiro, Brazil



## ARTICLE INFO

### Keywords:

Multi-phase flow  
Method of characteristics  
Concave relative permeability curves  
Immiscible flow

## ABSTRACT

Three-phase flow in porous media may appear in different scenarios during the production life of a hydrocarbon reservoir. The simultaneous flow of different phases is modeled by relative permeability curves which are fundamental to petroleum production analysis and forecast. Laboratory experiments are the main source of data for relative permeability curves. Mathematical solutions for multiphase flow in porous medium are key for determining relative permeability curves from laboratory data, to check numerical reservoir simulation results and for screening an enhanced oil recovery technique. The complexity of reservoir modeling and the use of numerical optimization to history match the laboratory data have shown the importance of concave relative permeability curves. In this paper we present the analytical solution for one-dimensional incompressible immiscible three-phase flow in porous media, where the relative permeability functions are described by concave curves. The hyperbolic system of equations that results from mass conservation is solved by the method of characteristics. The results show close agreement to numerical solutions.

## 1. Introduction

Multi-phase flow in porous medium is an important research area in the petroleum industry. Waterflooding is the most used recovery technique, and a third hydrocarbon phase can exist through a gas cap or it can be created during field production if it is depleted below bubble point. Darcy's law models the simultaneous flow of two or three phases, and the relative permeabilities relate the mobility of the phases. These curves are obtained using coreflood experiments, where one or two phases are injected in a core while the pressure and the effluent rates are measured. There are two kinds of experiments based in the flow regime: steady-state and transient.

For steady-state experiments, two or three phases are injected simultaneously in a core until a steady-state condition is achieved. The relationship among the phase rates creates a particular saturation in the core, and the relative permeability of each phase can be directly obtained using the Darcy's law. Details of experimental apparatus and results for different rocks are largely reported in literature [1–9].

In the transient approach, pressure and cumulative production are measured since the beginning of the experiment and the relative permeability curves are obtained through the solution of an inverse problem [10–15]. The main advantage of this method is that the permeability curves are obtained in a single experimental running, making this method faster and simpler. The main problem is that the experimental

curves depend on the hypothesis adopted for the inverse problem solution.

The inverse problem can be solved by two different ways: using analytical solutions of governing equations [10–13,16–19] and using numerical optimization techniques [20–29]. The first method is preferred because it is faster and free of numerical errors. However, for complex scenarios like miscible flooding, thermal effects and heavy oils; analytical solutions may not be available [28,29]. Thus, the development of new mathematical models and solutions considering different scenarios are fundamental.

Concave relative permeability curves are not as common as the convex ones, but it may appear in different conditions:

1. Steady-state experiments [13];
2. Transient experiments in which the original reservoir wettability is preserved [30];
3. Use of numerical optimization to solve the transient coreflood experiments [21,25,29,31];
4. History matching full-field production data changing not only geological parameters, but also the relative permeability curves used in reservoir simulators [32–35].

Thus, the analysis of the mathematical aspects of three-phase flow using concave relative permeability curves is important to better understand its recovery factor impact in reservoir simulation.

\* Corresponding author.

E-mail addresses: [wagnerqb@gmail.com](mailto:wagnerqb@gmail.com) (W.Q. Barros), [puime@lenep.uenf.br](mailto:puime@lenep.uenf.br) (A.P. Pires), [alvaroperes@lenep.uenf.br](mailto:alvaroperes@lenep.uenf.br) (A.M.M. Peres).

Analytical solutions for two-phase flow [36] considers one-dimensional transient oil displacement by an immiscible fluid (water or gas) in an homogeneous reservoir. Capillary and gravitational effects were further included by Sheldon and Cardwell [37], Fayers and Sheldon [38]. Two-phase solutions considering mass exchange between phases were built using tie-lines [39–42].

Analytical solutions for three-phase immiscible flow in horizontal and homogeneous porous medium, neglecting capillary, dispersion and gravitational forces, are classified in three main groups [43]: hyperbolic with a single umbilic point [44–49], hyperbolic with multiple umbilic points [43,45] and mixed hyperbolic and elliptic [45,50,51]. The existence of these regions creates new waves that are not fully described using the classical Riemann problem theory. For example, transitional shocks appears in problems with an unique umbilic point, in which the traditional Rankine–Hugoniot and Lax equations are insufficient to determine the solution stability [44,52,53].

Traditionally, all hypothesis with respect to Darcy’s law validity are assumed during construction of three-phase immiscible equations. However, both Darcy’s law and Buckley–Leverett equations can be obtained by modeling the microscopic creeping flow through proper upscaling by homogenization techniques [54] or using the mixture theory [55]. Relaxing the assumption that viscous friction within the fluid can be neglected it is possible to deduce the Brinkman and the Forchheimer’s terms creating more realistic models for flow in porous media [55,56]. Considering a pressure dependent viscosity model, it is possible to show a dependence of the relative permeability curve on the fluid pressure, even for rigid solid matrices, when considering the linear flow in thin channels [57,58]. If this dependence of viscosity on pressure is strong and the exponential viscosity model is used, the traditional Darcy’s approach may under-predict the pressure gradient field [56,59,60].

Understanding the mathematical structure of three-phase solutions can give us insights of how is the most efficient way to explore a petroleum reservoir. The final oil recovery is strongly affected by the reservoir characteristics (permeability, fluid viscosities, relative permeability curves), by the proportion of water and gas flowing simultaneously in the porous medium [47,61,62] and by the in-place oil saturation condition [63]. However, all of the solutions already published in literature considers only convex relative permeability curves. To the best of our knowledge, there are no published solutions for three-phase flow using concave relative permeability functions, typical of Corey’s exponents less than one.

In this work, we present the analytical solution for the displacement of oil by water and gas in one-dimensional porous media using concave relative permeability functions. In Section 2 we show the mathematical development and the general solution of the Riemann problem, including the stability conditions. Next section presents the general solution considering different injection conditions (Section 3). Then, some conclusions are addressed.

## 2. Mathematical model of three-phase immiscible flow

We consider the linear displacement of oil by a mixture of gas and water in a homogeneous and isotropic reservoir initially saturated with oil at irreducible water saturation. Additional hypothesis are:

1. Immiscible and isothermal flow;
2. Negligible dispersion, gravitational and capillary effects;
3. Incompressible fluids and porous media;
4. Constant viscosity;
5. Darcy’s law is valid;
6. Constant cross sectional area.

Under these assumptions, the transport equation for each phase is given by:

$$\frac{\partial S_\pi}{\partial t} + \frac{1}{\phi} \frac{\partial v_\pi}{\partial x} = 0, \text{ for } \pi = w, o, g \quad (1)$$

in which  $\phi$  is the rock porosity, and  $S_\pi$  and  $v_\pi$  are the saturation and velocity of phase  $\pi$ . In this work, the aqueous, oleic and gaseous phase are denoted by  $w, o, g$ , respectively. Using Darcy’s equation, the velocity of each phase can be calculated by:

$$v_\pi = -\frac{K k_{r\pi}}{\mu_\pi} \frac{\partial P}{\partial x} \quad (2)$$

where  $K$  and  $k_{r\pi}$  are the absolute and relative permeabilities,  $\mu_\pi$  the phase viscosity and  $P$  the fluid pressure. Phase normalized saturations are defined by:

$$\begin{cases} S_{nw} = \frac{S_w - S_{wi}}{1 - S_{wi} - S_{or}}, & S_w \in [S_{wi}, 1 - S_{or}] \\ S_{no} = \frac{S_o - S_{or}}{1 - S_{wi} - S_{or}}, & S_o \in [S_{or}, 1 - S_{wi}] \\ S_{ng} = \frac{S_g}{1 - S_{wi} - S_{or}}, & S_g \in [0, 1 - S_{wi} - S_{or}] \end{cases} \quad (3)$$

where  $S_{wi}$  is the irreducible water saturation and  $S_{or}$  the residual oil saturation. We define the following dimensionless time and space coordinates:

$$x_D = \frac{x}{L} \quad (4)$$

$$t_D = \frac{\int_0^t q(\tau) d\tau}{(1 - S_{wi} - S_{or}) AL\phi} \quad (5)$$

where  $L$  is the porous media length,  $A$  is the cross sectional area, and  $q$  is the total injected flow rate measured at the inlet point ( $x_D = 0$ ). Thus, Eq. (1) can be written in its dimensionless form as:

$$\frac{\partial S_{n\pi}}{\partial t_D} + \frac{\partial f_\pi}{\partial x_D} = 0, \text{ for } \pi = w, o, g \quad (6)$$

in which  $f_\pi$  is the fractional flow of phase  $\pi$ :

$$f_\pi = \frac{\lambda_\pi}{\lambda_T} = \frac{\frac{k_{r\pi}}{\mu_\pi}}{\frac{k_{rw}}{\mu_w} + \frac{k_{ro}}{\mu_o} + \frac{k_{rg}}{\mu_g}} \quad (7)$$

where  $\lambda_\pi$  is the mobility for phase  $\pi$  and  $\lambda_T$  is the total system mobility. The three-phase relative permeability curves are given by the power-law model (Corey’s model [4]). We also follow Sarem’s approach [12, 16], where the relative permeability of each phase is a function of its own saturation. Under these considerations, the relative permeability of each phase is given by:

$$\begin{cases} k_{rw} = k_{rw}^{S_{or}} (S_{nw})^{n_w} \\ k_{ro} = k_{ro}^{S_{wi}} (S_{no})^{n_o} \\ k_{rg} = k_{rg}^{S_{or}} (S_{ng})^{n_g} \end{cases} \quad (8)$$

in which  $k_{ro}^{S_{wi}}$  is the relative permeability of oil at  $S_{wi}$  and  $k_{rw}^{S_{or}}$  and  $k_{rg}^{S_{or}}$  are the relative permeability of water and gas phases at  $S_{or}$ . The terms  $n_w, n_o$ , and  $n_g$  are the Corey’s exponents for each phase.

For three-phase conservation laws, the  $2 \times 2$  system hyperbolicity depends on the eigenvalues of the Jacobian matrix of the flux vector and it is linked to the relative permeability curves model. When the eigenvalues are real and different, the problem is called strictly hyperbolic and the solutions are well known. However, depending on the relative permeability curves, there are umbilic points where two or more eigenvalues are real and equal, leading to issues regarding uniqueness and existence of solutions. Eventually there are regions in the domain in which the eigenvalues are complex, generating elliptic ill-posed problems [43,46,50,64,65].

In this work, we consider the problem for concave relative permeability curves, obtained when  $n \in (0, 1)$ . Fig. 1 compares the relative permeability and the water fractional flow for  $n_w = n_o = 0.5$  and for  $n_w = n_o = 2.0$ . Note that the relative permeability function concavity leads to different behavior of the fractional flow curve. For the concave case the  $f_w$  derivative tends to infinity when one phase saturation goes to zero. This behavior changes the saturation profile solution when compared to convex relative permeability curves problems.

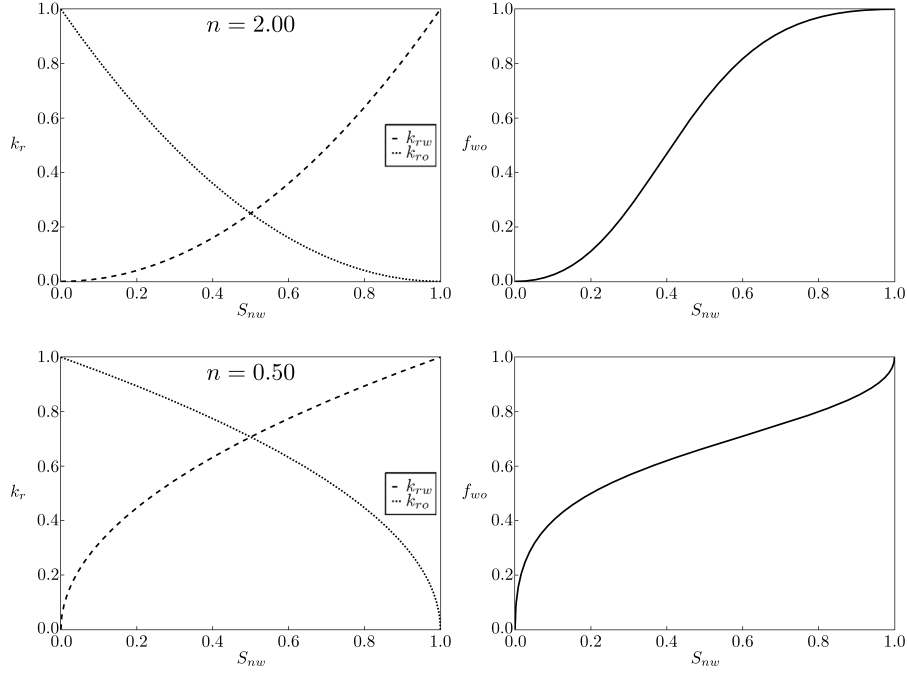


Fig. 1. Comparison between convex and concave relative permeability and water fractional flow curves using Corey's model ( $k_{rw}^{Sor}/\mu_w = 1.0$ ,  $k_{rw}^{Swi}/\mu_w = 0.5$  and  $k_{ro}^{Swi}/\mu_g = 2.0$ ).

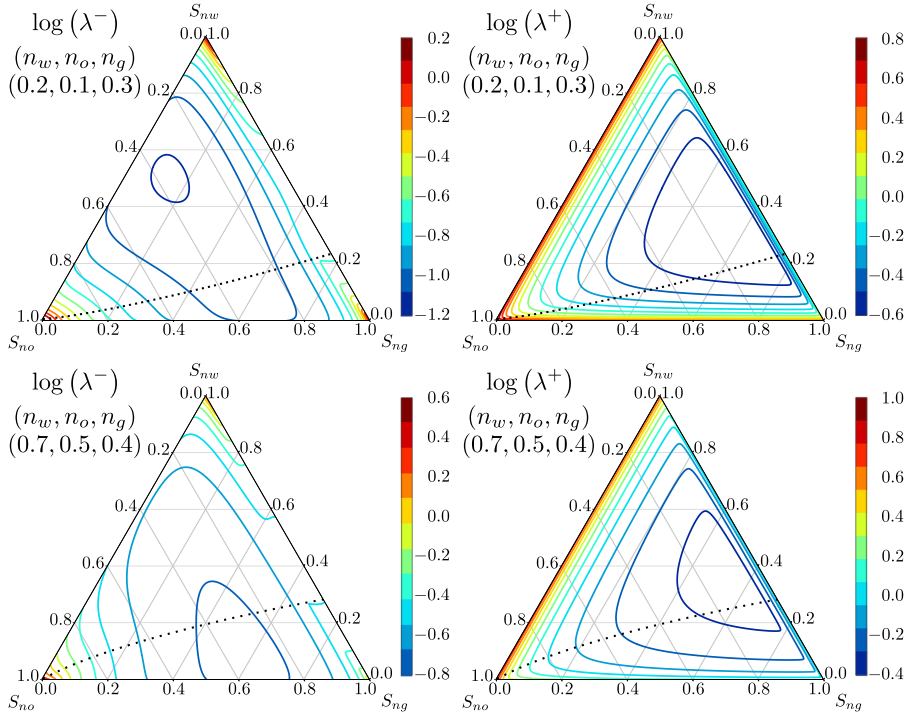


Fig. 2. Eigenvalues ( $\log(\lambda^-)$  and  $\log(\lambda^+)$ ) for  $(n_w, n_o, n_g) = (0.2, 0.1, 0.3)$  and  $(n_w, n_o, n_g) = (0.7, 0.5, 0.4)$  ( $k_{rw}^{Sor}/\mu_w = 1.0$ ,  $k_{rw}^{Swi}/\mu_w = 0.5$  and  $k_{ro}^{Swi}/\mu_g = 2.0$ ).

2.1. Solution in the saturation triangle

The saturations are limited by  $S_{nr} \in [0, 1]$  and by  $S_{nw} + S_{no} + S_{ng} = 1$ . As a consequence, we need to solve only two saturations. In this work we choose water and oil phases:

$$\begin{pmatrix} 1 & 0 \\ 0 & 1 \end{pmatrix} \begin{pmatrix} \frac{\partial S_{nw}}{\partial t_D} \\ \frac{\partial S_{no}}{\partial t_D} \end{pmatrix} + \begin{pmatrix} \frac{\partial f_w}{\partial S_{nw}} & \frac{\partial f_w}{\partial S_{no}} \\ \frac{\partial f_o}{\partial S_{nw}} & \frac{\partial f_o}{\partial S_{no}} \end{pmatrix} \begin{pmatrix} \frac{\partial S_{nw}}{\partial x_D} \\ \frac{\partial S_{no}}{\partial x_D} \end{pmatrix} = \begin{pmatrix} 0 \\ 0 \end{pmatrix} \quad (9)$$

Using Corey's model for relative permeabilities, the flux function is given by (Eq. (8)):

$$\begin{cases} f_w = \frac{\frac{k_{rw}^{Sor}}{\mu_w} S_{nw}^{n_w}}{\frac{k_{rw}^{Sor}}{\mu_w} S_{nw}^{n_w} + \frac{k_{rw}^{Swi}}{\mu_o} S_{no}^{n_o} + \frac{k_{rg}^{Sor}}{\mu_g} (1 - S_{nw} - S_{no})^{n_g}} \\ f_o = \frac{\frac{k_{ro}^{Swi}}{\mu_o} S_{no}^{n_o}}{\frac{k_{rw}^{Sor}}{\mu_w} S_{nw}^{n_w} + \frac{k_{ro}^{Swi}}{\mu_o} S_{no}^{n_o} + \frac{k_{rg}^{Sor}}{\mu_g} (1 - S_{nw} - S_{no})^{n_g}} \end{cases} \quad (10)$$

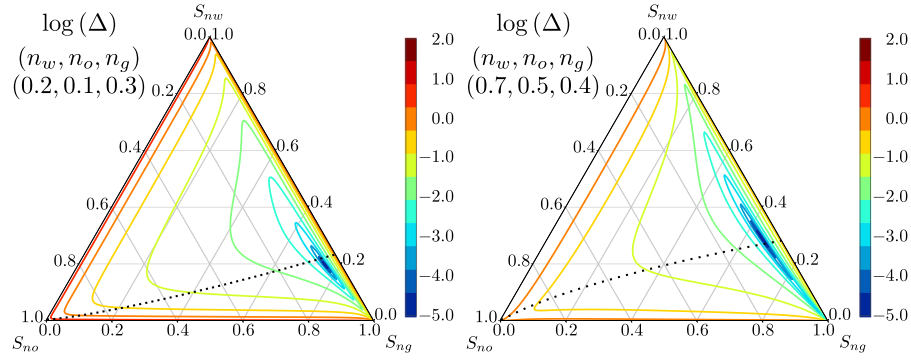


Fig. 3. Stability criteria ( $\log(\Delta)$ ) for  $(n_w, n_o, n_g) = (0.2, 0.1, 0.3)$  and  $(n_w, n_o, n_g) = (0.7, 0.5, 0.4)$  ( $k_{rw}^{S_{rw}}/\mu_w = 1.0$ ,  $k_{ro}^{S_{ro}}/\mu_o = 0.5$  and  $k_{rg}^{S_{rg}}/\mu_g = 2.0$ ).

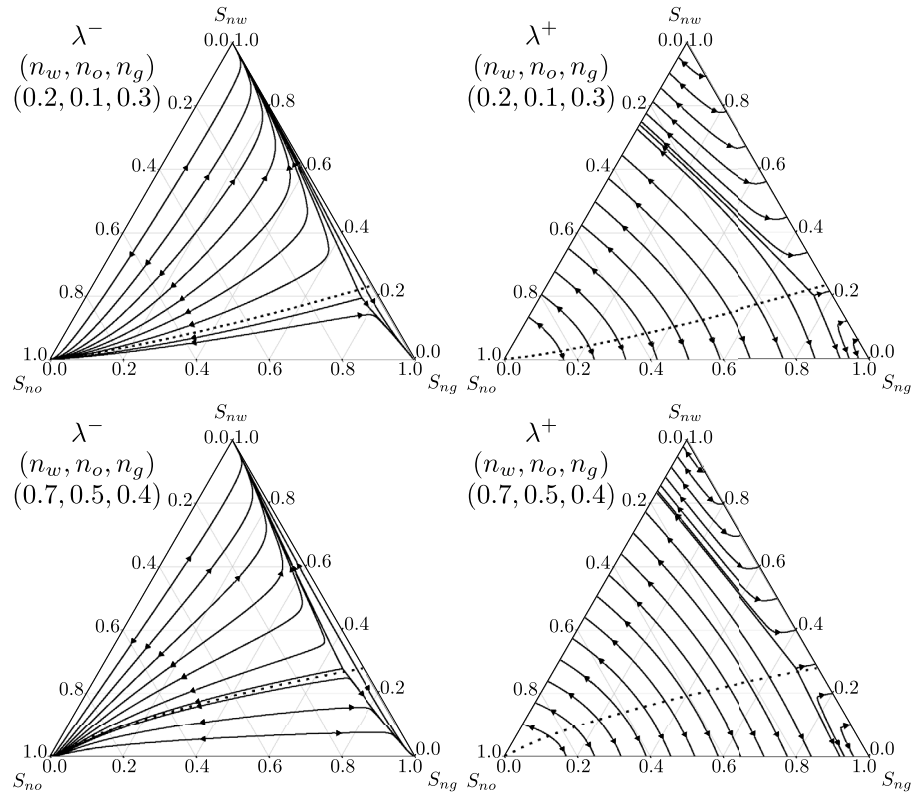


Fig. 4. Integral curves for  $(n_w, n_o, n_g) = (0.2, 0.1, 0.3)$  and  $(n_w, n_o, n_g) = (0.7, 0.5, 0.4)$  ( $k_{rw}^{S_{rw}}/\mu_w = 1.0$ ,  $k_{ro}^{S_{ro}}/\mu_o = 0.5$  and  $k_{rg}^{S_{rg}}/\mu_g = 2.0$ ).

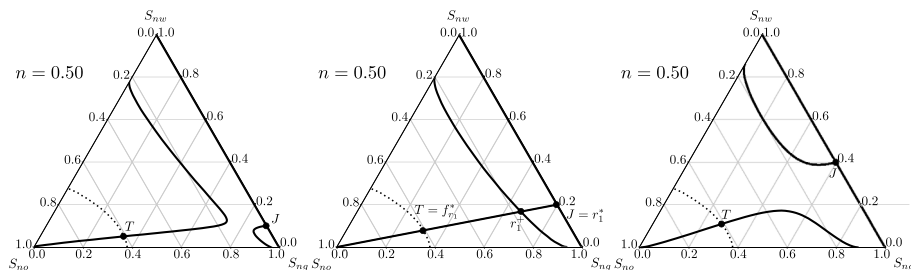


Fig. 5. Hugoniot locus for different  $J$  points along the  $\overline{S_{nw}S_{nsg}}$  edge ( $n = n_w = n_o = n_g = 0.5$ ,  $k_{rw}^{S_{rw}}/\mu_w = 1.0$ ,  $k_{ro}^{S_{ro}}/\mu_o = 0.5$  and  $k_{rg}^{S_{rg}}/\mu_g = 2.0$ ).

The eigenvalues of the Jacobian of flux vector (System (9)) are:

and the system is strictly hyperbolic if:

$$\lambda^\pm = \frac{1}{2} \left( \frac{\partial f_w}{\partial S_{nw}} + \frac{\partial f_o}{\partial S_{no}} \right) \pm \frac{1}{2} \sqrt{\left( \frac{\partial f_w}{\partial S_{nw}} - \frac{\partial f_o}{\partial S_{no}} \right)^2 + 4 \left( \frac{\partial f_w}{\partial S_{no}} \frac{\partial f_o}{\partial S_{nw}} \right)} \quad (11)$$

$$\Delta \equiv \left( \frac{\partial f_w}{\partial S_{nw}} - \frac{\partial f_o}{\partial S_{no}} \right)^2 + 4 \left( \frac{\partial f_w}{\partial S_{no}} \frac{\partial f_o}{\partial S_{nw}} \right) > 0 \quad (12)$$

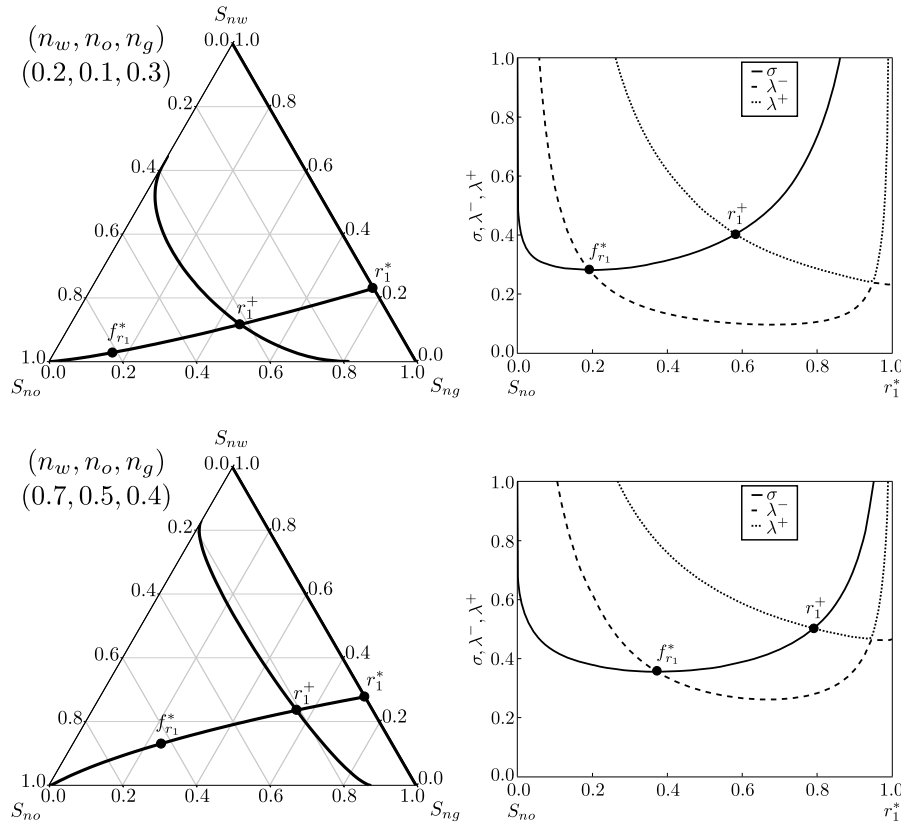


Fig. 6. Hugoniot locus and eigenvalues along  $r_1$  curve for  $(n_w, n_o, n_g) = (0.2, 0.1, 0.3)$  and  $(n_w, n_o, n_g) = (0.7, 0.5, 0.4)$  ( $k_{sw}^{S_w}/\mu_w = 1.0$ ,  $k_{sw}^{S_w}/\mu_w = 0.5$  and  $k_{sw}^{S_w}/\mu_w = 2.0$ ).

Table 1  
General solution of System (9) for concave relative permeability curves.

Case	$f'_{wg}(r_1^*) \leq \sigma(r_1^*, f_{r_1}^*)$	Injection condition	Solution profile
3.1-a	True	$J = S_{nw}$	$(J = S_{nw}) \rightarrow f_w^* - I$
3.1-b	True	$r_1^* < J < S_{nw}$	$(J) \rightarrow (r_1^*) \rightarrow f_{r_1}^* - I$
3.1-c	True	$\min f'_{gw} < J < r_1^*$	$(J) \rightarrow T - (r_1^*) \rightarrow f_{r_1}^* - I$
3.1-d	True	$r_1^* < J < \min f'_{gw}$	$(J) - (r_1^*) \rightarrow f_{r_1}^* - I$
3.1-e	True	$J = r_1^*$	$(J = r_1^*) \rightarrow f_{r_1}^* - I$
3.1-f	True	$S_{ng} < J < r_1^*$	$(J) \rightarrow (r_1^*) \rightarrow f_{r_1}^* - I$
3.1-g	True	$J = S_{ng}$	$(J = S_{ng}) \rightarrow f_g^* - I$
3.2-a	False	$J = S_{nw}$	$(J = S_{nw}) \rightarrow f_w^* - I$
3.2-b	False	$J \in (S_{nw}, S_{ng})$	$(J) \rightarrow T - I$
3.2-c	False	$J = S_{ng}$	$(J = S_{ng}) \rightarrow f_g^* - I$

For all points inside the ternary triangle  $\lambda^- < \lambda^+$  (slow and fast eigenvalues), except at the umbilic points where eigenvalues are equal. System (9) is solved by the method of characteristics [66–68].

### 2.1.1. Rarefaction waves

The rarefaction part of the solution is found by solving the following ODE system:

$$\frac{d\bar{S}_n}{d\xi} = \bar{r}_\pm(\bar{S}_n) \tag{13}$$

where  $\xi = x_D/t_D$  is the self-similar variable and  $\bar{r}_\pm$  are the fast and slow right eigenvectors of the Jacobian. The rarefaction waves follow a continuous path in the ternary triangle for each eigenvalue, written as:

$$\left(\frac{dS_{nw}}{dS_{no}}\right)^\pm = -\frac{\frac{\partial f_w}{\partial S_{no}}}{\left(\frac{\partial f_w}{\partial S_{nw}} - \lambda^\pm\right)} \tag{14}$$

Note that along each rarefaction curve, the solution is valid if the associated eigenvalue increases monotonically along the integral path [69], condition called geometrical compatibility criteria.

### 2.1.2. Shock waves

This problem also admits weak solutions, called shock waves. A valid shock must conserve the mass of all phases across a discontinuity, where each side is denoted by  $L$  (left) and  $R$  (right). This restriction is known as Rankine–Hugoniot condition and is used to calculate the shock speed  $\sigma = \sigma(L, R)$ :

$$\begin{cases} \sigma(S_{nw}^L - S_{nw}^R) = (f_w^L - f_w^R) \\ \sigma(S_{no}^L - S_{no}^R) = (f_o^L - f_o^R) \end{cases} \tag{15}$$

Fixing the  $L$  point in the domain it is possible to define the Hugoniot locus,  $\mathcal{H}(L)$ , as the geometrical place of all possible  $R$  points inside the ternary triangle, in which the Rankine–Hugoniot is satisfied. All points in  $\mathcal{H}(L)$  are possible weak solutions of System (9). To determine which one is the admissible, we are using both stability criteria defined by Liu [67,68] and Lax [66].

### 2.2. Numerical solution method

In order to check the analytical solutions, the saturation profiles are compared with a numerical first order explicit upwind method [70]. This scheme was chosen over other methods because, besides its simplicity, it does not generate numerical oscillation, allowing a comparison even at small shock regions. To minimize numerical diffusion effects the spatial domain is discretized with 100,000 cells in all cases shown in this work.

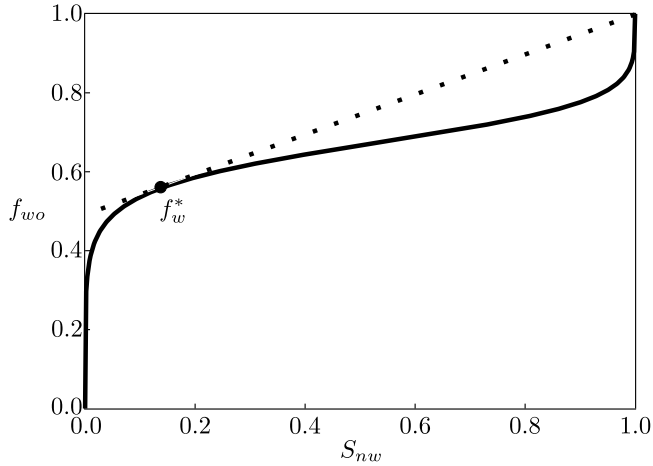


Fig. 7. Water-oil fractional flow and its tangent at  $f_w^*$  ( $n = n_w = n_o = n_g = 0.25$ ,  $k_{rw}^{Sor}/\mu_w = 1.0$ ,  $k_{ro}^{Swt}/\mu_o = 0.5$  and  $k_{rg}^{Sog}/\mu_g = 2.0$ ).

### 3. System solution

In this section we discuss the general solution of System (9) for the case of different Corey's exponent ( $n_w, n_o, n_g \in (0, 1)$ ), considering the displacement of oil by a gas-water mixture. The initial condition, defined by  $S_I$  or  $I$ , is the oil saturation at irreducible water ( $S_{no} = 1$ ). The boundary condition, defined by  $S_J$  or  $J$ , is the injection of a gas-water mixture, and lies on the  $\overline{S_{nw}S_{ng}}$  edge. Mathematically, these conditions are given by:

$$S_I(x_D, 0) = (0, 1, 0) \tag{16}$$

$$S_J(0, t_D) = (J, 0, 1 - J), \text{ for } J \in [0, 1] \tag{17}$$

Figs. 2 and 3 show the eigenvalues and the hyperbolicity ( $\log(\Delta)$ ) condition for  $(n_w, n_o, n_g) = (0.2, 0.1, 0.3)$  and  $(n_w, n_o, n_g) = (0.7, 0.5, 0.4)$ . All figures in this section were generated using the following phase mobilities  $k_{rw}^{Sor}/\mu_w = 1.0$ ,  $k_{ro}^{Swt}/\mu_o = 0.5$  and  $k_{rg}^{Sog}/\mu_g = 2.0$ . For the cases analyzed, there is an unique umbilic point inside the saturation triangle, where  $\Delta = 0$  and both eigenvalues are equal. This hypothesis is consistent with the topological arguments presented in [49].

The integral curves describe the rarefaction paths inside the domain. In Fig. 4 the arrows point toward increasing eigenvalues. For concave relative permeability curves, the slow rarefaction waves move to the triangle vertices while the fast waves move to the edges. In both cases, the associated eigenvalues approach infinity, meaning that for initial conditions located at any triangle vertices, the solutions will always be associated with an infinity speed rarefaction wave. Note that both slow and fast rarefaction curves collapse at the umbilic point, as expected.

The dotted line in Figs. 2–4 defines the  $r_1$  separatrix, the curve that separates two different topologies of Hugoniot locus constructed for points in  $\overline{S_{nw}S_{ng}}$  edge (Fig. 5) in saturation domain. Defining the point  $r_1^*$  as the intersection of  $r_1$  curve and the  $\overline{S_{nw}S_{ng}}$  edge, if  $J \in (S_{nw}, r_1^*)$  the Hugoniot locus has three branches, two locals and one non-local. The non-local branch starts and finishes at the  $\overline{S_{no}S_{ng}}$  edge. As  $S_{nw}$  approaches  $r_1^*$  the distance between local and the non-local branches decreases until they collapse at  $r_1^*$ . For  $J \in (S_{ng}, r_1^*)$  the non-local branch starts and finishes at the opposite  $\overline{S_{no}S_{nw}}$  edge. The dotted is the  $\lambda^-$  extension of  $\overline{S_{nw}S_{ng}}$  edge,  $E^-(\overline{S_{nw}S_{ng}})$ , where for each point  $T$  there is a point  $J$  in  $\overline{S_{nw}S_{ng}}$  where the shock speed  $\sigma(J, T)$  has the same value of the slow eigenvalue  $\lambda^-(T)$ . Mathematically, this curve is expressed by:

$$E^-(\overline{S_{nw}S_{ng}}) = \left\{ T : \exists J \in \overline{S_{nw}S_{ng}}, \text{ with } J \neq T, \right. \\ \left. \text{in which } T \in \mathcal{H}(J) \text{ and } \sigma(J, T) = \lambda^-(T) \right\} \tag{18}$$

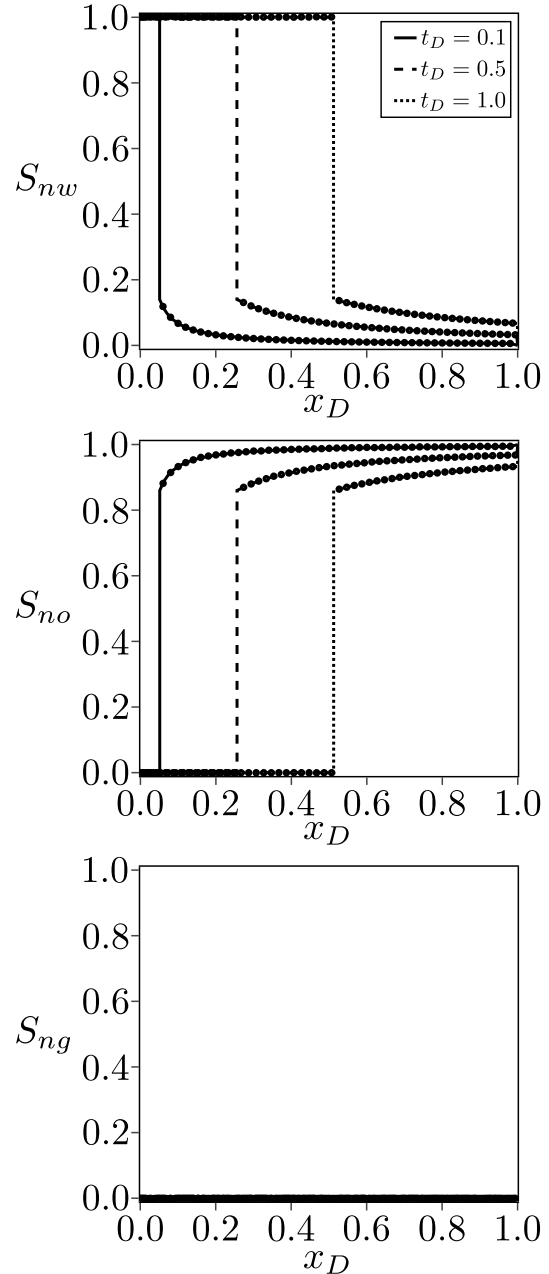


Fig. 8. Saturation profile for different injection times for Case 3.1-a ( $n = n_w = n_o = n_g = 0.25$ ,  $k_{rw}^{Sor}/\mu_w = 1.0$ ,  $k_{ro}^{Swt}/\mu_o = 0.5$  and  $k_{rg}^{Sog}/\mu_g = 2.0$ ), compared with numerical solution.

where for each  $J$  plotted in Fig. 5 there is a corresponding  $T$ . It is possible to note that  $J = r_1^*$  implies in  $T = f_{r_1}^*$ .

For the general case where each phase has its own  $n$  exponent, the  $r_1$  curve is constructed analyzing the Hugoniot locus along  $\overline{S_{nw}S_{ng}}$ . For the special case when all phases have the same Corey's exponent ( $n = n_w = n_o = n_g$ ), it is possible to define an explicit equation for  $r_1$ :

$$r_1 : S_{nw} = \left( \frac{k_{rg}^{Sog}/\mu_g}{k_{rw}^{Sor}/\mu_w} \right)^{\frac{1}{n-1}} S_{ng} \tag{19}$$

The analysis of  $r_1$  is important because the general solution is built based on the behavior of the shock speed and eigenvalues along this curve (Fig. 6), in which the shock curve was built fixing the  $r_1^*$  as the left condition of the shock. At point  $f_{r_1}^*$ , the slow eigenvalue and the shock speed are equal ( $\sigma(f_{r_1}^*, r_1^*) = \lambda^-(f_{r_1}^*)$ ) and, according to

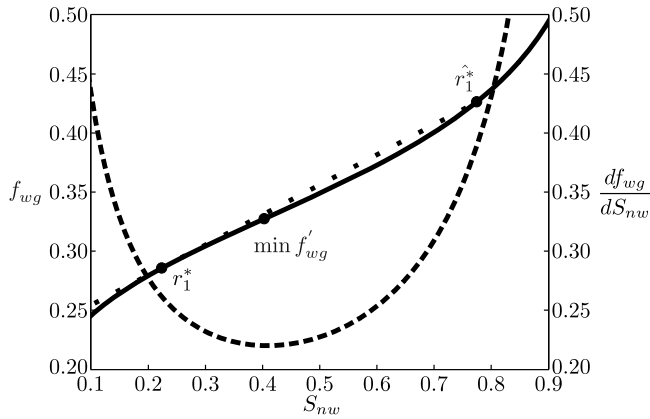


Fig. 9. Limit conditions on  $\overline{S_{nw}, S_{ng}}$  edge. Continuous curve is  $f_{wg}$ , dashed line is its derivative and dotted line is the tangent at  $r_1^*$  ( $(n_w, n_o, n_g) = (0.2, 0.1, 0.3)$ ,  $k_{nw}^{*sw}/\mu_w = 1.0$ ,  $k_{no}^{*sw}/\mu_o = 0.5$  and  $k_{ng}^{*sw}/\mu_g = 2.0$ ).

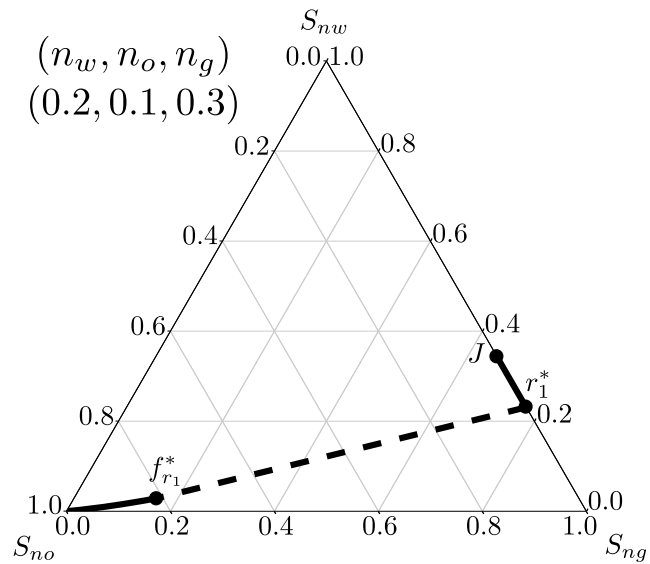


Fig. 10. Solution path in the ternary diagram for Case 3.1-d ( $(n_w, n_o, n_g) = (0.2, 0.1, 0.3)$ ,  $k_{nw}^{*sw}/\mu_w = 1.0$ ,  $k_{no}^{*sw}/\mu_o = 0.5$  and  $k_{ng}^{*sw}/\mu_g = 2.0$ ).

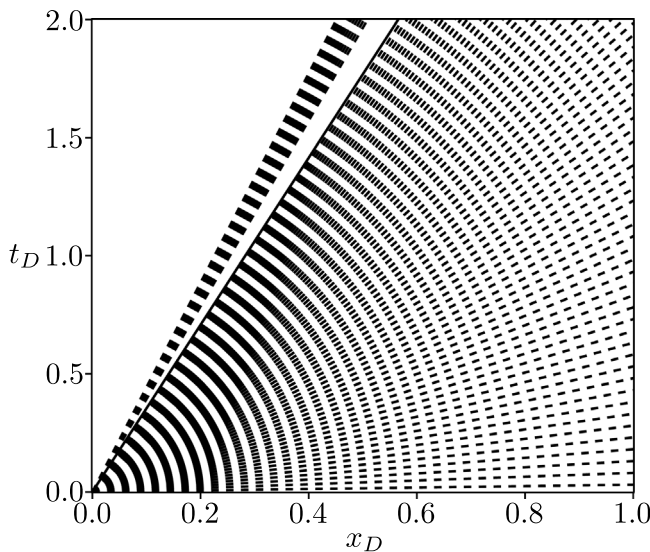


Fig. 11. Characteristic diagram for Case 3.1-d ( $(n_w, n_o, n_g) = (0.2, 0.1, 0.3)$ ,  $k_{nw}^{*sw}/\mu_w = 1.0$ ,  $k_{no}^{*sw}/\mu_o = 0.5$  and  $k_{ng}^{*sw}/\mu_g = 2.0$ ).

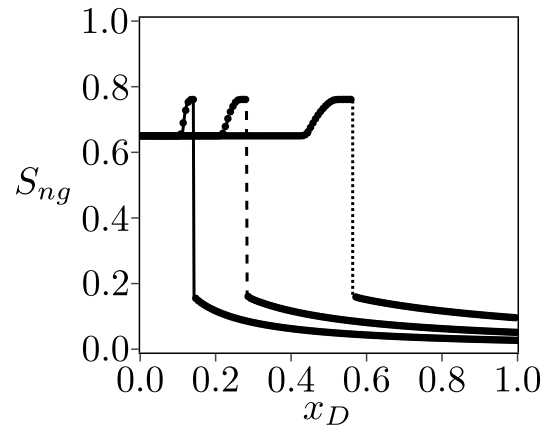
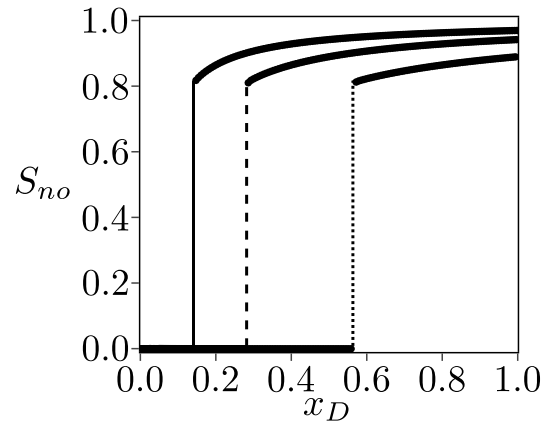
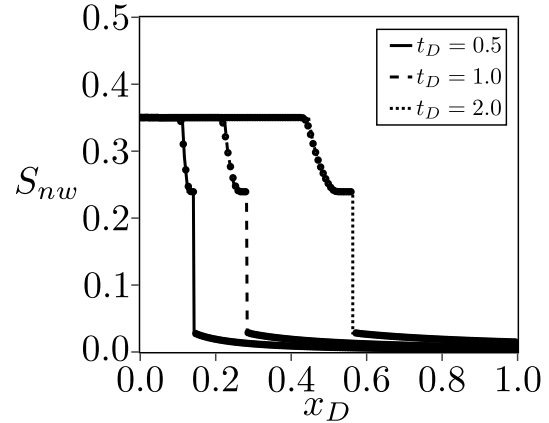


Fig. 12. Saturation profile for different injection times for Case 3.1-d ( $(n_w, n_o, n_g) = (0.2, 0.1, 0.3)$ ,  $k_{nw}^{*sw}/\mu_w = 1.0$ ,  $k_{no}^{*sw}/\mu_o = 0.5$  and  $k_{ng}^{*sw}/\mu_g = 2.0$ ), compared with numerical solution.

the Liu's stability criteria, this point is the most stable shock solution along the  $r_1$  curve. Note that at this point the shock speed is a local minimum, respecting the Bethe-Wendroff theorem [71,72]. The point  $r_1^+$  is a bifurcation manifold, in which two branches of  $r_1^*$  Hugoniot locus cross each other. At this point the shock curve changes its topology and the theorem of Bethe-Wendroff is not satisfied anymore (note that the shock speed is not at a critical point), implying that this point is not a stable solution [44].

Even though point  $f_{r_1}^*$  obeys Liu's stability criteria, it may or may not satisfy the geometrical compatibility criteria. This compatibility is obtained when the characteristics increase their velocities in the physical  $x_D - t_D$  plane, and it can be described by:

$$f'_{wg}(r_1^*) \leq \sigma(r_1^*, f_{r_1}^*) \tag{20}$$

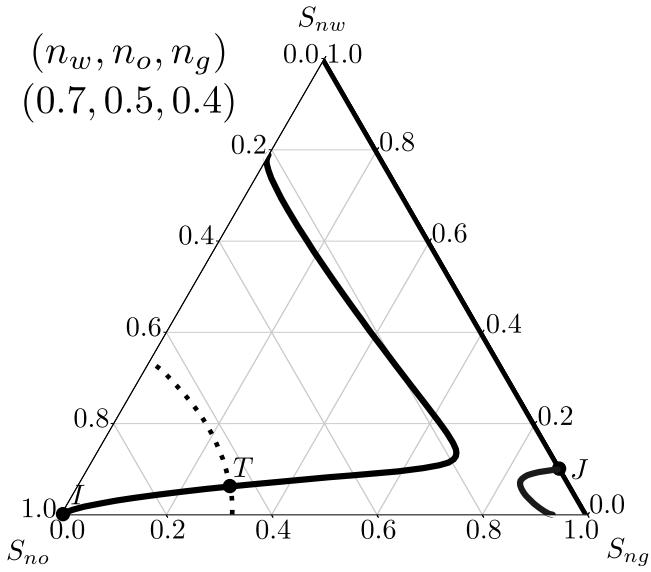


Fig. 13. Hugoniot locus of  $J$  in ternary diagram. Dotted curve is the extension  $E^- (\overline{S_{nw}, S_{ng}})$   $((n_w, n_o, n_g) = (0.7, 0.5, 0.4), k_{rw}^{sw}/\mu_w = 1.0, k_{rg}^{sw}/\mu_g = 0.5$  and  $k_{rg}^{sw}/\mu_g = 2.0$ ).

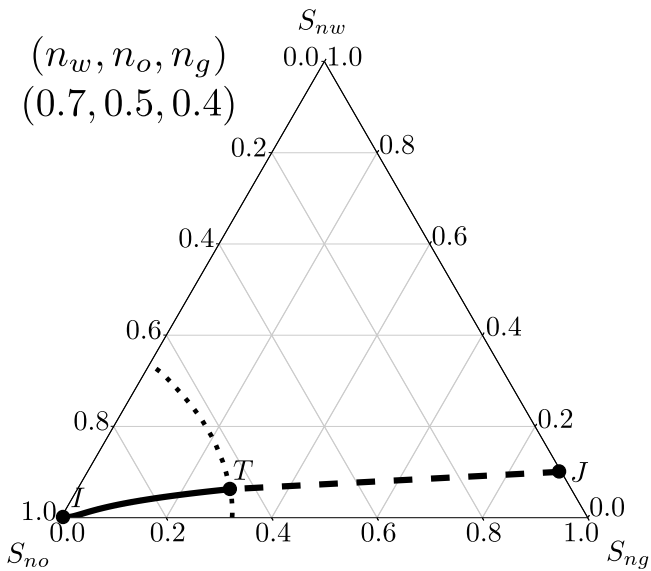


Fig. 14. Solution path in the ternary diagram for Case 3.2-b  $((n_w, n_o, n_g) = (0.7, 0.5, 0.4), k_{rw}^{sw}/\mu_w = 1.0, k_{rg}^{sw}/\mu_g = 0.5$  and  $k_{rg}^{sw}/\mu_g = 2.0$ ).

Observes that for concave relative permeability curves,  $\lambda^-(r_1^*) = f'_{wg}(r_1^*)$ , and  $(n_w, n_o, n_g) = (0.2, 0.1, 0.3)$  follows this condition, while  $(n_w, n_o, n_g) = (0.7, 0.5, 0.4)$  does not (Fig. 6).

The general solution of System (9) is presented in Table 1 for different injection conditions. The following notation is used to describe the solution waves:  $\rightarrow$  denotes a shock,  $-$  represents a rarefaction and a point in parenthesis indicates a constant state. Note that the solutions are divided in two major groups defined by Condition (20).

### 3.1. Solution for $f'_{wg}(r_1^*) \leq \sigma(r_1^*, f_{r_1}^*)$

The Cases 3.1-a and 3.1-g represent pure water and pure gas injection, respectively. Both solutions start with a shock from  $J$  to  $f_w^*$  or  $f_g^*$  and finish with a rarefaction wave to the initial point, where  $f_w^*$  and  $f_g^*$  are the tangent points of the water and gas fractional flow, depicted in Fig. 7 for the water case and  $n = n_w = n_o = n_g = 0.25$ .

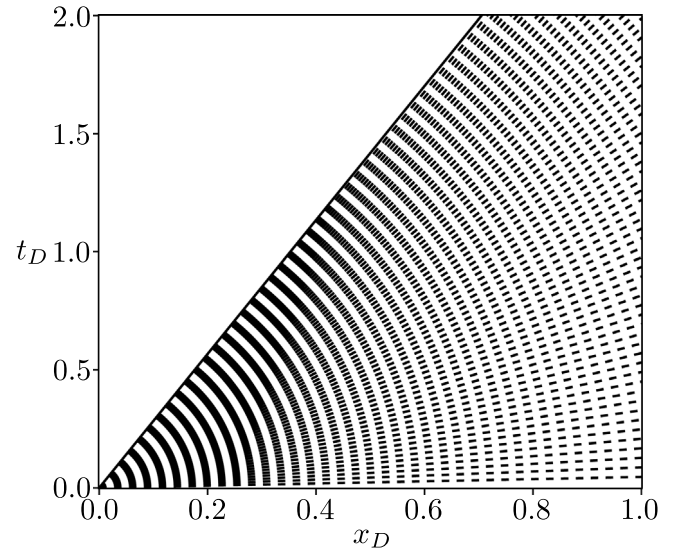


Fig. 15. Characteristic diagram for Case 3.2-b  $((n_w, n_o, n_g) = (0.7, 0.5, 0.4), k_{rw}^{sw}/\mu_w = 1.0, k_{rg}^{sw}/\mu_g = 0.5$  and  $k_{rg}^{sw}/\mu_g = 2.0$ ).

Comparing the saturation profile for this case with numerical solution, it can be observed that the breakthrough velocity is infinity and appears when injection begins, and the water saturation behind the shock is 100% (Fig. 8). This scenario is typical of highly heterogeneous low permeability rocks, where the presence of fractures creates a path for water phase, leading to an early breakthrough and recovery of almost all oil in the fracture system. After the production of the large channels, the low permeability matrix does not improve the oil recovery.

For Cases 3.1-b until 3.1-f, the shock from  $r_1^*$  to  $f_{r_1}^*$  is calculated using the geometrical compatibility criteria and all cases finish with the wave path  $(r_1^*) \rightarrow f_{r_1}^* - I$ . However, there are five different ways to reach the  $r_1^*$  point, depending on the structure of fractional flow curve in  $\overline{S_{nw}, S_{ng}}$  edge (Fig. 9). The point  $\hat{r}_1^*$  is the intersection between curve  $f_{wg}$  and its tangent at  $r_1^*$ , and it can be noted that every straight line connecting  $r_1^*$  and  $J \in (\hat{r}_1^*, S_{nw})$  is above the water-gas fractional flow curve  $f_{wg}$ . So, the solution for Case 3.1-b starts with a direct shock from  $J$  to  $r_1^*$ .

Due to the concave relative permeability functions, the derivative of  $f_{wg}$  with respect to the water saturation is strictly convex. So, the following relationship is valid:

$$\min f'_{wg} \in (r_1^*, \hat{r}_1^*) \quad (21)$$

where  $\min f'_{wg}$  is the minimum of  $f_{wg}$  derivative. This mathematical property allows us to build the solution for Case 3.1-c, in which, for every point  $T \in [r_1^*, \min f'_{wg}]$ , the tangent line of  $f_{wg}$  will cross a point  $J \in (\min f'_{wg}, \hat{r}_1^*)$ . Thus, the solution for this case starts with a shock from  $J$  to  $T$  followed by a rarefaction to  $r_1^*$ . Finally, the Cases 3.1-d and 3.1-e are part of Case 3.1-c, while Case 3.1-f has the same structure of Case 3.1-b. It must be stressed that all solutions in this section must follow the geometrical compatibility criteria, and exceptions are calculated following the same structure of cases where  $f'_{gw}(r_1^*) > \sigma(r_1^*, f_{r_1}^*)$  in Section 3.2.

The solution for the Case 3.1-d, when Condition (20) is satisfied, is presented in Figs. 10–12. Fig. 10 shows the solution path in the saturation triangle, and Figs. 11 and 12 show the characteristics and saturation profile, respectively. The solution starts with a rarefaction up to  $r_1^*$ , then a shock to  $f_{r_1}^*$ , followed by a rarefaction to the initial condition  $S_{no}$ . A low mobility fluid (oil) is replaced by a higher mobility mixture (gas + water), where the gas phase moves faster than water. It creates a gas slug in porous media, in which the gas saturation is higher

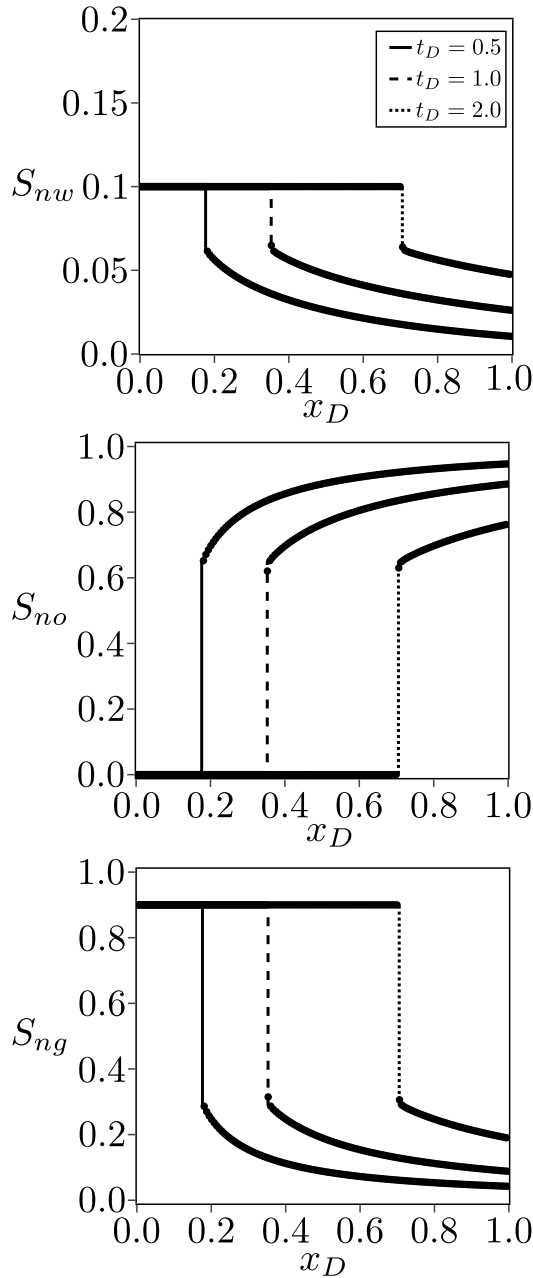


Fig. 16. Saturation profile for different injection times for Case 3.2-b ( $(n_w, n_o, n_g) = (0.7, 0.5, 0.4)$ ),  $k_{rw}^s/\mu_w = 1.0$ ,  $k_{ro}^s/\mu_o = 0.5$  and  $k_{rg}^s/\mu_g = 2.0$ ), compared with numerical solution.

than the injected saturation. Note that for Cases 3.1-b to 3.1-d the gas saturation in  $r_1^*$  is greater than injected saturation and a gas slug will be formed, while for Case 3.1-f a water slug will appear.

### 3.2. Solution for $f'_{wg}(r_1^*) > \sigma(r_1^*, f_{r_1}^*)$

When Condition (20) is not satisfied or the geometrical compatibility criteria fails at any point along the solutions presented in Section 3.1, the real solution must follow an integral curve outside the  $\overline{S_{nw}S_{ng}}$  edge. For each  $J$  on  $\overline{S_{nw}S_{ng}}$  there is an associated point  $T \in E^-(\overline{S_{nw}S_{ng}})$  in the  $\lambda^-$  extension curve (Eq. (18)). Except when  $J = r_1^*$ ,  $T$  always belongs to the non-local branch, thus a direct rarefaction solution is impossible. For the Case  $J = r_1^*$  the rarefaction is not possible due to the geometrical compatibility ( $f'_{wg}(r_1^*) > \sigma(r_1^*, f_{r_1}^*)$ ). The cases

when  $J = S_{nw}$  and  $J = S_{ng}$  (Cases 3.2-a and 3.2-c in Table 1) present the same solution structure of Cases 3.1-a and 3.1-g. For Case 3.2-b, the solution will consist of a shock from  $J$  to  $T$ , which obeys Liu's stability criteria, followed by a rarefaction to the initial condition  $I$ .

Fig. 13 shows the Hugoniot locus for a particular case when  $J \in (S_{nw}, S_{ng})$  and  $(n_w, n_o, n_g) = (0.7, 0.5, 0.4)$ , in which the dotted line is the extension  $E^-(\overline{S_{nw}S_{ng}})$ . The solution is given by Case 3.2-b, consisting of a shock from  $J$  to  $T$  followed by a rarefaction to the initial condition (Figs. 14–16). Note that all solutions when the Criteria (20) is not satisfied are composed by a shock followed by a rarefaction, so, no slugs appear in porous media.

## 4. Conclusions

This work presents a general analytical solutions for three-phase immiscible flow in an one-dimensional porous media with concave relative permeability curves. The mathematical key-points of the solution procedure by the method of characteristics are fully discussed for different scenarios and boundary conditions.

The saturation profiles are presented for the displacement of reservoir oil by a mixture of gas and water. The analytical solutions were compared with the results obtained by an explicit first-order upwind numerical method showing an excellent agreement. The solutions constructed in this paper can be used to validate numerical reservoir simulations or in inverse problems to compute concave relative permeability curves from core flood data.

### CRediT authorship contribution statement

Wagner Q. Barros: Conceptualization, Methodology, Software, Writing – original draft. Adolfo P. Pires: Supervision, Validation, Writing – review & editing. Alvaro M.M. Peres: Supervision, Validation, Writing – review & editing.

### Declaration of competing interest

The authors declare that they have no known competing financial interests or personal relationships that could have appeared to influence the work reported in this paper.

### Acknowledgments

The authors acknowledge Universidade Estadual do Norte Fluminense (UNEF), Brazil for financial support. This study was also financed in part by the Coordenação de Aperfeiçoamento de Pessoal de Nível Superior - Brazil (CAPES) - Finance Code 001.

## References

- [1] M. Leverett, Flow of oil-water mixtures through unconsolidated sands, Trans. AIME 132 (01) (1939) 149–171, <http://dx.doi.org/10.2118/939149-g>.
- [2] M. Leverett, W. Lewis, Steady flow of gas-oil-water mixtures through unconsolidated sands, Trans. AIME 142 (01) (1941) 107–116, <http://dx.doi.org/10.2118/941107-g>.
- [3] A.T. Corey, The interrelation between gas and oil relative permeabilities, Prod. Mon. (1954) 38–41.
- [4] A. Corey, C. Rathjens, J. Henderson, M. Wyllie, Three-phase relative permeability, J. Pet. Technol. 8 (11) (1956) 63–65, <http://dx.doi.org/10.2118/737-g>.
- [5] S. Reid, The flow of three immiscible fluids in porous media, Ph.D. thesis, University of Birmingham, 1956.
- [6] M. Oak, Three-phase relative permeability of water-wet berea, in: SPE/DOE Enhanced Oil Recovery Symposium, Society of Petroleum Engineers, 1990, <http://dx.doi.org/10.2118/20183-ms>.
- [7] M. Oak, L. Baker, D. Thomas, Three-phase relative permeability of berea sandstone, J. Pet. Technol. 42 (08) (1990) 1054–1061, <http://dx.doi.org/10.2118/17370-pa>.
- [8] L. Moghadasi, A. Guadagnini, F. Inzoli, M. Bartosek, D. Renna, Characterization of two- and three-phase relative permeability of water-wet porous media through X-Ray saturation measurements, J. Pet. Sci. Eng. 145 (2016) 453–463, <http://dx.doi.org/10.1016/j.petrol.2016.05.031>.

- [9] R.N. Moghaddam, M. Jamiolahmady, Steady-state relative permeability measurements of tight and shale rocks considering capillary end effect, *Transp. Porous Media* 128 (1) (2019) 75–96, <http://dx.doi.org/10.1007/s11242-019-01236-8>.
- [10] H.J. Welge, A simplified method for computing oil recovery by gas or water drive, *J. Pet. Technol.* 4 (04) (1952) 91–98, <http://dx.doi.org/10.2118/124-g>.
- [11] E. Johnson, D. Bossler, V.N. Bossler, Calculation of relative permeability from displacement experiments, *Petrol. Trans. AIME SPE-1023G* (1959).
- [12] A. Sarem, Three-phase relative permeability measurements by unsteady-state method, *Soc. Petrol. Eng. J.* 6 (03) (1966) 199–205, <http://dx.doi.org/10.2118/1225-pa>.
- [13] S. Jones, W. Roszelle, Graphical techniques for determining relative permeability from displacement experiments, *J. Pet. Technol.* 30 (05) (1978) 807–817, <http://dx.doi.org/10.2118/6045-pa>.
- [14] J.S. Kalbus, R.L. Christiansen, New data reduction developments for relative permeability determination, in: SPE Annual Technical Conference and Exhibition, Society of Petroleum Engineers, 1995, <http://dx.doi.org/10.2118/30799-ms>.
- [15] J. Toth, T. Bodi, P. Szucs, F. Civan, Convenient formulae for determination of relative permeability from unsteady-state fluid displacements in core plugs, *J. Pet. Sci. Eng.* 36 (1–2) (2002) 33–44, [http://dx.doi.org/10.1016/S0920-4105\(02\)00249-8](http://dx.doi.org/10.1016/S0920-4105(02)00249-8).
- [16] A. Grader, D. O'Meara, Dynamic displacement measurements of three-phase relative permeabilities using three immiscible liquids, in: SPE Annual Technical Conference and Exhibition, Society of Petroleum Engineers, 1988, <http://dx.doi.org/10.2118/18293-ms>.
- [17] S. Siddiqui, P. Hicks, A. Grader, Verification of Buckley-Leverett three-phase theory using computerized tomography, *J. Pet. Sci. Eng.* 15 (1) (1996) 1–21, [http://dx.doi.org/10.1016/0920-4105\(95\)00056-9](http://dx.doi.org/10.1016/0920-4105(95)00056-9).
- [18] R. Barroeta, L.G. Thompson, Estimation of relative permeability from displacement pressure data, in: SPE/DOE Symposium on Improved Oil Recovery, Society of Petroleum Engineers, 2006, <http://dx.doi.org/10.2118/99734-ms>.
- [19] P. Cao, S. Siddiqui, Three-phase unsteady-state relative permeability measurements in consolidated cores using three immiscible liquids, in: SPE Annual Technical Conference and Exhibition, Society of Petroleum Engineers, 2011, <http://dx.doi.org/10.2118/145808-ms>.
- [20] P. Kerig, A. Watson, Relative-permeability estimation from displacement experiments: An error analysis, *SPE Reserv. Eng.* 1 (02) (1986) 175–182, <http://dx.doi.org/10.2118/12589-pa>.
- [21] A. Watson, P. Richmond, P. Kerig, T. Tao, A regression-based method for estimating relative permeabilities from displacement experiments, *SPE Reserv. Eng.* 3 (03) (1988) 953–958, <http://dx.doi.org/10.2118/15064-pa>.
- [22] G.M. Mejia, A.T. Watson, J.E. Nordtvedt, Estimation of three-phase flow functions in porous media, *AICHE J.* 42 (7) (1996) 1957–1967, <http://dx.doi.org/10.1002/aic.690420716>.
- [23] N. Tokuda, S. Takahashi, M. Watanabe, T. Kurose, Application of genetic algorithm to history matching for core flooding, in: SPE Asia Pacific Oil and Gas Conference and Exhibition, Society of Petroleum Engineers, 2004, <http://dx.doi.org/10.2118/88621-ms>.
- [24] X. Sun, K.K. Mohanty, Estimation of flow functions during drainage using genetic algorithm, *SPE J.* 10 (04) (2005) 449–457, <http://dx.doi.org/10.2118/84548-pa>.
- [25] J. Wang, J.S. Buckley, Automatic history matching using differential evolution algorithm, in: International Symposium of the Society of Core Analysis, Trondheim, Norway, Society of Petroleum Engineers, 2006.
- [26] F. Le-Hussain, Y. Cinar, P.G. Bedrikovetsky, Comparison of methods for drainage relative permeability estimation from displacement tests, in: SPE Improved Oil Recovery Symposium, Society of Petroleum Engineers, 2010, <http://dx.doi.org/10.2118/129678-ms>.
- [27] H. Shahverdi, M. Sohrabi, M. Fatemi, M. Jamiolahmady, Three-phase relative permeability and hysteresis effect during WAG process in mixed wet and low IFT systems, *J. Pet. Sci. Eng.* 78 (3–4) (2011) 732–739, <http://dx.doi.org/10.1016/j.petrol.2011.08.010>.
- [28] M. Akhlaghinia, F. Torabi, C.W. Chan, Experimental investigation of temperature effect on three-phase relative permeability isoperms in heavy oil systems, *Fuel* 118 (2014) 281–290, <http://dx.doi.org/10.1016/j.fuel.2013.10.049>.
- [29] P. Mahzari, U. Taura, A. Cooke, M. Sohrabi, An improved approach to estimate three-phase relative permeability functions for heavy-oil displacement involving instability and compositional effects, *Energies* 10 (12) (2017) 2008, <http://dx.doi.org/10.3390/en10122008>.
- [30] P.L. Coyne, M.I. Omar, 20 years of laboratory oil-water relative permeability data in the Malay basin, in: SPE Asia Pacific Oil and Gas Conference and Exhibition, Society of Petroleum Engineers, 2000, <http://dx.doi.org/10.2118/64375-ms>.
- [31] P. Mahzari, A. AlMesmari, M. Sohrabi, Co-history matching: A way forward for estimating representative saturation functions, *Transp. Porous Media* 125 (3) (2018) 483–501, <http://dx.doi.org/10.1007/s11242-018-1129-8>.
- [32] F. Lomeland, B. Hasanov, E. Ebeltoft, M. Berge, A versatile representation of upscaled relative permeability for field applications, in: SPE Europe/EAGE Annual Conference, Society of Petroleum Engineers, 2012, <http://dx.doi.org/10.2118/154487-ms>.
- [33] Y. Zhang, Z. Fan, D. Yang, H. Li, S. Patil, Simultaneous estimation of relative permeability and capillary pressure for PUNQ-S3 model with a damped iterative-ensemble-Kalman-filter technique, *SPE J.* 22 (03) (2017) 971–984, <http://dx.doi.org/10.2118/177846-pa>.
- [34] M. Adibifard, M. Talebkeikhah, M. Sharifi, A. Hemmati-Sarapardeh, Iterative ensemble Kalman filter and genetic algorithm for automatic reconstruction of relative permeability curves in the subsurface multi-phase flow, *J. Pet. Sci. Eng.* 192 (2020) 107264, <http://dx.doi.org/10.1016/j.petrol.2020.107264>.
- [35] A.R. Valdez, B.M. Rocha, G. Chapiro, R.W. dos Santos, Uncertainty quantification and sensitivity analysis for relative permeability models of two-phase flow in porous media, *J. Pet. Sci. Eng.* 192 (2020) 107297, <http://dx.doi.org/10.1016/j.petrol.2020.107297>.
- [36] S. Buckley, M. Leverett, Mechanism of fluid displacement in sands, *Trans. AIME* 146 (01) (1942) 107–116, <http://dx.doi.org/10.2118/942107-g>.
- [37] J. Sheldon, W. Cardwell, One-dimensional, incompressible, noncapillary, two-phase fluid flow in a porous medium, *Trans. AIME* 216 (01) (1959) 290–296, <http://dx.doi.org/10.2118/978-g>.
- [38] F. Fayers, J. Sheldon, The effect of capillary pressure and gravity on two-phase fluid flow in a porous medium, *Trans. AIME* 216 (01) (1959) 147–155, <http://dx.doi.org/10.2118/1089-g>.
- [39] R. Johns, B. Dindoruk, F. Orr, Analytical theory of combined condensing/vaporizing gas drives, *SPE Adv. Technol. Ser.* 1 (02) (1993) 7–16, <http://dx.doi.org/10.2118/24112-pa>.
- [40] R. Johns, F. Orr, Miscible gas displacement of multicomponent oils, *SPE J.* 1 (01) (1996) 39–50, <http://dx.doi.org/10.2118/30798-pa>.
- [41] P. Bedrikovetsky, A. Shapiro, A. Pires, New analytical solutions for 1-D multi-component gas injection problems, in: Abu Dhabi International Conference and Exhibition, Society of Petroleum Engineers, 2004, <http://dx.doi.org/10.2118/88760-ms>.
- [42] A.P. Pires, P.G. Bedrikovetsky, A.A. Shapiro, A splitting technique for analytical modelling of two-phase multicomponent flow in porous media, *J. Pet. Sci. Eng.* 51 (1–2) (2006) 54–67, <http://dx.doi.org/10.1016/j.petrol.2005.11.009>.
- [43] R.E. Guzmán, F.J. Fayers, Mathematical properties of three-phase flow equations, *SPE J.* 2 (03) (1997) 291–300, <http://dx.doi.org/10.2118/35154-pa>.
- [44] E.L. Isaacson, D. Marchesin, B.J. Plohr, J.B. Temple, Multiphase flow models with singular Riemann problems, *Mat. Apl. Comput.* 11 (2) (1992) 147–166.
- [45] R.E. Guzmán, F.J. Fayers, Solutions to the three-phase Buckley-Leverett problem, *SPE J.* 2 (03) (1997) 301–311, <http://dx.doi.org/10.2118/35156-pa>.
- [46] D. Marchesin, B.J. Plohr, Wave structure in WAG recovery, *SPE J.* 6 (02) (2001) 209–219, <http://dx.doi.org/10.2118/71314-pa>.
- [47] A.V. Azevedo, A.J. de Souza, F. Furtado, D. Marchesin, B. Plohr, The solution by the wave curve method of three-phase flow in virgin reservoirs, *Transp. Porous Media* 83 (1) (2009) 99–125, <http://dx.doi.org/10.1007/s11242-009-9508-9>.
- [48] A.V. Azevedo, A.J. de Souza, F. Furtado, D. Marchesin, Uniqueness of the Riemann solution for three-phase flow in a porous medium, *SIAM J. Appl. Math.* 74 (6) (2014) 1967–1997, <http://dx.doi.org/10.1137/140954623>.
- [49] P. Castañeda, E. Abreu, F. Furtado, D. Marchesin, On a universal structure for immiscible three-phase flow in virgin reservoirs, *Comput. Geosci.* 20 (1) (2016) 171–185, <http://dx.doi.org/10.1007/s10596-016-9556-5>.
- [50] M. Shearer, J.A. Trangenstein, Loss of real characteristics for models of three-phase flow in a porous medium, *Transp. Porous Media* 4 (5) (1989) <http://dx.doi.org/10.1007/bf00179533>.
- [51] M.D. Jackson, M.J. Blunt, Elliptic regions and stable solutions for three-phase flow in porous media, *Transp. Porous Media* 48 (3) (2002) 249–269, <http://dx.doi.org/10.1023/a:1015726412625>.
- [52] E.L. Isaacson, D. Marchesin, B.J. Plohr, Transitional waves for conservation laws, *SIAM J. Math. Anal.* 21 (4) (1990) 837–866, <http://dx.doi.org/10.1137/0521047>.
- [53] D. Marchesin, A.A. Mailybaev, Dual-family viscous shock waves in n conservation laws with application to multi-phase flow in porous media, *Arch. Ration. Mech. Anal.* 182 (1) (2006) 1–24, <http://dx.doi.org/10.1007/s00205-005-0419-9>.
- [54] A. Mikelić, L. Paoli, On the derivation of the Buckley-Leverett model from the two fluid Navier-Stokes equations in a thin domain, *Comput. Geosci.* 1 (1) (1997) 59–83, <http://dx.doi.org/10.1023/a:1011509010432>.
- [55] K.R. Rajagopal, On a hierarchy of approximate models for flows of incompressible fluids through porous solids, *Math. Models Methods Appl. Sci.* 17 (02) (2007) 215–252, <http://dx.doi.org/10.1142/S0218202507001899>.
- [56] V. Savatorova, K. Rajagopal, Homogenization of a generalization of Brinkman's equation for the flow of a fluid with pressure dependent viscosity through a rigid porous solid, *ZAMM. J. Appl. Math. Mech./Z. Angew. Math. Mech.* 91 (8) (2011) 630–648, <http://dx.doi.org/10.1002/zamm.201000141>.
- [57] L. Fusi, A. Farina, G. Saccomandi, Buckley-leverett equation with viscosities and relative permeabilities depending on pressure, *SIAM J. Appl. Math.* 75 (5) (2015) 1983–2000, <http://dx.doi.org/10.1137/15100566x>.
- [58] L. Fusi, A. Farina, F. Rosso, Mathematical models for fluids with pressure-dependent viscosity flowing in porous media, *Internat. J. Engrg. Sci.* 87 (2015) 110–118, <http://dx.doi.org/10.1016/j.ijengsci.2014.11.007>.
- [59] S. Srinivasan, A. Bonito, K. Rajagopal, Flow of a fluid through a porous solid due to high pressure gradients, *J. Porous Media* 16 (3) (2013) 193–203, <http://dx.doi.org/10.1615/jpormedia.v16.i3.20>.
- [60] S. Srinivasan, K. Rajagopal, On the flow of fluids through inhomogeneous porous media due to high pressure gradients, *Int. J. Non-Linear Mech.* 78 (2016) 112–120, <http://dx.doi.org/10.1016/j.ijnonlinmec.2015.09.003>.

- [61] P.L. Andrade, A.J. de Souza, F. Furtado, D. Marchesin, Oil displacement by water and gas in a porous medium: the Riemann problem, *Bull. Braz. Math. Soc. (N.S.)* 47 (1) (2016) 77–90, <http://dx.doi.org/10.1007/s00574-016-0123-4>.
- [62] P. Andrade, A. de Souza, F. Furtado, D. Marchesin, Three-phase fluid displacements in a porous medium, *J. Hyperbolic Differ. Equ.* 15 (04) (2018) 731–753, <http://dx.doi.org/10.1142/s0219891618500236>.
- [63] L.F.L. Guerrero, D. Marchesin, Diffusive Riemann solutions for 3-phase flow in porous media, in: *Brazilian Society of Computational and Applied Mathematics*, 7, SBMAC, 2020, <http://dx.doi.org/10.5540/03.2020.007.01.0372>.
- [64] J.B. Bell, J.A. Trangenstein, G.R. Shubin, Conservation laws of mixed type describing three-phase flow in porous media, *SIAM J. Appl. Math.* 46 (6) (1986) 1000–1017, <http://dx.doi.org/10.1137/0146059>.
- [65] L. Holden, On the strict hyperbolicity of the buckley–leverett equations for three-phase flow in a porous medium, *SIAM J. Appl. Math.* 50 (3) (1990) 667–682, <http://dx.doi.org/10.1137/0150039>.
- [66] P.D. Lax, Hyperbolic systems of conservation laws II, *Comm. Pure Appl. Math.* 10 (4) (1957) 537–566, <http://dx.doi.org/10.1002/cpa.3160100406>.
- [67] T.-P. Liu, The Riemann problem for general 2x2 conservation laws, *Trans. Amer. Math. Soc.* 199 (1974) 89, <http://dx.doi.org/10.2307/1996875>.
- [68] T.-P. Liu, The Riemann problem for general systems of conservation laws, *J. Differential Equations* 18 (1) (1975) 218–234, [http://dx.doi.org/10.1016/0022-0396\(75\)90091-1](http://dx.doi.org/10.1016/0022-0396(75)90091-1).
- [69] L. Tai-Ping, *Hyperbolic and Viscous Conservation Laws*, CBMS-NSF Regional Conference Series in Applied Mathematics, Siam, 2007.
- [70] R. LeVeque, L. J. D. Crighton, *Finite Volume Methods for Hyperbolic Problems*, Cambridge Texts in Applied Mathematics, Cambridge University Press, 2002.
- [71] B. Wendroff, The Riemann problem for material with nonconvex equations of state I: Isentropic flow, *J. Math. Anal. Appl.* 38 (1972) 454–466.
- [72] B. Wendroff, The Riemann problem for material with nonconvex equations of state II: General flow, *J. Math. Anal. Appl.* 38 (1972) 640–658.

**3    *Book Chapter: Approximate  
Solution for One-Dimensional  
Compressible Two-Phase  
Immiscible Flow in Porous Media  
for Variable Boundary  
Conditions***

# Chapter 1

## Approximate Solution for One-Dimensional Compressible Two-Phase Immiscible Flow in Porous Media for Variable Boundary Conditions



W. Q. Barros, A. P. Pires, and Á. M. M. Peres

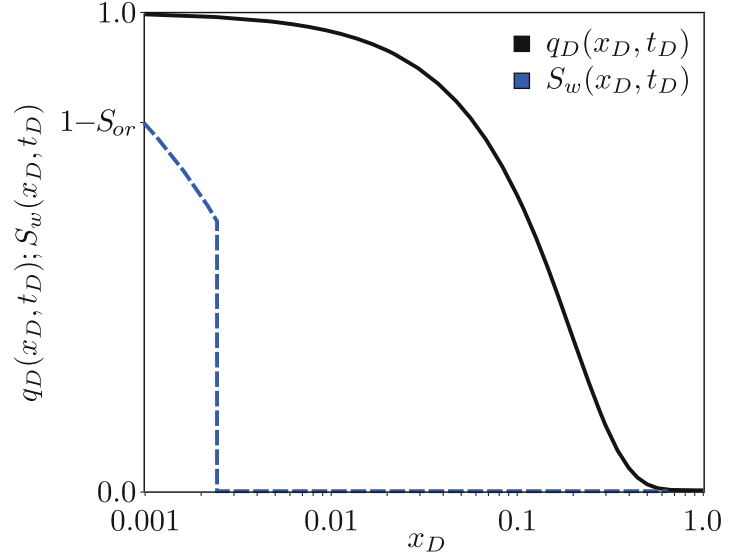
### 1.1 Introduction

In most petroleum reservoirs, there are at least two phases: oil and connate water. Usually, water is also injected to increase oil production and keep the reservoir pressure at some desired level. Oil displacement by injected water can be modeled by a system of two partial differential equations representing the mass conservation of each component and Darcy's law replacing momentum balance. For one-dimensional incompressible systems without mass transfer, the problem can be solved by the method of characteristics [BL42]. If the relative permeability curves are convex, the solution is given by a continuous two-phase saturation zone (rarefaction wave) followed by a discontinuity (shock). This solution was further expanded to include gravitational and capillary effects [SC59, FS59], to evaluate the pressure drop along porous medium [W52, JBN59], and for three-phase flow [IMPT92, GF97, AS09, CAFM16]. Analytical solutions for compressible two-phase problems are more difficult to develop because both pressure and saturation fields must be solved simultaneously. Approximate solutions were obtained for a two-zone system with constant saturation in each zone [HRM58, KMJ72]. Splitting the two-phase region in more segments improves the accuracy of the solution. The water saturation in each zone of this multi-region system is constant, and thus the velocity of water saturation front in the pressure solution can be neglected and a quasi-static approach can be used [AK89]. The authors of [BH90] proposed a different approximate solution superposing pressure transient effects on a previous saturation profile obtained by Buckley–Leverett solution. The authors of [TR97] generalized the theory for multiphase flow in a heterogeneous reservoir. In this approach, the

---

W. Q. Barros · A. P. Pires (✉) · Á. M. M. Peres  
Universidade Estadual do Norte Fluminense, Macaé, RJ, Brazil  
e-mail: [adolfo.puime@gmail.com](mailto:adolfo.puime@gmail.com); [alvaroperes@lenep.uenf.br](mailto:alvaroperes@lenep.uenf.br)

**Fig. 1.1** Typical water saturation and dimensionless flow rate profiles for constant injection rate for a fixed time



pressure and saturation zones move with different velocities, in which the saturation front is always within a steady-state flow-rate zone (Fig. 1.1). It is a simplified method to calculate the pressure profile for the problem of constant fluid injection, in which the saturation is obtained by the immiscible Buckley–Leverett problem and the flow rate by the single-phase compressible solution. The pressure solution is calculated integrating Darcy’s equation [BTR98, PR03, PBR04, PBR06].

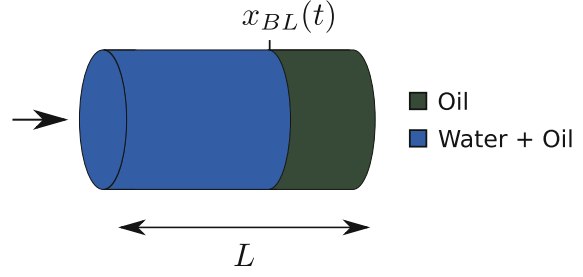
For constant boundary conditions, the Thompson–Reynolds conjecture provides good results when compared to numerical experiments. However, for non-constant boundary conditions, a new pressure perturbation along the reservoir appears and the conjecture cannot be applied. In this work, we present a new procedure to generalize the solution for non-constant boundary conditions. In Sect. 1.2, we derive the mathematical formulation and present an approximate solution. Next, we compare the solution with numerical results under different injection schedules and system compressibility (1.3). Finally, some conclusions are addressed (1.4).

## 1.2 Mathematical Model

In this work, it is considered a one-dimensional oil displacement by water in a homogeneous porous medium (Fig. 1.2). Additional hypothesis are:

- Immiscible and isothermal linear flow
- Constant cross-sectional area
- Negligible dispersion, gravitational and capillary effects
- Constant viscosity phases
- Constant phases and rock compressibility
- Darcy’s law is valid

**Fig. 1.2** Representation of 1D water flooding



The velocity of each phase can be calculated using Darcy's law,

$$v_{\pi} = -\frac{K k_{r\pi}}{\mu_{\pi}} \frac{\partial P}{\partial x}, \quad (1.1)$$

where  $K$  and  $k_{r\pi}$  are the absolute and phase relative permeabilities,  $\mu_{\pi}$  the phase viscosity, and  $\frac{\partial P}{\partial x}$  the linear pressure gradient; the subscript  $\pi$  denotes water  $w$  or oil  $o$  phase. Summing up the velocity for all phases and neglecting capillary effects, one gets

$$q_T(x, t) = -AK\lambda_T(x, t) \frac{\partial P(x, t)}{\partial x}, \quad (1.2)$$

where  $A$  is the cross-sectional area,  $q_T$  represents the total volumetric flow rate, and  $\lambda_T$  is the total mobility of the phases ( $\lambda_T = \frac{k_{rw}}{\mu_w} + \frac{k_{ro}}{\mu_o}$ ).

To determine the pressure profile along the porous medium length, we integrate Eq. 1.2 using a constant pressure external boundary condition

$$P(x = L, t) = P_i,$$

in which  $P_i$  denotes the initial pressure and  $L$  is the core length, resulting in

$$P(x, t) - P_i = \frac{1}{AK} \int_x^L \frac{q_T(x', t)}{\lambda_T(x', t)} dx'.$$

Now, we introduce dimensionless time and space coordinates,

$$x_D = \frac{x}{L}, \quad (1.3)$$

$$t_D = \frac{q_{ref} t}{(1 - S_{wi} - S_{or}) AL\phi}, \quad (1.4)$$

where  $q_{ref}$  is a reference flow rate, adopted as the first injection value, and  $\phi$  is the rock porosity. The irreducible water saturation and residual oil saturation are

denoted by  $S_{wi}$  and  $S_{or}$ , respectively. Thus, the pressure drop can be written in dimensionless variables as

$$P_D(x_D, t_D) = \int_{x_D}^1 \frac{q_D(x'_D, t_D)}{\lambda_{TD}(x'_D, t_D)} dx'_D, \quad (1.5)$$

where

$$P_D(x_D, t_D) = \frac{KA\hat{\lambda}_o}{q_{ref}L} (P(x, t) - P_i), \quad (1.6)$$

$$\lambda_{TD}(x_D, t_D) = \frac{\lambda_T(x, t)}{\hat{\lambda}_o}, \quad (1.7)$$

$$q_D(x_D, t_D) = \frac{q_T(x, t)}{q_{ref}}, \quad (1.8)$$

in which  $\hat{\lambda}_o$  is oil mobility at water irreducible saturation. Equation 1.5 relates the flow rate and mobility profiles to the pressure drop change at a given position  $x_D$ . In this work, we solve this problem for the case of step-change internal boundary condition. Thus, an approximation can be obtained based on two key hypotheses:

1. The mobility profile can be obtained by the incompressible problem solution.
2. The total flow rate can be calculated considering two regions with fixed interface position for compressible flow.

The total flow rate is obtained from a linear partial differential equation. Thus, Eq. 1.5 applied for the internal boundary condition  $P_D(x_D = 0, t_D) = P_{wD}(t_D)$  is written as

$$P_{wD}(t_D) = \int_0^1 \frac{q_D(x'_D, t_D)}{\lambda_{TD}(x'_D, t_D)} dx'_D, \quad (1.9)$$

where

$$q_D(x_D, t_D) = \sum_{j=1}^{Nsteps} \left[ q_{D_j}^{Inj} - q_{D_{j-1}}^{Inj} \right] q_{DC}(x_D, t_D - t_{D_{j-1}}).$$

The last equation is the flow-rate superposition, in which  $Nsteps$  is the number of flow-rate steps until  $t_D$ ,  $q_{D_j}^{Inj}$  is the injection flow rate in step  $j$ , and  $t_{D_j}$  is the time when  $q_{D_j}^{Inj}$  started. The terms inside parenthesis are the  $(x_D, t_D)$  coordinates where  $q_{DC}$  and  $\lambda_{TD}$  are evaluated. The function  $q_{DC}$  is the mathematical solution for the two-region problem under constant injection rate.

### 1.2.1 Approximation for $\lambda_{TD}(x_D, t_D)$

The mass conservation for simultaneous flow of oil and water in a linear porous media is modeled by the equations

$$\frac{\partial (\phi S_\pi \rho_\pi)}{\partial t} + \frac{\partial (\rho_\pi v_\pi)}{\partial x} = 0, \quad \pi = w, o, \quad (1.10)$$

where  $\rho_\pi$  is the phase density. Considering an incompressible system, we find

$$\frac{\partial S_\pi}{\partial t} + \frac{1}{\phi} \frac{\partial v_\pi}{\partial x} = 0, \quad \pi = w, o.$$

Defining the normalized water saturation as

$$S_{nw} = \frac{S_w - S_{wi}}{1 - S_{wi} - S_{or}}, \quad S_w \in [S_{wi}, 1 - S_{or}]$$

and applying the definitions of dimensionless variables (Eqs. 1.3, 1.4, and 1.8) together with Darcy's law (Eq. 1.1), we find [BL42]

$$\frac{\partial S_{nw}}{\partial t_D} + q_D(x_D = 0, t_D) \frac{\partial f_w}{\partial x_D} = 0,$$

in which  $f_w$  defines the water fractional flow

$$f_w = \frac{\frac{k_{rw}}{\mu_w}}{\frac{k_{rw}}{\mu_w} + \frac{k_{ro}}{\mu_o}}.$$

For convex relative permeability curves, the derivative  $\frac{df_w}{dS_{nw}}$  is not monotonic and the solution is not unique. To determine the most admissible solution, we apply the Lax [L57] and Oleinik [O57] stability criteria, and the solution is composed of a rarefaction wave followed by a shock. The shock must be a zero-diffusion limit of the solution given by traveling waves [L07]. The solution is given by

$$S_{nw} = \begin{cases} \frac{df_w}{dS_{nw}}^{-1} \left( \frac{1}{q_D(x_D=0, t_D)} \frac{x_D}{t_D} \right), & x_D \in (0, x_D^{BL}), \\ 0, & x_D \in (x_D^{BL}, 1), \end{cases} \quad (1.11)$$

where  $\left( \frac{1}{q_D(x_D=0, t_D)} \frac{x_D}{t_D} \right)$  is the self-similar variable where the inverse of  $\frac{df_w}{dS_{nw}}$  is evaluated. The shock position is denoted by  $x_D^{BL}$  (Fig. 1.2) and is calculated solving the Rankine–Hugoniot ODE condition.

$$\frac{dx_D^{BL}}{dt_D} = q_D(x_D = 0, t_D) \frac{f_w^{BL}}{S_{nw}^{BL}}.$$

### 1.2.2 Approximation for $q_{DC}(x_D, t_D)$

Applying Darcy's law (Eq. 1.1) in the mass conservation (Eq. 1.10), we find

$$S_\pi \left( \phi \frac{\partial \rho_\pi}{\partial P} + \rho_\pi \frac{\partial \phi}{\partial P} \right) \frac{\partial P}{\partial t} + (\phi \rho_\pi) \frac{\partial S_\pi}{\partial t} - \left( \rho_\pi \frac{\partial \left( \frac{K k_{r\pi}}{\mu_\pi} \frac{\partial P}{\partial x} \right)}{\partial x} + \frac{K k_{r\pi}}{\mu_\pi} \frac{\partial \rho_\pi}{\partial P} \left( \frac{\partial P}{\partial x} \right)^2 \right) = 0, \quad \pi = w, o \quad (1.12)$$

Using the rock and fluid compressibility definitions ( $c_\phi = \frac{1}{\phi} \frac{\partial \phi}{\partial P}$  and  $c_\pi = \frac{1}{\rho_\pi} \frac{\partial \rho_\pi}{\partial P}$ ) and summing for both phases, it is possible to derive

$$\frac{\partial \left( \lambda_T \frac{\partial P}{\partial x} \right)}{\partial x} + (c_w \lambda_w + c_o \lambda_o) \left( \frac{\partial P}{\partial x} \right)^2 = \frac{\phi c_t}{K} \frac{\partial P}{\partial t},$$

where  $c_t$  is the total compressibility, given by

$$c_t(x, t) = c_\phi + c_o(1 - S_w(x, t)) + c_w S_w(x, t).$$

For small pressure gradients and slightly compressible fluids, the quadratic term can be neglected. Thus, applying the dimensionless definitions (Eqs. 1.3, 1.4, and 1.5), we find the dimensionless PDE for the pressure in a compressible two-phase system,

$$\frac{1}{\lambda_{TD}} \frac{\partial \left( \lambda_{TD} \left( \frac{\partial P_D}{\partial x_D} \right) \right)}{\partial x_D} = \gamma_L \frac{\partial P_D}{\partial t_D},$$

where the term  $\gamma_L$  is given by

$$\gamma_L(x_D, t_D) = \frac{q_{ref} L}{(1 - S_{wi} - S_{or}) K A \lambda_T} c_t.$$

The terms  $\gamma_L$  and  $\lambda_{TD}$  depend on the saturation profile. To solve this equation, the domain is divided into two regions based on the shock position, and the saturation profile is considered constant in both zones

$$\begin{cases} \frac{\partial^2 P'_D}{\partial x_D^2} = \gamma_L^{IN} \frac{\partial P'_D}{\partial t_D}, & x_D \in (0, x_D^{BL}), \\ \frac{\partial^2 P'_D}{\partial x_D^2} = \hat{\gamma}_L \frac{\partial P'_D}{\partial t_D}, & x_D \in (x_D^{BL}, 1), \end{cases}$$

where  $\gamma_L^{IN}$  is the average gamma in the region behind the shock, and  $\hat{\gamma}_L$  is the gamma in the original oil condition. Note that  $P'$  indicates the pressure for the two-zone problem. The internal boundary condition (I.B.C.) in dimensionless variables is given by

$$\lim_{x_D \rightarrow 0} \left( \frac{\partial P'_D}{\partial x_D} \right) = -\frac{1}{\lambda_{TD}^{IN}} \text{ (I.B.C.)} .$$

The initial condition (I.C.) and external boundary condition (E.B.C.) are

$$P'_D(x_D = 1, t_D) = 0 \text{ (E.B.C.)} ,$$

$$P'_D(x_D, t_D = 0) = 0 \text{ (I.C.)} .$$

Thus, the equations that model the pressure in the inner zone are given by

$$\begin{cases} \frac{\partial^2 P'_D}{\partial x_D^2} = \gamma_L^{IN} \frac{\partial P'_D}{\partial t_D}, & x_D \in (0, x_D^{BL}) , \\ P'_D(x_D, t_D = 0) = 0 & \text{(I.C.)} , \\ \lim_{x_D \rightarrow 0} \left( \frac{\partial P'_D}{\partial x_D} \right) = -\frac{1}{\lambda_{TD}^{IN}} & \text{(I.B.C.)} . \end{cases}$$

The equations for the outer region are

$$\begin{cases} \frac{\partial^2 P'_D}{\partial x_D^2} = \hat{\gamma}_L \frac{\partial P'_D}{\partial t_D}, & x_D \in (x_D^{BL}, 1) , \\ P'_D(x_D, t_D = 0) = 0 & \text{(I.C.)} , \\ P'_D(x_D = 1, t_D) = 0 & \text{(E.B.C.)} . \end{cases}$$

The continuity of pressure and total flow rate at the interface of the two regions are used to close the problem.

$$\begin{aligned} \lim_{x_D \rightarrow x_D^{BL-}} P'_D(x_D, t_D) &= \lim_{x_D \rightarrow x_D^{BL+}} P'_D(x_D, t_D) \\ \left( \lambda_{TD}^{IN} \frac{\partial P_D(x_D, t_D)}{\partial x_D} \right)_{x_D^{BL-}} &= \left( \frac{\partial P_D(x_D, t_D)}{\partial x_D} \right)_{x_D^{BL+}} . \end{aligned}$$

The shock position  $x_D^{BL} = x_D^{BL}(t_D)$  characterizes a moving internal condition. However, as the speed of this boundary is small, we may use a quasi-stationary assumption, in which the effect of a moving interface is neglected in the solution. However, the interface position is updated every time  $t_D$  in order to evaluate the dimensionless pressure  $P_D(x_D, t_D)$ .

### 1.2.2.1 Solution by the Laplace Transform

The quasi-stationary hypothesis allows one to solve the two-region problem by the Laplace transform. Applying the transform in the PDE and in both boundary conditions and using the initial condition, the system can be written for the inner zone as

$$\begin{cases} \frac{\partial^2 \bar{P}'_D}{\partial x_D^2} = \gamma_L^{IN} u \bar{P}'_D, & x_D \in (0, x_D^{BL}) , \\ \lim_{x_D \rightarrow 0} \left( \frac{\partial \bar{P}'_D}{\partial x_D} \right) = -\frac{1}{u \lambda_{TD}^{IN}} \quad \text{(I.B.C.)} \end{cases}$$

and for the outer zone as

$$\begin{cases} \frac{\partial^2 \bar{P}'_D}{\partial x_D^2} = \hat{\gamma}_L u \bar{P}'_D, & x_D \in (x_D^{BL}, 1) , \\ \bar{P}'_D(x_D = x_{Ds}, u) = 0 \quad \text{(E.B.C.)} . \end{cases}$$

The coupling condition in Laplace's domain is given by

$$\lim_{x_D \rightarrow x_D^{BL-}} \bar{P}'_D(x_D, u) = \lim_{x_D \rightarrow x_D^{BL+}} \bar{P}'_D(x_D, u) \\ \left( \lambda_{TD}^{IN} \frac{\partial \bar{P}'_D(x_D, u)}{\partial x_D} \right)_{x_D^{BL-}} = \left( \frac{\partial \bar{P}'_D(x_D, u)}{\partial x_D} \right)_{x_D^{BL+}} .$$

The general solution is

$$\begin{aligned} \bar{P}'_D(x_D, u) &= A_0 e^{\sqrt{\gamma_L^{IN}} u x_D} + A_1 e^{-\sqrt{\gamma_L^{IN}} u x_D}, \quad \text{for } x_D \in (0, x_D^{BL}) , \\ \bar{P}'_D(x_D, u) &= A_2 e^{\sqrt{\hat{\gamma}_L} u x_D} + A_3 e^{-\sqrt{\hat{\gamma}_L} u x_D}, \quad \text{for } x_D \in (x_D^{BL}, 1) . \end{aligned}$$

Applying the boundary and coupling conditions, it is possible to write the following system of equations:

$$\begin{pmatrix} 1 & -1 & 0 & 0 \\ 0 & 0 & e^{\hat{\alpha}_L x_{Ds}} & e^{-\hat{\alpha}_L x_{Ds}} \\ e^{\alpha_L^{IN} x_D^{BL}} & e^{-\alpha_L^{IN} x_D^{BL}} & -e^{\hat{\alpha}_L x_D^{BL}} & -e^{-\hat{\alpha}_L x_D^{BL}} \\ \lambda_{TD}^{IN} \alpha_L^{IN} e^{\alpha_L^{IN} x_D^{BL}} & -\lambda_{TD}^{IN} \alpha_L^{IN} e^{-\alpha_L^{IN} x_D^{BL}} & -\hat{\alpha}_o e^{\hat{\alpha}_L x_D^{BL}} & \hat{\alpha}_o e^{-\hat{\alpha}_L x_D^{BL}} \end{pmatrix} \begin{pmatrix} A_0 \\ A_1 \\ A_2 \\ A_3 \end{pmatrix} = \begin{pmatrix} -\frac{1}{\lambda_{TD}^{IN}} \frac{1}{u \alpha_L^{IN}} \\ 0 \\ 0 \\ 0 \end{pmatrix} ,$$

with  $\alpha_L^{IN} = \sqrt{\gamma_L^{IN} u}$  and  $\hat{\alpha}_L = \sqrt{\hat{\gamma}_L u}$ . The coefficients  $A_0$ ,  $A_1$ ,  $A_2$ , and  $A_3$  are calculated through

$$A_0 = \frac{1}{\lambda_{TD}^{IN} \alpha_L^{IN} u} \left( \frac{2\lambda_{TD}^{IN} \alpha_L^{IN} \left( e^{-\hat{\alpha}_L x_D^{BL}} - e^{\hat{\alpha}_L (x_D^{BL}-2)} \right) - e^{-\alpha_L^{IN} x_D^{BL}} \Omega_L}{2 \cosh(\alpha_L^{IN} x_D^{BL}) \Omega_L} \right),$$

$$A_1 = \frac{1}{\lambda_{TD}^{IN} \alpha_L^{IN} u} \left( \frac{e^{\alpha_L^{IN} x_D^{BL}} \Omega_L + 2\lambda_{TD}^{IN} \alpha_L^{IN} \left( e^{-\hat{\alpha}_L x_D^{BL}} - e^{\hat{\alpha}_L (x_D^{BL}-2)} \right)}{2 \cosh(\alpha_L^{IN} x_D^{BL}) \Omega_L} \right),$$

$$A_2 = -\frac{2e^{-2\hat{\alpha}_L}}{u \Omega_L},$$

$$A_3 = \frac{2}{u \Omega_L},$$

in which

$$\begin{aligned} \Omega_L = & \left( \hat{\alpha}_L + \lambda_{TD}^{IN} \alpha_L^{IN} \right) \left( e^{(\alpha_L^{IN} - \hat{\alpha}_L) x_D^{BL}} + e^{\hat{\alpha}_L (x_D^{BL}-2) - \alpha_L^{IN} x_D^{BL}} \right), \\ & + \left( \hat{\alpha}_L - \lambda_{TD}^{IN} \alpha_L^{IN} \right) \left( e^{-(\alpha_L^{IN} + \hat{\alpha}_L) x_D^{BL}} + e^{\hat{\alpha}_L (x_D^{BL}-2) + \alpha_L^{IN} x_D^{BL}} \right). \end{aligned}$$

The coefficients  $A_0$ ,  $A_1$ ,  $A_2$ , and  $A_3$  are time dependent because the interface position between the regions moves. Finally, we can apply Darcy's law (Eq. 1.2) in the two-zone pressure solution and obtain the approximated flow-rate profile

$$\bar{q}_{DC}(x_D, u) = \begin{cases} -\lambda_{TD}^{IN} \sqrt{\gamma_L^{IN} u} e^{\sqrt{\gamma_L^{IN} u} x_D} A_0 + \lambda_{TD}^{IN} \sqrt{\gamma_L^{IN} u} e^{-\sqrt{\gamma_L^{IN} u} x_D} A_1 & \text{for } x_D < x_D^{BL}, \\ -\sqrt{\hat{\gamma}_L u} e^{\sqrt{\hat{\gamma}_L u} x_D} A_2 + \sqrt{\hat{\gamma}_L u} e^{-\sqrt{\hat{\gamma}_L u} x_D} A_3 & \text{for } x_D > x_D^{BL}. \end{cases} \quad (1.13)$$

These equations are inverted to real space using Stehfest's algorithm [GS70]. When the water front position reaches the external core face, Eq. 1.13 for  $x_D < x_D^{BL}$  is still valid; however, the terms  $\gamma_L^{IN}$  and  $\lambda_{TD}^{IN}$  must be averaged inside the core domain ( $x_D \in (0, 1)$ ).

### 1.3 Model Validation

In this section, we apply the developed solution for a set of typical laboratory core flood experiment parameter sets (Table 1.1). The relative permeability curves were generated using the Corey model [C56],

$$\begin{cases} k_{rw} = k_{rw}^{S_{or}^w} (S_{nw})^{n_w} , \\ k_{ro} = k_{ro}^{S_{wi}^w} (S_{no})^{n_o} , \end{cases}$$

using properties shown in Table 1.2 and Fig. 1.3. The mobility ratio is given by  $M = \frac{\hat{\lambda}_w}{\hat{\lambda}_o}$ , where  $\hat{\lambda}_w$  and  $\hat{\lambda}_o$  denote the water mobility at residual oil saturation and the oil mobility at irreducible water saturation. For the data shown in Table 1.2, we have  $M = 1.875$ .

All solutions discussed in this section are compared to numerical results.

#### 1.3.1 Injection Schedule 1

The first case analyzed is an isochronal schedule composed of three increasing injection flow rates followed by a falloff (Table 1.3). To generate the approximate solution, the first step is solving the incompressible problem (Eq. 1.11) using the fractional flow shown in Fig. 1.3. Comparing the incompressible solution with the

**Table 1.1** Typical rock and fluid properties for core flood experiments

Core length	$L = 15$	[cm]
Cross-sectional area	$A = 11.4$	[cm <sup>2</sup> ]
Porosity	$\phi = 0.1$	[-]
Absolute permeability	$K = 200$	[mD]
Initial injection rate	$q_T^0 = 0.54$	[cm <sup>3</sup> /min]
Water viscosity	$\mu_w = 1.0$	[cp]
Oil viscosity	$\mu_o = 5.0$	[cp]
Rock compressibility	$c_r = 9.8E - 6$	[1/Kgf/cm <sup>2</sup> ]
Water compressibility	$c_w = 1.0E - 6$	[1/Kgf/cm <sup>2</sup> ]
Oil compressibility	$c_o = 4.0E - 5$	[1/Kgf/cm <sup>2</sup> ]

**Table 1.2** Relative permeability curves parameters

$S_{wi} = 0.20$
$k_{ro}^{S_{wi}^w} = 0.80$
$S_{or}^w = 0.20$
$k_{rw}^{S_{or}^w} = 0.30$
$n_w = 2.2$
$n_o^w = 2.0$

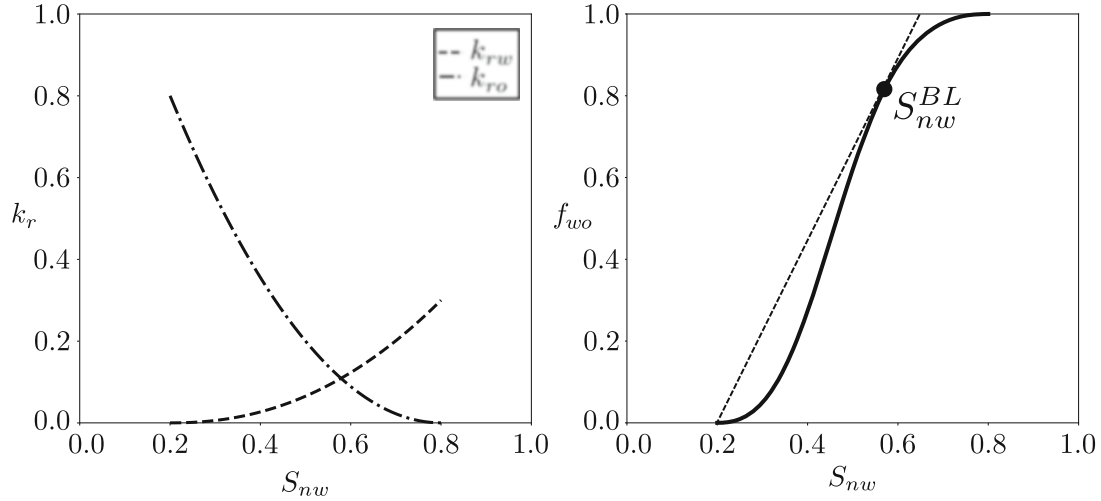


**Fig. 1.3** Relative permeability curves (left) and water fraction flow curve (right) for data shown in Tables 1.1 and 1.2

**Table 1.3** Injection schedule 1

$t_D$	$q_D^{INJ}$
0.00–0.05	1.0
0.05–0.10	2.0
0.10–0.15	3.0
0.15–0.20	0.0

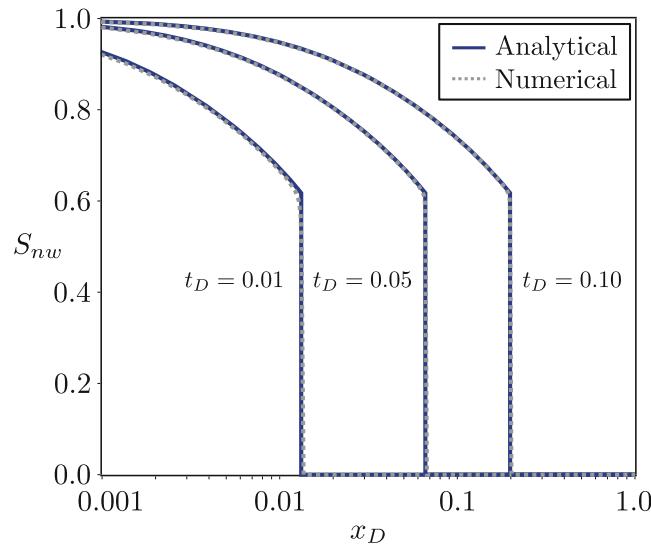


**Fig. 1.4** Analytical and numerical saturation profiles for schedule 1

numerical compressible solution (Fig. 1.4), it can be observed that the saturation profile matches for different injection times.

Once we have the saturation profile, we can solve Eq. 1.13 and obtain an approximate flow rate. In Fig. 1.5, three different  $\Delta t_D$  after the first flow-rate change ( $t_D = 0.05$ ) are compared. Note that the greatest difference between solutions

**Fig. 1.5** Analytical and numerical flow-rate profile for different  $\Delta t_D$  after  $t_D = 0.05$

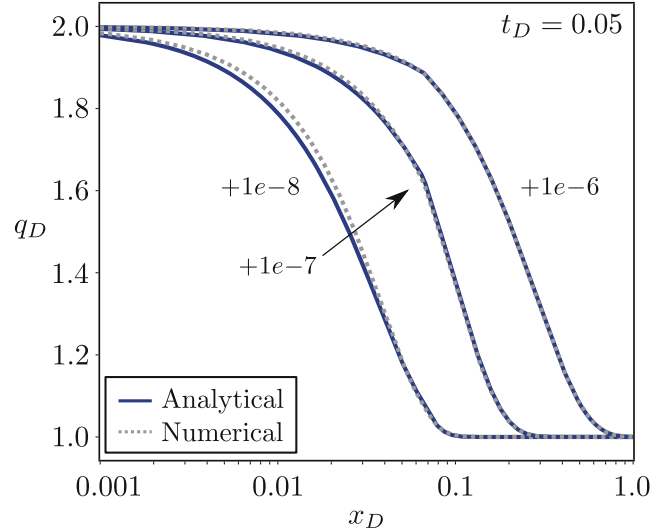
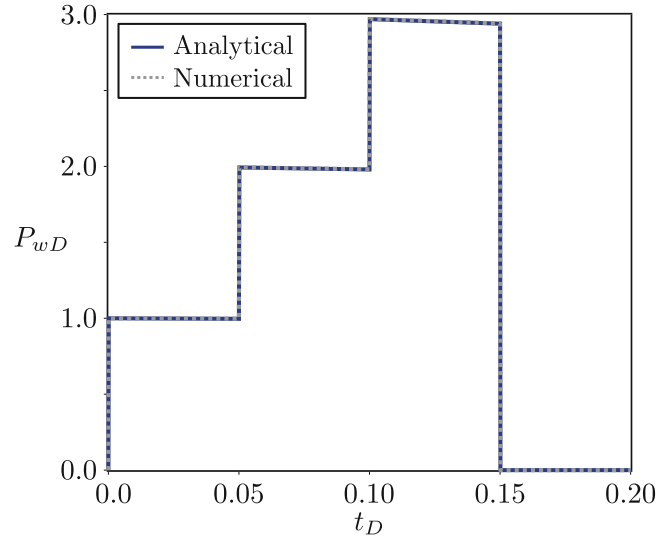


**Fig. 1.6** Analytical and numerical  $P_{wD}$  solution for schedule 1



appears at small times ( $\Delta t_D = 1e^{-8}$ ). After  $\Delta t_D = 1e^{-7}$ , the solutions present close agreement. Using the calculated  $\lambda_{TD}$  and  $q_D$ , it is possible to integrate Equation 1.9 and obtain the final solution (Fig. 1.6).

### 1.3.2 Injection Schedule 2

The second case changes the injection flow rate schedule (Table 1.4) using the same reservoir properties (Tables 1.1 and 1.2). Schedule 2 is composed of three isochronal decreasing flow rates, followed by a falloff. Figures 1.7 and 1.8 present the saturation and flow-rate profiles compared with the compressible numerical solutions. The presented profiles are calculated at three different  $\Delta t_D$  after the falloff

**Table 1.4** Injection schedule 2

$t_D$	$q_{Di}$
0.00–0.05	1.0
0.05–0.10	2/3
0.10–0.15	1/3
0.15–0.20	0.0

**Fig. 1.7** Analytical and numerical saturation profiles for different  $t_D$  for schedule 2

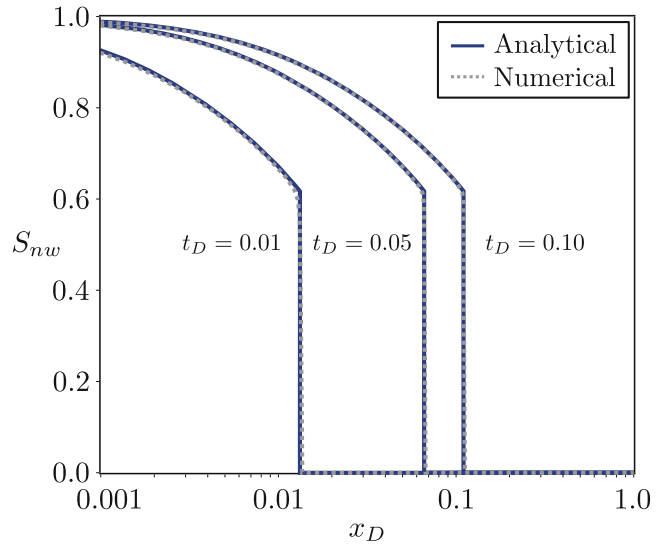
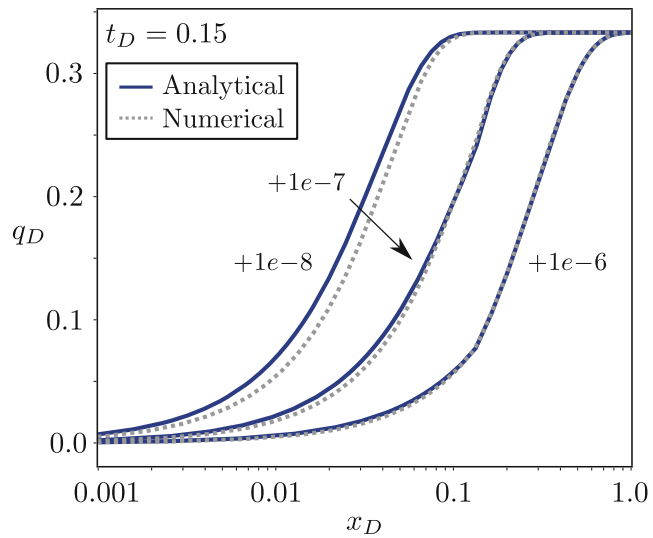


**Fig. 1.8** Analytical and numerical flow-rate profile for different  $\Delta t_D$  after  $t_D = 0.15$



( $t_D = 0.15$ ). It can be noted that both solutions agree and can be used to build the pressure solution of the original problem (Fig. 1.9). Note that our approximation of  $P_{wD}$  agrees with numerical simulation for all flow-rate steps.

**Fig. 1.9** Analytical and numerical  $P_{wD}$  solution for schedule 2

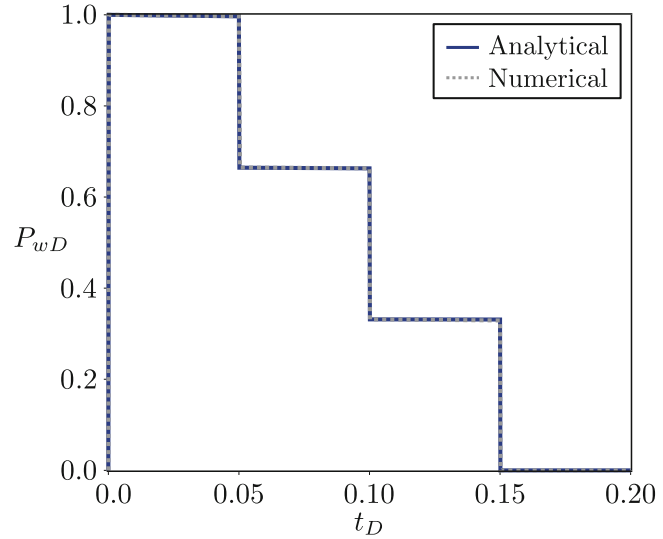
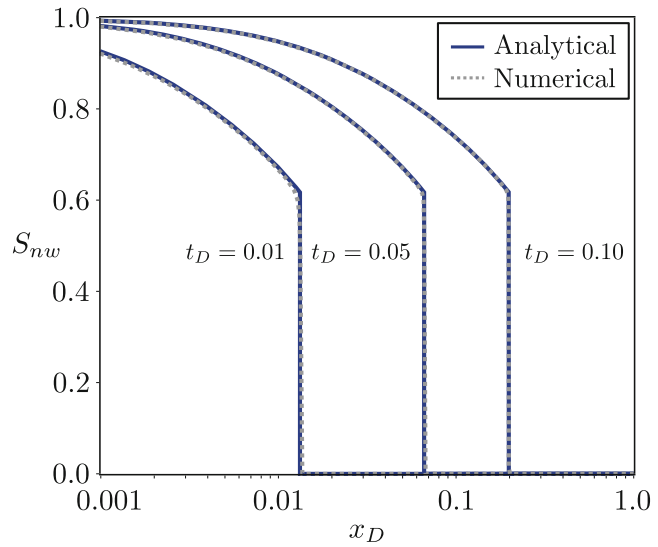


**Fig. 1.10** Analytical and numerical saturation profile for different  $t_D$  for a more compressible system



### 1.3.3 Compressibility Effect

Schedule 1 (Table 1.3) was used to analyze the compressibility effects in the results ( $c_r = 1.0E - 2$  1/MPa and  $c_o = 4.0E - 3$  1/Kgf/cm<sup>2</sup> keeping all other properties constant. Even increasing the compressibility by a factor of 100, the incompressible and compressible saturation profiles still match (Fig. 1.10). As this system is much more compressible, it is expected that the flow rate propagates slower in the reservoir (Fig. 1.11). It can be noted that both solutions agree after  $\Delta t_D = 1e^{-6}$ . The pressure solution is presented in Fig. 1.12 showing the excellent agreement with numerical compressible simulation.

**Fig. 1.11** Analytical and numerical flow-rate profile for different  $\Delta t_D$  after  $t_D = 0.10$

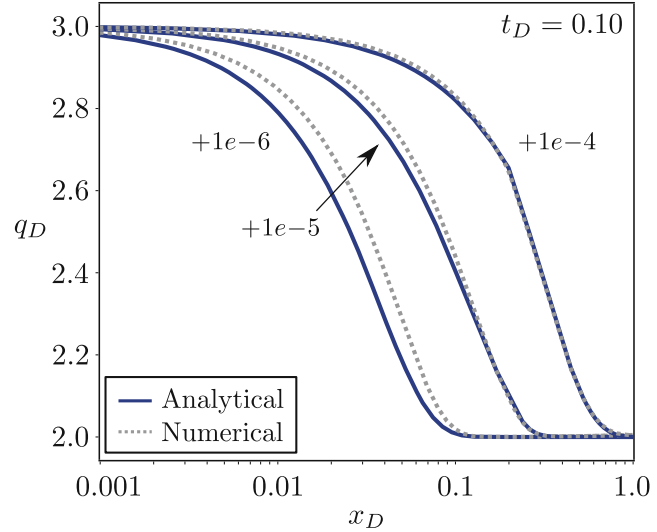
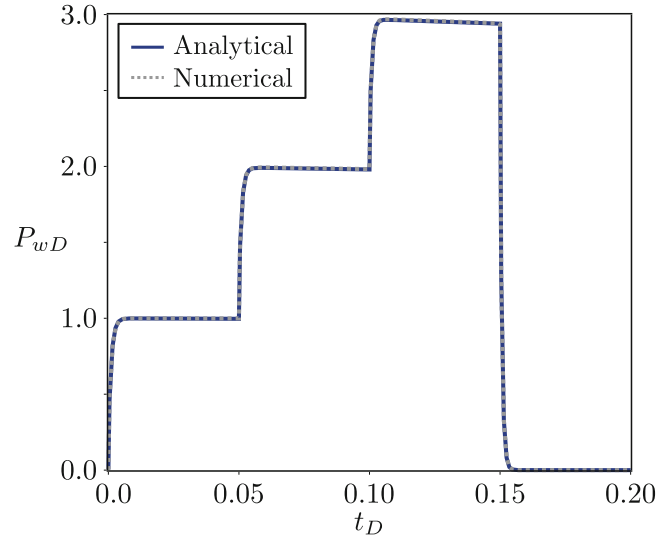


**Fig. 1.12** Analytical and numerical  $P_{wD}$  solution for a more compressible system



## 1.4 Conclusion

This work presents a new solution for the pressure drop along a linear porous medium considering immiscible two-phase oil displacement and a step-rate variable boundary condition. The solution is calculated based on two main hypothesis:

1. The mobility profile can be determined by the incompressible problem solution.
2. The total flow rate can be calculated by a dual-zone compressible problem.

The model was tested for two different flow rate schedules, and the results were compared to numerical solutions with excellent agreement. The analytical solution built in this work can be used to model laboratory core flood experiments.

**Acknowledgments** The authors acknowledge Universidade Estadual do Norte Fluminense (UENF) for financial support. This study was also financed in part by the Coordenação de Aperfeiçoamento de Pessoal de Nível Superior—Brasil (CAPES)—Finance Code 001.

## References

- [AK89] Abbaszadeh, M., & Kamal, M.: Pressure-transient testing of water-injection wells. *SPE Reserv. Eng.* **4**(01), 115–124 (1989). Society of Petroleum Engineers (SPE). <https://doi.org/10.2118/16744-pa>
- [AS09] Azevedo, A.V., Souza, A.J., Furtado, F., Marchesin, D., Plohr, B.: The solution by the wave curve method of three-phase flow in virgin reservoirs. *Trans. Porous Media* **83**(01), 99–125 (2009). Springer Science and Business Media LLC. <https://doi.org/10.1007/s11242-009-9508-9>
- [BH90] Bratvold, R.B., Horne, R.N.: Analysis of pressure-falloff tests following cold-water injection. *SPE Form. Evaluation* **5**(03), 293–302 (1990). Society of Petroleum Engineers (SPE). <https://doi.org/10.2118/18111-pa>
- [BL42] Buckley, S., Leverett, M.: Mechanism of fluid displacement in sands. *Trans. AIME* **146**(01), 107–116 (1942). Society of Petroleum Engineers (SPE). <https://doi.org/10.2118/942107-g>
- [BTR98] Banerjee, R., Thompson, L.G., Reynolds, A.C.: Injection/falloff testing in heterogeneous reservoirs. *SPE Reser. Evaluation Eng.* **1**(06), 519–527 (1998). Society of Petroleum Engineers (SPE). <https://doi.org/10.2118/52670-pa>
- [CAF16] Castañeda P., Abreu, E., Furtado, F., Marchesin, D.: On a universal structure for immiscible three-phase flow in virgin reservoirs, *Comput. Geosci.* **20**(01), 171–185 (2016). Springer Science and Business Media LLC. <https://doi.org/10.1007/s10596-016-9556-5>
- [C56] Corey, A.T., Rathjens, C.H., Henderson, J.H., Wyllie, M.R.J.: Three-phase relative permeability. *J. Petroleum Technol.* **8**(11), 63–65 (1956). Society of Petroleum Engineers (SPE). <https://doi.org/10.2118/737-g>
- [FS59] Fayers, F.J., Sheldon, J.W.: The effect of capillary pressure and gravity on two-phase fluid flow in a porous medium. *Trans. AIME* **216**(01), 147–155 (1959). Society of Petroleum Engineers (SPE). <https://doi.org/10.2118/1089-g>
- [GF97] Guzmán, R.E., Fayers, F.J.: Mathematical properties of three-phase flow equations. *SPE J.* **2**(03), 291–300 (1997). Society of Petroleum Engineers (SPE). <https://doi.org/10.2118/35154-pa>
- [GS70] Stehfest, H.: Algorithm 368: numerical inversion of laplace transforms. *Commun. ACM* **13**, 47–49 (1970)
- [HRM58] Hazebroek, P., Rainbow, H., Matthews, C.S.: Pressure fall-off in water injection wells. *Trans. AIME* **213**(01), 250–260 (1958). Society of Petroleum Engineers (SPE). <https://doi.org/10.2118/925-g>
- [IMPT92] Isaacson, E.L., Marchesin, D., Plohr, B.J., Temple, J.B.: Multiphase flow models with singular Riemann problems. *Mat. Apl. Comput.* **11**(02), 147–166 (1992). Sociedade Brasileira de Matemática Aplicada e Computacional
- [JBN59] Johnson, E.F., Bossler, D.P., Neumann, V.O.: Calculation of relative permeability from displacement experiments. *Trans. AIME* **216**, 370–372 (1959). Society of Petroleum Engineers (SPE), SPE-1023G
- [KMJ72] Kazemi, H., Merrill, L.S., Jargon, J.R.: Problems in interpretation of pressure fall-off tests in reservoirs with and without fluid banks. *J. Petrol. Technol.* **24**(09), 1147–1156 (1972). Society of Petroleum Engineers (SPE). <https://doi.org/10.2118/3696-pa>
- [L07] Liu, T.: *Hyperbolic and Viscous Conservation Laws*. CBMS-NSF Regional Conference Series in Applied Mathematics, vol. 01. SIAM, Philadelphia (2007)
- [L57] Lax, P.D.: Hyperbolic systems of conservation laws II. *Commun. Pure Appl. Math.* **10**(04), 537–566 (1957). Wiley. <https://doi.org/10.1002/cpa.3160100406>
- [O57] Oleinik, O.A.: On the uniqueness of the generalized solution of the Cauchy problem for a non-linear system of equations occurring in mechanics. *Uspekhi Mat. Nauk* **12**, 169–176 (1957)

- [PBR04] Peres, A.M.M., Boughrara, A.A., Reynolds, A.C.: Rate superposition for generating pressure falloff solutions for vertical and horizontal wells. SPE Annual Technical Conference and Exhibition, Society of Petroleum Engineers (SPE) (2004). <https://doi.org/10.2118/90907-ms>
- [PBR06] Peres, A.M.M., Boughrara, A.A., Reynolds, A.C.: Rate superposition for generating pressure falloff solutions. SPE J. **11**(03), 364–374 (2006). Society of Petroleum Engineers (SPE). <https://doi.org/10.2118/90907-pa>
- [PR03] Peres, A.M.M., Reynolds, A.C.: Theory and analysis of injectivity tests on horizontal wells. SPE J. **8**(02), 147–159 (2003). Society of Petroleum Engineers (SPE). <https://doi.org/10.2118/84957-pa>
- [SC59] Sheldon, J.W., Cardwell, W.T.: One-dimensional, incompressible, noncapillary, two-phase fluid flow in a porous medium. Trans. AIME **216**(01), 290–296 (1959). Society of Petroleum Engineers (SPE). <https://doi.org/10.2118/978-g>
- [TR97] Thompson, L., Reynolds, A.C.: Well testing for radially heterogeneous reservoirs under single and multiphase flow conditions. SPE Format. Evaluation **12**(01), 57–64 (1997). Society of Petroleum Engineers (SPE). <https://doi.org/10.2118/30577-pa>
- [W52] Welge, H.J.: A simplified method for computing oil recovery by gas or water drive. J. Petrol. Technol. **4**(04), 91–98 (1952). Society of Petroleum Engineers (SPE). <https://doi.org/10.2118/124-g>

**4    *Article: Approximated Solution  
for Linear Step-Rate Water  
Injectivity Test***

# Approximated Solution for Linear Step-Rate Water Injectivity Test

Wagner Q. Barros<sup>a</sup>, Adolfo P. Pires<sup>a,\*</sup>, Alvaro M. M. Peres<sup>a</sup>

<sup>a</sup>*Laboratório de Engenharia e Exploração de Petróleo - Universidade Estadual do Norte Fluminense Darcy Ribeiro, Macaé, RJ, Brazil*

---

## Abstract

Water injectivity test is an important method used in petroleum engineering to get dynamical reservoir data. It consists of a controlled flow-rate water injection followed by a falloff period (stop of injection), while the bottom hole pressure is measured during all process. To interpret such test, an inverse problem must be constructed using an analytical solution of the pressure equation.

For the water injection in oil reservoirs, the pressure and saturation fields must be solved together, creating mathematical difficulties to obtain a complete solution. At the moment, only approximated solutions for the continuous injection problem with a single falloff were obtained. In this article, we present a new approximated solution considering a step variable flow-rate injection, typical of step-rate tests. This solution is useful not only to interpret step-rate tests, but also for cases where for operational problems issues the injection flow-rate was not well controlled during the test.

*Keywords:* Pressure Well Tests, Method of Characteristics, Injectivity tests, Step-rate tests

---

---

\*mycorrespondingauthor  
Email address: [adolfo.puime@gmail.com](mailto:adolfo.puime@gmail.com) (Adolfo P. Pires)

## 1. Introduction

Injectivity and falloff tests in vertical wells are an useful tool to obtain dynamic reservoir data. The injected fluid has distinct properties when compared with original oil in place, creating a moving internal boundary. The inner zone is highly saturated with the injected phase having a different transmissibility of the outer oil zone, saturated with original oil.

The pressure solution for a dual-zone medium with compressible fluids is a well known problem, as well as the saturation solution considering immiscible and incompressible flow (knowing by Buckley-Leverett solution). However, deriving an analytical solution for the compressible injectivity test is a much more difficulty task because both pressure and saturation fields are coupled, creating a system of non-linear partial differential equations (PDE).

The first attempt to solve this coupled problem is divide the medium in two constant saturation zones, and treat the flow as a piston-like displacement (Hazebroek et al. (1958); Kazemi et al. (1972)). The more the two-phase zone is divided, better is the quality of such approach, however, this method does not consider the effect of compressibility in the saturations profile. For practical water injectivity tests, the water front is much slower than the pressure profile, and the saturation and pressure fields can be decoupled, known as a quasi-static approximation (Abbaszadeh and Kamal (1989)). Using this hypothesis, it is possible to superimpose the pressure-transient effects in the Buckley-Leverett saturation profile, producing satisfactory results for the continuous injectivity tests (Bratvold and Horne (1990)).

Thompson and Reynolds (1997) generalized the theory for compressible multi-phase flow in heterogeneous reservoirs. The problem was rewritten using spatial averages, where a moving weighting kernel determines the regions that has higher impacts in the solution. This process gives high weights for regions where the total mobility and the flow-rate are varying more rapidly with time. Considering the continuous injectivity test for traditional reservoir properties, the flow-rate changing zone is much faster than the saturation advancing front,

causing that the two-phase zone is always within a steady-state region, affirmation further known by Thompson Reynolds conjecture (Figure 1). As a direct consequence of this affirmation is that the saturation and flow-rate profiles can be decoupled and the final pressure solution is constructing simply integrating the multiphase Darcy's law (Banerjee et al. (1998); Peres and Reynolds (2003); Peres et al. (2004)).

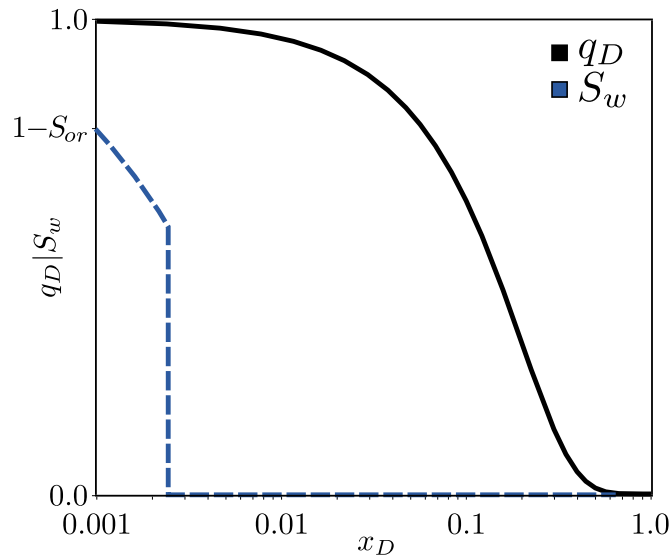


Figure 1: Illustration of the Thompson Reynolds conjecture for the linear waterflooding injection

The Thompson Reynolds conjecture gives excellent results for continuous water injection, in which an explicit criteria was derived to test its validity considering different coordinate systems (Peres and Reynolds (2003)). However its application for injectivity tests is based in the constant flow-rate injection hypothesis, in which due to operational issues is difficulty to obtain in practical field applications. Every time the flow-rate injection changes, a new transient is generating in the two-phase zone, invalidating completely the conjecture.

In this work we present an approximate solution for the linear step-rate injectivity tests, where we decoupled the saturation and pressure solutions using the

quasi-static approach. In Section 2 the mathematical formulation is discussed considering two different external boundary conditions: finite and infinity reservoir. The approximated solution was compared with numerical simulation in Sections 4 and 3 for both boundary conditions, respectively. Then we per-  
50 formed a sensitivity analysis over the dimensionless groups that impacts the approximation quality (Section 5) and we discussed some criterias for the solution validity. Some conclusions are then addressed in sequence. In Appendix A, a mathematical proof of the coupling condition, discussed in the mathematical formulation, is formulated. The pressure solution in Laplace's field is then  
55 presented in Appendix B.

## 2. Mathematical Model

A water injectivity test is defined by the controlled injection of water in a reservoir initially saturated with oil at irreducible water saturation (Figure 2). Additional hypothesis are:

- Reservoir is linear, homogeneous and with constant cross sectional area;
- Immiscible and isothermal flow;
- Dispersion, gravitational and capillary effects are neglected;
- Fluids having constant viscosity;
- Slightly compressible fluids and rock;
- Darcy's law hypothesis are valid.

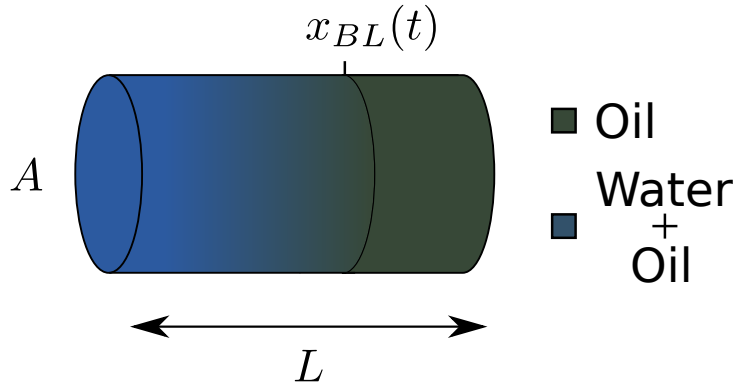


Figure 2: Linear water step-rate injection

The velocity of each phase can be calculated by the Darcy's law:

$$v_{\pi} = -\frac{Kk_{r\pi}}{\mu_{\pi}} \frac{\partial P}{\partial x}, \quad \pi = w, o \quad (1)$$

where  $K$  and  $k_{r\pi}$  are the absolute and relative permeabilities,  $\mu_{\pi}$  the phase viscosity and  $\frac{\partial P}{\partial x}$  the linear pressure gradient. Subscripts  $w$  and  $o$  are related

to water and oil phases, respectively. Summing both phases and neglecting the  
70 capillary effects:

$$q_T(x, t) = -AK\lambda_T(x, t) \frac{\partial P(x, t)}{\partial x} \quad (2)$$

where  $A$  is the cross sectional area,  $q_T$  is the total flow rate and  $\lambda_T$  is the total mobility of the system ( $\lambda_T = \frac{k_{rw}}{\mu_w} + \frac{k_{ro}}{\mu_o}$ ). The pressure profile can be obtained integrating this equation:

$$P(x, t) - P_i = \frac{1}{AK} \int_x^{x_s} \frac{q_T(x', t)}{\lambda_T(x', t)} dx' \quad (3)$$

where  $x_s$  is the position of the external reservoir boundary:

$$\begin{cases} x_s \rightarrow \infty, & \text{Infinity} \\ x_s = L, & \text{Finite} \end{cases} \quad (4)$$

75 and  $P_i$  is the initial reservoir pressure ( $P(x_s, t) = P_i$ ).

For this problem, we are defining the following dimensionless time and space coordinates:

$$x_D = \frac{x}{L_C} \quad (5)$$

$$t_D = \frac{q_{ref} t}{(1 - S_{wi} - S_{or}) AL_C \phi} \quad (6)$$

where  $L_C$  is a characteristic length ( $L_C = L$  for the finite case and any other characteristic dimension for infinity solution) and  $q_{ref}$  is a reference flow rate  
80 value, usually the first injection step.  $S_{wi}$  is the irreducible water saturation and  $S_{or}$  is the residual oil saturation. The pressure is then written by:

$$P_D(x_D, t_D) = \int_{x_D}^{x_{DS}} \frac{q_D(x'_D, t_D)}{\lambda_{TD}(x'_D, t_D)} dx'_D \quad (7)$$

where:

$$P_D(x, t) = \frac{KA\hat{\lambda}_o}{q_{ref}L_C} (P(x, t) - P_i) \quad (8)$$

$$\lambda_{TD}(x, t) = \frac{\lambda_T(x, t)}{\hat{\lambda}_o} \quad (9)$$

$$q_D(x, t) = \frac{q_T(x, t)}{q_{ref}} \quad (10)$$

in which  $\hat{\lambda}_o$  is the mobility of oil at water irreducible saturation. Note that  $x_{DS} = 1$  for finite boundary condition and  $x_{DS} \rightarrow \infty$  for the infinity case.

85 There is no reported analytical solution for Equation 7, most of because the pressure and saturation fields should be solved coupledly. In order to avoid such difficulty, we are proposing a decoupled approximated solution based in two main hypothesis:

1. The mobility profile ( $\lambda_{TD}$ ) can be approximated by the incompressible  
90 solution;
2. The flow-rate profile ( $q_D$ ) can be approximated by a two-zone, linear, quasi-static, compressible problem.

As it will be discussed, the flow-rate profile is obtained by a linear PDE, making valid the application of flow-rate time superposition (Duhamel's principle).

95 Thus, the pressure in the inlet face ( $P_{wD}$ ) is given by:

$$P_{wD}(t_D) = \int_0^{x_{DS}} \frac{1}{\lambda_{TD}(x'_D, t_D)} \sum_{j=1}^{Nsteps} [q_{D_j}^{Inj} - q_{D_{j-1}}^{Inj}] q_D(x'_D, t_D - t_{D_{j-1}}) dx'_D \quad (11)$$

where  $Nsteps$  is the number of flow-rate steps until  $t_D$ ,  $q_{D_j}^{Inj}$  is the injection flow-rate in step  $j$  and  $t_{D_j}$  is the time when  $q_{D_j}^{Inj}$  has started. The terms inside parenthesis are the  $(x_D, t_D)$  point where  $q_D$  and  $\lambda_{TD}$  will be evaluated and should not be confused with an algebraic multiplication.

### 100 2.1. Approximation for $\lambda_{TD}(x_D, t_D)$ (Hypothesis 1)

Considering the water and oil flow in porous medium, the mass conservation for each phase is written by:

$$\frac{\partial(\phi S_\pi \rho_\pi)}{\partial t} + \frac{\partial(\rho_\pi v_\pi)}{\partial x} = 0, \pi = w, o \quad (12)$$

Using the incompressibility assumption (Hypothesis 1):

$$\frac{\partial S_\pi}{\partial t} + \frac{1}{\phi} \frac{\partial v_\pi}{\partial x} = 0, \pi = w, o \quad (13)$$

Now we introduce the saturation normalization:

$$\begin{cases} S_{nw} = \frac{S_w - S_{wi}}{1 - S_{wi} - S_{or}}, & S_w \in [S_{wi}, 1 - S_{or}] \\ S_{no} = \frac{S_o - S_{or}}{1 - S_{wi} - S_{or}}, & S_o \in [S_{or}, 1 - S_{wi}] \end{cases} \quad (14)$$

105 Applying the dimensionless definitions (Equations 5-10) and the Darcy's equation (Equation 1), we deduce the mass conservation of water phase, also known by dimensionless Buckley-Leverett equation (Buckley and Leverett (1942)):

$$\frac{\partial S_{nw}}{\partial t_D} + \frac{\partial q_D f_w}{\partial x_D} = 0 \quad (15)$$

in which  $f_w$  defines the water fractional flow:

$$f_w = \frac{\frac{k_{rw}}{\mu_w}}{\frac{k_{rw}}{\mu_w} + \frac{k_{ro}}{\mu_o}} \quad (16)$$

### 2.1.1. Solution for $\lambda_{TD}(x_D, t_D)$

110 The Equation 15 is a hyperbolic PDE, whose solution is given by the method of characteristics. By this method, the solution is constant over characteristic paths:

$$\frac{dx_D}{dt_D} = q_D \frac{df_w}{dS_{nw}} \quad (17)$$

This work considers convex relative permeability curves, in which  $\frac{df_w}{dS_{nw}}$  is not monotonic in  $S_{nw} \in (0, 1)$ . Weak solutions admissibility is tested using both  
 115 Lax (Lax (1957)) and Oleinik (Oleinik (1957)) stability criteria. The solution can then be described by a continuous region followed by a moving discontinuity:

$$S_{nw} = \begin{cases} \frac{df_w}{dS_{nw}}^{-1} \left( \frac{1}{q_D(t_D)} \frac{x_D}{t_D} \right), & x_D \in (0, x_D^{BL}) \\ 0, & x_D \in (x_D^{BL}, x_{DS}) \end{cases} \quad (18)$$

where the term  $\frac{1}{q_D(t_D)} \frac{x_D}{t_D}$  inside parenthesis is called self-similar variable and is the point where the inverse of  $\frac{df_w}{dS_{nw}}$  should be evaluated. The discontinuity trajectory  $x_D^{BL}(t_D)$  is obtained by solving the Rankine-Hugoniot equation:

$$\frac{dx_D^{BL}}{dt_D} = q_D(t_D) \frac{f_w^{BL}}{S_{nw}^{BL}} \quad (19)$$

120 in which  $S_{nw}^{BL}$  and  $f_w^{BL}$  are the water saturation and fractional flow for  $\lim_{x_D \rightarrow x_D^{BL-}}$ . For a step-rate water injection  $q_D(t_D)$  is given by steps and the solution characteristics are described by a sequence of straight lines in  $x_D - t_D$  plane (Figure 3), where the dashed lines are used to represent the continuous part of the solution (rarefaction fan) while the solid line is the Buckley-Leverett shock.

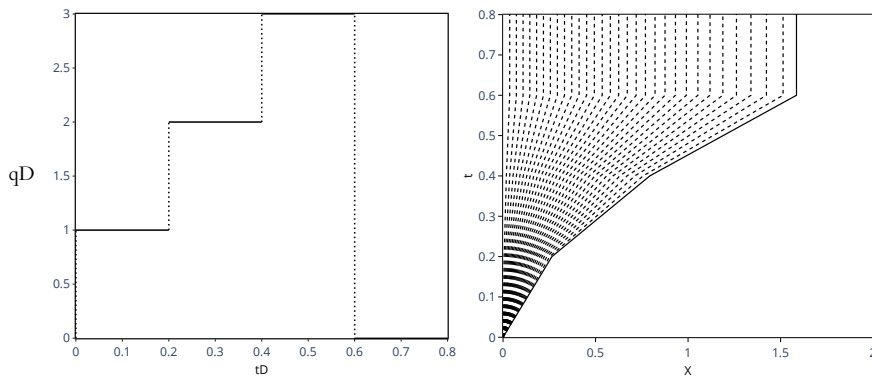


Figure 3: Characteristic diagram for a step-rate water injection

### 125 2.1.2. Validity of Hypothesis 1

To evaluate the validity of this hypothesis we need to analyze the magnitude of neglected terms when we assume incompressible flow. Expanding the original mass conservation (Equation 12) and applying the dimensionless definitions:

$$\rho_\pi \left( \frac{\partial S_{n\pi}}{\partial t_D} + \frac{\partial q_D f_\pi}{\partial x_D} \right) + S_\pi \frac{\partial (\phi \rho_\pi)}{\partial t_D} \frac{1}{(1 - S_{wi} - S_{or}) \phi} + f_\pi q_D \frac{\partial \rho_\pi}{\partial x_D} = 0, \quad \pi = w, o \quad (20)$$

Using the slightly compressibility rock and fluid definitions:

$$c_\phi = \frac{1}{\phi} \frac{d\phi}{dP} \quad (21)$$

$$c_\pi = \frac{1}{\rho_\pi} \frac{d\rho_\pi}{dP}, \quad \pi = w, o \quad (22)$$

130 We obtain:

$$\left( \frac{\partial S_{n\pi}}{\partial t_D} + \frac{\partial q_D f_\pi}{\partial x_D} \right) + S_\pi (\phi c_\pi + c_\phi \phi) \frac{\partial P}{\partial t_D} \frac{1}{(1 - S_{wi} - S_{or}) \phi} + f_\pi q_D c_\pi \frac{\partial P}{\partial x_D} = 0, \quad \pi = w, o \quad (23)$$

The first parenthesis is the Buckley-Leverett equation, the other terms are related to the error by neglected values. Summing for both phases, we can define a measure for the error introduced by incompressibility assumption:

$$\epsilon_L^{BL} = \frac{\partial P}{\partial t_D} \frac{c_t}{(1 - S_{wi} - S_{or})} + [f_w c_w + f_o c_o] \frac{\partial P}{\partial x_D} q_D \quad (24)$$

where  $c_t$  is the total compressibility of the system ( $c_t = c_\phi + S_w c_w + S_o c_o$ ). We  
 135 can relate terms  $\frac{\partial P}{\partial t_D}$  and  $\frac{\partial P}{\partial x_D}$  using the characteristic path (Equation 17) and the Darcy's equation (Equation 2:

$$\epsilon_L^{BL} = \left| \gamma_L \frac{df_w}{dS_{nw}} + \beta_L \right| (q_D)^2 \quad (25)$$

in which:

$$\gamma_L(x_D, t_D) = \frac{q_{ref} L_C}{(1 - S_{wi} - S_{or}) K A \lambda_T} \frac{c_t}{\lambda_T} \quad (26)$$

$$\beta_L(x_D, t_D) = [f_w c_w + f_o c_o] \frac{q_{ref} L_C}{K A \lambda_T} \quad (27)$$

This equation is written in dimensionless variables where  $\epsilon_L^{BL} = \epsilon_L^{BL}(x_D, t_D)$  because its dependency of the saturation field in the two-phase zone. Note that  $\epsilon_L^{BL}$  tends to zero in the limit when  $c_t \rightarrow 0$ , as expected. Then we can define an admissibility condition for Hypothesis 1:

$$\Psi_L^{BL} \equiv \max \left( \left| \gamma_L \frac{df_w}{dS_{nw}} + \beta_L \right| \right) \left( \max q_D^{Inj} \right)^2, \forall S_{nw} \in (S_{nw}^{BL}, 1) \quad (28)$$

## 2.2. Approximation for $q_D(x_D, t_D)$ (Hypothesis 2)

Starting from the mass conservation (Equation 12), applying the Darcy's law (Equation 1) and the compressibility definitions:

$$\phi \frac{\partial S_\pi}{\partial t} + \phi S_\pi (c_\pi + c_\phi) \frac{\partial P}{\partial t} - \left[ K \frac{\partial \lambda_\pi}{\partial x} \frac{\partial P}{\partial x} + K \lambda_\pi c_\pi \left( \frac{\partial P}{\partial x} \right)^2 \right] = 0, \pi = w, o \quad (29)$$

Summing both water and oil phases and applying the dimensionless definitions (Equations 5-10):

$$\frac{1}{\lambda_{TD}} \frac{\partial \lambda_{TD}}{\partial x_D} \frac{\partial P_D}{\partial x_D} + \lambda_{TD} \beta_L \left( \frac{\partial P_D}{\partial x_D} \right)^2 = \gamma_L \frac{\partial P_D}{\partial t_D} \quad (30)$$

For slow pressure gradients (validity of Darcy's law) the quadratic pressure gradient term is slow and can be neglected. Then:

$$\frac{1}{\lambda_{TD}} \frac{\partial \lambda_{TD}}{\partial x_D} \frac{\partial P_D}{\partial x_D} = \gamma_L \frac{\partial P_D}{\partial t_D} \quad (31)$$

Equation 31 is the general linear pressure in the porous medium. However, its solution is difficult because of the temporal and spatial dependence of terms  $\lambda_{TD}$  and  $\gamma_L$ . Instead of solving the pressure by this equation, we can approximate the flow-rate profile by the quasi-static approach, where for each  $t_D$  we consider a static saturation profile. The static  $\lambda_{TD}$  term can be decomposed in the spatial average plus a fluctuation term ( $\lambda_{TD} = \overline{\lambda_{TD}} + \lambda'_{TD}$ ):

$$\frac{1}{\lambda_{TD}} \frac{1}{1 + \frac{\lambda'_{TD}}{\lambda_{TD}}} \frac{\partial (\overline{\lambda_{TD}} + \lambda'_{TD})}{\partial x_D} \frac{\partial P_D}{\partial x_D} = \overline{\gamma_L} \frac{1 + \frac{c'_t}{c_t}}{1 + \frac{\lambda'_{TD}}{\lambda_{TD}}} \frac{\partial P_D}{\partial t_D} \quad (32)$$

155 where:

$$\overline{\gamma_L} = \frac{q_{ref} L_C}{(1 - S_{wi} - S_{or}) K A \overline{\lambda_{TD}}} \overline{c_t} \quad (33)$$

and  $c_t = \overline{c_t} + c_t'$ . Note that  $c_t(S_{nw})$  is a linear function and  $c_t'(S_{nw}) = c_t(S_{nw}') \approx c_r$ . Thus, both  $\frac{c_t'}{\overline{c_t}}$  and  $\frac{\lambda'_{TD}}{\lambda_{TD}}$  are small terms and the PDE becomes:

$$\overline{\lambda_{TD}} \frac{\partial^2 P_D}{\partial x_D^2} + \frac{\partial \lambda'_{TD}}{\partial x_D} \frac{\partial P_D}{\partial x_D} = \overline{\lambda_{TD}} \overline{\gamma_L} \frac{\partial P_D}{\partial t_D} \quad (34)$$

The domain can be divided in two zones by the Buckley-Leverett shock position ( $x_D^{BL}$ ). For the single-phase zone,  $\lambda'_{TD}$  is already null and for two-phase zone we will consider  $\lambda'_{TD} \approx 0$ . Applying the initial (I.C.), internal boundary (I.B.C.) and external boundary (E.B.C.) conditions, we have a PDE for each zone:

$$\begin{cases} \frac{\partial^2 P_D}{\partial x_D^2} = \overline{\lambda_{TD}^{2Ph}} \frac{\partial P_D}{\partial t_D}, & x_D \in (0, x_D^{BL}) \\ P_D(x_D, t_D = 0) = 0 & \text{(I.C.)} \\ \lim_{x \rightarrow 0} \left( \frac{\partial P_D}{\partial x_D} \right) = -\frac{q_D^{inj}}{\lambda_{TD}^{2Ph}} & \text{(I.B.C)} \end{cases} \quad (35)$$

$$\begin{cases} \frac{\partial^2 P_D}{\partial x_D^2} = \hat{\gamma}_L \frac{\partial P_D}{\partial t_D}, & x_D \in (x_D^{BL}, x_{DS}) \\ P_D(x_D, t_D = 0) = 0 & \text{(I.C.)} \\ P_D(x_D = x_{DS}, t_D) = 0 & \text{(E.B.C)} \end{cases} \quad (36)$$

where  $\overline{\lambda_{TD}^{2Ph}}$  and  $\overline{\gamma_L^{2Ph}}$  are the spatial average in the two-phase zone (constant before the breakthrough due to the self-similar Buckley-Leverett solution). To couple both systems we are using the pressure and flow-rate continuity (Appendix A):

$$\lim_{x_D \rightarrow x_D^{BL-}} P_D(x_D, t_D) = \lim_{x_D \rightarrow x_D^{BL+}} P_D(x_D, t_D) \quad (37)$$

$$\left( \overline{\lambda_{TD}^{2Ph}} \frac{\partial P_D(x_D, t_D)}{\partial x_D} \right)_{x_D^{BL-}} = \left( \frac{\partial P_D(x_D, t_D)}{\partial x_D} \right)_{x_D^{BL+}}$$

It must be remembered that because of the quasi-static approach the pressure that we are calculating in Equations 35-37 is different of the pressure solution (Equation 7) and should not be confused.

170 *2.2.1. Solution for  $q_D(x_D, t_D)$*

To solve Equations 35-37 we apply the Laplace's transform in both PDE's and in the coupling conditions:

$$\begin{cases} \frac{\partial^2 \tilde{P}_D}{\partial x_D^2} = \overline{\gamma_L^{2Ph}} u \tilde{P}_D, & x_D \in (0, x_D^{BL}) \\ \lim_{x \rightarrow 0} \left( \frac{\partial \tilde{P}_D}{\partial x_D} \right) = -\frac{q_D^{Inj}}{\lambda_{TD}^{2Ph}} \frac{1}{u} \quad \text{(I.B.C)} \end{cases} \quad (38)$$

$$\begin{cases} \frac{\partial^2 \tilde{P}_D}{\partial x_D^2} = \hat{\gamma}_L u \tilde{P}_D, & x_D \in (x_D^{BL}, x_{DS}) \\ \tilde{P}_D(x_D = x_{DS}, u) = 0 \quad \text{(E.B.C)} \end{cases} \quad (39)$$

$$\begin{aligned} \lim_{x_D \rightarrow x_D^{BL-}} \tilde{P}_D(x_D, u) &= \lim_{x_D \rightarrow x_D^{BL+}} \tilde{P}_D(x_D, u) \\ \left( \lambda_{TD}^{2Ph} \frac{\partial \tilde{P}_D(x_D, u)}{\partial x_D} \right)_{x_D^{BL-}} &= \left( \frac{\partial \tilde{P}_D(x_D, u)}{\partial x_D} \right)_{x_D^{BL+}} \end{aligned} \quad (40)$$

Solving the system and applying the Darcy's law in Laplace's domain (Equation 2), the flow-rate can be then determined by:

$$\tilde{q}_D(x_D, u) = \begin{cases} -\frac{\lambda_{TD}^{2Ph}}{\lambda_{TD}^{2Ph}} \sqrt{\overline{\gamma_L^{2Ph}}} u e^{\sqrt{\overline{\gamma_L^{2Ph}}} u x_D} A_0 + \frac{\lambda_{TD}^{2Ph}}{\lambda_{TD}^{2Ph}} \sqrt{\overline{\gamma_L^{2Ph}}} u e^{-\sqrt{\overline{\gamma_L^{2Ph}}} u x_D} A_1, & \text{for } x_D < x_D^{BL} \\ -\sqrt{\hat{\gamma}_L} u e^{\sqrt{\hat{\gamma}_L} u x_D} A_2 + \sqrt{\hat{\gamma}_L} u e^{-\sqrt{\hat{\gamma}_L} u x_D} A_3, & \text{for } x_D > x_D^{BL} \end{cases} \quad (41)$$

175 where the system solution and coefficients  $A_0$ ,  $A_1$ ,  $A_2$  and  $A_3$  are described in Appendix B. Once calculated the flow-rate in Laplace's domain, the result is inverted to real field using the Stehfest's algorithm Stehfest (1970).

*2.2.2.  $q_D(x_D, t_D)$  Solution After Breakthrough*

180 For finite reservoir, as long the water injection persists, the Buckley-Leverett front approximates to the outlet face ( $x_D = 1$ ). After the breakthrough, the  $q_D$  solution given by Equation 41 cannot be used, because  $x_D^{BL}$  is outside the domain. For this case, the flow-rate solution should be construct using:

$$\tilde{q}_D(x_D, u) = -\frac{\lambda_{TD}^{BT}}{\lambda_{TD}^{BT}} \sqrt{\overline{\gamma_L^{BT}}} u e^{\sqrt{\overline{\gamma_L^{BT}}} u x_D} A_0^{BT} + \frac{\lambda_{TD}^{BT}}{\lambda_{TD}^{BT}} \sqrt{\overline{\gamma_L^{BT}}} u e^{-\sqrt{\overline{\gamma_L^{BT}}} u x_D} A_1^{BT} \quad (42)$$

where  $\overline{\lambda_{TD}^{BT}}$  and  $\overline{\gamma_L^{BT}}$  are spatial averages inside domain only  $x_D \in (0, 1)$ . The coefficients  $A_0^{BT}$  and  $A_1^{BT}$  are calculated using  $x_D^{BL} = 1$  in coefficients  $A_0$  and  $A_1$  for finite case.

### 2.2.3. Validity of Hypothesis 2

During the construction of flow-rate solution we have made two simplifications: slow pressure gradients and average properties in two-phase zone. For the first simplification, the associated error is given by:

$$\epsilon_L^P = \left| \lambda_{TD} \beta_L \left( \frac{\partial P_D}{\partial x_D} \right)^2 \right| \quad (43)$$

Applying the Darcy's equation:

$$\epsilon_L^P = \left| \frac{\beta_L q_D^2}{\lambda_{TD}} \right| \quad (44)$$

The flow-rate is always lower than the maximum injected flow-rate ( $q_D(x_D, t_D) \leq \max q_D^{Inj}$ ). The admissibility condition is then defined by:

$$\Psi_L^P \equiv \max \left( \frac{\beta_L}{\lambda_{TD}} \right) \left( \max q_D^{Inj} \right)^2, \forall S_{nw} \in (S_{nw}^{BL}, 1) \quad (45)$$

For the average properties assumption, we will define the average error as:

$$\epsilon_L^M = \int_0^{x_D^{BL}} \frac{\partial \lambda_{TD}' \frac{\partial P_D}{\partial x_D}}{\partial x_D} dx_D \quad (46)$$

By Darcy's law, the estimated pressure gradient is given by  $\frac{\partial P_D}{\partial x_D} = \frac{q_D}{\lambda_{TD}}$ , thus evaluating the integral:

$$\epsilon_L^M = \left( \frac{\lambda_{TD}^{BL} - \overline{\lambda_{TD}}}{\lambda_{TD}} q_D \right)_{x_D=x_D^{BL}} - \left( \frac{M - \overline{\lambda_{TD}}}{\lambda_{TD}} q_D \right)_{x_D=0} \quad (47)$$

where  $\lambda_{TD}^{BL}$  is the mobility using  $S_{nw}^{BL}$  and  $M = \frac{\lambda_{Sor}}{\lambda_o}$ . The admissibility for this assumption is defined using maximizing the error:

$$\Psi_L^M \equiv \left| \frac{(\lambda_{TD}^{BL} - M)}{\lambda_{TD}} \right| q_D^{INJ} \quad (48)$$

Note that if the saturation changes sharply in two-phase zone,  $\Psi_L^M$  will assume high values leading to inadmissible errors for Hypothesis 2. This limitation can  
200 be overcome dividing the two-phase region in more zones and repeating the process discussed in this section. However, as it will be discussed, for the values we tested the approximated solution, this refinement was not necessary and all results showed in this paper were generated using only a single zone for the two-phase region.

205 **3. Infinity Reservoir Solution**

In this section we will compare the infinity reservoir solution ( $x_{DS} \rightarrow \infty$ ) with numerical simulation using the properties showed in Table 1. The approximation of infinity reservoir is typically used in well test analysis, where the well radius is orders of magnitude lower than the reservoir length, and also the injected volumes are small compared with the original oil in-place. To write the space dimensionless variable (Equation 5) we are considering the reservoir length as the characteristic length ( $L_C$ ). Rock and fluid properties are calculated using the properties showed in Table 2 and Figure 4.

Table 1: Linear infinity reservoir properties

Length	$L = 10000$	[m]
Cross Section Area	$A = 4000$	[m <sup>2</sup> ]
Starting Flow Rate	$q_T^0 = 25$	[m <sup>3</sup> /d]

Table 2: Rock and Fluid physical properties

Fluid Properties		
Water Viscosity	$\mu_w = 1.0$	[cp]
Water Compressibility	$c_w = 1.0E - 6$	[1/Kgf/cm2]
Oil Viscosity	$\mu_o = 5.0$	[cp]
Oil Compressibility	$c_o = 4.0E - 5$	[1/Kgf/cm2]
Rock Properties		
Porosity	$\phi = 0.1$	[-]
Absolute Permeability	$K = 500$	[mD]
Rock Compressibility	$c_r = 1.0E - 4$	[1/MPa]
Relative Permeability Curves		
Irreducible Water Saturation	$S_{wi} = 0.20$	[-]
$k_{ro}$ in $S_{wi}$ Saturation	$k_{ro}^{S_{wi}} = 0.80$	[-]
Residual Oil Saturation	$S_{or} = 0.20$	[-]
$k_{rw}$ in $S_{or}$ Saturation	$k_{rw}^{S_{or}} = 0.30$	[-]
Water Corey's Parameter	$n_w = 2.2$	[-]
Oil Corey's Parameter	$n_o = 2.0$	[-]

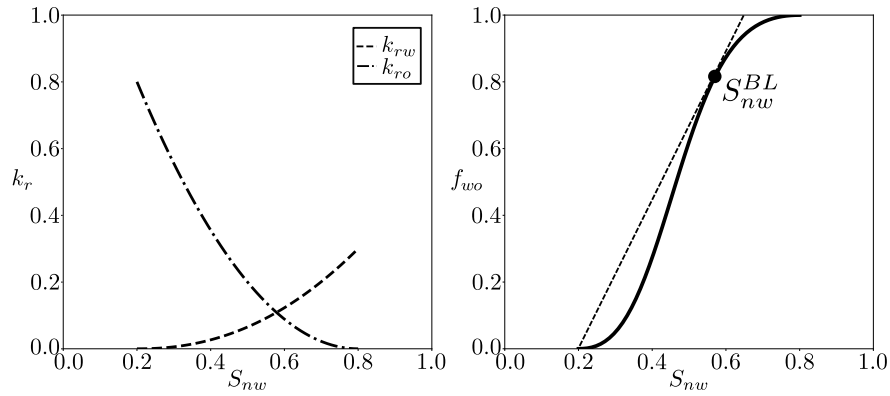


Figure 4: Relative permeability and fractional flow curves for properties showed in Table 2

The injectivity test schedule is composed by a three isochronal steps fol-

215 lowed by a falloff of same length (Table 3). The Figure 5 shows the flow-rate  
 $\Delta t_D = 1x10^{-7}$ ,  $\Delta t_D = 1x10^{-6}$  and  $\Delta t_D = 1x10^{-5}$  after each flow-rate change.  
 Note that the flow-rate propagation front does not react the reservoir outlet  
 any moment during the test, validating the use of the infinity hypothesis. For  
 this case, both numerical and analytical solutions agree very well, in which the  
 220 stability conditions are:  $(\Psi_L^{BL}, \Psi_L^P, \Psi_L^M) = (2.0x10^{-1}, 1.1x10^{-2}, 2.9)$ . The nu-  
 merical simulations were run using an uniform mesh grid with 20,000 cells, with  
 a controlled time-step size in order to maintain  $CFL < 0.1$ . The saturation  
 profile comparison is not needed because the water saturation front entered less  
 than 0.2% of the total reservoir length.

Table 3: Step-rate schedule for infinity reservoir test

$\Delta t_D (x10^{-4})$	$q_D^{Inj}$
0.00-1.00	1.0
1.00-2.00	2.0
2.00-3.00	3.0
3.00-4.00	0.0

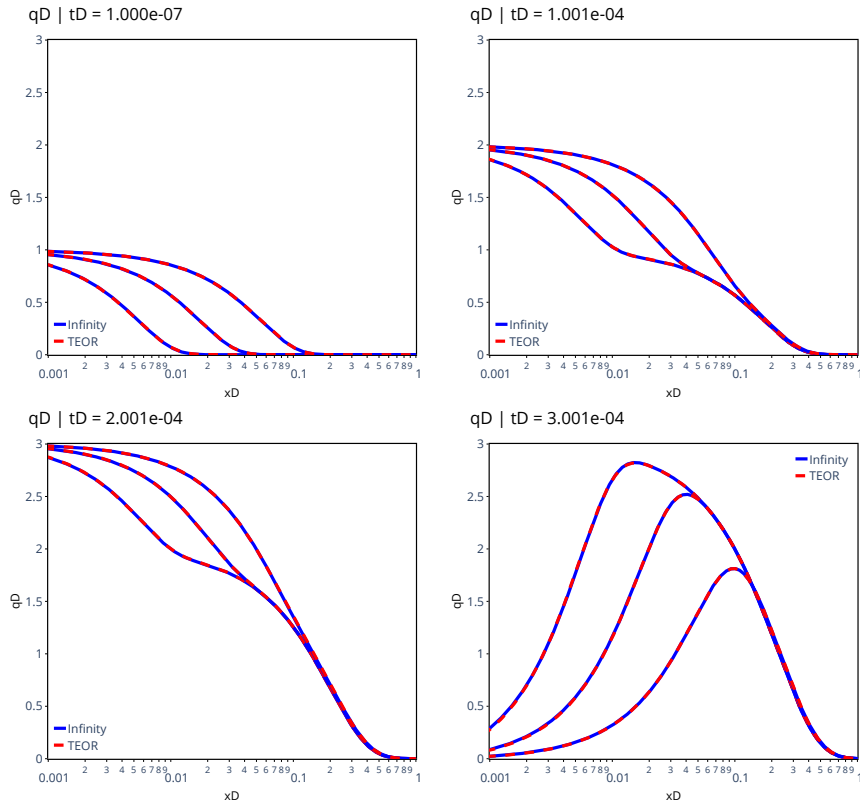


Figure 5: Numerical and analytical flow-rate profile comparison for  $\Delta t_D = 1x10^{-7}$ ,  $\Delta t_D = 1x10^{-6}$  and  $\Delta t_D = 1x10^{-5}$  after each flow-rate change considering the infinity reservoir solution

225 Now we have the mobility and the flow-rate profile along the reservoir, the pressure solution in the inlet face is calculated by Equation 11 (Figure 6). Every time the flow-rate is increased a new transient starts in the reservoir, increasing the pressure rate. Then, in the falloff period, the pressure stops to increase and falls in order to restore the original pressure in the reservoir. We may note the  
 230 excellent agreement between numerical and analytical solutions for the infinity reservoir case.

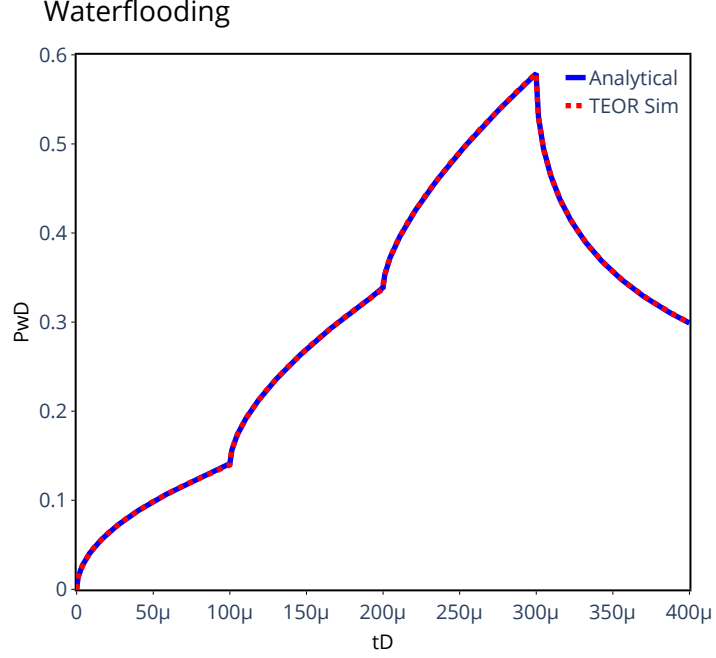


Figure 6: Numerical and analytical pressure in inlet face ( $P_{wD}$ ) for the infinity reservoir solution

### 3.1. Well-Test Analysis

The standard tool for well-test analysis is using the derivative of pressure with respect to the natural logarithm of time (Bourdet's analysis). However, before use this technique, we need to diminish the effect of the injection flow-rate variation from the pressure data, in order to improve the reservoir component of data. For this we will use the equivalent time concept, based in the convolution scheme.

The equivalent time for the linear flow ( $t_{eDl}$ ) can be defined by the time when the pressure data in a particular time  $\Delta t$  after a step change has the same magnitude of the pressure produced by the linear solution with constant injection flow-rate. Mathematically:

$$\frac{P_{wD}(t_{D_{N-1}}) - P_{wD}(t_{D_{N-1}} + \Delta t_D)}{q_{D_{N-1}} - q_{D_N}} = C_1 \sqrt{t_{eDl}} + C_2 \quad (49)$$

where  $t_{D_{N-1}}$  is the time where the flow-rate step  $N$  starts,  $q_{D_N}$  is the flow-rate in step  $N$  and  $C_1\sqrt{t_{eDl}} + C_2$  is the linear solution for the infinity reservoir, with  $C_1$  and  $C_2$  given by arbitrary constants depending of the linear problem. The dimensionless pressure in time  $t_{D_{N-1}} + \Delta t_D$  can be written using the Duhamel's principle:

$$P_{wD}(t_{D_{N-1}} + \Delta t_D) = \sum_{j=1}^N [q_{D_j} - q_{D_{j-1}}] \left( C_1 \sqrt{(t_{D_{N-1}} + \Delta t_D - t_{D_{j-1}})} + C_2 \right) \quad (50)$$

then, combining both equations we have the equivalent time definition:

$$\sqrt{t_{eDl}} = \sum_{j=1}^{N-1} \left( \frac{q_{D_j} - q_{D_{j-1}}}{q_{D_{N-1}} - q_{D_N}} \right) \left[ \sqrt{(t_{D_{N-1}} - t_{D_{j-1}})} - \sqrt{(t_{D_{N-1}} + \Delta t_D - t_{D_{j-1}})} \right] + \sqrt{\Delta t_D} \quad (51)$$

Note that for the first injection step ( $N = 1$ ) the equivalent time is the exact time  $t_{eDl} = \Delta t_D = t_D$ .

Now we can use the pressure derivative with respect to the equivalent time  $\left( \frac{dP_{wD}}{d\log(t_{eDl})} \right)$  for any particular time-step to obtain the reservoir properties (Figure 7). When the equivalent time concept is applied for the infinity case, the derivative for any time-step follows a straight line with  $\frac{1}{2}$  slop, typical of the linear flow. For real well-tests the reservoir properties are obtained using only the falloff period (Figure 8), because the pressure data is smoother not influenced by injection and operational noises. Comparing the multi-step solution with the single-phase one, we can conclude that for the infinity reservoir case, the single-phase hypothesis is an excellent approximation for the test analysis, where the reservoir properties can be obtained adjusting the derivative curve.

### Infinity PwD Linear Waterflooding

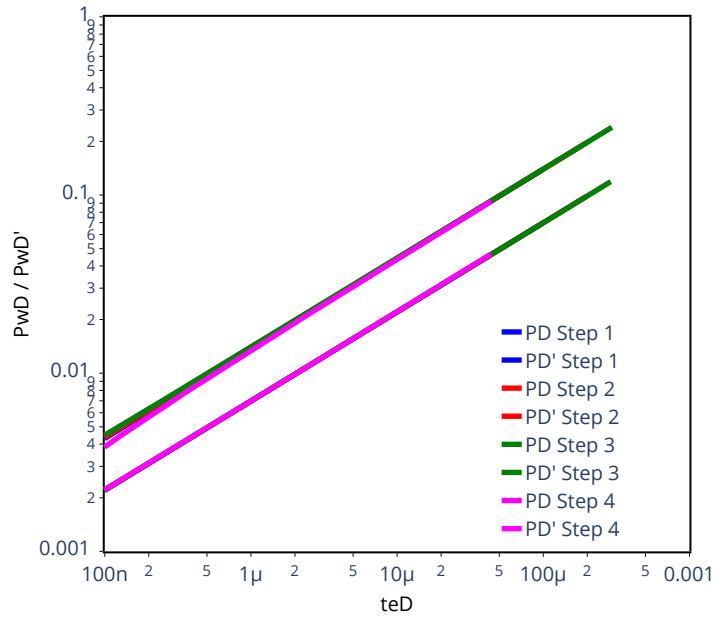


Figure 7:  $P_{wD}$  and  $\frac{dP_{wD}}{d\log(teD)}$  for the infinity reservoir solution

### Infinity PwD Linear Waterflooding

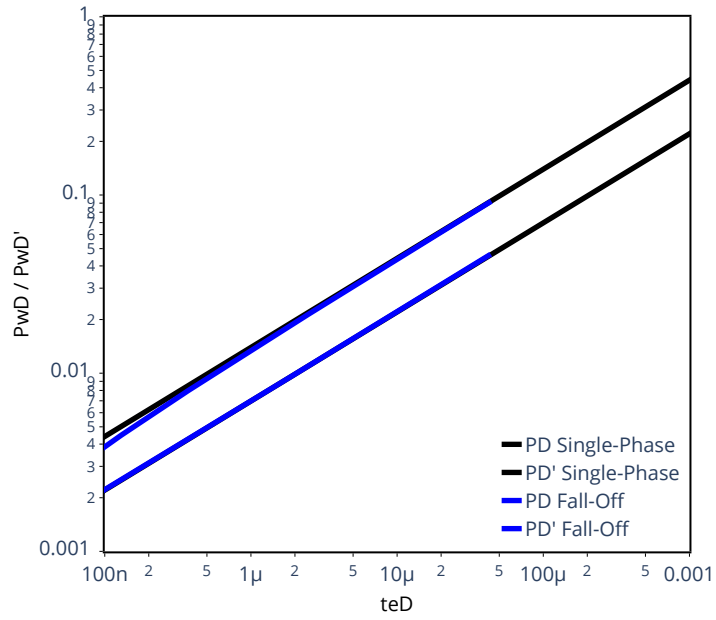


Figure 8:  $P_{wD}$  and  $\frac{dP_{wD}}{d\log(teD)}$  for the infinity reservoir solution compared with the single-phase linear solution

#### 4. Finite Reservoir Solution

For long duration tests, when the injected volume is not neglected when compared with original oil in place, the outlet reservoir face interferes in the pressure solution and the infinity approximation cannot be used. In this section a laboratory coreflooding experiment is modeled using the finite model (Table 4), where the injection flow-rate is controlled in the core inlet and the pressure drop along the rock core is monitored during all the experiment. The rock and fluid properties are the same shown in Table 2 and Figure 4.

Table 4: Linear finite reservoir properties

Length	$L = 30$	[cm]
Diameter	$D = 1.5$	[in]
Starting Flow Rate	$q_T^0 = 0.25$	[cm <sup>3</sup> /min]

The injection schedule for this coreflooding experiment is composed by three isochronal flow-rate steps followed by a fall-off period (Table 5 and Figure 3). If we compare the water front advance over time between our approximated solution and one obtained by numerical simulation that considers fluid and rock compressibility (Figure 9), we conclude that the first hypothesis gives outstanding results for stability conditions that we are dealing ( $(\Psi_L^{BL}, \Psi_L^P, \Psi_L^M) = (2.9 \times 10^{-4}, 1.6 \times 10^{-5}, 2.9)$ ). The water breakthrough happens in time  $t_D \approx 0.45$  where the shock wave leaves the domain, where the compressible and incompressible solutions still agree. Note that, because the horizontal flow hypothesis, the water profile does not change in the falloff period, most of because phase segregation is not acting in this system.

The flow-rate along reservoir is compared with numerical solutions for times  $\Delta t_D = 1 \times 10^{-8}$ ,  $\Delta t_D = 1 \times 10^{-7}$  and  $\Delta t_D = 1 \times 10^{-6}$  after each flow-rate change (Figure 10). Both solutions agree for the case we are studying, showing the validity of Hypothesis 2. Note that solutions still agrees after the breakthrough, time when the porous medium is highly saturated with water.

Table 5: Step-rate schedule for finite reservoir test

$\Delta t_D$	$q_D^{Inj}$
0.00-0.20	1.0
0.20-0.40	2.0
0.40-0.60	3.0
0.60-0.80	0.0

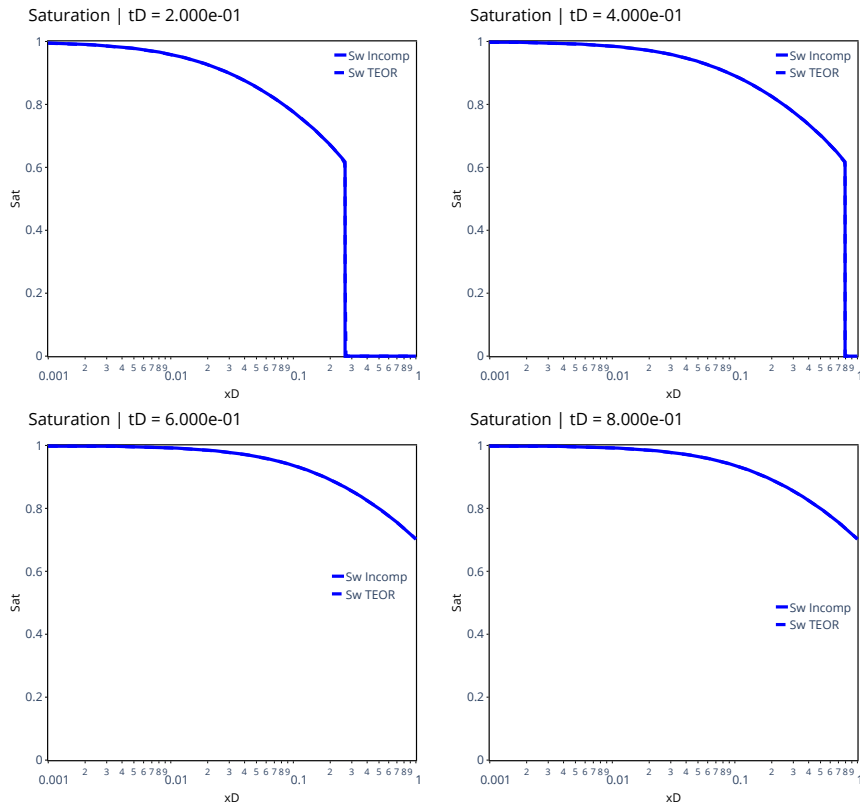


Figure 9: Numerical and analytical water saturation profile comparison for  $t_D = 0.2$ ,  $t_D = 0.4$ ,  $t_D = 0.8$  and  $t_D = 0.8$  considering the finite reservoir solution

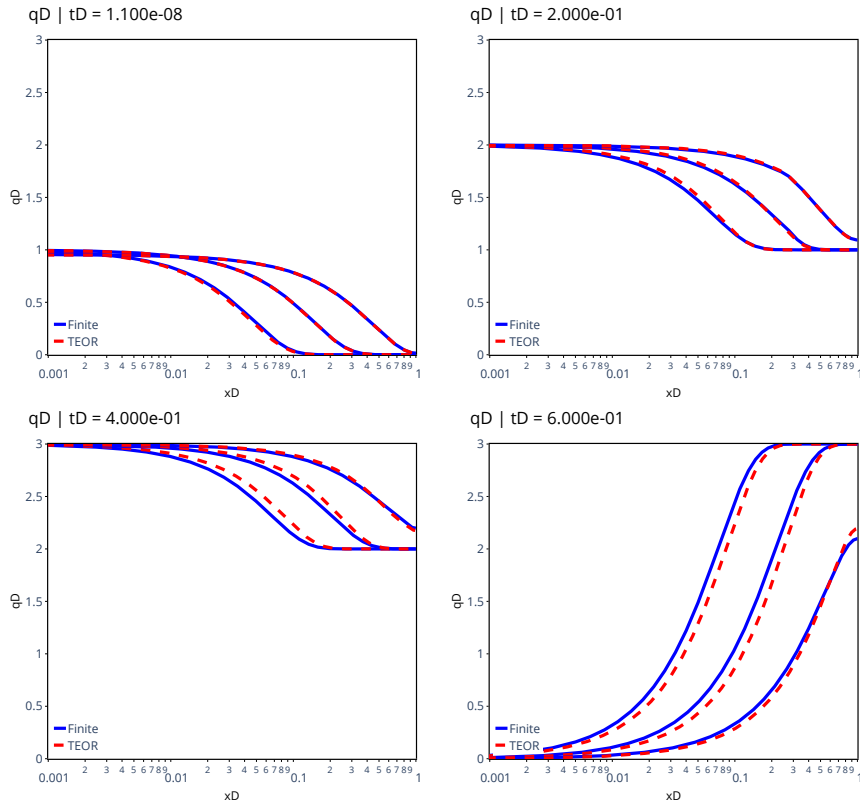


Figure 10: Numerical and analytical flow-rate profile comparison for  $\Delta t_D = 1 \times 10^{-8}$ ,  $\Delta t_D = 1 \times 10^{-7}$  and  $\Delta t_D = 1 \times 10^{-6}$  after each flow-rate change considering the finite reservoir solution

285      Once we have calculated both  $\lambda_{TD}$  and  $q_D$  profiles, we are able to evaluate the Equation 11 and calculate the pressure in the inlet face (Figure 11). As expected, both solution agrees because this case satisfies both Hypothesis 1 and 2. The breakthrough time ( $t_D^{BT}$ ) can be well identified in the pressure plot because of the pressure rate changing.

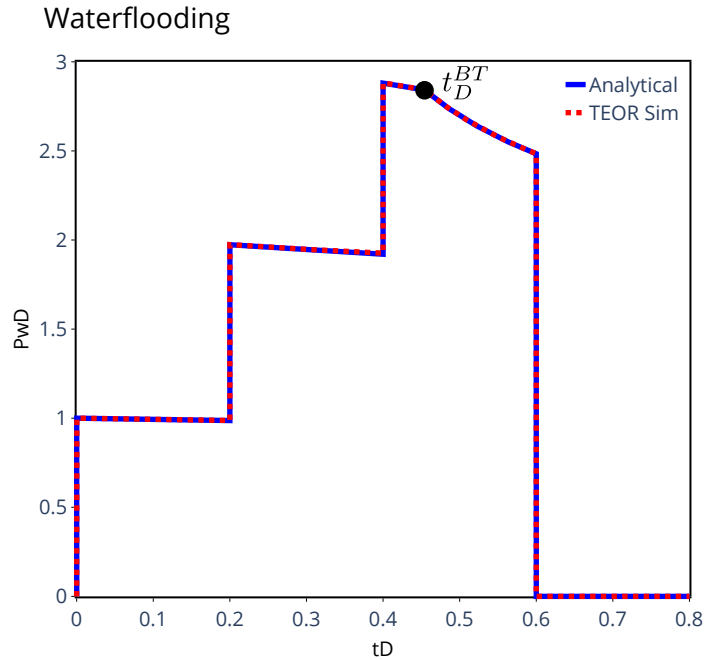


Figure 11: Numerical and analytical pressure in the inlet face ( $P_{wD}$ ) for the finite reservoir solution

290 *4.1. Well-Test Analysis*

To analyze the results of a well-test using the finite reservoir solution we will try to use the derivative technique using the same equivalent time definition that we used in infinity case (Equation 51). However, if we compare the  $\frac{dP_{wD}}{d\log(t_{eDt})}$  for each test period we conclude that we cannot use the same approach. This is more evident if we compare the falloff period with the analytical single-phase solution.

Thus, to interpret tests where the reservoir limit interferes the solution we have two options: analyze only the initial times of data (period where the infinity approach is valid), or if it is not possible, we need to solve an inverse problem matching experimental and the pressure solution given by Equation 11.

300

### Finite PwD Linear Waterflooding

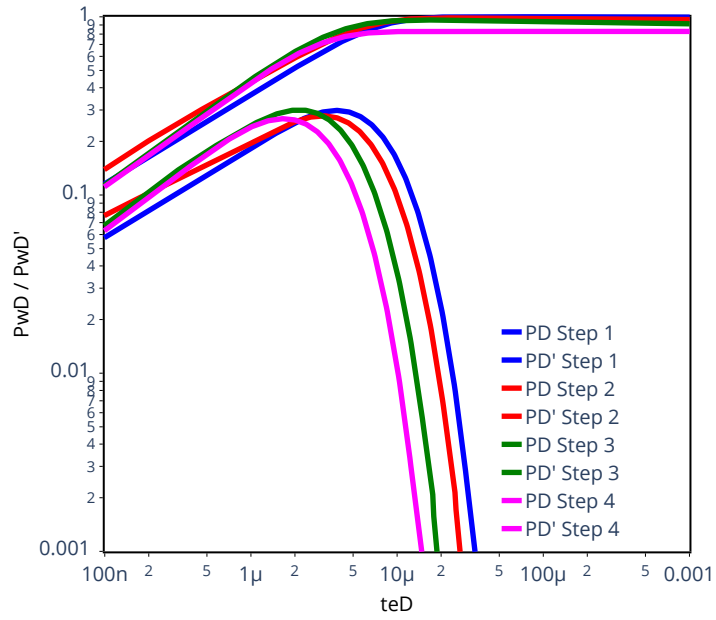


Figure 12:  $P_{wD}$  and  $\frac{dP_{wD}}{d\log(teD)}$  for the finite reservoir solution

### Finite PwD Linear Waterflooding

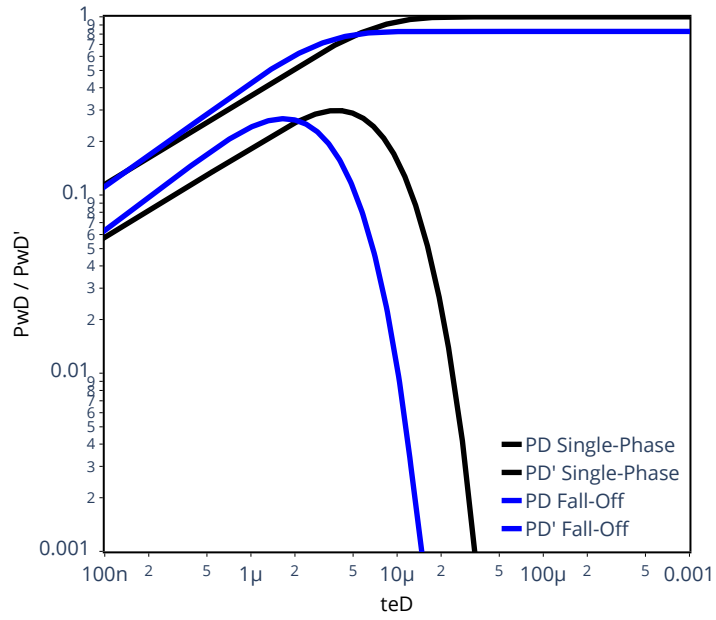


Figure 13:  $P_{wD}$  and  $\frac{dP_{wD}}{d\log(teD)}$  for the finite reservoir solution compared with the single-phase linear solution

## 5. Sensitivity Analysis

In order to analyze the quality of the approximate solution, we made a sensitivity analysis comparing the stability parameters and the error between numerical and analytical solutions. The base case is the finite model, generated using properties described in Tables 2, 4 and Schedule giving by Table 5.

### 5.1. $\Psi_L^{BL}$ Parameter Analysis

First comparison is fixing all physical properties except the fluid and rock compressibilities, that are multiplied by the same constant, changing the value of  $c_t$ . The Figure 14 shows how the  $\Psi_L^{BL}$  value interfere in the saturation solution. The error was calculated comparing the incompressible analytical (Equation 18) and the compressible numerical solution for  $t_D = 0.4$ . For  $\Psi_L^{BL} < 0.1$ , the incompressible saturation profile is an excellent approximation for the compressible problem. For comparison purposes the saturation profile was plotted for two different  $\Psi_L^{BL}$  values (Figure 15), in which can be observed that the compressible saturation front becomes slower with the increasing of  $\Psi_L^{BL}$ , generating the deviation in results.

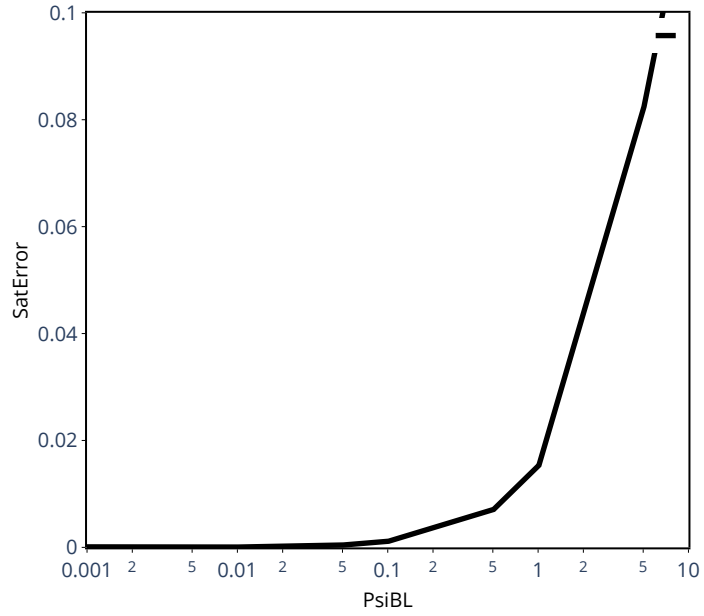


Figure 14:  $\Psi_L^{BL}$  versus the error in saturation solution for the finite case

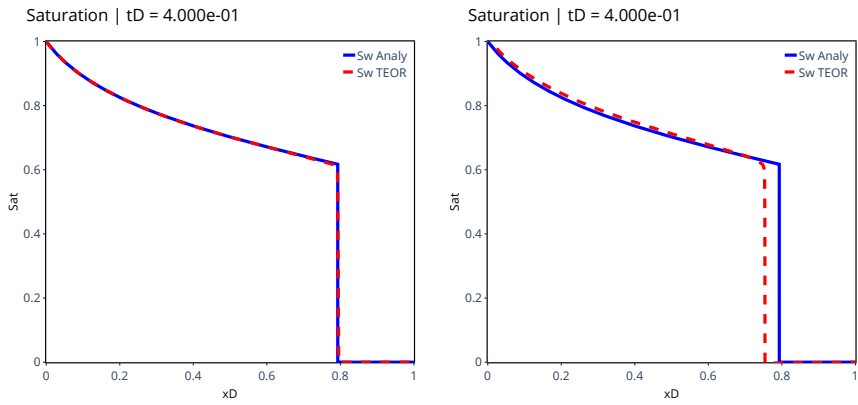


Figure 15: Numerical and analytical saturation profile comparison for  $t_D = 0.4$  and  $\Psi_L^{BL} = 0.01$  and  $\Psi_L^{BL} = 1.0$

### 5.2. $\Psi_L^P$ Parameter Analysis

To analyze the  $\Psi_L^P$  impact in the flow-rate approximation we fixed all properties and changed the starting flow-rate velocity (reference flow-rate  $q_{ref}$ ). To calculate the error we compared the flow-rate profile for  $\Delta t_D = 1 \times 10^{-6}$  after the beginning of the second step ( $t_D = 0.20$ ).

As showed in Figure 16, the  $\Psi_L^P$  approximation produces relative low errors for  $\Psi_L^P < 0.01$ , point where the errors increases fast. The Figure 17 presents the flow-rate profile for two  $\Psi_L^P$  values, in which can be noted that the solution loses accuracy for high  $\Psi_L^P$  values.

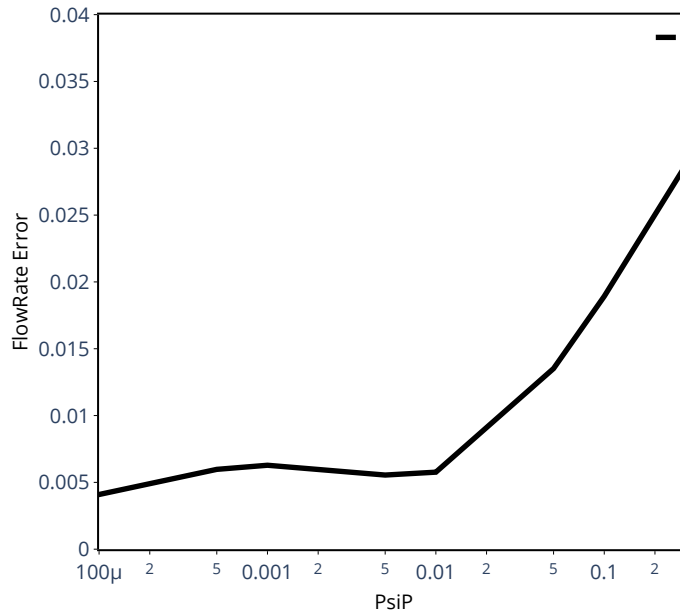


Figure 16:  $\Psi_L^P$  versus the error in flow-rate profile for  $\Delta t_D = 1 \times 10^{-6}$  after  $t_D = 0.2$ , for the finite case

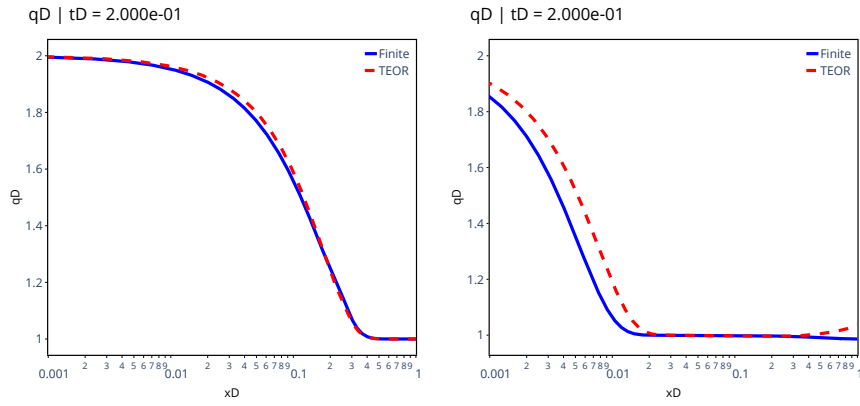


Figure 17: Numerical and analytical flow-rate profile comparison for  $\Delta t_D = 1 \times 10^{-6}$  after  $t_D = 0.2$ , for  $\Psi_L^P = 1 \times 10^{-4}$  and  $\Psi_L^M = 1 \times 10^{-1}$

### 5.3. $\Psi_L^M$ Parameter Analysis

The  $\Psi_L^M$  parameter is related to the average mobility profile assumption in the two-phase zone. To evaluate this we changed the oil viscosity of the base case. The Figure 18 presents the error when compared the numerical and analytical flow-rate profile for  $\Delta t_D = 1 \times 10^{-6}$  after the beginning of the second step ( $t_D = 0.20$ ). Observes that errors start to increase fast after  $\Psi_L^M > 5$ .

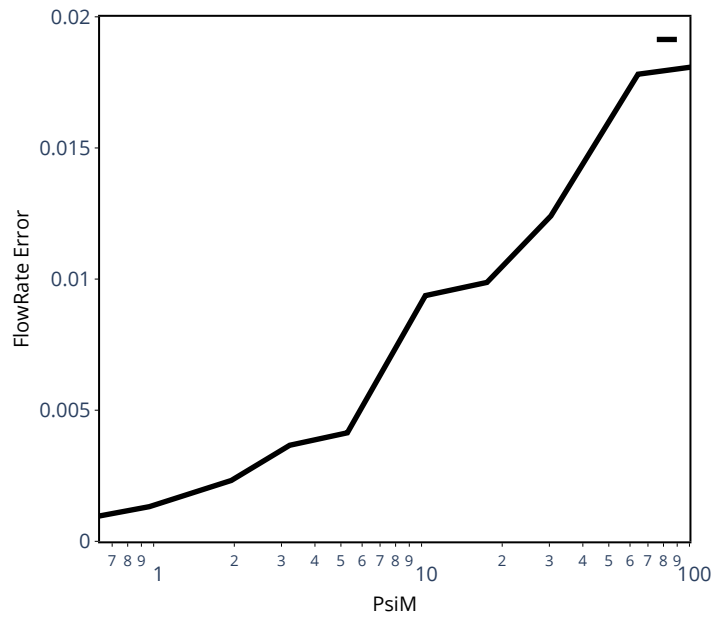


Figure 18:  $\Psi_L^M$  versus the error in flow-rate profile for  $\Delta t_D = 1 \times 10^{-6}$  after  $t_D = 0.2$ , for the finite case

## 6. Conclusions

In this work it has been presented an approximated solution for step variable flow-rate injectivity tests for linear coordinate system. The analytical solution  
335 proposed considers both infinity and finite reservoir extension, with applications in laboratory and field scale experiments. The comparison between numerical and analytical solution shows excellent agreement.

In addition to the presented solution, it was discussed the approximations done during mathematical formulation, creating three dimensionless parameters  
340  $(\Psi_L^{BL}, \Psi_L^P$  and  $\Psi_L^M)$ . Those were studied in an sensitivity analysis, generating a coherent criteria for the solution validity.

## References

- Abbaszadeh, M., Kamal, M., 1989. Pressure-transient testing of water-injection wells. SPE Reservoir Engineering 4, 115–124. URL: <https://doi.org/10.2118/16744-pa>, doi:10.2118/16744-pa.
- 345
- Banerjee, R., Thompson, L., Reynolds, A., 1998. Injection/falloff testing in heterogeneous reservoirs. SPE Reservoir Evaluation & Engineering 1, 519–527. URL: <https://doi.org/10.2118/52670-pa>, doi:10.2118/52670-pa.
- Bratvold, R., Horne, R., 1990. Analysis of pressure-falloff tests following cold-water injection. SPE Formation Evaluation 5, 293–302. URL: <https://doi.org/10.2118/18111-pa>, doi:10.2118/18111-pa.
- 350
- Buckley, S., Leverett, M., 1942. Mechanism of fluid displacement in sands. Transactions of the AIME 146, 107–116. doi:10.2118/942107-g.
- Hazebroek, P., Rainbow, H., Matthews, C., 1958. Pressure fall-off in water injection wells. Transactions of the AIME 213, 250–260. URL: <https://doi.org/10.2118/925-g>, doi:10.2118/925-g.
- 355
- Kazemi, H., Merrill, L., Jargon, J., 1972. Problems in interpretation of pressure fall-off tests in reservoirs with and without fluid banks. Journal of Petroleum Technology 24, 1147–1156. URL: <https://doi.org/10.2118/3696-pa>, doi:10.2118/3696-pa.
- 360
- Lax, P.D., 1957. Hyperbolic systems of conservation laws II. Communications on Pure and Applied Mathematics 10, 537–566. doi:10.1002/cpa.3160100406.
- Oleinik, O.A., 1957. Discontinuous solutions of non-linear differential equations. Uspekhi Matematicheskikh Nauk 12, 3–73.
- 365
- Peres, A.M., Boughrara, A.A., Reynolds, A., 2004. Rate superposition for generating pressure falloff solutions for vertical and horizontal wells, in: SPE Annual Technical Conference and Exhibition, SPE. URL: <https://doi.org/10.2118/90907-ms>, doi:10.2118/90907-ms.

Peres, A.M., Reynolds, A.C., 2003. Theory and analysis of injectivity tests on  
370 horizontal wells. SPE Journal 8, 147–159. URL: [https://doi.org/10.2118/  
84957-pa](https://doi.org/10.2118/84957-pa), doi:10.2118/84957-pa.

Stehfest, H., 1970. Algorithm 368: Numerical inversion of laplace transforms.  
Commun. ACM 13, 47–49.

Thompson, L., Reynolds, A., 1997. Well testing for radially heterogeneous  
375 reservoirs under single and multiphase flow conditions. SPE Formation Eval-  
uation 12, 57–64. URL: <https://doi.org/10.2118/30577-pa>, doi:10.2118/  
30577-pa.

## Appendix A. Flow-Rate Coupling Condition

380 During the flow-rate approximation, we use the continuity of pressure and flow-rate profiles for coupling the equations in the two zones (Equation 37). In this section we will demonstrate these two affirmations.

### Appendix A.1. Proof of Pressure Field Continuity

The pressure profile can be expressed using the Darcy's equation (Equation 385 2) as an integral function:

$$P(x, t) - P_i = \frac{1}{AK} \int_x^{x_s} \frac{q_T(x', t)}{\lambda_T(x', t)} dx' \quad (\text{A.1})$$

Then, if the argument of the integral has a countable set of discontinuities, then the pressure is Riemann integrable and continuous.

### Appendix A.2. Proof of Flow-Rate Continuity

Using the two-phase pressure equation in the dimensional form (Equation 390 31):

$$\frac{\partial \lambda_T \frac{\partial P}{\partial x}}{\partial x} = \frac{\phi c_t}{K} \frac{\partial P}{\partial t} \quad (\text{A.2})$$

Applying the Darcy's equation (Equation 2):

$$\frac{\partial q_T}{\partial x} = -A\phi c_t \frac{\partial P}{\partial t} \quad (\text{A.3})$$

We define the flow-rate in the inlet face, then we can write:

$$q_T(x, t) - q_T^{Inj}(t) = - \int_0^x A\phi c_t \frac{\partial P}{\partial t} dx \quad (\text{A.4})$$

395 For the same arguments of pressure, for the time intervals where  $q_T^{Inj}(t)$  is continuous, the total flow-rate is Riemann integrable and continuous. Observes that this proof is valid only for the total flow-rate, and each phase flow-rate can assume discontinuities, like the Buckley-Leverett shock.

## Appendix B. Flow-Rate Coefficients

The general solution for the PDE's 38-39 in Laplace's domain is giving by:

$$\begin{aligned}\tilde{P}_D(x_D, u) &= A_0 e^{\alpha_L^{2Ph} x_D} + A_1 e^{-\alpha_L^{2Ph} x_D}, \text{ for } x_D < x_D^{BL} \\ \tilde{P}_D(x_D, u) &= A_2 e^{\hat{\alpha}_L x_D} + A_3 e^{-\hat{\alpha}_L x_D}, \text{ for } x_D > x_D^{BL}\end{aligned}\quad (\text{B.1})$$

where  $\alpha_L^{2Ph} = \sqrt{\gamma_L^{2Ph} u}$ ,  $\hat{\alpha}_L = \sqrt{\hat{\gamma}_L u}$ . Substituting the boundary and initial  
400 conditions, we construct the following linear system:

$$\begin{pmatrix} 1 & -1 & 0 & 0 \\ 0 & 0 & e^{\hat{\alpha}_L x_{Ds}} & e^{-\hat{\alpha}_L x_{Ds}} \\ e^{\alpha_L^{2Ph} x_D^{BL}} & e^{-\alpha_L^{2Ph} x_D^{BL}} & -e^{\hat{\alpha}_L x_D^{BL}} & -e^{-\hat{\alpha}_L x_D^{BL}} \\ \frac{\lambda_{TD}^{2Ph} \alpha_L^{2Ph} e^{\alpha_L^{2Ph} x_D^{BL}}}{-\lambda_{TD}^{2Ph} \alpha_L^{2Ph} e^{-\alpha_L^{2Ph} x_D^{BL}}} & -\frac{\lambda_{TD}^{2Ph} \alpha_L^{2Ph} e^{-\alpha_L^{2Ph} x_D^{BL}}}{-\lambda_{TD}^{2Ph} \alpha_L^{2Ph} e^{-\alpha_L^{2Ph} x_D^{BL}}} & -\hat{\alpha}_L e^{\hat{\alpha}_L x_D^{BL}} & \hat{\alpha}_L e^{-\hat{\alpha}_L x_D^{BL}} \end{pmatrix} \begin{pmatrix} A_0 \\ A_1 \\ A_2 \\ A_3 \end{pmatrix} = \begin{pmatrix} -\frac{q_D^{Inj}}{\lambda_{TD}^{2Ph} u \alpha_L^{2Ph}} \\ 0 \\ 0 \\ 0 \end{pmatrix} \quad (\text{B.2})$$

### Appendix B.1. Solution for Infinity System

For the infinity system,  $x_{Ds} \rightarrow \infty$ , and in order to maintain real and limited coefficients,  $A_2 = 0$ . Thus, the coefficients are written by:

$$A_0 = \frac{q_D^{Inj}}{\lambda_{TD}^{2Ph} \alpha_L^{2Ph} u} \left( \frac{(\lambda_{TD}^{2Ph} \alpha_L^{2Ph} - \hat{\alpha}_L) (1 + e^{-2\alpha_L^{2Ph} x_D^{BL}})^2}{2(1 + e^{-2\alpha_L^{2Ph} x_D^{BL}}) [\hat{\alpha}_L + (\hat{\alpha}_L + \lambda_{TD}^{2Ph} \alpha_L^{2Ph}) \cosh(2\alpha_L^{2Ph} x_D^{BL}) - \lambda_{TD}^{2Ph} \alpha_L^{2Ph} e^{-2\alpha_L^{2Ph} x_D^{BL}}]} \right) \quad (\text{B.3})$$

$$A_1 = \frac{q_D^{Inj}}{\lambda_{TD}^{2Ph} \alpha_L^{2Ph} u} \left( \frac{2(\hat{\alpha}_L + \lambda_{TD}^{2Ph} \alpha_L^{2Ph}) (1 + \cosh(2\alpha_L^{2Ph} x_D^{BL}))}{2(1 + e^{-2\alpha_L^{2Ph} x_D^{BL}}) [\hat{\alpha}_L + (\hat{\alpha}_L + \lambda_{TD}^{2Ph} \alpha_L^{2Ph}) \cosh(2\alpha_L^{2Ph} x_D^{BL}) - \lambda_{TD}^{2Ph} \alpha_L^{2Ph} e^{-2\alpha_L^{2Ph} x_D^{BL}}]} \right) \quad (\text{B.4})$$

$$A_2 = 0 \quad (\text{B.5})$$

$$A_3 = \frac{q_D^{Inj}}{\lambda_{TD}^{2Ph} \alpha_L^{2Ph} u} \left( \frac{\lambda_{TD}^{2Ph} \alpha_L^{2Ph}}{e^{-\hat{\alpha}_L x_D^{BL}} ((\hat{\alpha}_L + \lambda_{TD}^{2Ph} \alpha_L^{2Ph}) \cosh(\alpha_L^{2Ph} x_D^{BL}) - \lambda_{TD}^{2Ph} \alpha_L^{2Ph} e^{-\alpha_L^{2Ph} x_D^{BL}})} \right) \quad (\text{B.6})$$

Appendix B.2. Solution for Finite System

405 For finite system,  $x_{Ds} \rightarrow 1$ . The coefficients are written by:

$$A_0 = \frac{q_D^{Inj}}{\lambda_{TD}^{2Ph} \alpha_L^{2Ph} u} \left( \frac{2\overline{\lambda_{TD}^{2Ph}} \alpha_L^{2Ph} \left( e^{-\hat{\alpha}_L x_D^{BL}} - e^{\hat{\alpha}_L (x_D^{BL}-2)} \right) - e^{-\alpha_L^{2Ph} x_D^{BL}} \Omega_L}{2\cosh(\alpha_L^{2Ph} x_D^{BL}) \Omega_L} \right) \quad (\text{B.7})$$

$$A_1 = \frac{q_D^{Inj}}{\lambda_{TD}^{2Ph} \alpha_L^{2Ph} u} \left( \frac{e^{\alpha_L^{2Ph} x_D^{BL}} \Omega_L + 2\overline{\lambda_{TD}^{2Ph}} \alpha_L^{2Ph} \left( e^{-\hat{\alpha}_L x_D^{BL}} - e^{\hat{\alpha}_L (x_D^{BL}-2)} \right)}{2\cosh(\alpha_L^{2Ph} x_D^{BL}) \Omega_L} \right) \quad (\text{B.8})$$

$$A_2 = -\frac{2q_D^{Inj} e^{-2\hat{\alpha}_L}}{u\Omega_L} \quad (\text{B.9})$$

$$A_3 = \frac{2q_D^{Inj}}{u\Omega_L} \quad (\text{B.10})$$

in which:

$$\begin{aligned} \Omega_L = & \left( \hat{\alpha}_L + \overline{\lambda_{TD}^{2Ph}} \alpha_L^{2Ph} \right) \left( e^{(\alpha_L^{2Ph} - \hat{\alpha}_L) x_D^{BL}} + e^{\hat{\alpha}_L (x_D^{BL}-2) - \alpha_L^{2Ph} x_D^{BL}} \right) \\ & + \left( \hat{\alpha}_L - \overline{\lambda_{TD}^{2Ph}} \alpha_L^{2Ph} \right) \left( e^{-(\alpha_L^{2Ph} + \hat{\alpha}_L) x_D^{BL}} + e^{\hat{\alpha}_L (x_D^{BL}-2) + \alpha_L^{2Ph} x_D^{BL}} \right) \quad (\text{B.11}) \end{aligned}$$

**5    *Book Chapter: Approximate  
Analytical Solutions for 1-D  
Immiscible Water-Alternated-Gas***

# Approximate Analytical Solutions for 1-D Immiscible Water-Alternated-Gas

Adolfo P. Pires<sup>a,\*</sup>, Wagner Q. Barros<sup>a</sup>, Alvaro M. M. Peres<sup>a</sup>

<sup>a</sup>*Universidade Estadual do Norte Fluminense Darcy Ribeiro, Brazil*

---

## Abstract

Water-Alternated-Gas (WAG) flooding is largely used as an Enhanced Oil Recovery (EOR) method in oil fields. It is based on the high sweep efficiency of the water phase and the high displacement efficiency of the gas phase. Additionally, other components may be dissolved in both displacing phases, increasing the oil recovery factor and leading to modern WAG schemes such as PWAG (Polymer WAG), MWAG (Miscible WAG), and others. In this chapter we present approximate analytical solutions for the linear immiscible Water-Alternated-Gas problem. The mathematical model is composed by a  $2 \times 2$  system of non-linear hyperbolic Partial Differential Equations (PDE), solved by the Method of Characteristics (MOC) for a set of reservoir properties. The analytical solution is compared with numerical simulation showing the accuracy and robustness of the method under different WAG conditions. The solutions can be used to analyze laboratory WAG experiments or used for screening the best recovery technique for a particular field in a fast and efficient way.

*Keywords:* Enhanced Oil Recovery, Three Phase Flow, Water Alternated Gas

---

## 1. Introduction

The choice of the most suited recovery technique for a particular reservoir depends on reliable fluid-rock data and the economic evaluation of the

---

\*Corresponding author

*Email address:* [adolfo.puime@gmail.com](mailto:adolfo.puime@gmail.com) (Adolfo P. Pires)

possible options. In general, this analysis is performed using numerical and analytical mathematical tools.

Reservoir simulation is a widespread used technique to generate field production forecasts for different scenarios. It is used to optimize the oil recovery as a function of the number of wells, injection and production flow rates, and others (Lin and Poole, 1991). However, numerical simulations are time consuming, and it is not possible to simulate local phenomena and field scale in the same run (Christensen et al., 1998; Li et al., 2003). Another issue is that commercial codes are limited to well established physical problems, which do not fit new challenges. Then, new models must be built, and analytical solutions for simplified problems are used to validate these codes.

One dimensional immiscible, incompressible two-phase flow in porous media for constant initial and boundary conditions is modeled by a hyperbolic partial differential equation, and this problem can be solved by the Method of Characteristics (MOC) (Buckley and Leverett, 1942). Two-phase problems considering capillary and gravitational effects were also solved (Fayers and Sheldon, 1959; Sheldon and Cardwell, 1959), and also including mass exchange between injected gas and reservoir fluid (Johns and Orr, 1996; Bedrikovetsky et al., 2004). Three-phase immiscible problems generate a  $2 \times 2$  system of equations (Bell et al., 1986; Holden, 1990). In general, the solution for these problems considers the simultaneous injection of water and gas as the boundary condition, and the oil saturation at the beginning of the injection as initial condition.

Injection of alternated water and gas slugs in oil reservoirs is one of the most interesting Enhanced Oil Recovery (EOR) techniques. The use of the so called Water-Alternated-Gas (WAG) method can improve oil recovery by up to 20%, depending on fluid and rock characteristics (Sanchez, 1999; Christensen et al., 2001). Several rock and fluid properties, such as rock heterogeneity, natural faults, fluids miscibility, and surface tension, among others, impact the efficiency of this process (Sohrabi et al., 2004; Holtz, 2016).

The mathematical model of the WAG method leads to a variable boundary condition problem. The change of the boundary condition introduces new characteristic waves that interact with the existing ones in the solution domain. Marchesin and Plohr (2001) analyzed the wave structure that appears in the WAG recovery scheme.

In this chapter we propose a simplified method to solve the WAG displacement problem. At the end of each injection step, the saturations are averaged and are considered constant at the beginning of the next step, avoid-

ing the interaction waves problem. Results are generated for different WAG conditions and are compared to numerical solutions with excellent agreement.

Next section presents the mathematical details involved with the WAG problem. The general solution is presented in Section 3, followed by the comparison of the approximate solution in different scenarios. Finally some conclusions are addressed.

## 2. Mathematical Model

The physical problem analyzed in this chapter considers the simultaneous flow of water, oil and gas in an one-dimensional porous medium. Additional hypothesis are:

1. One dimensional isothermal horizontal flow;
2. Homogeneous and incompressible porous medium;
3. Negligible dispersion and capillary effects;
4. No chemical reactions nor components adsorption;
5. Incompressible and constant viscosity phases.

Under these assumptions, the mass conservation of each phase is written as:

$$\frac{\partial S_\pi}{\partial t} + \frac{1}{\phi} \frac{\partial v_\pi}{\partial x} = 0, \text{ for } \pi = w, o, g \quad (1)$$

where  $\phi$  is the rock porosity,  $S_\pi$  and  $v_\pi$  are the phase  $\pi$  saturation and velocity and  $w$ ,  $o$  and  $g$  relate to water, oil and gas phases, respectively. Each phase velocity is calculated using Darcy's equation:

$$v_\pi = -\frac{K k_{r\pi}}{\mu_\pi} \frac{\partial P}{\partial x}, \text{ for } \pi = w, o, g \quad (2)$$

in which  $K$  is the absolute permeability,  $k_{r\pi}$  is the relative permeability of phase  $\pi$  and  $\mu_\pi$  is the phase viscosity. The relation  $\frac{k_{r\pi}}{\mu_\pi}$  is also called the phase mobility  $\lambda_\pi$ . The phase fractional flow function is defined as:

$$f_\pi = \frac{v_\pi}{v_T} = \frac{\lambda_\pi}{\lambda_T} \quad (3)$$

where  $v_T$  and  $\lambda_T$  are the total velocity and total mobility. Then, applying the fractional flow definition in Equation 1 we obtain:

$$\frac{\partial S_\pi}{\partial t} + \frac{v_T}{\phi} \frac{\partial f_\pi}{\partial x} = 0, \text{ for } \pi = w, o, g \quad (4)$$

Equation 4 can be rewritten as a function of the following dimensionless space and time coordinates

$$x_D = \frac{x}{L} \quad (5)$$

$$t_D = \int_0^t \frac{v_T(\tau)}{\phi L (1 - S_{wi} - S_{om})} d\tau \quad (6)$$

to become

$$\frac{\partial S_\pi}{\partial t_D} + \frac{\partial f_\pi}{\partial x_D} = 0, \text{ for } \pi = w, o, g \quad (7)$$

### 2.1. Method of Characteristics

Equation 7 can be solved using the method of characteristics. As the sum of the saturations is one, it is necessary to solve only two equations:

$$\begin{cases} \frac{\partial S_w}{\partial t_D} + \frac{\partial f_w(S_w, S_o)}{\partial x_D} = 0 \\ \frac{\partial S_o}{\partial t_D} + \frac{\partial f_o(S_w, S_o)}{\partial x_D} = 0 \end{cases} \quad (8)$$

or, in matrix form

$$\begin{pmatrix} 1 & 0 \\ 0 & 1 \end{pmatrix} \begin{pmatrix} S_w \\ S_o \end{pmatrix}_{t_D} + \begin{pmatrix} \frac{\partial f_w}{\partial S_w} & \frac{\partial f_w}{\partial S_o} \\ \frac{\partial f_o}{\partial S_w} & \frac{\partial f_o}{\partial S_o} \end{pmatrix} \begin{pmatrix} S_w \\ S_o \end{pmatrix}_{x_D} = \begin{pmatrix} 0 \\ 0 \end{pmatrix} \quad (9)$$

where the  $t_D$  and  $x_D$  subscripts denote partial derivatives. The system eigenvalues are calculated by:

$$\lambda^\pm = \frac{1}{2} \left( \frac{\partial f_w}{\partial S_w} + \frac{\partial f_o}{\partial S_o} \right) \pm \frac{1}{2} \sqrt{\left( \frac{\partial f_w}{\partial S_w} - \frac{\partial f_o}{\partial S_o} \right)^2 + 4 \left( \frac{\partial f_w}{\partial S_o} \frac{\partial f_o}{\partial S_w} \right)} \quad (10)$$

in which  $\lambda^+$  and  $\lambda^-$  are called fast and slow eigenvalues.

### 2.1.1. Rarefaction Waves

System 9 can be rewritten as a function of a self-similar independent variable  $\xi = x_D/t_D$ :

$$\begin{pmatrix} \frac{\partial f_w}{\partial S_w} - \xi & \frac{\partial f_w}{\partial S_o} \\ \frac{\partial f_o}{\partial S_w} & \frac{\partial f_o}{\partial S_o} - \xi \end{pmatrix} \begin{pmatrix} \frac{\partial S_w}{\partial \xi} \\ \frac{\partial S_o}{\partial \xi} \end{pmatrix} = \begin{pmatrix} 0 \\ 0 \end{pmatrix} \quad (11)$$

This independent variable is an eigenvalue of the system and the continuous part of the solution (rarefaction waves) can be found solving the following system:

$$\frac{d\vec{S}}{d\xi} = \vec{r}_{\pm} \quad (12)$$

where  $\vec{r}_{\pm}$  are the fast and slow right-eigenvector of the Jacobian matrix. Note that the fast and slow rarefaction solutions are also given by the following equations:

$$\left( \frac{dS_w}{dS_o} \right)^{\pm} = - \frac{\frac{\partial f_w}{\partial S_o}}{\left( \frac{\partial f_w}{\partial S_w} - \lambda^{\pm} \right)} \quad (13)$$

### 2.1.2. Shock Waves

This system of equations also admits discontinuous solutions that must conserve mass:

$$\begin{cases} \sigma (S_w^L - S_w^R) = (f_w^L - f_w^R) \\ \sigma (S_o^L - S_o^R) = (f_o^L - f_o^R) \end{cases} \quad (14)$$

This system is known as Rankine-Hugoniot conditions, where  $\sigma$  is the shock speed, and superscripts  $L$  and  $R$  denote left and right shock conditions, respectively.

### 2.1.3. Numerical Solution Method

The analytical solutions developed in this chapter are compared with a numerical first order explicit method (LeVeque et al., 2002). To minimize numerical diffusion issues, all runs were performed using the condition  $CFL = 0.1$  and the spatial domain composed by 10.000 cells.

### 3. Approximate Analytical Solution

In this section we describe the approximate analytical solution of the Water-Alternated-Gas problem. The relative permeability for each phase is calculated using the modified Stone I model (Stone, 1970; Aziz and Settari, 1979):

$$\begin{cases} k_{rw} = k_{rw}(S_w) \\ k_{ro} = k_{ro}(S_w, S_o, S_g) = (1 - S_{wi} - S_{om}) \frac{S_o - S_{om}}{k_{ro}^{S_{wi}}} \left( \frac{k_{ro}^w}{1 - S_w - S_{om}} \right) \left( \frac{k_{ro}^g}{1 - S_g - S_{wi} - S_{om}} \right) \\ k_{rg} = k_{rg}(S_g) \end{cases} \quad (15)$$

where  $S_{wi}$  is the irreducible water saturation,  $S_{om}$  is the lowest oil residual saturation determined from waterflooding and gasflooding experiments ( $S_{om} = \min(S_{or}^w, S_{or}^g)$ ); and  $k_{ro}^w$  and  $k_{ro}^g$  are the relative permeability from waterflooding and gasflooding experiments. Note that the oil relative permeability depends on the saturations of all phases. The waterflooding and gasflooding two-phase relative permeability are calculated using a power law model (Corey et al., 1956):

$$\begin{cases} k_{rw} = k_{rw}^{S_{or}^w} \left( \frac{S_w - S_{wi}}{1 - S_{wi} - S_{or}^w} \right)^{n_w} \\ k_{ro}^{w|g} = k_{ro}^{S_{wi}} \left( \frac{S_o - S_{or}^{w|g}}{1 - S_{wi} - S_{or}^{w|g}} \right)^{n_o^{w|g}} \\ k_{rg} = k_{rg}^{S_{or}^g} \left( \frac{S_g}{1 - S_{wi} - S_{or}^g} \right)^{n_g} \end{cases} \quad (16)$$

in which the terms  $k_{rw}^{S_{or}^w}$ ,  $k_{ro}^{S_{wi}}$  and  $k_{rg}^{S_{or}^g}$  are the water, oil and gas relative permeabilities calculated at the points  $S_{or}^w$ ,  $S_{wi}$  and  $S_{or}^g$ . Note that for the region where  $S_o \in (S_{or}^w, S_{or}^g)$  the water relative permeability curve is linearly extrapolated using the point  $k_{rw}(S_w = 1) = 1$ . Figures 1 and 2 show the two and three phase relative permeability curves calculated with the data shown in Table 1. All cases run in this section use the water, oil and gas viscosity equal to  $\mu_w = 1.0$ ,  $\mu_o = 2.0$  and  $\mu_g = 0.05$ .

Table 1: Corey's parameters used in the Base Case simulations.

Waterflooding	Gasflooding
$S_{wi} = 0.20$	$S_{wi} = 0.20$
$k_{ro}^{S_{wi}} = 0.80$	$k_{ro}^{S_{wi}} = 0.80$
$S_{or}^w = 0.40$	$S_{or}^g = 0.20$
$k_{rw}^{S_{or}^w} = 0.40$	$k_{rg}^{S_{or}^g} = 0.80$
$n_w = 2.20$	$n_g = 1.80$
$n_o^w = 2.00$	$n_o^g = 2.10$

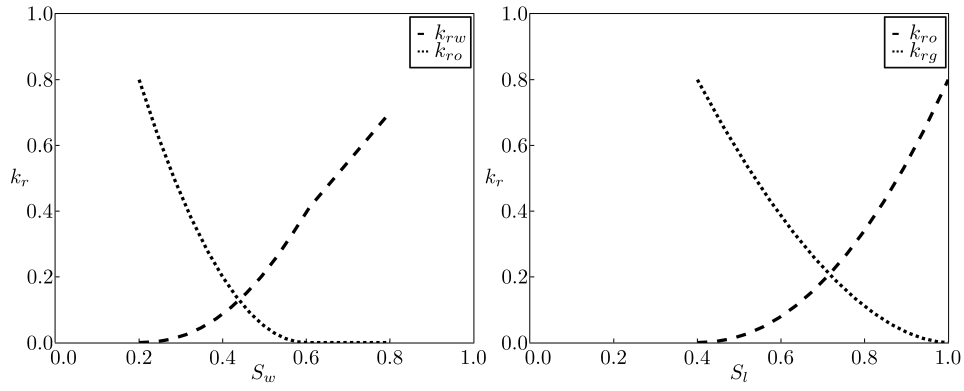


Figure 1: Water-Oil and Gas-Oil relative permeability curves

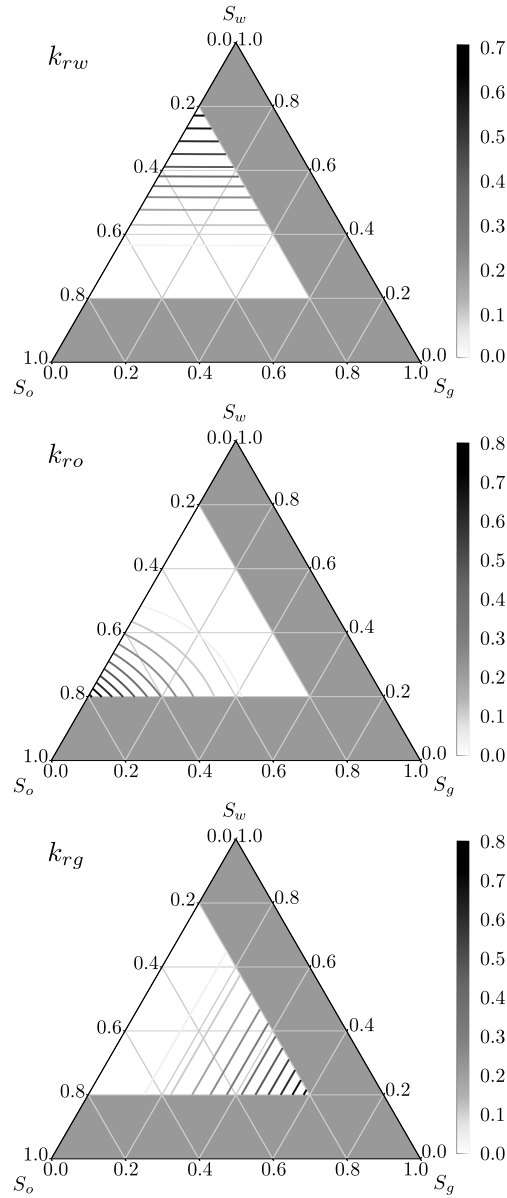


Figure 2: Three phase relative permeability curves

The residual oil saturation depends on the injected fluid along the WAG displacement process. As a consequence, the integral curves also change (Figure 3). In this figure the arrows point toward the associated eigenvalue

increasing direction. For the fast integral curves, there are three points where the curves collapse:  $I = (S_w, S_o, S_g) = (S_{wi}, 1 - S_{wi}, 0)$ ,  $J_w = (S_w, S_o, S_g) = (1 - S_{or}^w, S_{or}^w, 0)$  and  $J_g = (S_w, S_o, S_g) = (S_{wi}, S_{or}^g, 1 - S_{wi} - S_{or}^g)$ . Figure 4 expands the region around  $J_w$ . Initial reservoir saturation is denoted by  $I$ , where there is only oil at irreducible water saturation. Points  $J_w$  and  $J_g$  are the injection boundary condition when  $S_o > \max(S_{or}^w, S_{or}^g)$ . One may note that in the region where  $S_o \in (S_{or}^w, S_{or}^g)$ , the fast integral curves are parallel to the  $\overline{S_w S_g}$  edge in the region near to the water vertex.

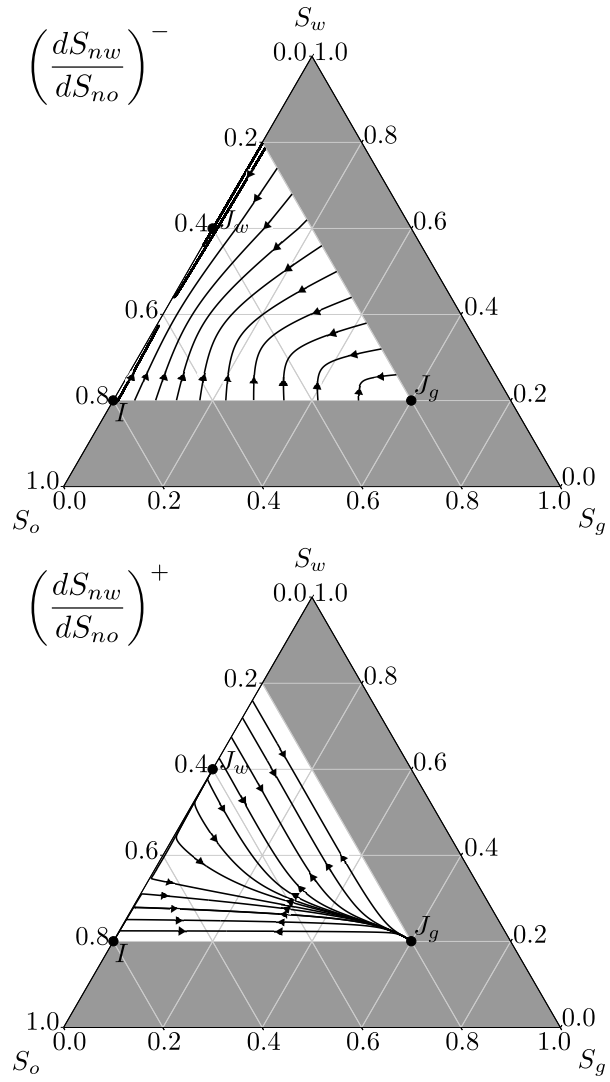


Figure 3: Slow and fast integral curves for data shown in Table 1

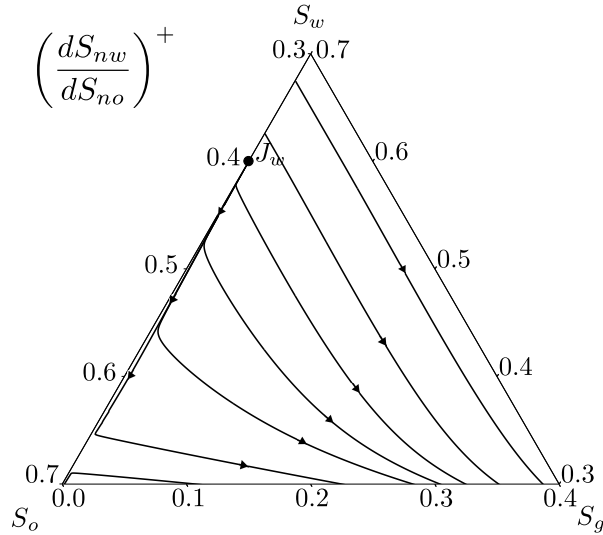


Figure 4: Detail of the fast integral curve around  $J_w$  for data shown in Table 1

To solve the complete WAG problem, every time the boundary condition is changed a new wave interacts with the waves in the solution, generating a new Riemann problem for each interaction (Rhee et al., 1970). To overcome this limitation we propose a simplified method where at the end of each injection step of the WAG cycle we calculate the average saturation in the porous medium and start a new initial-boundary value problem. This new problem is divided in two different cases based on the average oil saturation  $\bar{S}_o$ .

### 3.1. Solution for $\bar{S}_o > \max(S_{or}^w, S_{or}^g)$

For the case when  $\bar{S}_o > \max(S_{or}^w, S_{or}^g)$ , the injection condition will be either the  $J_w$  or the  $J_g$  point. In this example we consider that the first injected fluid of the WAG cycle is water. So, the initial and boundary conditions are given by:

$$\begin{cases} I^{1st} = I = (S_{wi}, 1 - S_{wi}, 0) \\ J^{1st} = J_w = (1 - S_{or}^w, S_{or}^w, 0) \end{cases} \quad (17)$$

The solution for this first step is composed by a rarefaction wave followed by a shock wave (Figure 5). In the left plot of this figure the dashed lines are a continuous rarefaction fan and the solid line is a shock. This solution

is also known as a fast composite wave because the shock speed is equal to the last rarefaction fast eigenvalue. Figure 6 shows the saturation profile for three different times after the beginning of the water injection, compared to a numerical solution. For this particular problem the WAG steps last  $t_D = 1.0$ . Note that the water breakthroughs after  $t_D = 0.55$ , and at the end of the injection step the saturation profile is a smooth curve. The saturation trajectory can be seen in the ternary plot (Figure 5), where the minimum water saturation is approximately  $S_w = 0.48$ , given by the left shock condition.

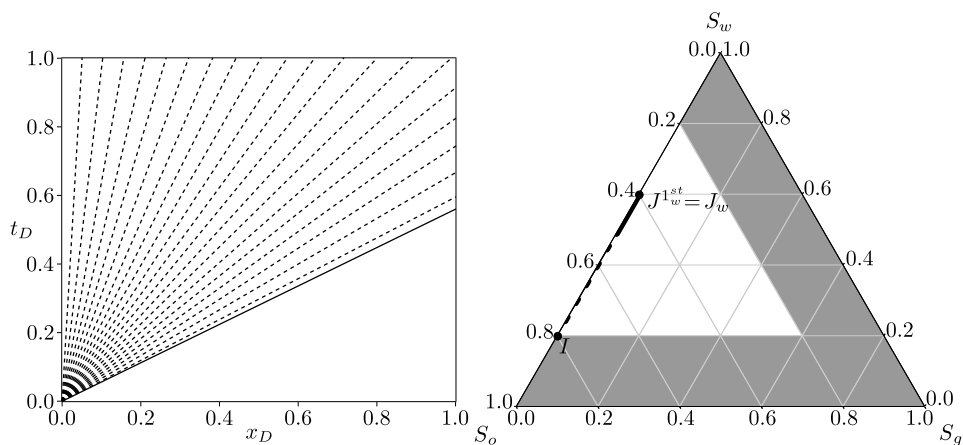


Figure 5: Characteristic diagram and saturation path for the first water injection step for the Base Case

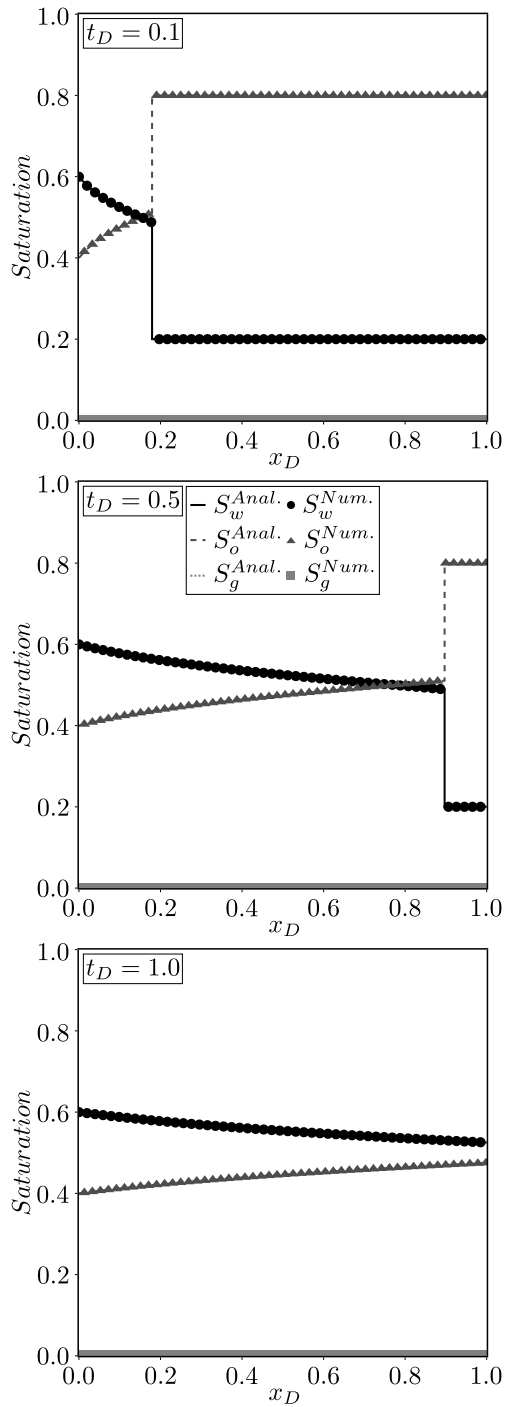


Figure 6: Saturation profile for the first water injection step for the Base Case

At the end of the water step the saturations spatial average are determined and the first gas injection step starts with the following conditions:

$$\begin{cases} I_g^{1st} = (0.5566, 0.4434, 0.0000) \\ J_g^{1st} = J_g = (S_{wi}, S_{or}^g, 1 - S_{or}^g) \end{cases} \quad (18)$$

where  $\bar{S}_o > S_{or}^w$ . The solution is given by a fast composite wave starting at  $J_g$  (Figures 7 and 8). The gas mobility is greater than the water mobility ( $\lambda_g > \lambda_w$ ) leading to a faster gas breakthrough. For this data set the oil residual saturation for gasflooding experiments is smaller than for waterflooding, increasing the recoverable oil during the gas step.

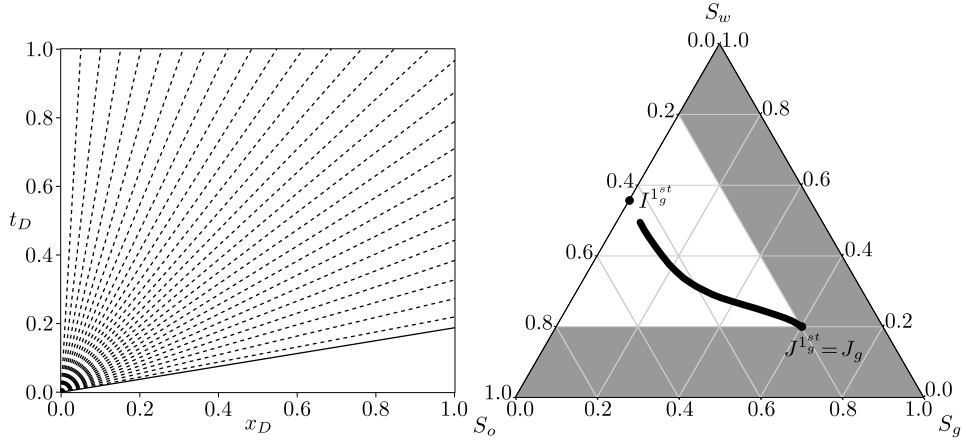


Figure 7: Characteristic diagram and saturation path for the first gas injection step for the Base Case

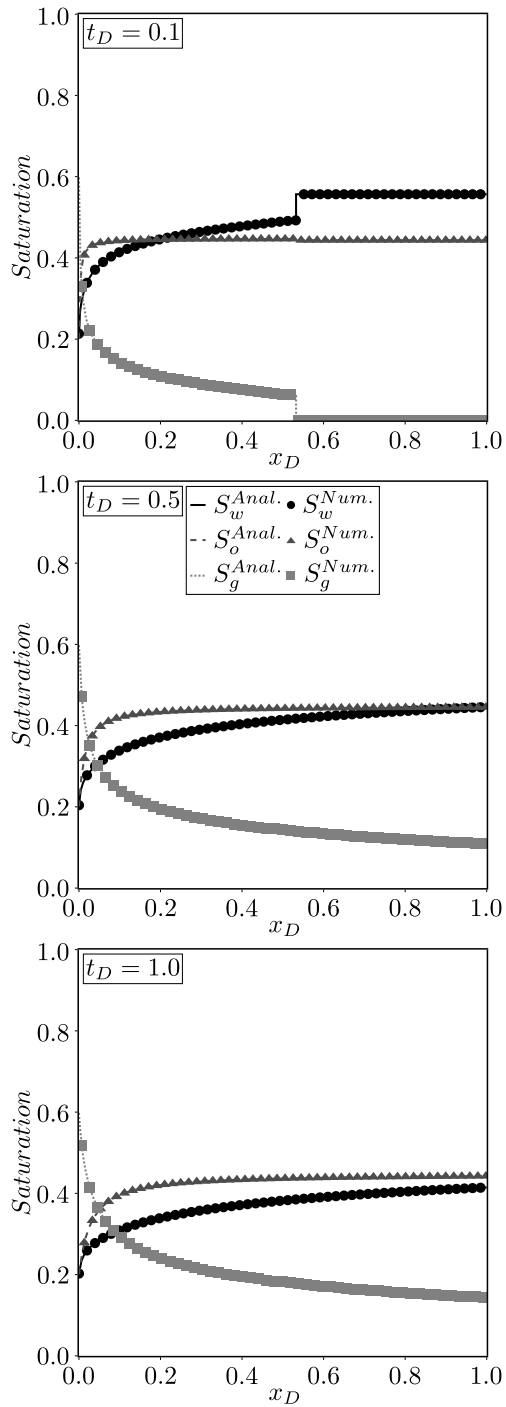


Figure 8: Saturation profile for the first gas injection step for the Base Case

After the gas injection step the saturations are averaged and the second WAG cycle starts:

$$\begin{cases} I_w^{2nd} = (0.3694, 0.4246, 0.2060) \\ J_w^{2nd} = J_w = (1 - S_{or}^w, S_{or}^w, 0) \end{cases} \quad (19)$$

Note that at the start of the second water step  $\bar{S}_o > S_{or}^w$  and the injection condition is given by  $J_w$ . Figures 9 and 10 show the characteristic diagram and the saturation profile for this injection step. The new water breakthrough is slower than the one for the gas cycle but is faster than the one for pure waterflooding, stressing the gas injection effect in the solution profile.

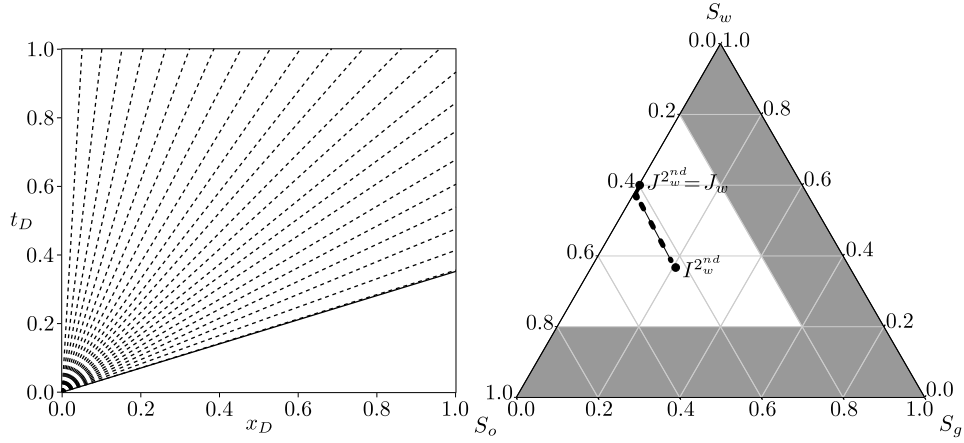


Figure 9: Characteristic diagram and saturation path for the second water injection step for the Base Case

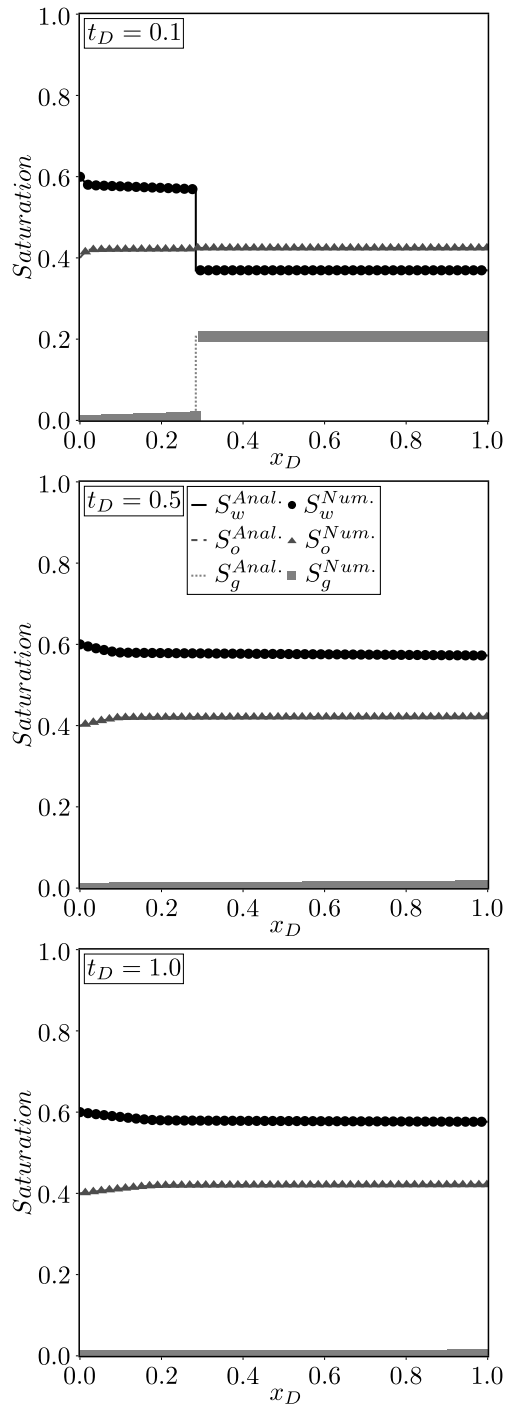


Figure 10: Saturation profile for the second water injection step for the Base Case

### 3.2. Solution for $\bar{S}_o < \max(S_{or}^w, S_{or}^g)$

Usually the residual oil saturation for waterflooding is greater than for gasflooding. As a consequence, a water injection step may start at a condition where  $\bar{S}_o < \max(S_{or}^w, S_{or}^g)$ . The water injection condition for this case ( $J_w^*$ ) is the point in the  $\bar{S}_w\bar{S}_o$  edge in which  $J_w^* = (1 - \bar{S}_o, \bar{S}_o, 0)$ .

Using the Base Case as example, at the beginning of the fourth WAG cycle,  $\bar{S}_o < S_{or}^w$ . The initial and boundary conditions for this cycle are given by:

$$\begin{cases} I_w^{4th} = (0.3895, 0.3955, 0.2150) \\ J_w^{4th} = J_w^* = (1 - \bar{S}_o, \bar{S}_o, 0) \end{cases} \quad (20)$$

Figures 11 and 12 show the solution for this particular case. The solution structure is composed by a fast composite wave. Analyzing the saturation profile, we can observe that this water step cannot extract any additional oil from the reservoir, however it is still important because the gas saturation decreases, and the next gas step can recover additional oil.

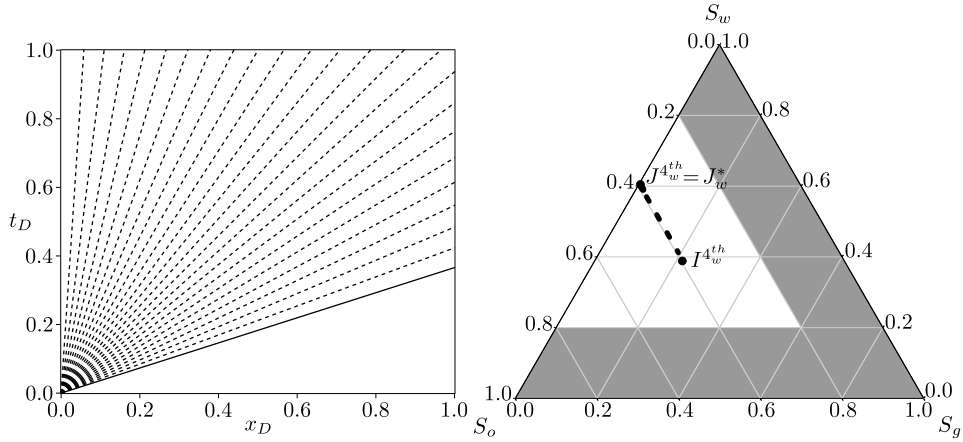


Figure 11: Characteristic diagram and saturation path for the fourth water injection step for the Base Case

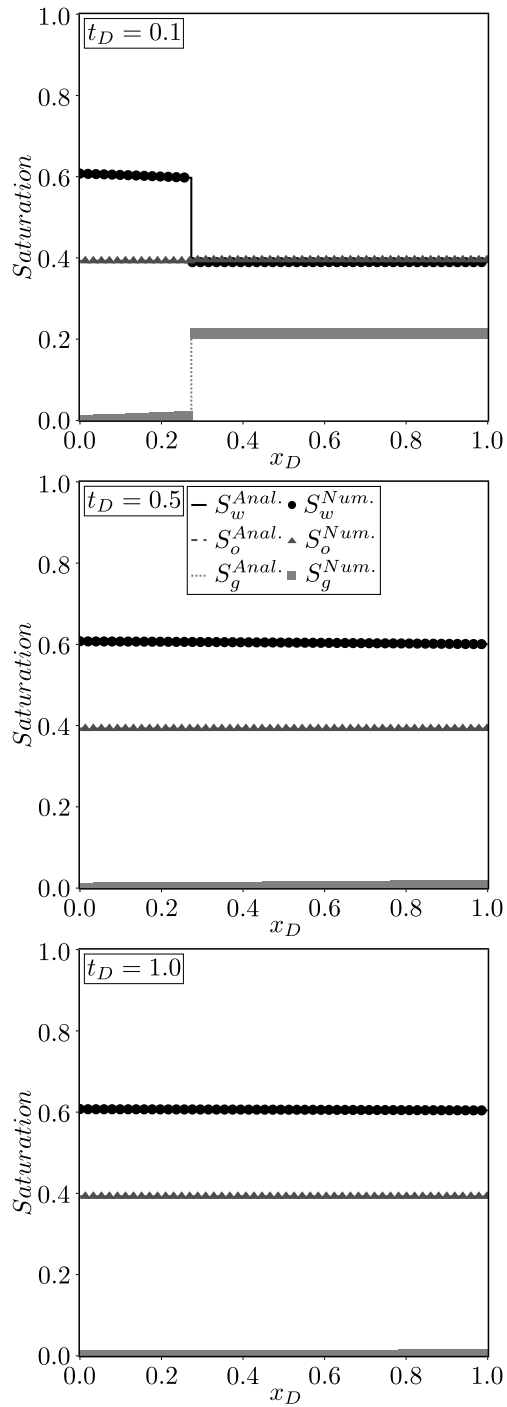


Figure 12: Saturation profile for the fourth water injection step for the Base Case

#### 4. Approximate Solution Validation

In this section we evaluate the proposed approximate analytical solution comparing it with numerical results. Figure 13 presents the accumulated production of each phase after two WAG cycles for the case presented in previous section, denoted Base Case. The difference of the accumulated oil recovery between the approximate proposed solution and the numerical solution is  $-0.0162\%PV$  (Pore Volume). Figure 14 shows the saturation profile at the end of each injection step.

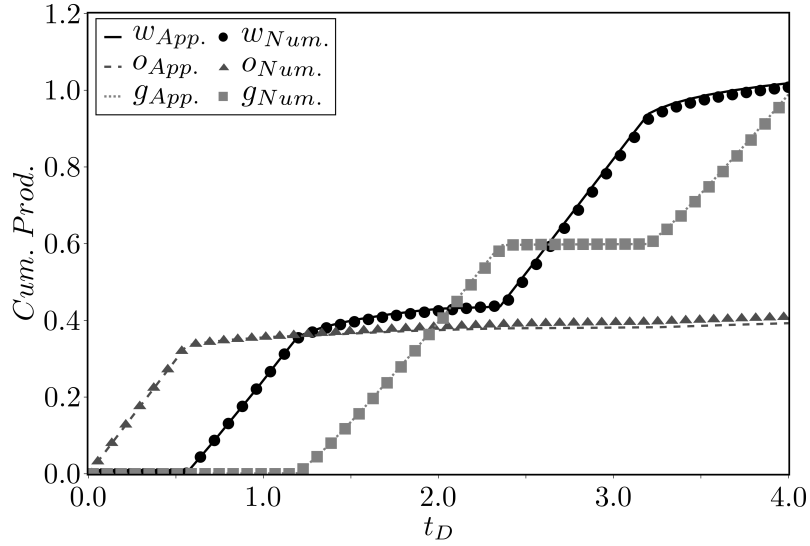


Figure 13: Accumulated production of each phase for the Base Case

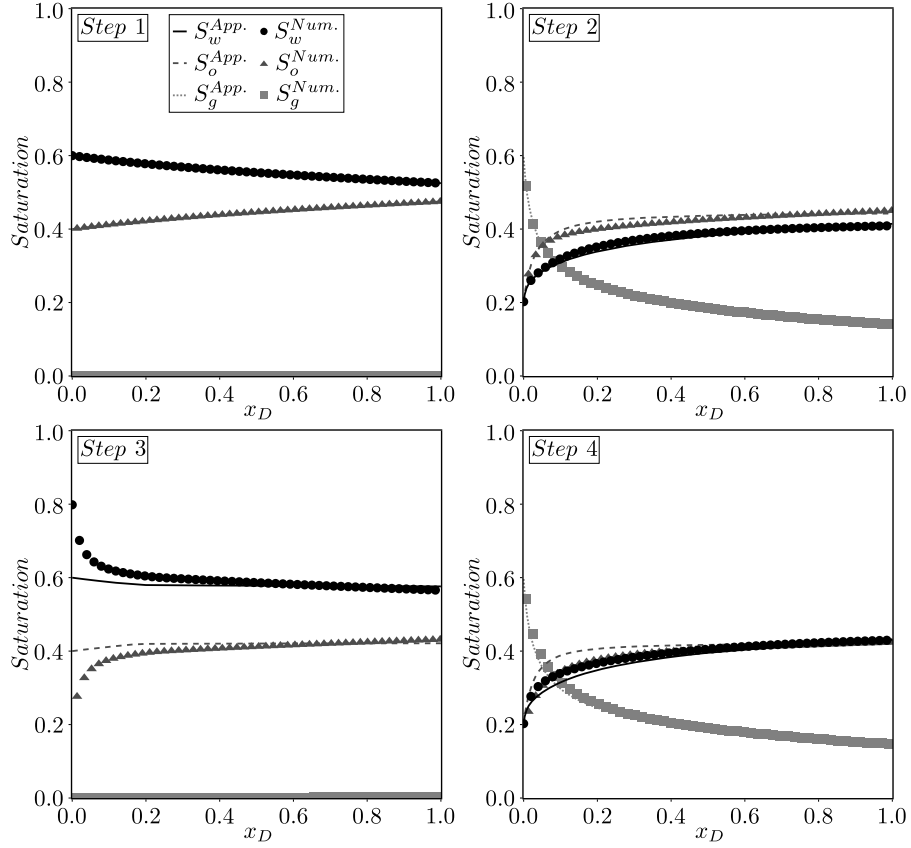


Figure 14: Saturation profile after each injection step for the Base Case

The Base Case solution was also developed considering the WAG process starting with gas injection (Figure 15). For this case the oil recovery was approximately 1% smaller at the end of the second cycle. The difference between the approximate and the numerical solutions for the oil recovery was  $-0.0191\%PV$ .

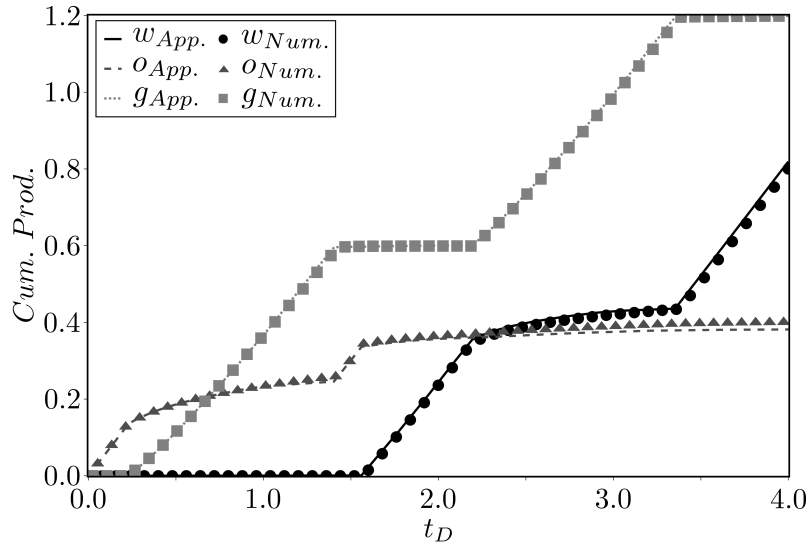


Figure 15: Accumulated production of each phase for the Base Case starting with gas injection

#### 4.1. Sensitivity analysis for injection time and number of WAG cycles

The approximate solution depends on the saturation averaging, which is highly influenced by the water and gas volumes injected, or the dimensionless injection time for each step. Figure 16 presents the accumulated production after two WAG cycles for two different injection times,  $t_D = 0.16$  and  $t_D = 4.00$ . For the smaller injection time the analytical solution does not present good results because the saturation profile is not smooth (Figure 17).

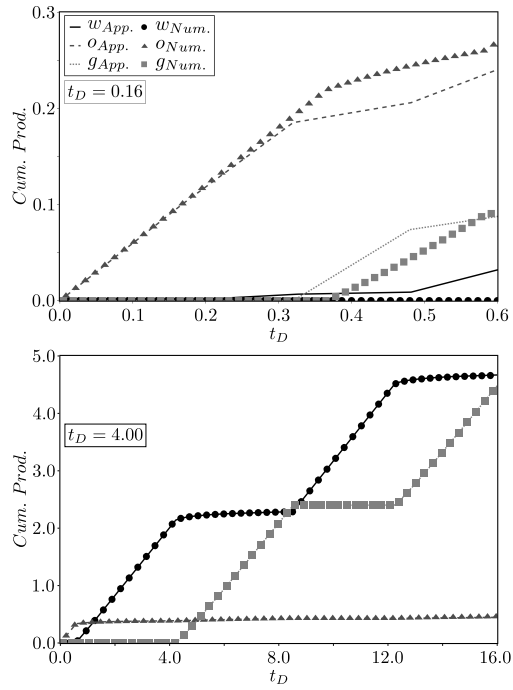


Figure 16: Accumulated production of each phase for the Base Case after two WAG cycles for injection time  $t_D = 0.16$  and  $t_D = 4.00$

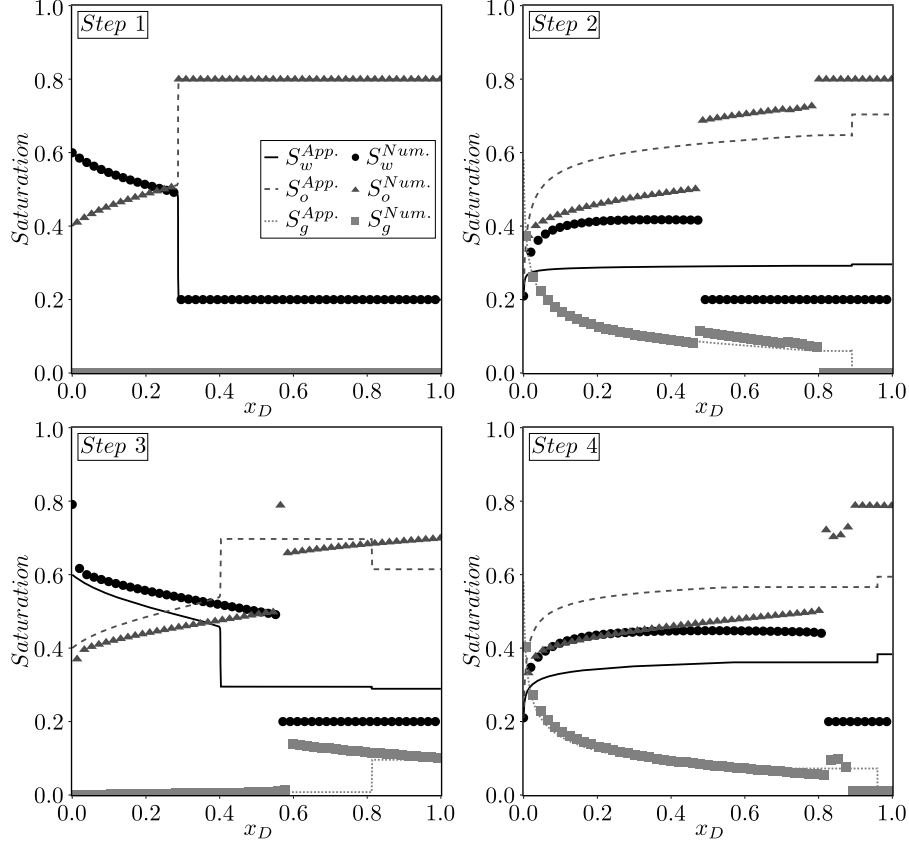


Figure 17: Saturation profile after each injection step for the Base Case with injection time  $t_D = 0.16$

We define oil recovery difference between our approximate and numerical solution as relative cumulative oil error ( $e = 1 - \frac{OR^{Anal.}}{OR^{Num.}}$ ), where  $OR^{Anal.}$  and  $OR^{Num.}$  are the oil recovery at the end of the last injection step calculated with the analytical and numerical methods. Figure 18 presents this error after two WAG cycles for different injection times. For very small injection times the error is also small because there is no injected fluids breakthrough and only oil is produced. As injection time increases the error also increases because the average saturation is not a good approximation for the WAG problem. However, after the injection time is long enough to the breakthrough of all phases (approximately  $t_D = 0.5$  for this particular case), the relative error decreases and the approximate solution becomes an excellent

tool to model the WAG injection problem.

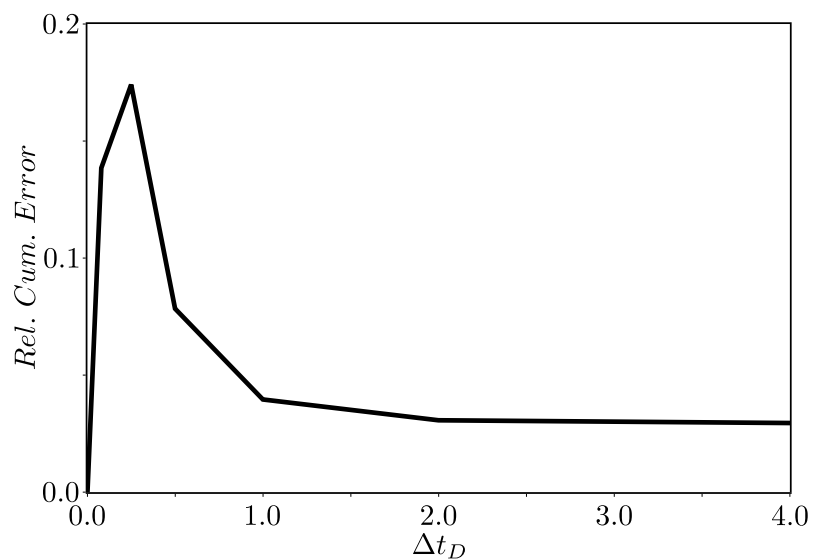


Figure 18: Oil recovery relative error between analytical and numerical solution after two WAG cycles for different injection times

Figure 19 presents oil recovery relative error as a function of the number of injection steps for four different injection times. Note that for all cases the marginal error decreases with the increase in the number of steps. For short injection times the first injection steps present greater errors, because of the sharp discontinuities in the saturation solution.

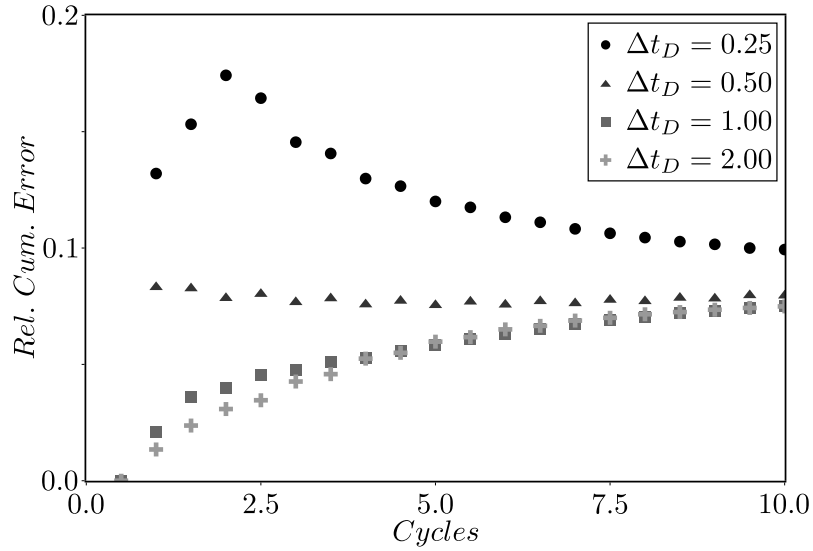


Figure 19: Oil recovery relative error between analytical and numerical solution for different number of WAG cycles

#### 4.2. Sensitivity analysis for the injected mobility ratio

Water and gas phases present different physical properties and interact with oil in different ways during immiscible displacement. Water phase is more viscous than gas phase, while oil residual saturation for a gasflooding is much smaller than for a waterflooding. We evaluate how the gas-water relative mobility ratio ( $\frac{\lambda_g}{\lambda_w}$ ) changes the results of the Base Case (Figure 20).

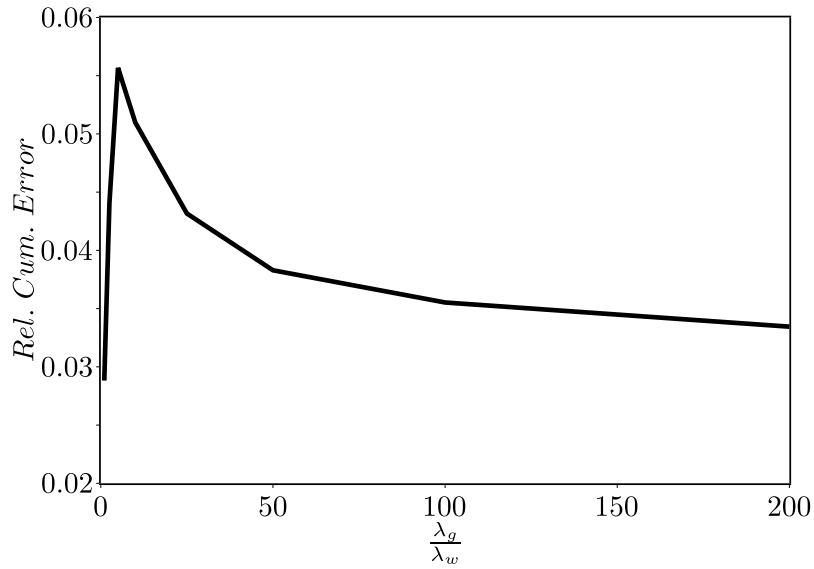


Figure 20: Effect of the gas-water relative mobility ratio ( $\frac{\lambda_g}{\lambda_w}$ ) on the oil recovery relative error

When  $\frac{\lambda_g}{\lambda_w} = 1$  the error of the approximate solution is small, because the saturation profile is well approximated by its average (Figure 21). As the relative mobility increases the error also increases, because of the difference in the saturation profiles (Figure 22). However, this effect reaches a maximum because as the gas mobility is increased, the gas breakthrough is decreased, which improves the solution quality.

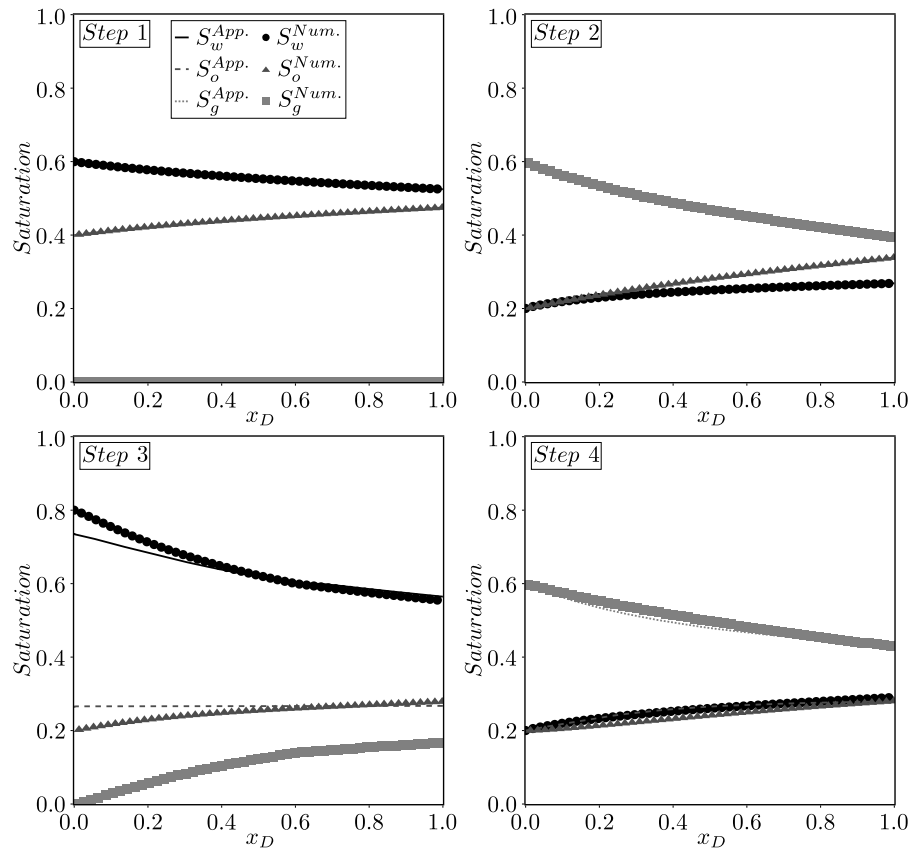


Figure 21: Saturation profile after each injection step for the Base Case for  $\frac{\lambda_g}{\lambda_w} = 1$

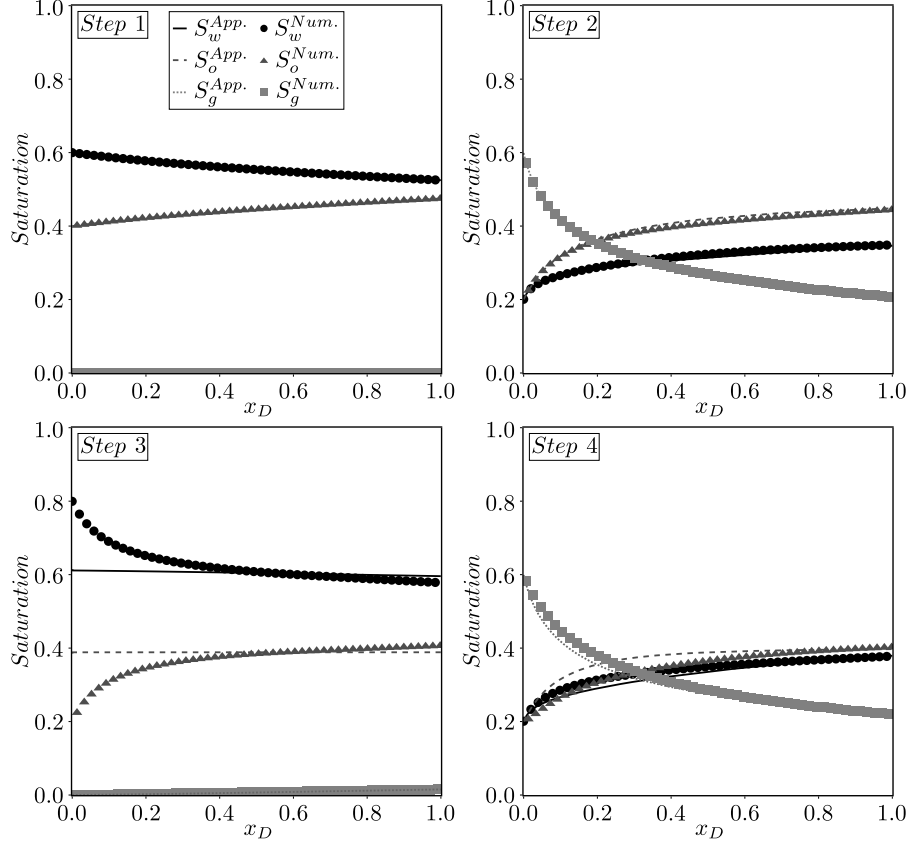


Figure 22: Saturation profile after each injection step for the Base Case for  $\frac{\lambda_g}{\lambda_w} = 10$

## 5. Conclusion

In this chapter we present an approximate analytical solution for the Water Alternated Gas (WAG) method of oil recovery. The mathematical model was based on the assumption of one-dimensional immiscible, incompressible, isothermal three-phase flow in porous media. The conservation laws for each phase leads to a  $2 \times 2$  system of hyperbolic partial differential equations, solved by the method of characteristics for a set of reservoir properties and relative permeability curves. It was considered that the residual oil saturation was different for waterflooding and gasflooding. At the end of each injection step, the saturations were averaged and considered constant along the porous media at the beginning of the following step, generating a new initial boundary

value problem with constant saturation, avoiding the necessity to solve wave interactions problems. The analytical solution was compared to the results of a numerical simulator with excellent agreement. Injection time, number of injection cycles and gas-water mobility ratio were changed to evaluate the robustness of the proposed technique. It was shown that the approximate solution is as good as the saturation profile can be approximated by its average. Larger WAG cycles led to better results, mainly after the injected fluids breakthrough.

### Acknowledgements

This research was financed in part by the Coordenação de Aperfeiçoamento de Pessoal de Nível Superior - Brasil (CAPES) - Finance Code 001. Alvaro Peres acknowledges the Universidade Estadual do Norte Fluminense Darcy Ribeiro (UENF) for financial support.

### References

- Aziz, K., Settari, A., 1979. Petroleum reservoir simulation. Applied Science Publishers.
- Bedrikovetsky, P., Shapiro, A., Pires, A., 2004. New analytical solutions for 1-d multicomponent gas injection problems, in: Abu Dhabi International Conference and Exhibition, Society of Petroleum Engineers. URL: <https://doi.org/10.2118/88760-ms>, doi:10.2118/88760-ms.
- Bell, J.B., Trangenstein, J.A., Shubin, G.R., 1986. Conservation laws of mixed type describing three-phase flow in porous media. SIAM Journal on Applied Mathematics 46, 1000–1017. URL: <https://doi.org/10.1137/0146059>, doi:10.1137/0146059.
- Buckley, S., Leverett, M., 1942. Mechanism of fluid displacement in sands. Transactions of the AIME 146, 107–116. URL: <https://doi.org/10.2118/942107-g>, doi:10.2118/942107-g.
- Christensen, J., Stenby, E., Skauge, A., 1998. Compositional and relative permeability hysteresis effects on near-miscible WAG, in: SPE/DOE Improved Oil Recovery Symposium, SPE. URL: <https://doi.org/10.2118/39627-ms>, doi:10.2118/39627-ms.

- Christensen, J., Stenby, E., Skauge, A., 2001. Review of WAG field experience. *SPE Reservoir Evaluation & Engineering* 4, 97–106. URL: <https://doi.org/10.2118/71203-pa>, doi:10.2118/71203-pa.
- Corey, A., Rathjens, C., Henderson, J., Wyllie, M., 1956. Three-phase relative permeability. *Journal of Petroleum Technology* 8, 63–65. URL: <https://doi.org/10.2118/737-g>, doi:10.2118/737-g.
- Fayers, F., Sheldon, J., 1959. The effect of capillary pressure and gravity on two-phase fluid flow in a porous medium. *Transactions of the AIME* 216, 147–155. URL: <https://doi.org/10.2118/1089-g>, doi:10.2118/1089-g.
- Holden, L., 1990. On the strict hyperbolicity of the buckley–leverett equations for three-phase flow in a porous medium. *SIAM Journal on Applied Mathematics* 50, 667–682. URL: <https://doi.org/10.1137/0150039>, doi:10.1137/0150039.
- Holtz, M.H., 2016. Immiscible water alternating gas (IWAG) EOR: Current state of the art, in: *SPE Improved Oil Recovery Conference*, Society of Petroleum Engineers. URL: <https://doi.org/10.2118/179604-ms>, doi:10.2118/179604-ms.
- Johns, R., Orr, F., 1996. Miscible gas displacement of multicomponent oils. *SPE Journal* 1, 39–50. URL: <https://doi.org/10.2118/30798-pa>, doi:10.2118/30798-pa.
- LeVeque, R., J, L., Crighton, D., 2002. *Finite Volume Methods for Hyperbolic Problems*. Cambridge Texts in Applied Mathematics, Cambridge University Press.
- Li, D., Kumar, K., Mohanty, K.K., 2003. Compositional simulation of WAG processes for a viscous oil, in: *SPE Annual Technical Conference and Exhibition*, SPE. URL: <https://doi.org/10.2118/84074-ms>, doi:10.2118/84074-ms.
- Lin, E., Poole, E., 1991. Numerical evaluation of single-slug, WAG, and hybrid CO<sub>2</sub> injection processes, dollarhide devonian unit, andrews county, texas. *SPE Reservoir Engineering* 6, 415–420. URL: <https://doi.org/10.2118/20098-pa>, doi:10.2118/20098-pa.

- Marchesin, D., Plohr, B.J., 2001. Wave structure in WAG recovery. SPE Journal 6, 209–219. URL: <https://doi.org/10.2118/71314-pa>, doi:10.2118/71314-pa.
- Rhee, H.K., Aris, R., Amundson, N.R., 1970. On the theory of multicomponent chromatography. Philosophical Transactions of the Royal Society of London. Series A, Mathematical and Physical Sciences 267, 419–455. URL: <https://doi.org/10.1098/rsta.1970.0050>, doi:10.1098/rsta.1970.0050.
- Sanchez, N.L., 1999. Management of water alternating gas (WAG) injection projects, in: Latin American and Caribbean Petroleum Engineering Conference, Society of Petroleum Engineers. URL: <https://doi.org/10.2118/53714-ms>, doi:10.2118/53714-ms.
- Sheldon, J., Cardwell, W., 1959. One-dimensional, incompressible, noncapillary, two-phase fluid flow in a porous medium. Transactions of the AIME 216, 290–296. URL: <https://doi.org/10.2118/978-g>, doi:10.2118/978-g.
- Sohrabi, M., Tehrani, D., Danesh, A., Henderson, G., 2004. Visualization of oil recovery by water-alternating-gas injection using high-pressure micromodels. SPE Journal 9, 290–301. URL: <https://doi.org/10.2118/89000-pa>, doi:10.2118/89000-pa.
- Stone, H., 1970. Probability model for estimating three-phase relative permeability. Journal of Petroleum Technology 22, 214–218. URL: <https://doi.org/10.2118/2116-pa>, doi:10.2118/2116-pa.

**6     *Article: An Immiscible Water  
Alternating Gas (WAG)  
Analytical Solution Based in  
Wave Interaction Theory***

# An Immiscible Water Alternating Gas (WAG) Analytical Solution Based on Wave Interaction Theory

Wagner Q. Barros<sup>a</sup>, Adolfo P. Pires<sup>a,\*</sup>, Álvaro M. M. Peres<sup>a</sup>

<sup>a</sup>*Laboratório de Engenharia e Exploração de Petróleo - Universidade Estadual do Norte  
Fluminense Darcy Ribeiro, Macaé, RJ, Brazil*

---

## Abstract

Water-Alternating-Gas (WAG) process is the alternated injection of water and gas slugs in the reservoir that allies the good microscopy displacement efficiency of the gas with the mobility control provided by the water. In recent years the use of this technique has been increased because of the good results in field applications and the relative low costs when compared to others Enhanced Oil Recovery (EOR) processes. In this work we present an analytical solution for the linear, incompressible, immiscible WAG process. The three-phase flow in porous media was modeled using the Darcy's law and the governing equations were solved using the method of characteristics. The wave interactions that appears due to the injection of slugs with different mobilities are identified and solved. This technique can be applied with any traditional three-phase relative permeability curve and no consideration was made for slug lengths and order, showing the great robustness of the model. Results were compared to numerical solutions with close agreement.

*Keywords:* Water-Alternating-Gas, Method of Characteristics, Enhanced Oil Recovery, Analytical Solution, Immiscible Flow

---

---

\*Corresponding author

*Email address:* Adolfo.Puime@gmail.com (Adolfo P. Pires)

## 1. Introduction

The WAG process is an EOR technique where alternated slugs of gas and water are injected in the reservoir. This method combines the high displacement efficiency during the gas cycle with the mobility control provided by the water slug, increasing both vertical and horizontal sweep efficiency and stabilizing the gas injection front. The first reported application was in North Pembina field in Canada, operated by Mobil in 1957 and its usage has largely since then (Christensen et al. (2001)). The incremental recovery efficiency varies between 1 to 13% of original oil in place (OOIP) for immiscible applications (Holtz (2016)) and between 2 and 20% for miscible cases (Christensen et al. (2001)).

A WAG project is divided in two main phases: screening and implementation. During screening phase, laboratory, mathematical modeling and simulation studies are performed to evaluate the impact of rock and fluid properties in the additional oil recovery. The implementation phase then starts with the pilot well, usually in a relatively isolated part of reservoir for performance evaluation (Nadeson et al. (2004)). One may observe that all information gathered during the screening phase reduces the risks involved in implementation, showing the importance of mathematical modeling and phenomenological understanding.

The mathematical problem of the WAG process can be understood as the interaction among the waves that appears during the injection of different fluid slugs in porous media. Thus understanding the multiphase flow in porous media is fundamental for WAG solutions. For the two-phase, linear, immiscible oil displacement by water or gas, the solution is well established by Buckley-Leverett equations (Buckley and Leverett (1942)).

Three-phase immiscible solutions are more complicated, because some standard assumptions of the Buckley-Leverett equation can create non real eigenvalues of the system of equations, leading to mathematically ill-posed problems (Bell et al. (1986); Holden (1990); Marchesin and Plohr (2001)). However, using the most common three-phase relative permeability models (Stone (1970); Baker (1988); Delshad and Pope (1989)) and rock/fluid properties usually found

in reservoirs, the elliptical regions are usually small and do not cause numerical instabilities during numerical simulations (Shearer and Trangenstein (1989)) nor create physically inadmissible solutions (Guzmán and Fayers (1997a,b)). A complete review of three-phase immiscible solutions can be found in Marchesin and Plohr (2001).

The three-phase immiscible solutions can be a good approximation for the WAG process, making a Riemann problem with a constant right state (initial saturation) and the left state being the temporal average of the injected fluid (Marchesin and Plohr (2001)). This approximation shows that the WAG process can be seen as a superposition of a non-linear self-similar three-phase displacement and a decaying oscillatory wave accounting the wave interactions. Numerical simulation of these simplified model showed a good agreement for small slug sizes, in which in the limit when the slugs length tends to zero, the simultaneous solution matches perfectly with the numerical WAG solution (LaForce and Jessen (2010)).

However, in real WAG modeling, the injected fluid properties changes after each cycle creating discontinuities in boundary condition, in which non-linear waves propagating with different speeds will interact along the space-time plane. Thus, self-similar solutions of three-phase immiscible flow cannot be used to describe this phenomenon. When two characteristic waves cross in the space-time plane, it can be seen as a new Riemann problem, centered in the exact crossing point and with limits given by both sides of initial waves (Rhee et al. (1970)). This technique has already been applied in the theory of two-phase slug injection of chemicals in reservoir (Borazjani et al. (2016); Khorsandi et al. (2016); Apolinário et al. (2020); Apolinário and Pires (2021)). However, for the best of our knowledge, there is no analytical solution reported in literature for a three-phase problem considering the wave interaction among different slugs.

In this work, we present the analytical solution of the WAG process in a linear, immiscible and incompressible system. This solution considers different water-flood and gas-flood residual oil saturations, to incorporate the displacement efficiency into the model. The system was solved by the method of char-

acteristics in which all wave interactions that appears due to the different slugs interactions were identified and solved. In Section 2 we show the mathematical modeling of the problem and the general solution of the simpler propagating waves. Next section we classify all wave interactions that appears in the WAG process and show how to resolve each. Then, in Section 4, it is presented a complete WAG analytical solution using the wave interactions discussed previously. After, some conclusions are addressed.

## 2. Mathematical Model of WAG Immiscible Flow

70 We consider the linear displacement of oil by the injection of alternated slugs  
of water and gas. The porous media is homogeneous and initially saturated with  
oil at irreducible water saturation. Additional hypothesis are:

- Immiscible and isothermal flow;
- Negligible dispersion, gravitational and capillary effects;
- 75 • Incompressible fluids and porous media;
- Fluids having constant viscosity;
- Darcy's law hypothesis are valid;
- Constant cross sectional area;
- Neglecting hysteresis of relative permeability curves;
- 80 • Absence of gas critical saturation.

Under these assumptions, the transport equation for each phase is given by:

$$\frac{\partial S_\pi}{\partial t} + \frac{1}{\phi} \frac{\partial v_\pi}{\partial x} = 0, \text{ for } \pi = w, o, g \quad (1)$$

in which  $\phi$  is the rock porosity and  $S_\pi$  and  $v_\pi$  are the saturation and velocity of  
phase  $\pi$ . The aqueous, oil and gaseous phase are denoted by  $w, o, g$ , respectively.

Using the Darcy equation, the velocity of each phase can be calculated by:

$$v_\pi = -\frac{K k_{r\pi}}{\mu_\pi} \frac{\partial P}{\partial x} \quad (2)$$

85 where  $K$  and  $k_{r\pi}$  are the absolute and relative permeabilities,  $\mu_\pi$  the phase  
viscosity and  $\frac{\partial P}{\partial x}$  the linear pressure gradient.

The interfacial tension between oil and gas are orders of magnitude lower  
than the oil-water, causing a lower residual oil by gasflooding ( $S_{or}^g$ ) than by  
waterflooding ( $S_{or}^w$ ). This phenomenon affects the displacement efficiency and  
90 is modeled by the introduction of the minimum residual oil saturation:

$$S_{om} = \min(S_{or}^w, S_{or}^g) \quad (3)$$

Thus, the phase saturations are all normalized by:

$$\begin{cases} S_{nw} = \frac{S_w - S_{wi}}{1 - S_{wi} - S_{om}}, & S_w \in [S_{wi}, 1 - S_{or}] \\ S_{no} = \frac{S_o - S_{om}}{1 - S_{wi} - S_{om}}, & S_o \in [S_{or}, 1 - S_{wi}] \\ S_{ng} = \frac{S_g}{1 - S_{wi} - S_{om}}, & S_g \in [0, 1 - S_{wi} - S_{or}] \end{cases} \quad (4)$$

where  $S_{wi}$  is the irreducible water saturation.

We define the dimensionless time and space coordinates:

$$x_D = \frac{x}{L} \quad (5)$$

$$t_D = \frac{\int_0^t q(\tau) d\tau}{(1 - S_{wi} - S_{om}) AL\phi} \quad (6)$$

where  $L$  is the core length,  $A$  is the cross sectional area,  $q$  is the total injected  
 95 flow rate measured at the inlet point ( $x_D = 0$ ) and  $\tau$  is the integral variable.

Thus, Equation 1 can be written in its dimensionless form as:

$$\frac{\partial S_{n\pi}}{\partial t_D} + \frac{\partial f_\pi}{\partial x_D} = 0, \text{ for } \pi = w, o, g \quad (7)$$

in which  $f_\pi$  defines the fractional flow of phase  $\pi$ :

$$f_\pi = \frac{\lambda_\pi}{\lambda_T} = \frac{\frac{k_{r\pi}}{\mu_\pi}}{\frac{k_{rw}}{\mu_w} + \frac{k_{ro}}{\mu_o} + \frac{k_{rg}}{\mu_g}} \quad (8)$$

where  $\lambda_\pi$  is the mobility for phase  $\pi$  and  $\lambda_T$  is the total system mobility.

### 2.1. Three-Phase Relative Permeability

100 Three-phase relative permeability models have a huge impact on the mathematical structure of immiscible solutions (Guzmán and Fayers (1997a,b)). The traditional approach is based in using empirical models that converts two-phase relative permeability curves into three-phase surfaces (Stone (1970); Baker (1988)). Those models are usually based in the channel flow theory, postulated

105 for a water wetting medium by three rules (Leverett (1939); Leverett and Lewis  
(1941); Corey et al. (1956)):

1. The relative permeability of the water phase depends only on its own saturation;
2. The relative permeability of the gas phase depends only on its own saturation;
- 110 3. The relative permeability of oil phase depends on the saturation of all three phases.

To model the two-phase relative permeability curves we are using the power-law model (Corey's model Corey et al. (1956)), given by:

$$\begin{cases} k_{rw} = k_{rw}^{S_{or}^w} (S_{nw})^{n_w} \\ k_{ro}^{w|g} = k_{ro}^{S_{wi}} (S_{no})^{n_o^{w|g}} \\ k_{rg} = k_{rg}^{S_{or}^g} (S_{ng})^{n_g} \end{cases} \quad (9)$$

115 where the superscript  $w|g$  indicates if the oil permeability was obtained either by the waterflooding or by gasflooding experiment. All cases presented in this work were generated considering the parameters in Table 1 and illustrated in Figure 1. It is important to observe that the water relative permeability curve was extrapolated by a line connecting  $S_w = 1 - S_{or}^w$  and  $S_w = 1$ , assuming  
120 that  $k_{rw}(S_w = 1) = 1$ , this is necessary to compatibilize these curves with the three-phase empirical model.

Table 1: Corey's model variables used in all cases

Waterflooding	Gasflooding
$S_{wi} = 0.20$	$S_{wi} = 0.20$
$k_{ro}^{S_{wi}} = 0.80$	$k_{ro}^{S_{wi}} = 0.80$
$S_{or}^w = 0.40$	$S_{or}^g = 0.20$
$k_{rw}^{S_{or}^w} = 0.30$	$k_{rg}^{S_{or}^g} = 0.70$
$n_w = 2.2$	$n_g = 2.4$
$n_o^w = 2.0$	$n_o^g = 1.8$

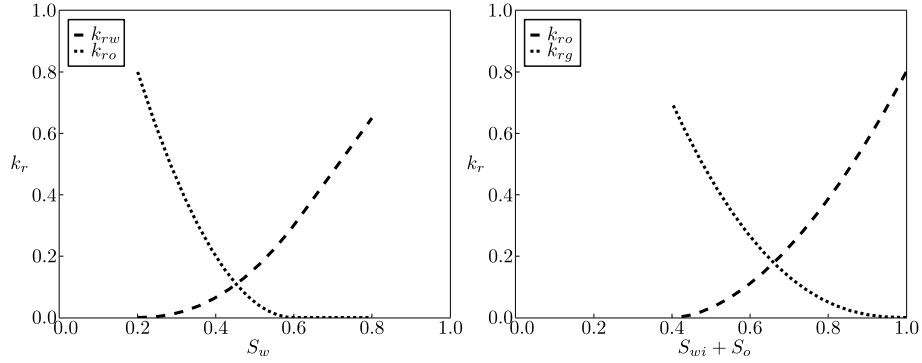


Figure 1: Two-phase relative permeability curves obtained from Corey's model

To convert the two-phase curves into three-phase we are using the modified Stone I model (Stone (1970); Aziz and Settari (1979)):

$$\begin{cases} k_{rw} = k_{rw}(S_{nw}) \\ k_{ro} = k_{ro}(S_{nw}, S_{no}, S_{ng}) = \frac{S_{no}}{k_{ro}^{swi}} \left( \frac{k_{ro}^w}{1-S_{nw}} \right) \left( \frac{k_{ro}^g}{1-S_{ng}} \right) \\ k_{rg} = k_{rg}(S_{ng}) \end{cases} \quad (10)$$

The Figure 10 presents the three-phase relative permeability curves obtained  
 125 from the parameters in Table 1 and used in all cases of this work. It is important  
 to observe that only the oil relative permeability curves are not straight lines,  
 showing its dependence on the saturation of all the three phases and obeying  
 the channel flow theory.

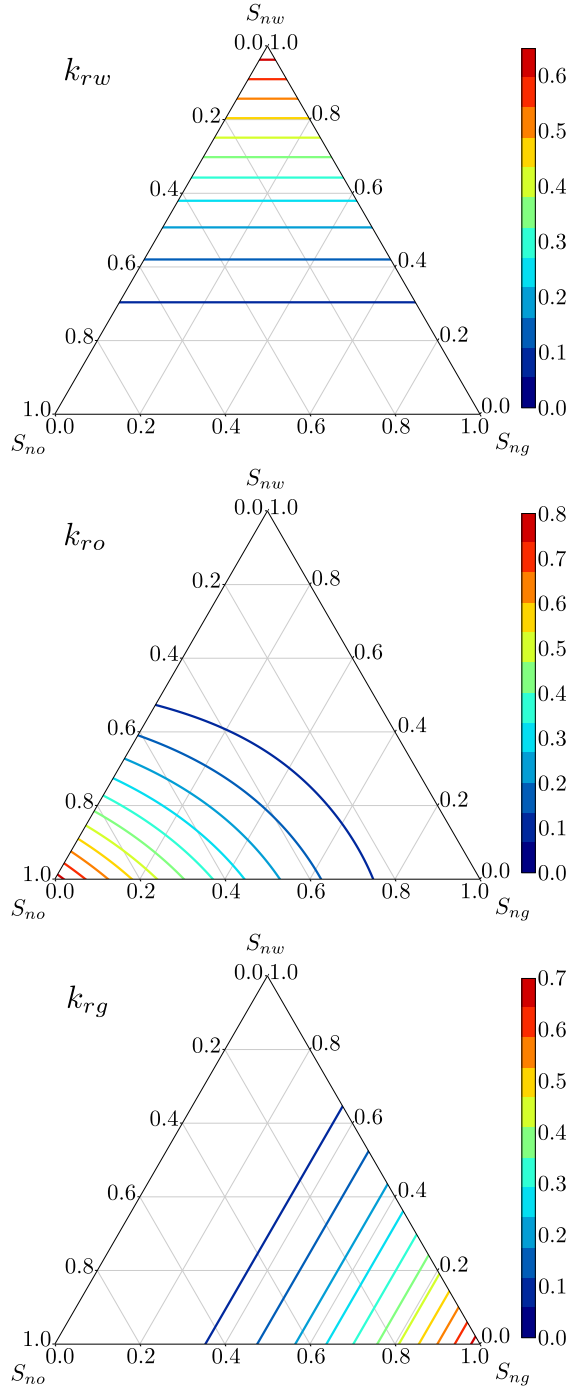


Figure 2: Three-phase relative permeability curves inside the ternary diagram for Stone's I model

## 2.2. Method of Characteristics and Fundamental Waves

130 Physically, the saturations are limited by  $S_\pi \in [0, 1]$  and by  $S_w + S_o + S_g = 1$ .  
Using these restrictions we write the gas saturation as a function of others and  
the governing equations (Equation 7) can be written in a matrix form:

$$\begin{pmatrix} 1 & 0 \\ 0 & 1 \end{pmatrix} \begin{pmatrix} \frac{\partial S_{nw}}{\partial t_D} \\ \frac{\partial S_{no}}{\partial t_D} \end{pmatrix} + \begin{pmatrix} \frac{\partial f_w}{\partial S_{nw}} & \frac{\partial f_w}{\partial S_{no}} \\ \frac{\partial f_o}{\partial S_{nw}} & \frac{\partial f_o}{\partial S_{no}} \end{pmatrix} \begin{pmatrix} \frac{\partial S_{nw}}{\partial x_D} \\ \frac{\partial S_{no}}{\partial x_D} \end{pmatrix} = \begin{pmatrix} 0 \\ 0 \end{pmatrix} \quad (11)$$

The right eigenvalues of the Jacobian of flux vector are written by:

$$\lambda^\pm = \frac{1}{2} \left( \frac{\partial f_w}{\partial S_{nw}} + \frac{\partial f_o}{\partial S_{no}} \right) \pm \frac{1}{2} \sqrt{\left( \frac{\partial f_w}{\partial S_{nw}} - \frac{\partial f_o}{\partial S_{no}} \right)^2 + 4 \left( \frac{\partial f_w}{\partial S_{no}} \frac{\partial f_o}{\partial S_{nw}} \right)} \quad (12)$$

135 in which  $\lambda^-$  and  $\lambda^+$  are called slow and fast eigenvalues with  $\lambda^- < \lambda^+$  in all  
points that satisfies the following criteria:

$$\Delta \equiv \left( \frac{\partial f_w}{\partial S_{nw}} - \frac{\partial f_o}{\partial S_{no}} \right)^2 + 4 \left( \frac{\partial f_w}{\partial S_{no}} \frac{\partial f_o}{\partial S_{nw}} \right) > 0 \quad (13)$$

Applying the relative permeability model (Figure 2) in Equation 12, there  
is a simply connected region inside domain in which the eigenvalues are not  
real ( $\Delta < 0$ ), called elliptic region (marked in gray in Figure 3). Inside the  
elliptic region the problem is ill-posed and cannot be solved by the method  
140 of characteristics (Castañeda et al. (2016)). For the WAG process, the initial  
and boundary conditions are always positioned outside this region. Thus, using  
the fact that the rarefaction paths do not enter the elliptic region, we can safely  
apply the method of characteristics. Then, the WAG immiscible solution can be  
described by a sequence of elementary nonlinear waves (Lax (1957); Liu (1974,  
145 1975)), showed in sequence.

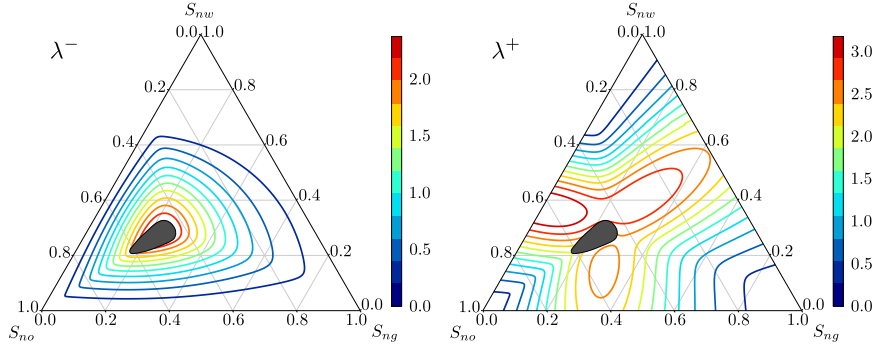


Figure 3: Slow and fast eigenvalues inside the ternary diagram for Stone's I model

### 2.2.1. Rarefaction Waves

Continuous solutions arise in the form of rarefaction waves, constructed by calculating the orbits of the following eigenvector field:

$$\frac{d\vec{S}_n}{d\xi} = \vec{r}_\pm(\vec{S}_n) \quad (14)$$

where  $\vec{r}_\pm$  are the slow and the fast right eigenvectors of the Jacobian of flux vector and  $\xi = x_D/t_D$ . Each of these orbits is called integral curves (rarefaction paths) and the set completely fills the ternary diagram excluding the elliptic region (Figure 3, in which the arrows point toward the eigenvalue increase direction). Applying the eigenvectors of the Jacobian of the flux vector (System 11), the integral curves are given by:

$$\left(\frac{dS_{nw}}{dS_{no}}\right)^\pm = -\frac{\frac{\partial f_w}{\partial S_{no}}}{\left(\frac{\partial f_w}{\partial S_{nw}} - \lambda^\pm\right)} \quad (15)$$

The slow integral paths are transverse to the triangle edges, behavior already discussed in literature (Marchesin and Plohr (2001)). However, the normalization that we introduce created a point of converging fast rarefaction paths in point  $(S_w, S_o, S_g) = (1 - S_{or}^w, S_{or}^w, 0)$ , causing that the fast integral paths are not approximately parallel of  $\overline{S_{nw}S_{no}}$  edge (expected behavior discussed in literature). This point can be physically interpreted by the limitation of waterflooding, in which additional oil can only be recovery by gas injection.

The solution along a particular integral curve is valid if the associated eigenvalue is strict increasing along this path (Tai-Ping (2007)). Observes that, for real values, the integral curves are not defined inside the elliptic region.

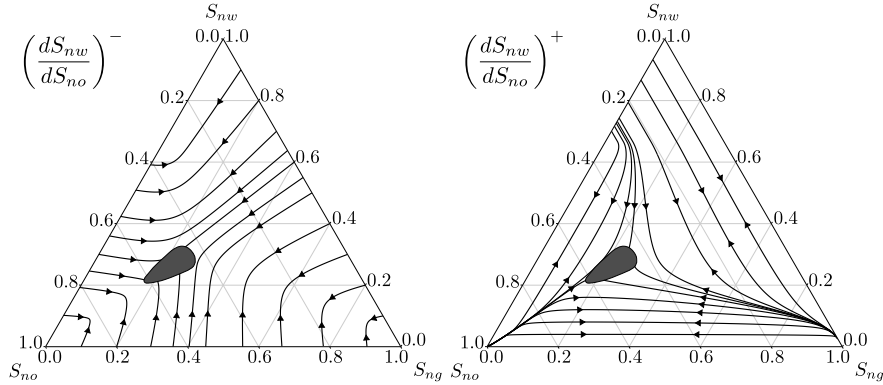


Figure 4: Slow and fast integral paths inside the ternary diagram for Stone's I model

165 2.2.2. Shock Waves

The System 11 admits weak solutions in the form of moving discontinuities, called shock waves. A valid shock must balance the flux of all phases across the discontinuity, where we call  $L$  and  $R$  the states immediately left ( $S^L = (S_{nw}^L, S_{no}^L)$ ) and right ( $S^R = (S_{nw}^R, S_{no}^R)$ ) of the discontinuity. This restriction is known by Rankine-Hugoniot condition and is used to calculate the shock speed  $\sigma = \sigma(S^L, S^R)$ :

$$\begin{cases} \sigma (S_{nw}^L - S_{nw}^R) = (f_w^L - f_w^R) \\ \sigma (S_{no}^L - S_{no}^R) = (f_o^L - f_o^R) \end{cases} \quad (16)$$

For a fixed left state  $S^L$ , we can define the Hugoniot locus ( $\mathcal{H}(S^L)$ ) as the geometrical place of all possible right states that obeys the Rankine-Hugoniot condition, mathematically described by:

$$\mathcal{H}(S^L) = \{T : \exists \sigma = \sigma(S^L, T) \text{ obeying Equation 16 with } T \neq S^L\} \quad (17)$$

175 The Figure 5 shows the Hugoniot locus for a particular point inside the  
ternary diagram. This locus has only two local branches meeting in the primary  
bifurcation point  $S^L$ , but more complicated bifurcations are found for WAG  
process (Marchesin and Plohr (2001)). In Section 4 we will show that Hugoniot  
loci with secondary bifurcation play an important rule in the WAG solution  
180 structure.

All points in  $\mathcal{H}(S^L)$  are possible weak solutions of System 11. To determine  
which point is the an admissible solution we are using the Lax (Lax (1957)) and  
Liu (Liu (1974, 1975)) stability criteria, where the characteristics waves should  
converge to the shock space-time path and the shock velocity must be in a critical  
185 point along a  $\mathcal{H}(S^L)$  branch. Additionally, a stable shock must be a zero-  
diffusion limit of the solution given by traveling waves, called vanishing viscosity  
condition (Marchesin and Plohr (2001); Tai-Ping (2007)), where a stable solution  
is obtained when there is at least one orbit in the vanishing viscosity phase plane  
connecting both shock sides.

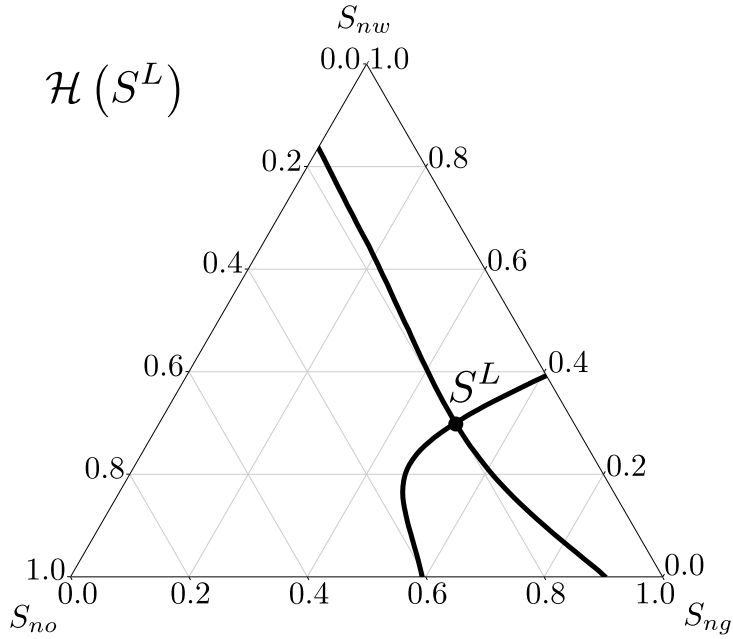


Figure 5: Hugoniot locus for  $S^L(S_{nw}, S_{no}, S_{ng}) = (0.3, 0.2, 0.5)$

190 *2.2.3. Composite Waves*

A composite wave or so called contact discontinuity can be defined by a shock with speed equal to the eigenvalue of the upstream state ( $\lambda^\pm(S^L)$ ):

$$\sigma(S^L, S^R) = \lambda^\pm(S^L) \quad (18)$$

where  $\pm$  indicates if it is either a fast or a slow composite wave. For stable composite waves,  $\sigma$  must be in a critical point in the  $\mathcal{H}(S^L)$  (Liu (1974, 1975)),  
 195 respecting the Bethe-Wendroff theorem (Wendroff (1972a,b)), and obeying the vanishing viscosity criteria (Marchesin and Plohr (2001); Tai-Ping (2007)).

*2.3. Numerical Solution Method*

In order to check the analytical solutions, the saturation profiles were compared with simulations using the first order, explicit, Upwind method LeVeque  
 200 et al. (2002):

$$\frac{(S_{n\pi})_n^{t+1} - (S_{n\pi})_n^t}{\Delta t_D} + \frac{(f_\pi)_{n-1}^t - (f_\pi)_n^t}{\Delta x_D} = 0, \quad \pi = w, o, g \quad (19)$$

where  $n$  and  $t$  are the spatial and temporal discretization index. This scheme do not produce numerical oscillation in the discontinuities, allowing a reliable comparison between analytical and numerical solution. To minimize numerical diffusion effects the spatial domain was discretized using 100,000 cells in all cases shown in this work, with the  $\Delta t_D$  subject to the CFL condition to maintain the simulation stability.

### 3. Wave Interactions

After each cycle in WAG scheme, the changes in fluid properties generates discontinuities in boundary condition, in which non-linear waves propagating with different speeds will interact along the space-time plane. These interactions can then interact with other waves generating new interactions in domain. In this section we will describe all interactions that arises in the immiscible WAG problem (Table 2). We treat all interactions as a new Riemann problem, centered in the crossing point and with lateral limits given by the two initial waves (Rhee et al. (1970)). For all saturation profiles shown in this and in the next section, the plotted dots are results obtained numerically.

There are basically two different kind of interactions: superposition and transmission. As showed in Figure 4, except for some particular points, the integral curves associated with the same eigenvalue (slow and fast) do not intercept themselves inside the ternary diagram. Thus, if two waves are interacting or either they are associated with different eigenvalues (slow with fast eigenvalues) or they are in the same integral path. For interactions associated with the same integral curve we call superposition phenomenon, and associated with different eigenvalues we call transmission.

Table 2: Summary of the wave interactions in WAG injection

		Slow Wave	Fast Wave
SSS	Shock-Shock Superposition	Shock	Shock
CCS	Composite-Composite Superposition	Composite	Composite
SRS	Shock-Rarefaction Superposition	Shock	Rarefaction
RSS	Rarefaction-Shock Superposition	Rarefaction	Shock
RCS	Rarefaction-Composite Superposition	Rarefaction	Composite
SRT	Shock-Rarefaction Transmission	Shock	Rarefaction
RRT	Rarefaction-Rarefaction Transmission	Rarefaction	Rarefaction
RCT	Rarefaction-Composite Transmission	Rarefaction	Composite
SCT	Shock-Composite Transmission	Shock	Composite

225 3.1. Shock-Shock Superposition (SSS) and Composite-Composite Superposition  
(CCS)

When the left state of fast wave and the right state of slow wave respects the Rankine-Hugoniot condition (Equation 16), there is a superposition of both shock waves (or composite wave for CCS case) resulting in a new propagating  
230 shock (Figures 6 and 7). Observe that the two shocks belong to the same integral curve: the  $\overline{S_{nw}S_{no}}$  edge.

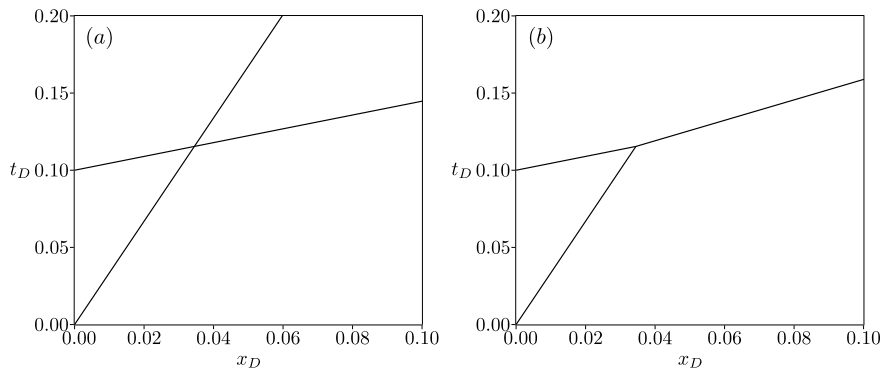


Figure 6: Characteristic plot before (a) and after (b) the SSS wave interaction solution

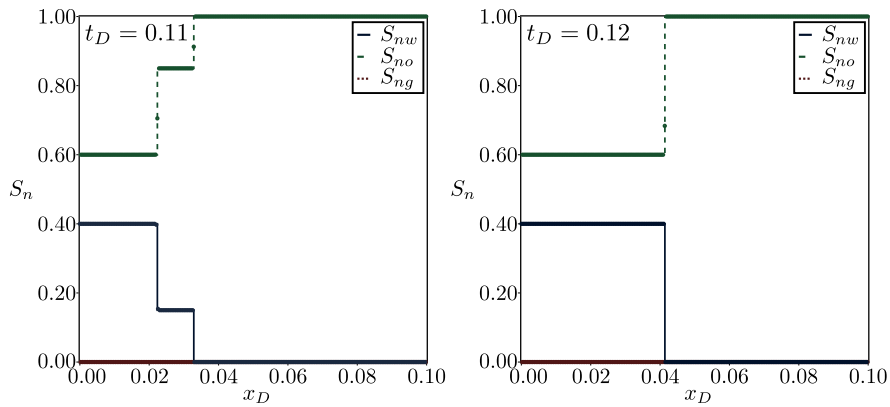


Figure 7: Saturation profile before ( $t_D = 0.11$ ) and after ( $t_D = 0.12$ ) the SSS wave interaction, compared with numerical solution

### 3.2. Shock-Rarefaction Superposition (SRS) and Rarefaction-Shock Superposition (RSS)

For shocks and rarefactions associated to the same integral curve, the interaction causes a superposition in which the shock changes its speed continuously until the end of the rarefaction fan (Figures 8 and 9). Observes that at each interaction point the Rankine-Hugoniot condition is satisfied. The unique difference between SRS and RSS interaction is which wave is the slow and which is the fast during the interaction.

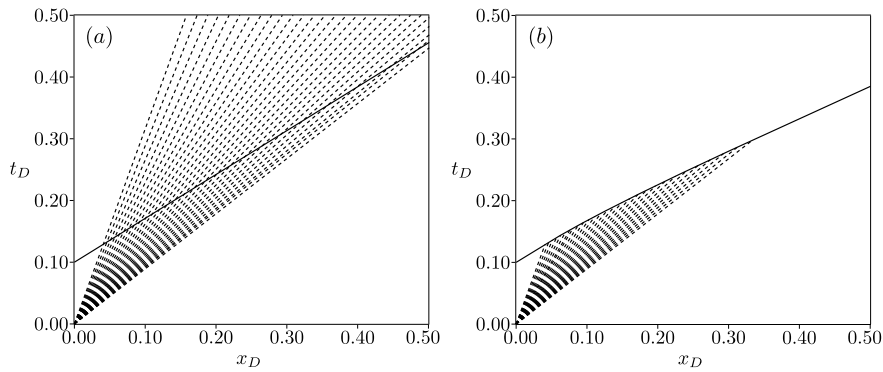


Figure 8: Characteristic plot before and after the RSS wave interaction solution

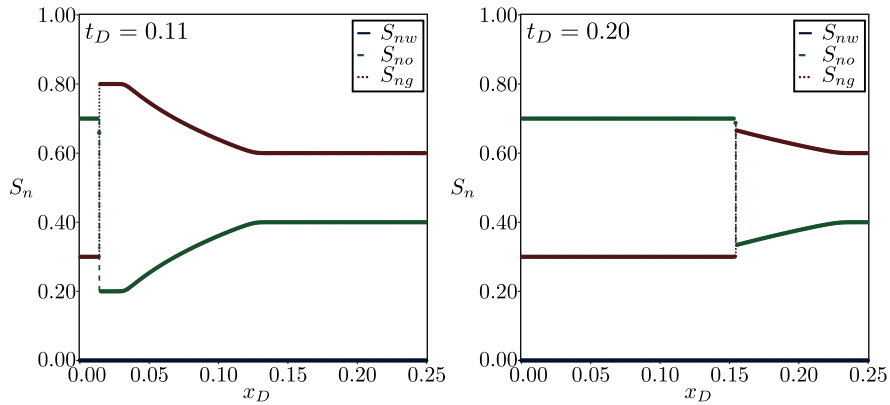


Figure 9: Saturation profile before ( $t_D = 0.11$ ) and during ( $t_D = 0.2$ ) the RSS wave interaction, compared with numerical solution

240 3.3. Rarefaction-Composite Superposition (RCS)

In the RCS interaction the continuous interaction between the rarefaction and the composite wave cause an acceleration of the shock, opening space in the composite fan. We interpret this phenomenon as a decompression of composite wave, where at each point the rarefaction eigenvalue is equal to the shock speed, characteristic of composite waves (Figures 10 and 11). Observes that after the interaction, only the composite wave remains with an expanded rarefaction fan.

245

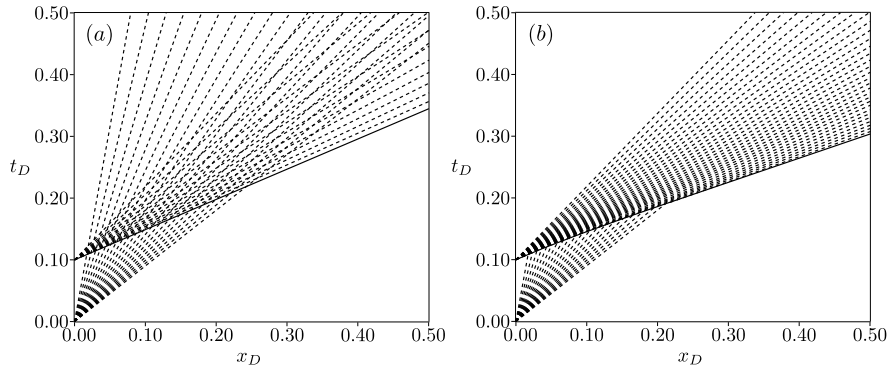


Figure 10: Characteristic plot before and after the RCS wave interaction solution

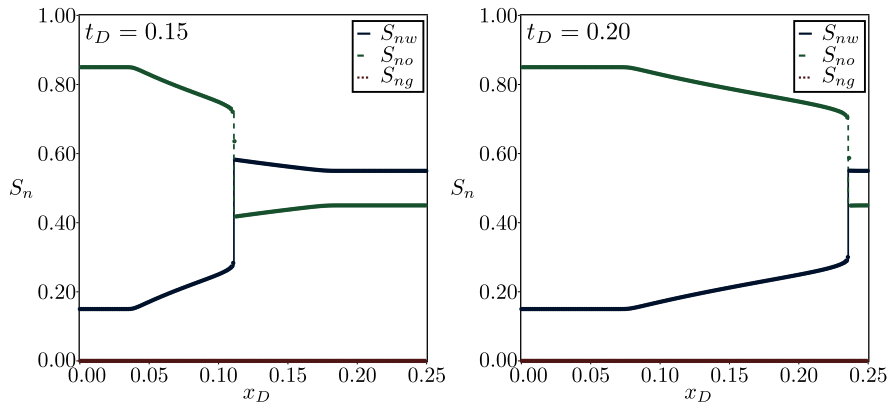


Figure 11: Saturation profile during ( $t_D = 0.15$ ) and after ( $t_D = 0.20$ ) the RCS wave interaction, compared with numerical solution

### 3.4. Shock-Rarefaction Transmission (SRT)

The transmission phenomenon occurs when waves of different integral curves are interacting. In the SRT case, rarefaction fan is continuously interacting with the shock wave, and as result, both waves change their direction and speed (Figures 12 and 13). At each crossing point, the Rankine-Hugoniot condition must be satisfied, making the rarefaction wave jumps to the integral path of the right shock state.

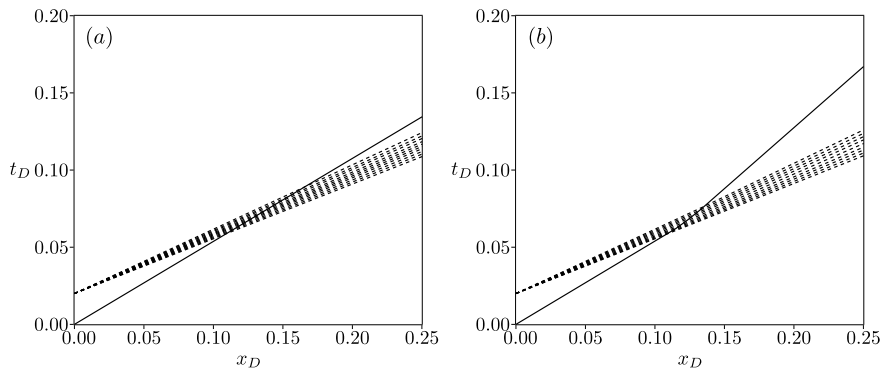


Figure 12: Characteristic plot before and after the SRT wave interaction solution

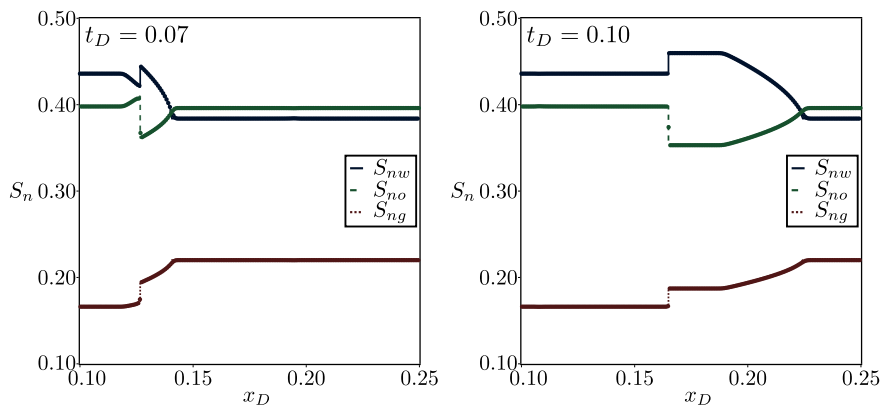


Figure 13: Saturation profile during ( $t_D = 0.07$ ) and after ( $t_D = 0.10$ ) the SRT wave interaction, compared with numerical solution

### 3.5. Rarefaction-Rarefaction Transmission (RRT)

255 In this interaction, the rarefactions are associated with the  $\left(\frac{dS_{nw}}{dS_{no}}\right)^-$  and  
 $\left(\frac{dS_{nw}}{dS_{no}}\right)^+$  integral curves, respectively. Thus, for each crossing point, the result-  
ing rarefaction is found by the crossing point of both integral paths (Figures 14  
and 15). In this case, both rarefaction fans are continuous solution, then the  
process to solve is discretize the fan in rarefaction waves and solve the interac-  
260 tion two by two, same procedure proposed by Rhee et al. (1970). It is important  
to observe that the final result is a continuous region among rarefaction interac-  
tions in the space-time plane, where we show both characteristics crossing in  
the same position only for illustration purposes.

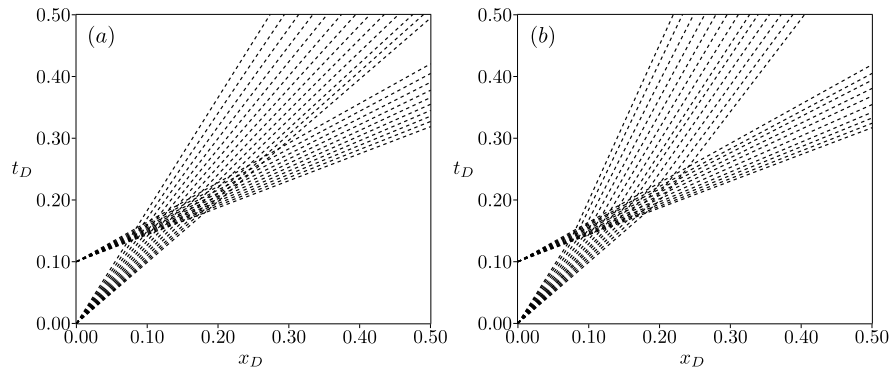


Figure 14: Characteristic plot before and after the RRT wave interaction solution

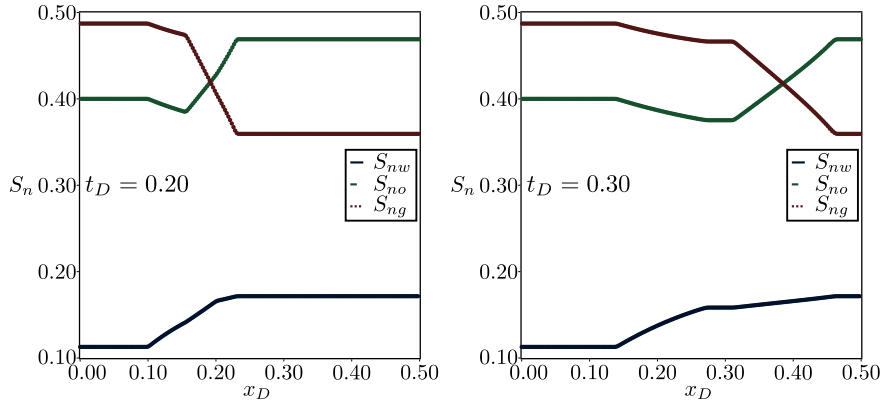


Figure 15: Saturation profile during ( $t_D = 0.20$ ) and after ( $t_D = 0.30$ ) the RRT wave interaction, compared with numerical solution

### 3.6. Rarefaction-Composite Transmission (RCT) and Shock-Composite Transmission (SCT)

265

In the RCT interaction, first the rarefaction interacts with the shock, accelerating the composite wave and opening space for new rarefactions (similar to interaction RCS). Then, the rarefaction fan transmits over the shock and interacts with the other fan above the composite wave (similar to the RRT).

270

Thus this case is a combination of RCS and RRT behavior.

For the SCT case, the waves were generated by previous interactions and the correct way to deal this case is solving a new Riemann problem centered in the interaction point and positioning the solution as resulting waves. The SCT and RCT waves will be illustrated in the next section, in the context of the WAG solutions.

275

## 4. WAG Analytical Solution

In this section the complete solution for the immiscible WAG process will be discussed. The solution procedure is divided in two parts: the initial wave positioning, where we build analytical solutions without consider the interaction among the cycles, and the wave interactions, solved by the application of the methodology described in Section 3.

### 4.1. Initial Wave Positioning

The initial wave positioning is constructed identifying the boundary condition and the inlet rock face saturation at beginning of each cycle (Table 3). Initially the porous media is saturated with oil at irreducible water saturation and at  $t_D = 0.0$  we start the injection of pure water. In the second cycle ( $t_D = 0.05$ ), the porous media is saturated with water at  $S_{or}^w$  condition and we start the injection the gas slug. From the third cycle onwards ( $t_D = 0.15$ ) the boundary and the inlet face conditions will alternate between  $(S_w, S_o, S_g) = (0, S_{or}^g, 1 - S_{or}^g)$  and  $(S_w, S_o, S_g) = (1 - S_{or}^g, S_{or}^g, 0)$  depending if it is a gas or water cycle. Observes that the first two cycles are different from the others only because  $S_{or}^g < S_{or}^w$  and the oil saturation in the inlet face do not reach  $S_{om}$ . After the 3<sup>rd</sup> cycle the solution pattern repeats indefinitely, not generating new wave interactions.

We construct the solution injecting cycles with small lengths ( $\Delta t_D < 1.0$ ) in order to maintain all wave interactions inside the domain  $x_D \in [0.0, 1.0]$ , allowing comparison with the numerical solution. However, the method can be applied for any WAG configuration. It is important to observe that all saturations reported in Table 3 must be normalized before the solution construction (Equation 4).

Table 3: Initial position wave

Cycle	$t_D$	Boundary Condition	Inlet Face Condition
		$B_C = (S_w, S_o, S_g)$	$I_F = (S_w, S_o, S_g)$
1 <sup>st</sup> Water	0.00	$(1 - S_{or}^w, S_{or}^w, 0)$	$(S_{wi}, 1 - S_{wi}, 0)$
2 <sup>nd</sup> Gas	0.05	$(0, S_{or}^g, 1 - S_{or}^g)$	$(1 - S_{or}^w, S_{or}^w, 0)$
3 <sup>rd</sup> Water	0.15	$(1 - S_{or}^g, S_{or}^g, 0)$	$(0, S_{or}^g, 1 - S_{or}^g)$

#### 4.1.1. 1<sup>st</sup> Cycle

The first cycle is the displacement of original oil by water injection and is described by the traditional Buckley-Leverett solutions (Figures 16 and 17). The boundary condition is obtained using  $f_w = 1$  that implies  $S_w = 1 - S_{or}^w$ .  
 305 The solution is then a composite wave connecting the boundary and the initial states.

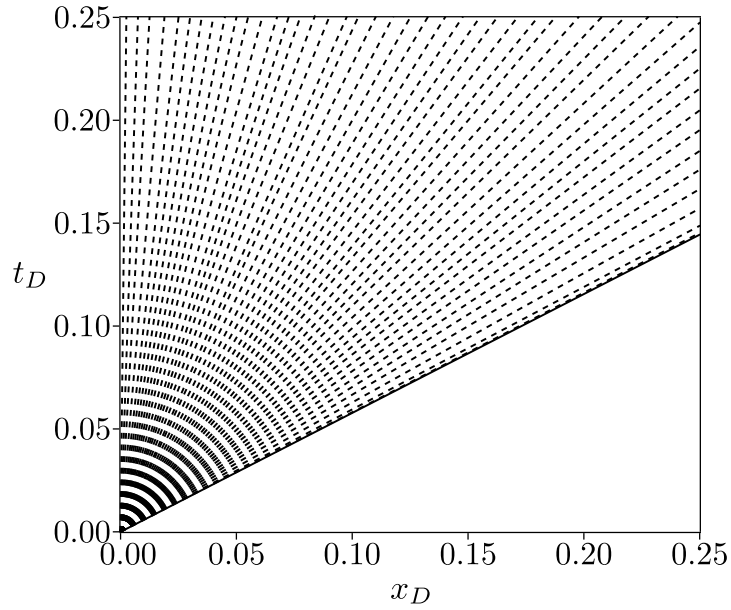


Figure 16: Characteristic diagram for the first cycle wave positioning

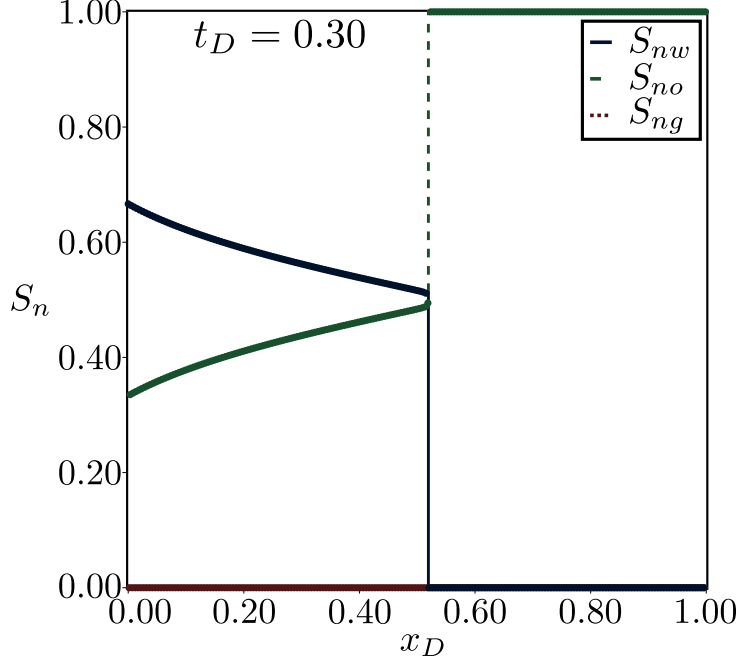


Figure 17: Saturation profile ( $t_D = 0.30$ ) for the first cycle wave positioning, compared with numerical solution

#### 4.1.2. 2<sup>nd</sup> Cycle

The second cycle starts the gas injection with the left rock face saturated with water at  $1 - S_{or}^w$ . The direct composite wave connecting boundary and left face conditions is not allowed, because do not respect the stability criteria. Thus the solution must necessarily pass through a point in  $\overline{S_{nw}S_{no}}$  edge.

The Figure 18 shows the hugoniot locus for three different  $J$  points along  $\overline{S_{nw}S_{no}}$  around a neighborhood of point  $J_{S_{nw}S_{no}}^*$ . Observes that each Hugoniot locus is formed by three branches, two locals and one non-local, in which the  $\overline{S_{nw}S_{no}}$  edge is always one of the local branches. For  $J$  below  $J_{S_{nw}S_{no}}^*$  the other local branch always connects  $\overline{S_{nw}S_{no}}$  and  $\overline{S_{no}S_{ng}}$  edges, while for  $J$  above  $J_{S_{nw}S_{no}}^*$   $\overline{S_{nw}S_{no}}$  and  $\overline{S_{nw}S_{ng}}$  edges are connected. The non-local branch change its behavior as well, for  $J$  below  $J_{S_{nw}S_{no}}^*$  the non-local branch starts and finishes in  $\overline{S_{nw}S_{ng}}$  and for  $J$  above  $J_{S_{nw}S_{no}}^*$  it starts and finishes in  $\overline{S_{no}S_{ng}}$  edge.

320 Thus, it can be seen that  $J_{S_{nw}S_{no}}^*$  is a separatrix point, in which the Hugoniot locus locally changes its topology and the local and non-local branches collapses themselves in a single point. The  $J_{S_{nw}S_{no}}^*$  point plays an important role in WAG solution because this point forms a stable orbit in the phase plane for the vanishing viscosity stability criteria using the identity viscosity matrix  
325 (Tai-Ping (2007)) (Figure 19). The  $T$  point marked in each Hugoniot locus is the point where  $\sigma(T, J) = \lambda^+(T)$ , representing the most stable shock in that branch according to Liu's criteria (Liu (1974, 1975)).

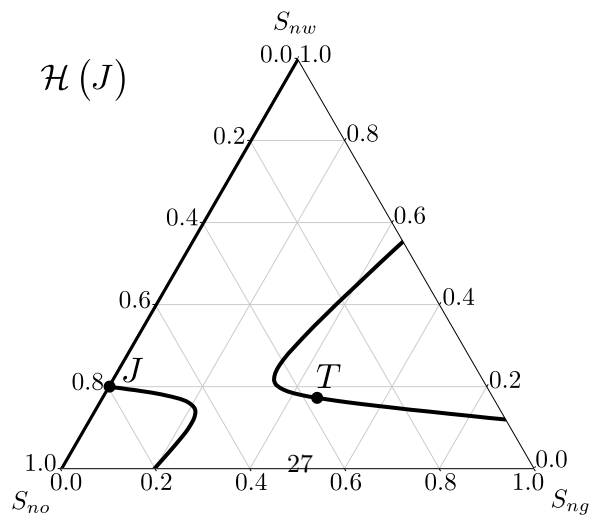
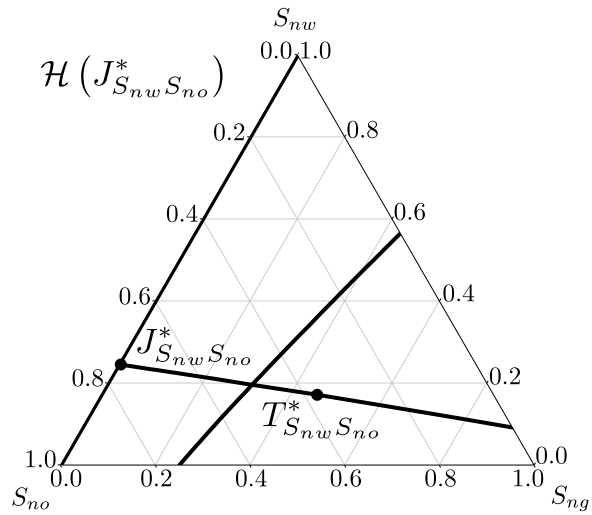
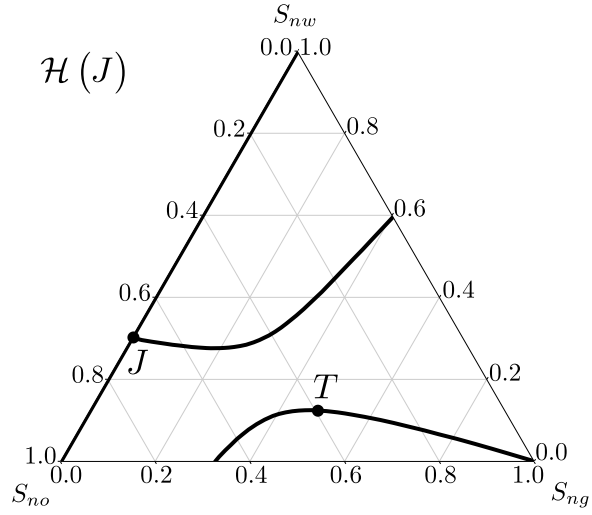


Figure 18: Hugoniot locus for three different positions along the  $\overline{S_{nw} S_{no}}$  edge

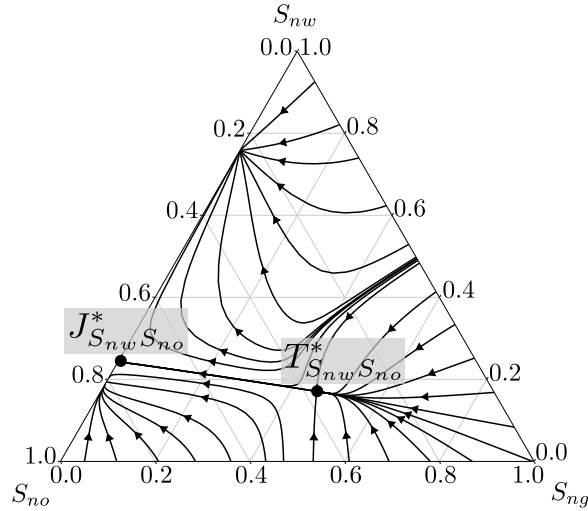


Figure 19: Phase plane for the vanishing viscosity stability criteria, for the second cycle wave

The solution for the second cycle is then described by a composite wave connecting  $T_{S_{nw}S_{no}}^*$  and  $J_{S_{nw}S_{no}}^*$ , followed by other fast composite wave connecting  $J_{S_{nw}S_{no}}^*$  to the inlet face condition of the second cycle (Figures 20 and 21). Depending on the relative permeability curves adopted, the condition  $\sigma(J_{S_{nw}S_{no}}^*, I_F^{2nd}) > \lambda^+(J_{S_{nw}S_{no}}^*)$  will not be satisfied and the second composite wave will not have rarefaction curves above (Figure 20). However, the wave interactions with the first cycle will accelerate this shock, as discussed in Section 3.3, appearing the rarefactions of this composite wave when  $\sigma(J_{S_{nw}S_{no}}^*, I_F^{2nd}) > \lambda^+(J_{S_{nw}S_{no}}^*)$ .

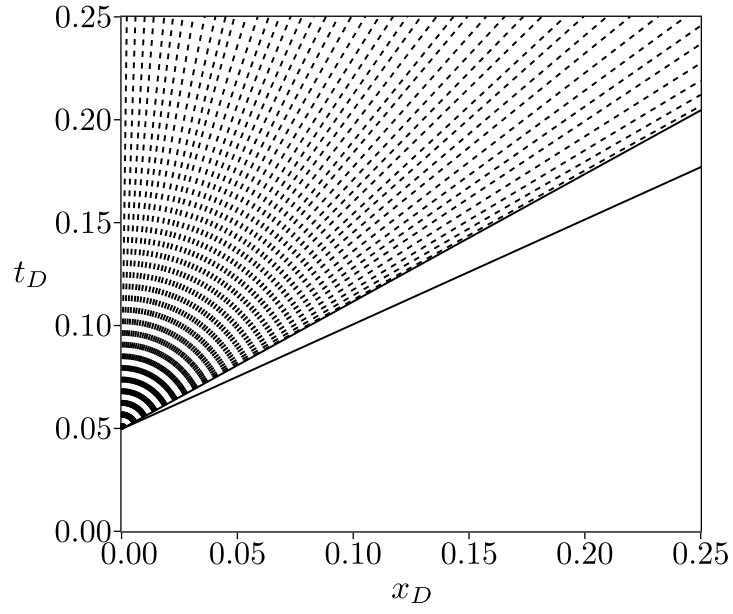


Figure 20: Characteristic diagram for the second cycle wave positioning

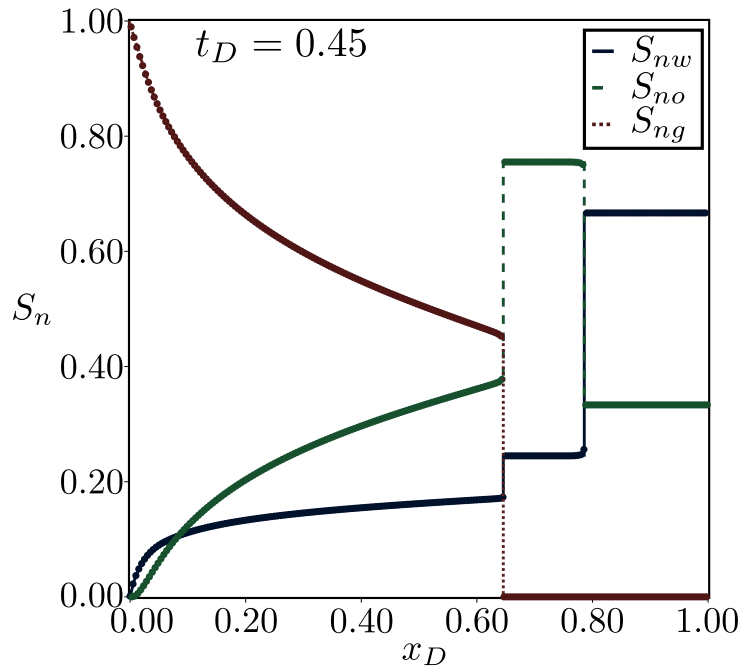


Figure 21: Saturation profile ( $t_D = 0.45$ ) for the second cycle wave positioning, compared with numerical solution

#### 4.1.3. 3<sup>rd</sup> Cycle

For the third cycle onwards the wave positioning is always in the  $\overline{S_{nw}S_{ng}}$  edge, changing only the boundary and the inlet face conditions. The solution of this case is also the traditional Buckley-Leverett equations considering the gas-water displacement (Figures 22 and 23), in which the solution consists of a fast composite wave connecting both vertices of  $\overline{S_{nw}S_{ng}}$ . As discussed, from this cycle, the residual oil in the inlet face reaches  $S_{om}$  and no more additional oil will be displaced in this point.

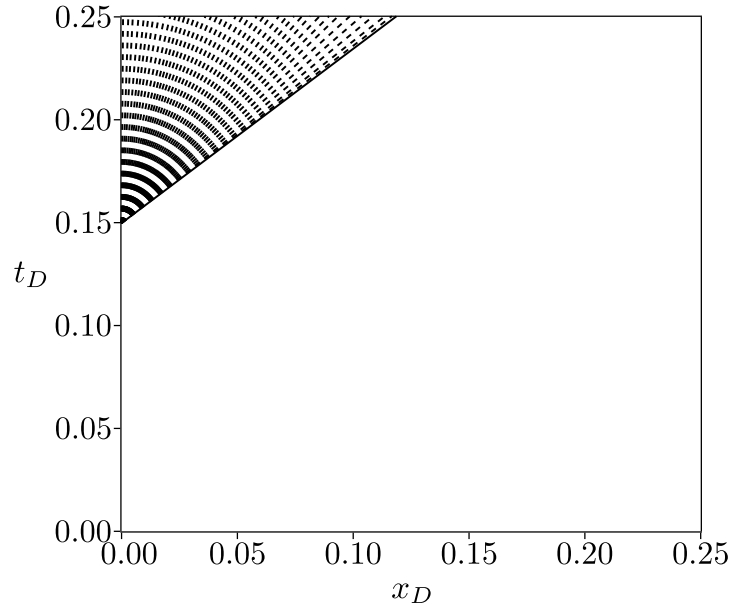


Figure 22: Characteristic diagram for the third cycle wave positioning

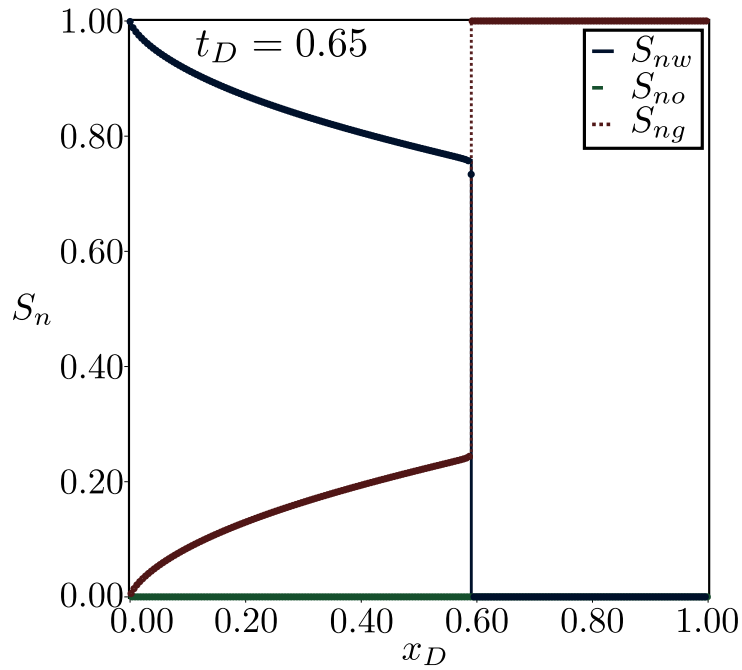


Figure 23: Saturation profile ( $t_D = 0.65$ ) for the second cycle wave positioning, compared with numerical solution

345 The Figure 24 presents the diagram characteristic after positioning the three first WAG cycles. There are wave interactions occurring in all domain and the order that we chose to solve these interactions can alter the final result. Thus we apply the causality principle determining that wave events happening first in time must be solved firstly, affecting only further events.

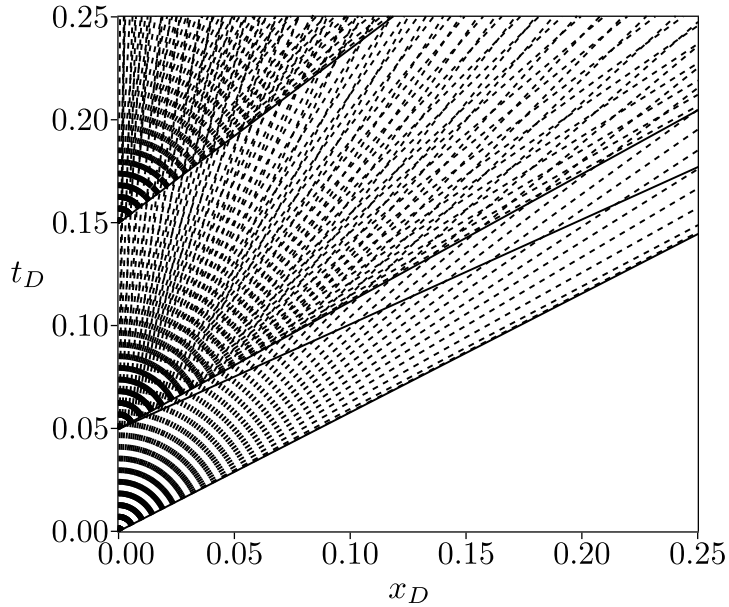


Figure 24: Characteristic diagram after wave positioning without solving the wave interactions

350 *4.2. WAG Wave Interactions*

In this section we will present the WAG scheme solution with wave interactions after application of the causality principle. The Figure 25 presents the characteristic diagram after solving all wave interactions, in which we are identifying the wave interactions using the keywords described in Table 2.

355 As discussed by [Marchesin and Plohr \(2001\)](#) the WAG scheme should present cyclic solutions, in which some patterns should repeat in characteristic diagram. Thus we divided the wave interaction in four different groups, and as it will be discussed, after the third WAG cycle the solution is a repetition of groups 02, 03 and 04, correctly positioned in the space-time plane.

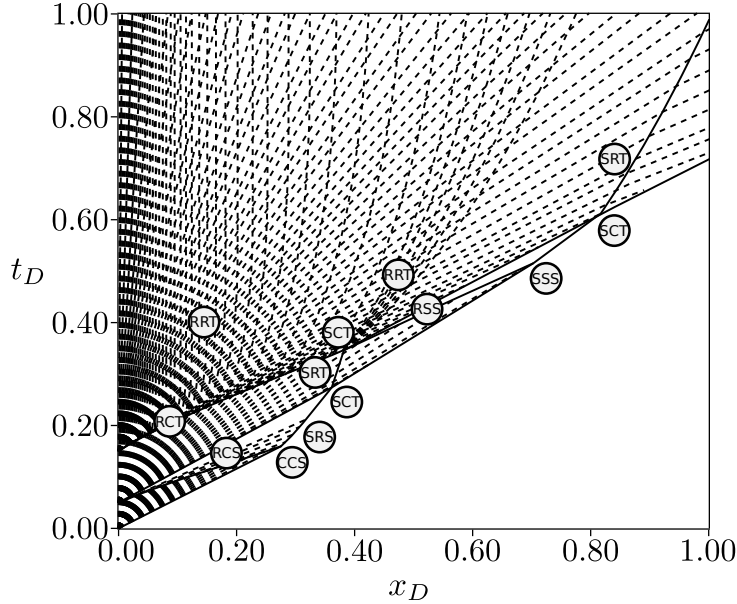


Figure 25: Characteristic diagram after solving all wave interactions

360 4.2.1. Group 01 - Composite-Composite Superposition

The Group 01 is the interaction of the first water cycle and the second composite wave of the next gas injection (Figure 26). All waves integrating this group belong to the same integral curve, the  $\overline{S_{nw}S_{no}}$  edge, thus we expect to see interactions of superposition type. One may observe that the Group 01 interactions only occurs once between the first and the second cycle if, and only if, the residual oil of the second displacement is lower than the first (in this case we start the WAG with water injection and  $S_{or}^g < S_{or}^w$ ).

The water rarefactions superposes with the second composite wave by a RCS interaction. This interaction accelerates the shock and expands the rarefaction fan. This phenomenon occurs until the crossing of both composite shocks, creating a CCS interaction. Then the new shock generated by the CCS will relate with the rarefaction fan by a SRS interaction.

The Figure 27 shows the saturation profile before ( $t_D = 0.15$ ) and after the ( $t_D = 0.18$ ) the CCS interaction. As it can be observed, the two composite

375 waves are approximating before the CCS point and, because the superposition  
phenomenon, only one resulting shock continues propagating in porous me-  
dia. Comparing the numerical and analytical solutions we can see the excellent  
agreement among them, where the numerical scheme could capture all these  
complicated wave interactions. However it was only possible because the high  
380 discretization that we used in this work.

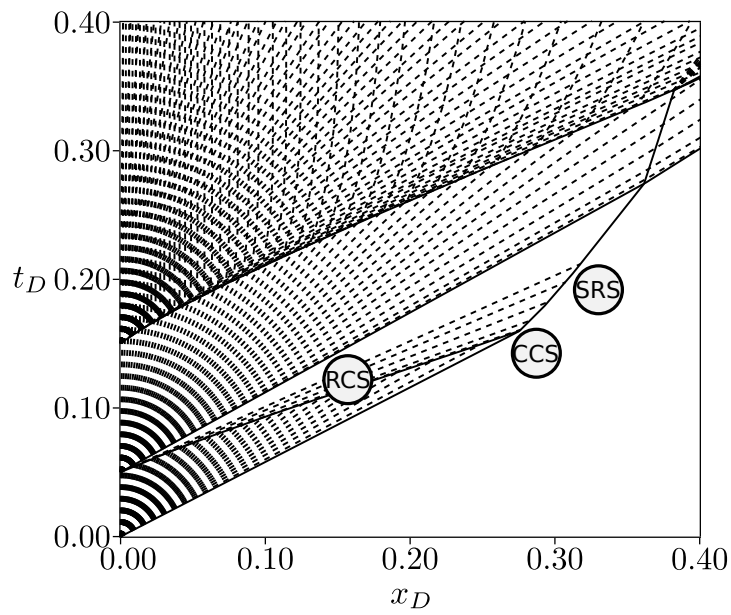


Figure 26: First group of interactions - RCS, CCS and SRS

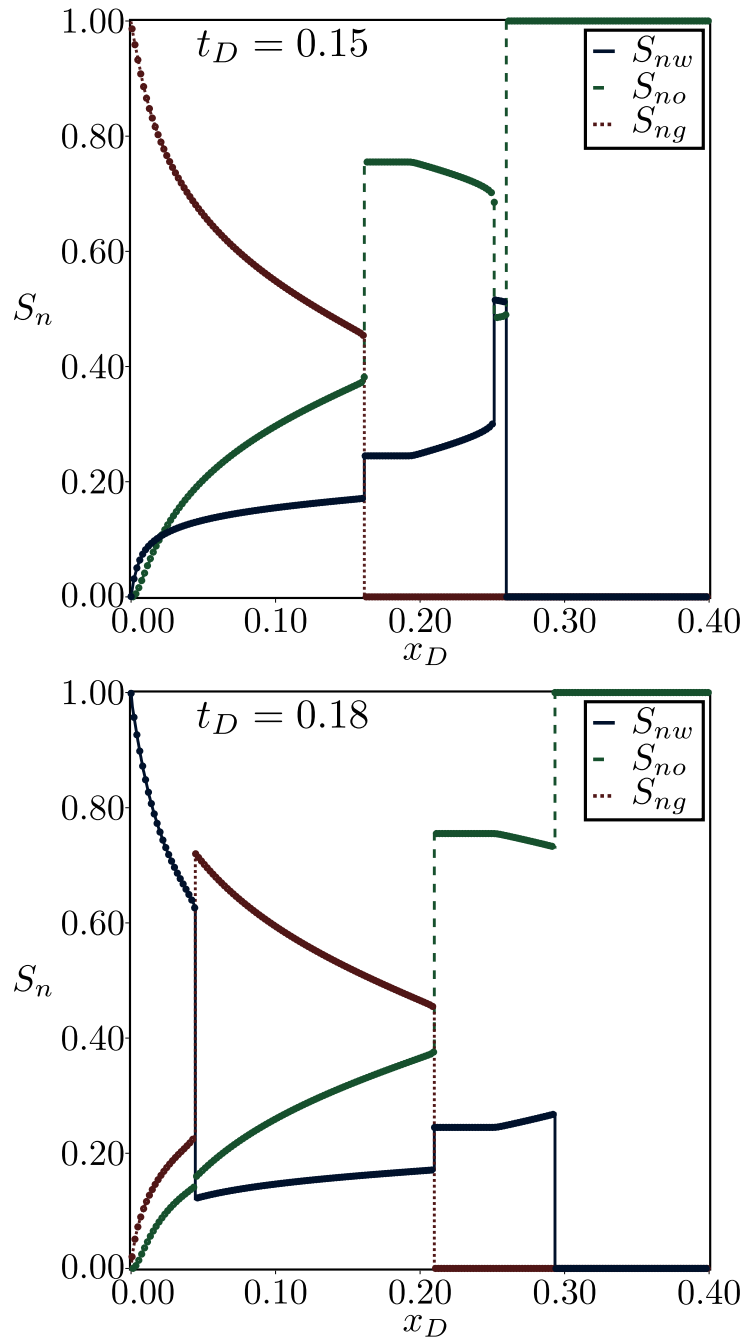


Figure 27: Saturation profile before ( $t_D = 0.15$ ) and after the ( $t_D = 0.18$ ) the CCS interaction for the Group 01 of WAG interactions, compared with numerical solution

#### 4.2.2. Group 02 - Slow Shock Transmission

For every cycle after the first the solution needs to pass through the  $\overline{S_{nw}S_{no}}$  or the  $\overline{S_{no}S_{ng}}$  edge. As it will be explained in Group 04, the points  $J_{S_{nw}S_{no}}^*$  and  $J_{S_{no}S_{ng}}^*$  will always appear in the solution in the form of a constant state  
385 bounded by a shock in the right side. Thus the Group 02 is formed by the interaction of these slow shocks and the composite wave of the next injection cycle (Figure 28).

Because of these waves are in different integral paths, it will occur a SCT transmission, generating slow and fast shocks. The slow shock will propagate  
390 along the rarefactions fan of the next composite wave in the form of a SRT transmission, changing both shock and rarefaction speeds.

The Figure 29 presents the saturation profile before ( $t_D = 0.25$ ) and after the ( $t_D = 0.30$ ) the SCT interaction. Before the SCT, the composite wave is approximating of the slow shock making the constant state of  $J_{S_{nw}S_{no}}^*$  contin-  
395 uously smaller with time (this region is showed in  $x_D \approx 0.35$  for  $t_D = 0.25$ ). After the SCT interaction the constant state vanishes and the rarefaction waves transmits by a SRT interaction, generating a new rarefaction fan separated by a shock discontinuity.

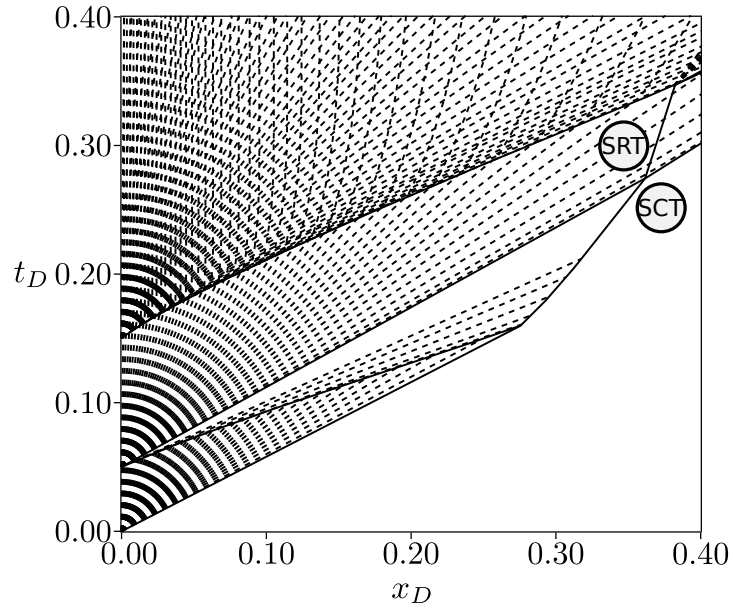


Figure 28: Second group of interactions - SCT and SRT

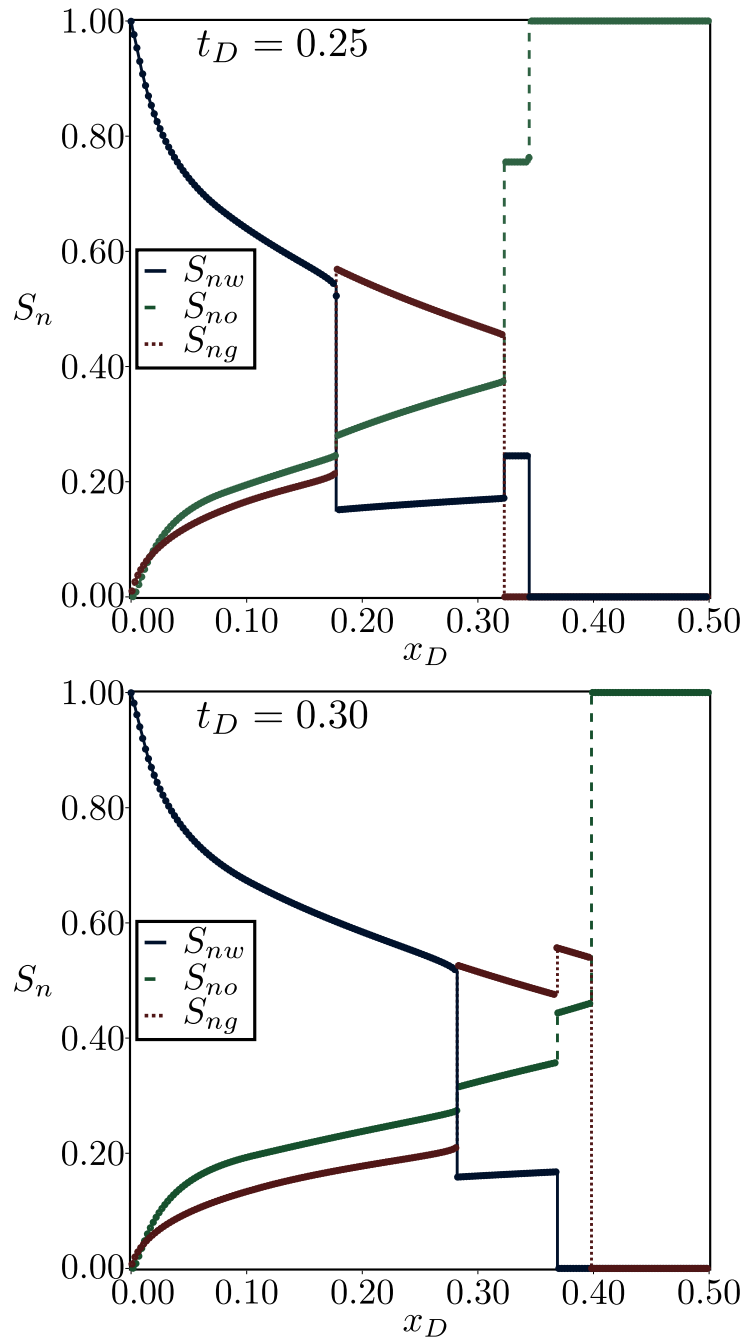


Figure 29: Saturation profile before ( $t_D = 0.25$ ) and after the ( $t_D = 0.30$ ) the SCT interaction for the Group 02 of WAG interactions, compared with numerical solution

#### 4.2.3. Group 03 - Slow Rarefaction Transmission

400 After the residual oil saturation in the inlet face reaches  $S_{om}$ , the solution of  
each cycle is always a composite wave in  $\overline{S_{nw}S_{ng}}$  edge. Thus, the rarefaction of  
a particular cycle will always interact with the next composite wave by a RCT  
transmission (Figure 30). This interaction accelerates the composite wave and,  
consequently, expands of the rarefaction fan, appearing new rarefaction waves.  
405 Rarefactions transmitted in RCT will interact with all rarefaction fan above the  
composite wave in the form of RRT transmission.

Both RCT and RRT interactions can be seen in Figure 27 in  $x_D \approx 0.05$  for  
 $t_D = 0.18$ . It is important to observe that due to the RRT interactions, the  
rarefaction fan above the composite wave does not belong to the  $\overline{S_{nw}S_{ng}}$  edge  
410 as before (showed in Figure 23). As discussed in Section 3.5, the RRT region  
comprises a continuous solution where besides we show two characteristics in  
the same position, it is used only to exemplify, because they have same value in  
each point.

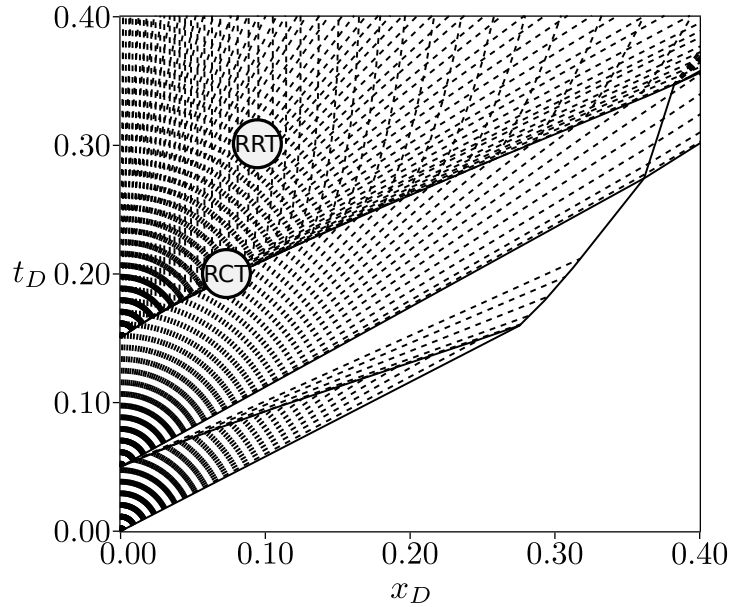


Figure 30: Third group of interactions - RCT and RRT

4.2.4. Group 04 - Transmitted Shock-Composite Transmission

415 In the Group 02 there is a transmission of a slow shock in space-time plane in the form of SRT interaction. At some moment, this slow shock will collide with the composite wave of the next cycle, in the form of a SCT transmission (Figure 31). The way to solve this interaction is evaluate both sides of the associated Riemann problem (Section 3.6).

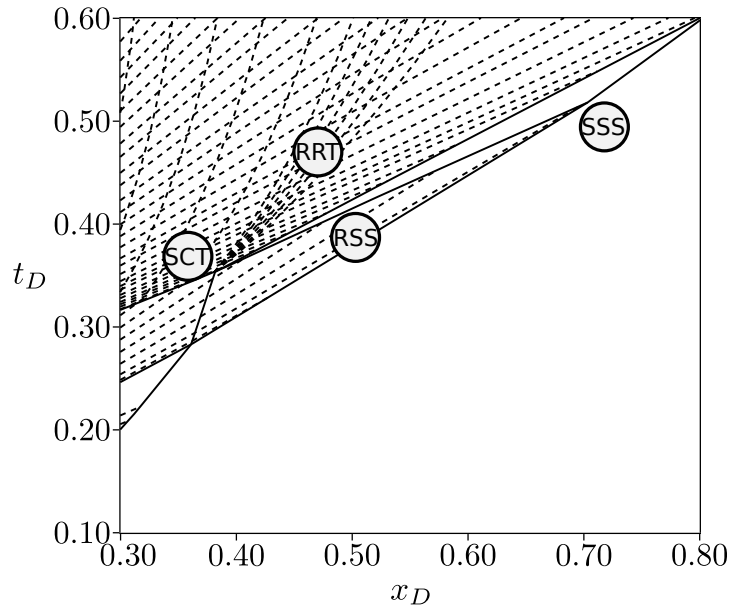


Figure 31: Fourth group of interactions - SCT, RSS and SSS

420 The left side of the associated Riemann problem is the composite wave state after all RCT interactions described in Group 03, while the right state is the right side of the slow shock after all SRT transmissions of Group 02. It is important to observe that the right state will be always either in  $\overline{S_{nw}S_{no}}$  or the  $\overline{S_{no}S_{ng}}$  edge. The Figure 32 presents the Hugoniot locus of the left state of the associated Riemann problem in the ternary diagram, in which  $S^L$  and  $S^R$   
 425 are the left and right sides of this associated problem, respectively. As it can be seen, there is no direct shock between these states, and the solution must necessarily pass through a point in  $\overline{S_{no}S_{ng}}$  edge.

Using the same arguments described in Section 4.1.2, there is a separatrix  
 430 point  $J_{S_{no}S_{ng}}^*$  where the Hugoniot locus locally changes its topology, forming a  
 stable orbit for the vanishing viscosity criteria (Figure 33). Thus, the solution  
 of this Riemann problem is composed by three parts:

1. Expansion of the left composite wave until the shock for the separatrix  
 point becomes allowed;
- 435 2. Shock to the separatrix point (either  $J_{S_{nw}S_{no}}^*$  or  $J_{S_{no}S_{ng}}^*$ ) creating a con-  
 stant state in this point;
3. Shock to the right state of the associated Riemann problem.

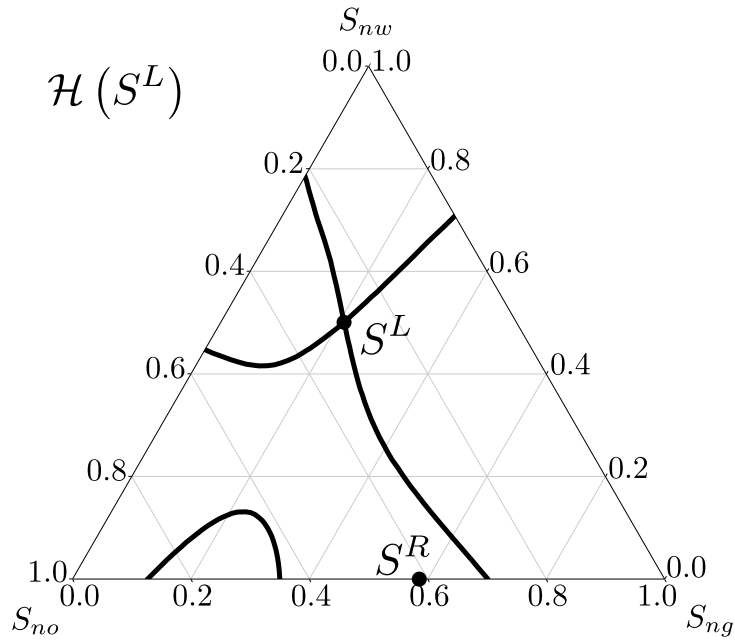


Figure 32: Hugoniot locus for the left state of the SCT interaction in Group 04

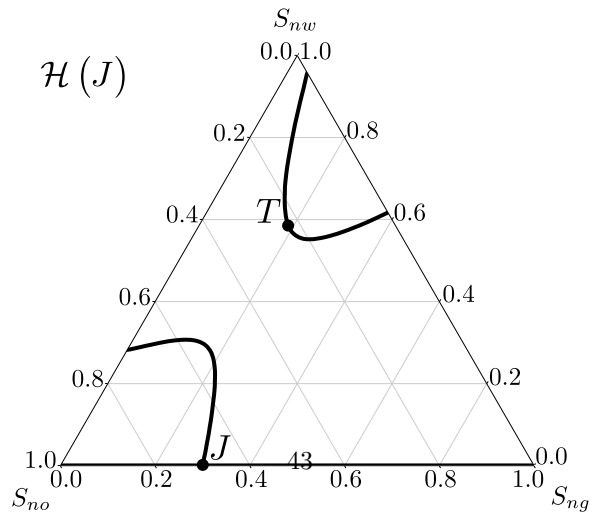
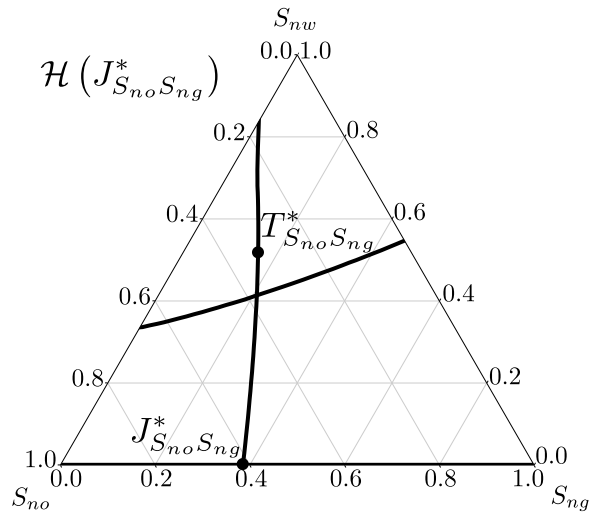
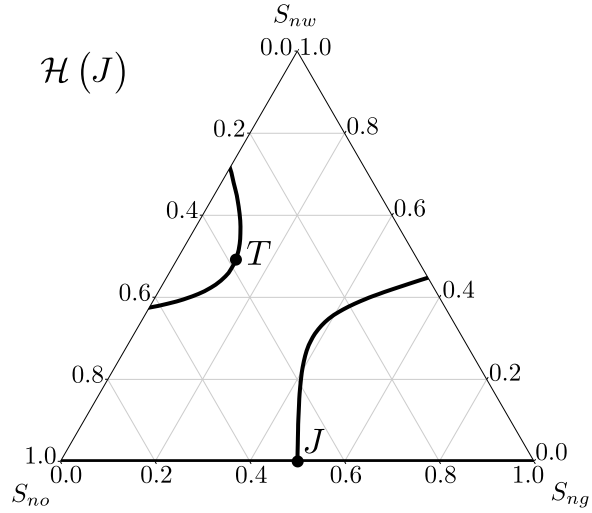


Figure 33: Hugoniot locus for three different positions along the  $\overline{S_{no}S_{ng}}$  edge

The Figure 34 shows the saturation profile before ( $t_D = 0.34$ ) and after ( $t_D = 0.39$ ) the SCT interaction. The expansion of the left composite wave creates rarefactions that interacts with the transmitted rarefactions of Group 03, by a RRT transmission, changing continuously the rarefaction fan of left state (showed in the form of a ramp in  $x_D \approx 0.40$  for  $t_D = 0.39$ ). After this RRT interaction there is a composite shock followed by a constant state of  $J_{S_{no}S_{ng}}^*$  point and finishing with a shock to the right state of the Riemann associated problem ( $x_D \approx 0.45$  for  $t_D = 0.39$ ).

The last shock of SCT interaction is in the same edge of the transmitted waves of Group 02 ( $\overline{S_{no}S_{ng}}$  for the third cycle) generating a continuous RSS superposition and diminishing the rarefaction fan in front of this shock ( $x_D \approx 0.65$  for  $t_D = 0.48$  in Figure 35). At some point this shock will superpose with the fast shock generated in Group 02, in the form of SSS interaction, creating a single shock that bounds the  $J_{S_{no}S_{ng}}^*$  constant state ( $x_D \approx 0.75$  for  $t_D = 0.54$  in Figure 35).

One may observe that for water cycles, this process creates a constant state in  $J_{S_{no}S_{ng}}^*$  point bounded by a shock in  $\overline{S_{no}S_{ng}}$  edge and for gas cycles it is created a constant state in point  $J_{S_{nw}S_{no}}^*$  bounded by a shock in  $\overline{S_{nw}S_{no}}$  edge. These constant states generated in this Group 04 will vanish in the SCT interaction of the Group 02 for the next WAG slug starting a new solution cycle ( $x_D \approx 0.85$  for  $t_D = 0.55$  in Figure 25).

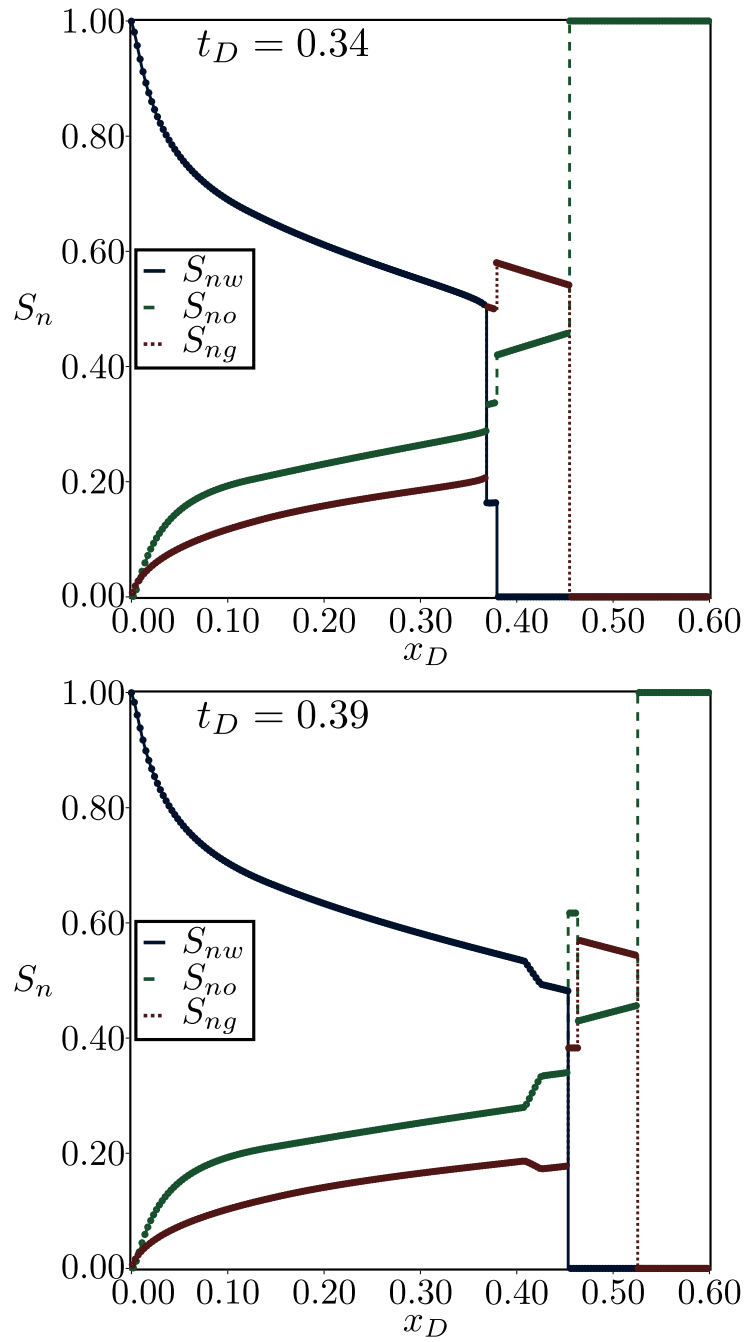


Figure 34: Saturation profile before ( $t_D = 0.34$ ) and after the ( $t_D = 0.39$ ) the SCT interaction for the Group 04 of WAG interactions, compared with numerical solution

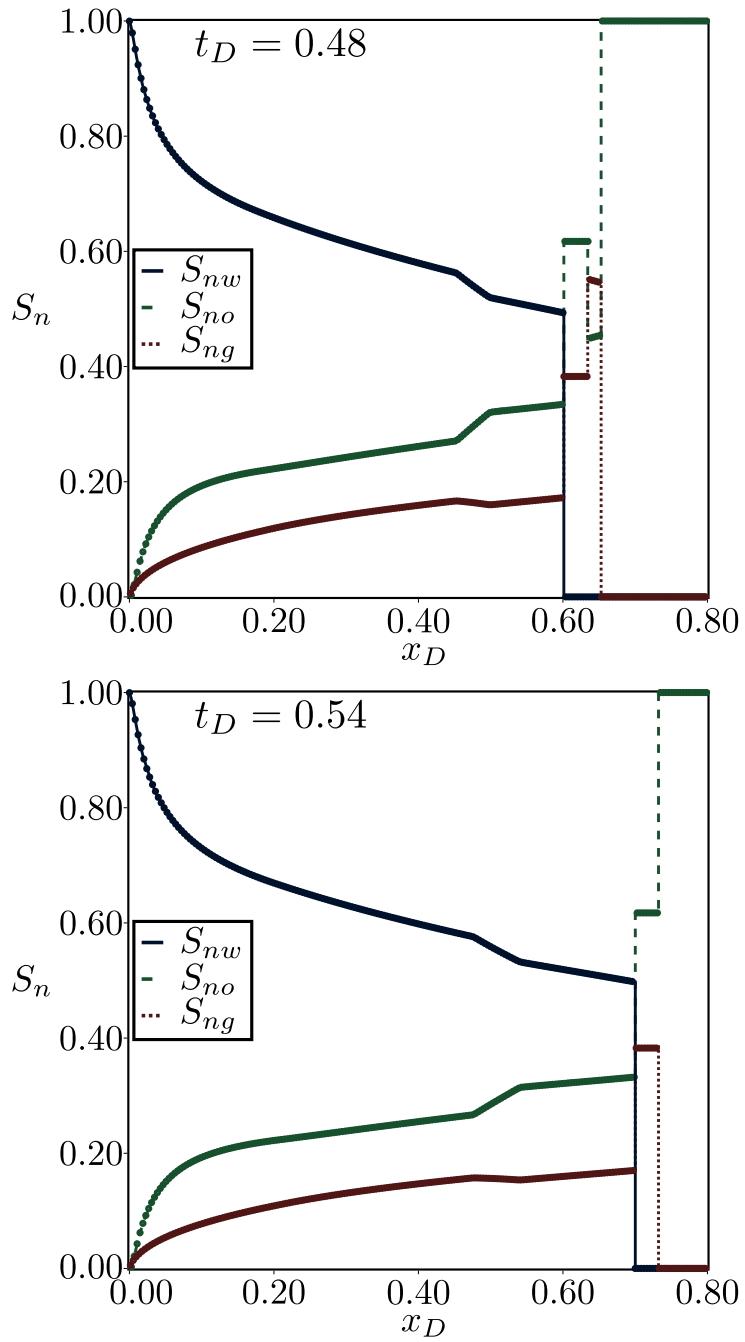


Figure 35: Saturation profile before ( $t_D = 0.48$ ) and after the ( $t_D = 0.54$ ) the SSS interaction for the Group 04 of WAG interactions, compared with numerical solution

## 5. Conclusions

460 We present the analytical solution of WAG scheme considering the wave interactions among different injected slugs. The mathematical solution was obtained using the method of characteristics where we classify and discuss the mathematical keys involved in all wave interactions.

The WAG scheme shows a cyclic wave interactions where after we identify 465 the main groups involved, the solution can be extended for any number of injected cycles. The difference of displacement efficiency between water and gas injection is observed after the first cycle, in which additional oil is mobilized in porous media. All results were compared with numerical simulations, showing a good agreement. The results obtained in this paper improves our mathematical 470 understanding of WAG scheme and can be used to validate reservoir numerical simulators.

## 6. Acknowledgments

The authors acknowledges the Universidade Estadual do Norte Fluminense (UENF) for financial support. This study was also financed in part by the 475 Coordenação de Aperfeiçoamento de Pessoal de Nível Superior - Brasil (CAPES) - Finance Code 001.

## References

- 480 Apolinário, F.O., de Paula, A.S., Pires, A.P., 2020. Injection of water slug containing two polymers in porous media: Analytical solution for two-phase flow accounting for adsorption effects. *Journal of Petroleum Science and Engineering* 188, 106927. URL: <https://doi.org/10.1016/j.petrol.2020.106927>, doi:10.1016/j.petrol.2020.106927.
- 485 Apolinário, F.O., Pires, A.P., 2021. Oil displacement by multicomponent slug injection: An analytical solution for langmuir adsorption isotherm. *Journal of Petroleum Science and Engineering* 197, 107939. URL: <https://doi.org/10.1016/j.petrol.2020.107939>, doi:10.1016/j.petrol.2020.107939.
- Aziz, K., Settari, A., 1979. *Petroleum reservoir simulation*. Applied Science Publishers.
- 490 Baker, L., 1988. Three-phase relative permeability correlations, in: *SPE Enhanced Oil Recovery Symposium*, Society of Petroleum Engineers. URL: <https://doi.org/10.2118/17369-ms>, doi:10.2118/17369-ms.
- Bell, J.B., Trangenstein, J.A., Shubin, G.R., 1986. Conservation laws of mixed type describing three-phase flow in porous media. *SIAM Journal on Applied Mathematics* 46, 1000–1017. URL: <https://doi.org/10.1137/0146059>, doi:10.1137/0146059.
- 495 Borazjani, S., Bedrikovetsky, P., Farajzadeh, R., 2016. Analytical solutions of oil displacement by a polymer slug with varying salinity. *Journal of Petroleum Science and Engineering* 140, 28–40. URL: <https://doi.org/10.1016/j.petrol.2016.01.001>, doi:10.1016/j.petrol.2016.01.001.
- 500 Buckley, S., Leverett, M., 1942. Mechanism of fluid displacement in sands. *Transactions of the AIME* 146, 107–116. URL: <https://doi.org/10.2118/942107-g>, doi:10.2118/942107-g.

- 505 Castañeda, P., Abreu, E., Furtado, F., Marchesin, D., 2016. On a universal structure for immiscible three-phase flow in virgin reservoirs. *Computational Geosciences* 20, 171–185. URL: <https://doi.org/10.1007/s10596-016-9556-5>, doi:10.1007/s10596-016-9556-5.
- Christensen, J., Stenby, E., Skauge, A., 2001. Review of WAG field experience. *SPE Reservoir Evaluation & Engineering* 4, 97–106. URL: <https://doi.org/10.2118/71203-pa>, doi:10.2118/71203-pa.
- 510 Corey, A., Rathjens, C., Henderson, J., Wyllie, M., 1956. Three-phase relative permeability. *Journal of Petroleum Technology* 8, 63–65. URL: <https://doi.org/10.2118/737-g>, doi:10.2118/737-g.
- Delshad, M., Pope, G., 1989. Comparison of the three-phase oil relative permeability models. *Transport in Porous Media* 4. URL: <https://doi.org/10.1007/bf00134742>, doi:10.1007/bf00134742.
- 515 Guzmán, R.E., Fayers, F.J., 1997a. Mathematical properties of three-phase flow equations. *SPE Journal* 2, 291–300. URL: <https://doi.org/10.2118/35154-pa>, doi:10.2118/35154-pa.
- Guzmán, R.E., Fayers, F.J., 1997b. Solutions to the three-phase buckley-leverett problem. *SPE Journal* 2, 301–311. URL: <https://doi.org/10.2118/35156-pa>, doi:10.2118/35156-pa.
- 520 Holden, L., 1990. On the strict hyperbolicity of the buckley-leverett equations for three-phase flow in a porous medium. *SIAM Journal on Applied Mathematics* 50, 667–682. URL: <https://doi.org/10.1137/0150039>, doi:10.1137/0150039.
- 525 Holtz, M.H., 2016. Immiscible water alternating gas (IWAG) EOR: Current state of the art, in: *SPE Improved Oil Recovery Conference*, Society of Petroleum Engineers. URL: <https://doi.org/10.2118/179604-ms>, doi:10.2118/179604-ms.

- 530 Khorsandi, S., Qiao, C., Johns, R.T., 2016. Displacement efficiency for low-salinity polymer flooding including wettability alteration. SPE Journal 22, 417–430. URL: <https://doi.org/10.2118/179695-pa>, doi:10.2118/179695-pa.
- LaForce, T., Jessen, K., 2010. Analytical and numerical investigation of multi-  
535 component multiphase WAG displacements. Computational Geosciences 14, 745–754. URL: <https://doi.org/10.1007/s10596-010-9185-3>, doi:10.1007/s10596-010-9185-3.
- Lax, P.D., 1957. Hyperbolic systems of conservation laws II. Communications on Pure and Applied Mathematics 10, 537–566. URL: <https://doi.org/10.1002/cpa.3160100406>, doi:10.1002/cpa.3160100406.  
540
- LeVeque, R., J, L., Crighton, D., 2002. Finite Volume Methods for Hyperbolic Problems. Cambridge Texts in Applied Mathematics, Cambridge University Press.
- Leverett, M., 1939. Flow of oil-water mixtures through unconsolidated sands. Transactions of the AIME 132, 149–171. URL: <https://doi.org/10.2118/939149-g>, doi:10.2118/939149-g.  
545
- Leverett, M., Lewis, W., 1941. Steady flow of gas-oil-water mixtures through unconsolidated sands. Transactions of the AIME 142, 107–116. URL: <https://doi.org/10.2118/941107-g>, doi:10.2118/941107-g.
- 550 Liu, T.P., 1974. The riemann problem for general 2x2 conservation laws. Transactions of the American Mathematical Society 199, 89. URL: <https://doi.org/10.2307/1996875>, doi:10.2307/1996875.
- Liu, T.P., 1975. The riemann problem for general systems of conservation laws. Journal of Differential Equations 18, 218–234. URL: [https://doi.org/10.1016/0022-0396\(75\)90091-1](https://doi.org/10.1016/0022-0396(75)90091-1), doi:10.1016/0022-0396(75)90091-1.  
555

- Marchesin, D., Plohr, B.J., 2001. Wave structure in WAG recovery. SPE Journal 6, 209–219. URL: <https://doi.org/10.2118/71314-pa>, doi:10.2118/71314-pa.
- 560 Nadeson, G., Anua, N.A.B., Singhal, A., Ibrahim, R.B., 2004. Water-alternating-gas (WAG) pilot implementation, a first EOR development project in dulang field, offshore peninsular malaysia, in: SPE Asia Pacific Oil and Gas Conference and Exhibition, Society of Petroleum Engineers. URL: <https://doi.org/10.2118/88499-ms>, doi:10.2118/88499-ms.
- 565 Rhee, H.K., Aris, R., Amundson, N.R., 1970. On the theory of multicomponent chromatography. Philosophical Transactions of the Royal Society of London. Series A, Mathematical and Physical Sciences 267, 419–455. URL: <https://doi.org/10.1098/rsta.1970.0050>, doi:10.1098/rsta.1970.0050.
- 570 Shearer, M., Trangenstein, J.A., 1989. Loss of real characteristics for models of three-phase flow in a porous medium. Transport in Porous Media 4. URL: <https://doi.org/10.1007/bf00179533>, doi:10.1007/bf00179533.
- Stone, H., 1970. Probability model for estimating three-phase relative permeability. Journal of Petroleum Technology 22, 214–218. URL: <https://doi.org/10.2118/2116-pa>, doi:10.2118/2116-pa.
- 575 Tai-Ping, L., 2007. Hyperbolic and Viscous Conservation Laws. CBMS-NSF Regional Conference Series in Applied Mathematics, Siam.
- Wendroff, B., 1972a. The riemann problem for materials with nonconvex equations of state i: Isentropic flow. Journal of Mathematical Analysis and Applications 38, 454–466. URL: [https://doi.org/10.1016/0022-247x\(72\)90103-5](https://doi.org/10.1016/0022-247x(72)90103-5), doi:10.1016/0022-247x(72)90103-5.
- 580 Wendroff, B., 1972b. The riemann problem for materials with nonconvex equations of state ii: General flow. Journal of Mathematical Analysis and Applications 38, 640–658. URL: [https://doi.org/10.1016/0022-247x\(72\)90075-3](https://doi.org/10.1016/0022-247x(72)90075-3), doi:10.1016/0022-247x(72)90075-3.



**7     *Article: Analytical Solution for  
the Miscible Water Alternating  
Gas (MWAG) Recovery Method***

# Analytical Solution for the Miscible Water Alternating Gas (MWAG) Recovery Method

Wagner Q. Barros<sup>a</sup>, Adolfo P. Pires<sup>a,\*</sup>, Alvaro M. M. Peres<sup>a</sup>

<sup>a</sup>*Laboratório de Engenharia e Exploração de Petróleo - Universidade Estadual do Norte Fluminense Darcy Ribeiro, Rodovia Amaral Peixoto, Km 163, Imboassica, Macaé, 27925-310, Rio de Janeiro, Brazil*

---

## Abstract

With the Brazilian pre-salt discoveries the use of the Miscible Water Alternating Gas (MWAG) recovery technique has recently increase. This method is useful in fields with a large amount of  $CO_2$  where the produced gas should be re-injected into the reservoir, and using only gasflooding the recovery factors do not achieve satisfactory values. Mathematical solutions are in paramount of importance to understand MWAG schemes, because it brings insights that cannot be obtained only using numerical simulations. In this paper we present a new mathematical three-phase formulation where oil and gas exchanges mass while water is considered an immiscible phase. This new approach is very useful because the hydrodynamic and thermodynamic equations are decoupled by the splitting technique allowing that the hydrocarbon phases can be described for any number of components. The equations are solved by the method of characteristics and the time variable boundary conditions, inherent of MWAG methods, are solved by the wave interaction technique. Analytical solutions are compared with numerical methods showing a close agreement.

*Keywords:* Water Alternating Gas, Enhanced Oil Recovery, WAG, Miscible Methods, Method of Characteristics

---

\*Corresponding author

*Email addresses:* [wagnerqb@gmail.com](mailto:wagnerqb@gmail.com) (Wagner Q. Barros), [adolfo.puime@gmail.com](mailto:adolfo.puime@gmail.com) (Adolfo P. Pires), [alvaroperes@lenep.uenf.br](mailto:alvaroperes@lenep.uenf.br) (Alvaro M. M. Peres)

## 1. Introduction

The Water Alternating Gas (WAG) technique combines the high displacement efficiency of the gas injection with the mobility control provided by water slugs, increasing the sweep efficiency and stabilizing the gas injection front Christensen et al. (2001). Regarding to the injected gas characteristics we can divided the WAG scheme in two major groups (Shahverdi et al., 2011; Shahverdi and Sohrabi, 2013):

1. Miscible WAG (MWAG): the composition of the injected gas and the original oil creates a miscible displacement, in which the lack of interfacial tension between phases drastically increases the displacement efficiency (Shahverdi et al., 2011; Shahverdi and Sohrabi, 2013; Afzali et al., 2018). Generation and maintenance of an stable miscible front is governed by equilibrium thermodynamic concepts and depends of fluids composition, pressure and temperature.
2. Immiscible WAG (IWAG): when the miscibility effect in reservoir's pressure and temperature is not achieved, it will occur the simultaneous flow of oil, gas and water in reservoir. The existence of surface tension between fluids decreases the displacement efficiency when compared to the MWAG, however, due to relative permeability hysteresis effects, this method reaches higher recovery factors when compared to waterflooding or gasflooding injections;

The incremental recovery factor when using WAG schemes varies between 1% unit 13% for IWAG and from 2% until 20% for MWAG applications (Christensen et al., 2001; Holtz, 2016). This huge performance range depends mainly of reservoir factors like fluid channeling, presence of sealing faults and the balance between gravity and viscous forces (Sanchez, 1999; Afzali et al., 2018). From the mathematical perspective the MWAG injection is a combination of hydrodynamic hyperbolic equations with an accurate thermodynamic description that can captures the mas transfer among phases.

Solutions for the hydrodynamic system started with the Buckley-Leverett equations (Buckley and Leverett, 1942; Leverett, 1939), where it was considered the transient oil displacement by an immiscible fluid injection in an one-dimensional reservoir. The system was described in terms of a non-linear hyperbolic partial differential equation and solved by the method of characteristics. Improved solutions of two-phase immiscible flow included capillary

and gravitational effects (Welge, 1952; Sheldon and Cardwell, 1959; Fayers and Sheldon, 1959).

Three-phase immiscible solutions follows the same principle where a system of non-linear partial differential equations is solved by the same method. However, depending on the relative permeability curves used to model the three-phase flow in the porous medium, it can appear points (umbilic) or regions where the system loses its hyperbolicity (Guzmán and Fayers, 1997a). Then, the solution for three-phase immiscible flow are divided in three main groups: Hyperbolic with a single umbilic point (Isaacson et al., 1990, 1992; Guzmán and Fayers, 1997b; Marchesin and Plohr, 2001; Marchesin and Mailybaev, 2006; Azevedo et al., 2009, 2014; Castañeda et al., 2016; Guerrero and Marchesin, 2020; Barros et al., 2021), hyperbolic with multiple umbilic points (Guzmán and Fayers (1997a,b)) and mixed hyperbolic and elliptic (Shearer and Trangenstein (1989); Guzmán and Fayers (1997b); Jackson and Blunt (2002)). Additional issues appear in the solution when we solve the immiscible system with variable boundary conditions (WAG principle), because new waves are constantly entering in the medium and interacting with the one previously in the system (Andrade et al., 2016, 2018).

All the solutions described before do not consider the mass exchange between injected and displaced phases. Traditionally the thermodynamic equilibrium between components in gas and oil phases can be described using the tie-line approximation (Wachmann, 1964; Hirasaki, 1981; Dumoré et al., 1984; Monroe et al., 1990; Johns et al., 1993; Johns and Orr, 1996; Orr Jr., 2007). By this approach, the liquid-vapor equilibrium is completely described by a map between composition and a virtual line that connects both phases. The thermodynamic equations are coupled with hydrodynamic ones, creating a hyperbolic partial differential equation system that is solved by the application of the method of characteristics. Additional efforts were made by Bedrikovetsky et al. (2004); Dutra et al. (2009) in order to decouple hydrodynamic and thermodynamic in different systems (splitting technique), allowing the solution of multi-component mixtures having more than three components.

Three-phase miscible solutions were found extending the tie-line concept for three-phase space (LaForce and Johns, 2005; LaForce et al., 2006; LaForce and Jessen, 2010). Using this approach and taking advantage of the Gibbs freedom rule the three phase system is divided in different spaces where the traditional immiscible theory applies. The main issue of this technique is that the complexity increase with the number of components in the mixture.

Despite all the methods that treat miscible flow reported in literature, for the best of our knowledge, there is not a mathematical description for the three-phase flow in a linear porous medium where only oil and gas can exchange mass and water is treated as an immiscible phase. This approach is useful because the splitting technique can be applied and problem can be solved for any number of components.

In this work we formulate a new mathematical system that describes the three-phase flow in a linear porous medium, where oil and gas can exchange mass while water is treated as an immiscible phase. We solve this problem considering time variable boundary conditions, describing the main aspects of the miscible WAG scheme. In Section 2 we present the physical and mathematical model, where we apply the splitting scheme to decouple thermodynamic and hydrodynamic equations. Next we described the general solution of both systems using the method of characteristics (Section 3). In the next two sections we solve the thermodynamic and hydrodynamic systems using an example to illustrate the solution (Sections 4 and 5). Finally we address some conclusion.

## 2. Physical and Mathematical Model

We are investigating the alternated water and gas injection in a reservoir initially containing oil at irreducible water saturation (Figure 1). Gas and oil phases are allowed to exchange mass while water is considered immiscible. Additional hypothesis are:

1. One-dimensional, linear and homogeneous porous medium with constant cross sectional area;
2. Instantaneous thermodynamic equilibrium between components in gas and oil phases;
3. Isothermal flow with absence of chemical reactions and molecular diffusion;
4. Negligible dispersive, gravitational and capillary effects;
5. Hypothesis considered in Darcy's equation are valid;
6. Low pressure gradient along porous medium;
7. Water and rock are treated as incompressible phases;
8. Ideal mixing is valid for oil and gas phases (Amagat's hypothesis).

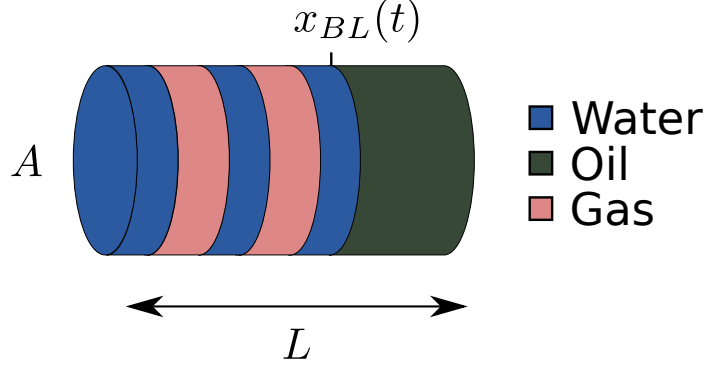


Figure 1: Mathematical model for the Miscible Water Alternating Gas (MWAG) problem.

Using the water immiscibility consideration and applying the mole conservation of hydrocarbon component  $i$ :

$$\begin{cases} \phi \frac{\partial}{\partial t} (S_o \rho_o x_{io} + S_g \rho_g x_{ig}) + \frac{\partial}{\partial x} (\rho_o x_{io} u_o + \rho_g x_{ig} u_g) = 0, & i = 1, \dots, n \\ \phi \frac{\partial S_w}{\partial t} + \frac{\partial u_w}{\partial x} = 0 \end{cases} \quad (1)$$

in which  $S_\pi$ ,  $\rho_\pi$  and  $u_\pi$  are the saturation, molar density and velocity of the generic phase  $\pi$  ( $\pi$  can be water ( $w$ ), oil ( $o$ ) or gas ( $g$ ));  $\phi$  is the rock porosity,  $x_{i\pi}$  is the mole fraction of component  $i$  in phase  $\pi$  and  $n$  is the number of hydrocarbon components considered in the problem. By the ideal mixing hypothesis the molar density of hydrocarbon phases ( $\rho_{o|g}$ ) may be written by:

$$\rho_{(o|g)} = \left( \sum_{i=1}^n \frac{x_{i(o|g)}}{\rho_{ci}} \right)^{-1} \quad (2)$$

where  $\rho_{ci}$  is the molar density of the pure component  $i$  at same pressure and temperature of the original system. We now define the volume fraction of component  $i$  in hydrocarbon phases:

$$c_{i(o|g)} = \frac{\frac{x_{i(o|g)}}{\rho_{ci}}}{\sum_{k=1}^n \frac{x_{k(o|g)}}{\rho_{ck}}} \quad (3)$$

and after some algebraic manipulation in Equation 1 we have:

$$\begin{cases} \phi \frac{\partial}{\partial t} (S_o c_{io} + S_g c_{ig}) + \frac{\partial}{\partial x} (u_o c_{io} + u_g c_{ig}) = 0, & i = 1, \dots, n \\ \phi \frac{\partial S_w}{\partial t} + \frac{\partial u_w}{\partial x} = 0 \end{cases} \quad (4)$$

The phase velocity is related with the gradient pressure by the Darcy's equation:

$$u_\pi(x, t) = \frac{q_\pi}{A} = -K \lambda_\pi(x, t) \frac{\partial P(x, t)}{\partial x} \quad (5)$$

where  $K$  is the reservoir absolute permeability,  $q_\pi$  is the phase volumetric flow and  $\lambda_\pi$  is the phase mobility, defined by:

$$\lambda_\pi = \frac{k_{r\pi}}{\mu_\pi} \quad (6)$$

in which  $k_{r\pi}$  and  $\mu_\pi$  are the relative permeability and viscosity of phase  $\pi$ . It is important to note that the relative permeability is function of the saturation of all phases ( $k_{r\pi} = k_{r\pi}(S_w, S_o, S_g)$ ) and for hydrocarbon phases the viscosity is function of the phase volumetric composition ( $\mu_\pi = \mu_\pi(c_{1\pi}, \dots, c_{n\pi})$ ).

Defining the fractional flow for phase  $\pi$ :

$$f_\pi = \frac{u_\pi}{u_w + u_o + u_g} = \frac{\lambda_\pi}{\lambda_w + \lambda_o + \lambda_g} \quad (7)$$

and manipulating Equation 4, we have:

$$\begin{cases} \phi \frac{\partial}{\partial t} (S_o c_{io} + S_g c_{ig}) + \frac{q_T}{A} \frac{\partial}{\partial x} (f_o c_{io} + f_g c_{ig}) = 0, & i = 1, \dots, n \\ \phi \frac{\partial S_w}{\partial t} + \frac{q_T}{A} \frac{\partial f_w}{\partial x} = 0 \end{cases} \quad (8)$$

in which  $q_T = q_T(t)$  is the volumetric total flow rate ( $q_T = q_w + q_o + q_g$ ) and  $A$  is the porous medium cross sectional area.

Considering  $L$  the porous medium length we introduce the dimensionless spatial and temporal variables:

$$x_D = \frac{x}{L} \quad (9)$$

$$t_D = \frac{\int_0^t q_T(x=0, \tau) d\tau}{AL\phi} \quad (10)$$

then, we obtain the dimensionless form of the mass conservation system:

$$\begin{cases} \frac{\partial}{\partial t_D} (S_o c_{io} + S_g c_{ig}) + \frac{\partial}{\partial x_D} (f_o c_{io} + f_g c_{ig}) = 0, & i = 1, \dots, n \\ \frac{\partial S_w}{\partial t_D} + \frac{\partial f_w}{\partial x_D} = 0 \end{cases} \quad (11)$$

### 2.1. Tie-Line Equilibrium Formulation

As we are considering that only oil and gas phases are allowed to exchange mass it is natural to describe the solution in terms of normalized hydrocarbon saturations:

$$\begin{cases} S_o^{HC} = \frac{S_o}{S_o + S_g} = \frac{S_o}{1 - S_w} \\ S_g^{HC} = \frac{S_g}{S_o + S_g} = \frac{S_g}{1 - S_w} \end{cases} \quad (12)$$

and normalized hydrocarbon fractional flow:

$$\begin{cases} f_o^{HC} = \frac{v_o}{v_o + v_g} = \frac{f_o}{1 - f_w} \\ f_g^{HC} = \frac{v_g}{v_o + v_g} = \frac{f_g}{1 - f_w} \end{cases} \quad (13)$$

where the superscript  $HC$  means that this property is normalized by hydrocarbon phases. Then, defining the total composition of component  $i$ :

$$C_i = S_o^{HC} c_{io} + S_g^{HC} c_{ig} \quad (14)$$

and the total fractional flow of the same component:

$$F_i = f_o^{HC} c_{io} + f_g^{HC} c_{ig} \quad (15)$$

we can rewrite the Equation 11 in the form:

$$\begin{cases} \frac{\partial S_{HC} C_i}{\partial t_D} + \frac{\partial f_{HC} F_i}{\partial x_D} = 0, & i = 1, \dots, n \\ \frac{\partial S_w}{\partial t_D} + \frac{\partial f_w}{\partial x_D} = 0 \end{cases} \quad (16)$$

where  $S_{HC} = 1 - S_w$  and  $f_{HC} = 1 - f_w$ . Additional restrictions are:

$$S_w + S_o + S_g = 1 \quad (17)$$

$$S_o^{HC} + S_g^{HC} = 1 \quad (18)$$

$$f_w + f_o + f_g = 1 \quad (19)$$

$$f_o^{HC} + f_g^{HC} = 1 \quad (20)$$

$$\sum_{i=1}^n C_i = \sum_{i=1}^n (S_o^{HC} c_{io} + S_g^{HC} c_{ig}) = 1 \quad (21)$$

$$\sum_{i=1}^{N_c} F_i = \sum_{i=1}^{N_c} (f_o^{HC} c_{io} + f_g^{HC} c_{ig}) = 1 \quad (22)$$

To model the thermodynamic equilibrium between hydrocarbon phases, we will relate the composition of component  $i$  with the composition of the last hydrocarbon component ( $C_n$ ):

$$C_i = \alpha_i C_n + \beta_i \quad (23)$$

in which  $\alpha_i$  and  $\beta_i$  are known by tie-line coefficients, calculated after some manipulation in Equation 14:

$$\begin{cases} \alpha_i = \frac{c_{io} - c_{ig}}{c_{no} - c_{ng}} \\ \beta_i = c_{ig} - \alpha_i c_{ng} \end{cases} \quad (24)$$

Note that if we manipulate the Equation 15 we have:

$$F_i = \alpha_i F_n + \beta_i \quad (25)$$

and consequently the final form of the mass conservation system:

$$\begin{cases} \frac{\partial S_{HC}(\alpha_i C_n + \beta_i)}{\partial t_D} + \frac{\partial f_{HC}(\alpha_i F_n + \beta_i)}{\partial x_D} = 0, \quad i = 2, \dots, n-1 & \text{(a)} \\ \frac{\partial S_{HC} C_n}{\partial t_D} + \frac{\partial f_{HC} F_n}{\partial x_D} = 0 & \text{(b)} \\ \frac{\partial S_w}{\partial t_D} + \frac{\partial f_w}{\partial x_D} = 0 & \text{(c)} \end{cases} \quad (26)$$

Note that the first part of this PDE (Partial Differential Equation) system has  $n - 2$  equations. This happens because we are modeling the thermodynamic system in terms of the last component composition ( $C_n$ ) and using restrictions showed in Equations 21 and 22.

For any system in thermodynamic equilibrium the Gibb's rule states that the mathematical freedom of the system is calculated by  $F = n - N_p + 2$ , where  $N_p$  is the number of phases. With only oil and gas as hydrocarbon phases and assuming constant pressure and temperature along porous medium (low

pressure gradient hypothesis), any tie-line can be uniquely identified by  $F = N_c - 2$  variables. This means that we can write the  $\alpha_i$  variable as  $\alpha_i = \alpha_i(\beta_2, \dots, \beta_{n-1})$ .

## 2.2. System's Splitting

Equation 26 is a system of  $n$  non-linear partial differential equations that describes the miscible WAG flow in a linear porous medium. In order to obtain an analytical solution for such system we will apply the splitting technique (Pires et al., 2006) to decouple the thermodynamic and hydrodynamic parts of the PDE system. Integrating the Equation 26-(a) in  $(0, x_D) \times (0, t_D)$  domain and applying the Green's theorem:

$$\int_0^{t_D} \int_0^{x_D} \left[ \frac{\partial S_{HC}(\alpha_i C_n + \beta_i)}{\partial t_D} + \frac{\partial f_{HC}(\alpha_i F_n + \beta_i)}{\partial x_D} \right] dx_D dt_D = \oint [-f_{HC}(\alpha_i F_n + \beta_i) dt_D + S_{HC}(\alpha_i C_n + \beta_i) dx_D] = 0 \quad (27)$$

We may now define two auxiliary variables for this problem

$$d\varphi = -f_{HC}F_n dt_D + S_{HC}C_n dx_D \quad (28)$$

$$d\psi = f_{HC}dt_D - S_{HC}dx_D \quad (29)$$

and substituting in Equation 27 we obtain:

$$\oint [\alpha_i d\varphi - \beta_i d\psi] = 0 \quad (30)$$

Applying again the Green's theorem we have the final form or the auxiliary thermodynamic system:

$$\frac{\partial \alpha_i}{\partial \psi} + \frac{\partial \beta_i}{\partial \varphi} = 0, \quad i = 2, \dots, n-1 \quad (31)$$

note that by the Gibb's rule we can write  $\alpha_i = \alpha_i(\beta_2, \dots, \beta_{n-1})$  and consequently Equation 31 depends exclusively of thermodynamic variables.

### 2.3. Velocity Projection

It is necessary a rule to convert the solution from  $(\varphi, \psi)$  to  $(x_D, t_D)$  spaces. Using the characteristics definition  $x_D = x_D(t_D)$  in Equations 28 and 29 manipulating we have:

$$\frac{d\varphi}{d\psi} = \frac{-f_{HC}F_n + S_{HC}C_n \frac{dx_D}{dt_D}}{f_{HC} - S_{HC} \frac{dx_D}{dt_D}} \quad (32)$$

and:

$$\frac{dx_D}{dt_D} = \frac{f_{HC} \left( F_n + \frac{d\varphi}{d\psi} \right)}{S_{HC} \left( C_n + \frac{d\varphi}{d\psi} \right)} \quad (33)$$

these equations are used to convert characteristic speeds from both planes, helping the solution of the WAG problem.

## 3. General Solution of Miscible WAG System

The application of the splitting technique decoupled the equation system and isolated the thermodynamic part of the solution. In this section we will discuss the general analytical solution of the miscible WAG problem in term of thermodynamic and hydrodynamic systems.

### 3.1. General Solution of Thermodynamic System

Equation 31 is a non-linear hyperbolic equation system. To solve it we apply the method of characteristics, describing the solution in terms of travelling shock and rarefaction waves (Tai-Ping, 2007).

#### 3.1.1. Shock Waves in Thermodynamic System

A shock wave is a weak solution of an hyperbolic equation system where the mass flux of all components is balanced between both sides of the discontinuity, denoted by  $L$  and  $R$ . Mathematically this condition is achieved if, and only if, the following equation system is satisfied (Rankine-Hugoniot condition):

$$\sigma_{(\varphi, \psi)} (\vec{\alpha}_R - \vec{\alpha}_L) = \left( \vec{\beta}_R - \vec{\beta}_L \right) \quad (34)$$

where  $\vec{\alpha} = (\alpha_2, \dots, \alpha_{n-1})$ ,  $\vec{\beta} = (\beta_2, \dots, \beta_{n-1})$  and  $\sigma_{(\varphi, \psi)}$  is the shock speed calculated in  $(\varphi, \psi)$  plane. Fixing a left point ( $L$ ) it is possible to write the geometrical place of all possible right points ( $R$ ) that respects the Rankine-Hugoniot condition, called Hugoniot locus ( $\mathcal{H}(L)$ ). To determine which of these points is the real admissible solution for the problem we are employing the so called Lax, Liu and Entropy criterias (Lax, 1957; Liu, 1974, 1975).

### 3.1.2. Rarefaction Waves in Thermodynamic System

Rarefaction waves may have deduced by application of the chain rule in Equation 31 and writing in matrix notation:

$$\frac{\partial \vec{\alpha}}{\partial \vec{\beta}} \frac{\partial \vec{\beta}}{\partial \psi} + \mathbf{I} \frac{\partial \vec{\beta}}{\partial \varphi} = 0 \quad (35)$$

where  $\frac{\partial \vec{\alpha}}{\partial \vec{\beta}}$  is the Jacobian matrix of  $\vec{\alpha}$  and  $\mathbf{I}$  is the identity matrix. Defining  $\xi_{(\varphi, \psi)} = \varphi/\psi$  the self-similar variable and manipulating Equation 35 we find that the rarefaction path must obey the following ordinary differential equation system:

$$\frac{d\vec{\beta}}{d\xi_{(\varphi, \psi)}} = \frac{\vec{r}_i}{\left\langle \frac{d\lambda_i}{d\vec{\beta}}, \vec{r}_i \right\rangle} \quad (36)$$

where  $\lambda_i$  and  $\vec{r}_i$  are the  $i$ -esim eigenvalue and eigenvector of the inverse of the jacobian matrix  $(\frac{\partial \vec{\alpha}}{\partial \vec{\beta}})$ . Note that because the system is hyperbolic all eigenvalues are real and we have  $n - 2$  different rarefaction paths passing for each point in domain. In order to exclude invalid solutions, a rarefaction solution must always increase the eigenvalue along the  $\xi_{(\varphi, \psi)}$  path.

## 3.2. General Solution of Hydrodynamic System

Once we have determined the solution of thermodynamic system, the next step is solving the hydrodynamic variables ( $S_w$  and  $C_n$ ). The strategy we are adopting for hydrodynamic variables is solving the Equation 26 direct in  $(x_D, t_D)$  space by the velocity conversion of  $\beta$  solution from  $(\varphi, \psi)$  space by Equations 32 and 33.

### 3.2.1. Shock Waves in Hydrodynamic System

There are two different situations to consider for shock solution in hydrodynamic variables, shock with constant  $\vec{\beta}$  where only  $S_w$  and  $C_n$  change

across the discontinuity and complete shocks where all variables change. For the first case, Equation 26-(a) has trivial solution and the Rankine-Hugoniot condition is written using only terms (b) and (c):

$$\begin{cases} \sigma_{(x_D, t_D)} = \frac{f_{HC}^R F_n^R - f_{HC}^L F_n^L}{S_{HC}^R C_n^R - S_{HC}^L C_n^L} & \text{(b)} \\ \sigma_{(x_D, t_D)} = \frac{f_w^R - f_w^L}{S_w^R - S_w^L} & \text{(c)} \end{cases} \quad (37)$$

where the subscript  $(x_D, t_D)$  indicates the domain where the speed is calculated. For the particular case when both  $C_n$  and  $\vec{\beta}$  are constant across the shock, the shock speed is calculated using only Equation 37-(c), that is known by the Buckley-Leverett shock.

For the complete shock case, the shock speed was already calculated in  $(\varphi, \psi)$  plane by Equation 34 and the speed can be converted by application of Equation 33:

$$\sigma_{(x_D, t_D)} = \frac{f_{HC}^L (F_n^L + \sigma_{(\varphi, \psi)})}{S_{HC}^L (C_n^L + \sigma_{(\varphi, \psi)})} = \frac{f_{HC}^R (F_n^R + \sigma_{(\varphi, \psi)})}{S_{HC}^R (C_n^R + \sigma_{(\varphi, \psi)})} \quad (38)$$

An interesting particular case of Equation 38 is when one side of the shock has only water and a single hydrocarbon phase (oil or gas) saturating the porous medium. Supposing this condition is valid for the left shock side ( $L$ ), then we have  $F_n^L = C_n^L$  and Equation 38 resumes to:

$$\sigma_{(x_D, t_D)} = \frac{f_{HC}^L}{S_{HC}^L} = \frac{f_{HC}^R (F_n^R + \sigma_{(\varphi, \psi)})}{S_{HC}^R (C_n^R + \sigma_{(\varphi, \psi)})} \quad (39)$$

that means that the shock speed depends unique and exclusively of the left condition and all points in this hugoniot locus ( $\mathcal{H}(L)$ ) have the same shock speed.

Another particular case of Equation 38 is when both sides of the shock are saturated with water and only one hydrocarbon phase. For this case we have  $\frac{f_{HC}^L}{S_{HC}^L} = \frac{f_{HC}^R}{S_{HC}^R}$  with different  $\vec{\beta}$  values in each shock side. Such situation is not real because even if we accept this solution as a valid shock in  $(x_D, t_D)$  space, it cannot be converted to  $(\varphi, \psi)$  by application of Equation 32. Thus we conclude that does not exist  $\vec{\beta}$  shocks when both sides has only one hydrocarbon phase.

### 3.2.2. Rarefaction Waves in Hydrodynamic System

There are two different cases to consider in order to find rarefaction solutions in the hydrodynamic system: constant  $\bar{\beta}$  rarefactions and complete rarefactions. The complete rarefaction case is simpler because we already have calculated the rarefaction speed in  $(\varphi, \psi)$  domain and we only need to convert to  $(x_D, t_D)$  space using Equation 33.

For the rarefactions with constant beta, first we need to manipulate Equations 26-(b) and (c) and write in a matrix form:

$$\begin{aligned} & \begin{pmatrix} C_n \\ S_w \end{pmatrix}_{t_D} + \\ & \begin{pmatrix} \frac{1}{S_{HC}} \left( f_{HC} \frac{\partial F_n}{\partial C_n} + (C_n - F_n) \frac{\partial f_w}{\partial C_n} \right) & \frac{1}{S_{HC}} \left( f_{HC} \frac{\partial F_n}{\partial S_w} + (C_n - F_n) \frac{\partial f_w}{\partial S_w} \right) \\ \frac{\partial f_w}{\partial C_n} & \frac{\partial f_w}{\partial S_w} \end{pmatrix} \begin{pmatrix} C_n \\ S_w \end{pmatrix}_{x_D} \\ & = \begin{pmatrix} 0 \\ 0 \end{pmatrix} \quad (40) \end{aligned}$$

Defining the self-similar variable  $\xi_{(x_D, t_D)} = \frac{x_D}{t_D}$  and manipulating the Equation 40, we find that the rarefaction paths for the hydrodynamic system must solve the following ODE system:

$$\begin{pmatrix} \frac{dC_n}{d\xi_{(x_D, t_D)}} \\ \frac{dS_w}{d\xi_{(x_D, t_D)}} \end{pmatrix} = \frac{\vec{r}'_{\pm}}{\left\langle \left( \frac{\partial \lambda_{\pm}}{\partial C_n}, \frac{\partial \lambda_{\pm}}{\partial S_w} \right) \cdot \vec{r}'_{\pm} \right\rangle} \quad (41)$$

where  $\lambda_{\pm}$  and  $\vec{r}'_{\pm}$  are the eigenvalue and eigenvector associated to the flux matrix of Equation 40. The sub-indexes  $\pm$  indicates that this matrix has two different eigenvalues and consequently for each point there are two rarefaction paths, one associated to the slow eigenvalue ( $-$ ) and one to the fast ( $+$ ).

One important particular case occurs when there is only one hydrocarbon phase (oil or gas) in system, because we have  $C_n = F_n$  and the System 40 reduces to:

$$\begin{pmatrix} C_n \\ S_w \end{pmatrix}_{t_D} + \begin{pmatrix} \frac{f_{HC}}{S_{HC}} & 0 \\ \frac{\partial f_w}{\partial C_n} & \frac{\partial f_w}{\partial S_w} \end{pmatrix} \begin{pmatrix} C_n \\ S_w \end{pmatrix}_{x_D} = \begin{pmatrix} 0 \\ 0 \end{pmatrix} \quad (42)$$

where the eigenvalues of flux matrix are the Buckley-Leverett rarefaction  $\left( \frac{\partial f_w}{\partial S_w} \right)$  and the trivial solution for single phase compositional flows  $\left( \frac{f_{HC}}{S_{HC}} \right)$  (Orr Jr., 2007).

## 4. Thermodynamic Description and Solution

The last section we presented the general solution for the miscible flow of water, oil and gas in an one-dimensional porous medium. In this section we will present a practical example of a hydrocarbon mixture and solve the thermodynamic partial differential equations. In the next section we will solve the hydrodynamic part of the system and show how waves can interact in a changing boundary condition problem like WAG injection.

### 4.1. Thermodynamic Description

We may relate two phases in thermodynamic equilibrium using tie-lines by direct application of Equation 24 where  $c_{i_o}$  and  $c_{i_g}$  are the volumetric compositions of component  $i$  in oil and gas phases. We can relate the volumetric composition of each component with  $\vec{\beta}$  values by adjusting the following surface to the thermodynamic data:

$$c_{i(o|g)}(\vec{\beta}) = \sum_{i_2=0}^2 \dots \sum_{i_{n-1}=0}^2 a_{i_2 \dots i_{n-1}} \beta_2^{i_2} \dots \beta_{n-1}^{i_{n-1}} \quad (43)$$

in which  $a_{i_2 \dots i_{n-1}}$  are the adjusted coefficients that models the thermodynamic equilibrium. Once we have a formula to calculate the hydrocarbon phase compositions, the viscosity of each of them are calculated by:

$$\mu_{(o|g)} = \sum_{i=1}^n c_{i(o|g)} \mu_i^0 \quad (44)$$

where  $\mu_i^0$  is the viscosity of the pure component at the same pressure and temperature. Note that the water viscosity is constant because it does not exchange mass with other components.

### 4.2. Thermodynamic Example

Considering the pressure of 100bar and 300K we applied the Peng-Robinson equation of state (Robinson and Peng, 1978) to calculate the thermodynamic equilibrium of a component mixture described in Table 1 for different mixture compositions, where  $p_c$  and  $T_c$  are the critical pressure and temperature,  $M_w$  is the molecular weight,  $\omega$  is the acentric factor and  $\mu^0$  is the viscosity of the pure component.

Table 1: Pure component thermodynamic properties

Comp.	$p_c$ (bar)	$T_c$ (K)	$M_w$ (g/mol)	$\omega$	$\mu^0$ (cp)
C1	45.99	190.56	16.043	0.011	0.01
C3	42.48	369.83	44.097	0.152	0.10
C6	30.25	507.60	86.177	0.300	1.00
C10	21.10	617.70	142.285	0.490	5.00

To correctly capture the thermodynamic equilibrium at the given pressure and temperature for any composition we performed more than 50,000 two-phase flash calculations for different composition points. After that, we used the least squares method to adjust the volumetric composition surface of each phase using Equation 43 (Table 2). The Figures 2 and 3 show the quality of the adjusted surface over the calculated data for the oil and gas phases. It can be noted the high R-score even using a huge number of points, showing the applicability of the proposed technique.

Table 2: Liquid and vapor volumetric composition coefficients

	$a_{00}$	$a_{01}$	$a_{02}$	$a_{10}$	$a_{11}$	$a_{12}$	$a_{20}$	$a_{21}$	$a_{22}$	$R^2$
Liquid										
$c_{1o}$	$4.2343x10^{-1}$	$1.1426x10^1$	$2.3066x10^2$	$1.6713x10^0$	$3.4732x10^0$	0.0	$5.2042x10^0$	0.0	0.0	0.99993
$c_{2o}$	$-4.9563x10^{-3}$	$9.1915x10^{-1}$	$-2.0770x10^1$	$4.0229x10^0$	$-2.0074x10^1$	0.0	$-1.4276x10^1$	0.0	0.0	0.99793
$c_{3o}$	$-2.7404x10^{-3}$	$4.2609x10^1$	$-2.2384x10^2$	$2.7770x10^{-2}$	$-3.5911x10^2$	0.0	$8.9073x10^{-1}$	0.0	0.0	0.99928
$c_{4o}$	$5.8427x10^{-1}$	$-5.4955x10^1$	$1.3953x10^1$	$-5.7220x10^0$	$3.7571x10^2$	0.0	$8.1811x10^0$	0.0	0.0	0.99958
Vapor										
$c_{1g}$	$9.9898x10^{-1}$	$-9.6938x10^{-1}$	$-7.4891x10^{-2}$	$-9.9002x10^{-1}$	$-1.3535x10^0$	0.0	$-3.9344x10^{-1}$	0.0	0.0	0.99997
$c_{2g}$	$1.2164x10^{-4}$	$-1.0963x10^{-2}$	$-2.0044x10^{-1}$	$9.8582x10^{-1}$	$1.2330x10^0$	0.0	$3.7252x10^{-1}$	0.0	0.0	0.99997
$c_{3g}$	$5.0189x10^{-5}$	$1.0431x10^0$	$1.6582x10^0$	$-5.0414x10^{-3}$	$1.3839x10^0$	0.0	$6.0591x10^{-2}$	0.0	0.0	0.99989
$c_{4g}$	$8.4314x10^{-4}$	$-6.2790x10^{-2}$	$-1.3829x10^0$	$9.2444x10^{-3}$	$-1.2634x10^0$	0.0	$-3.9671x10^{-2}$	0.0	0.0	0.99399

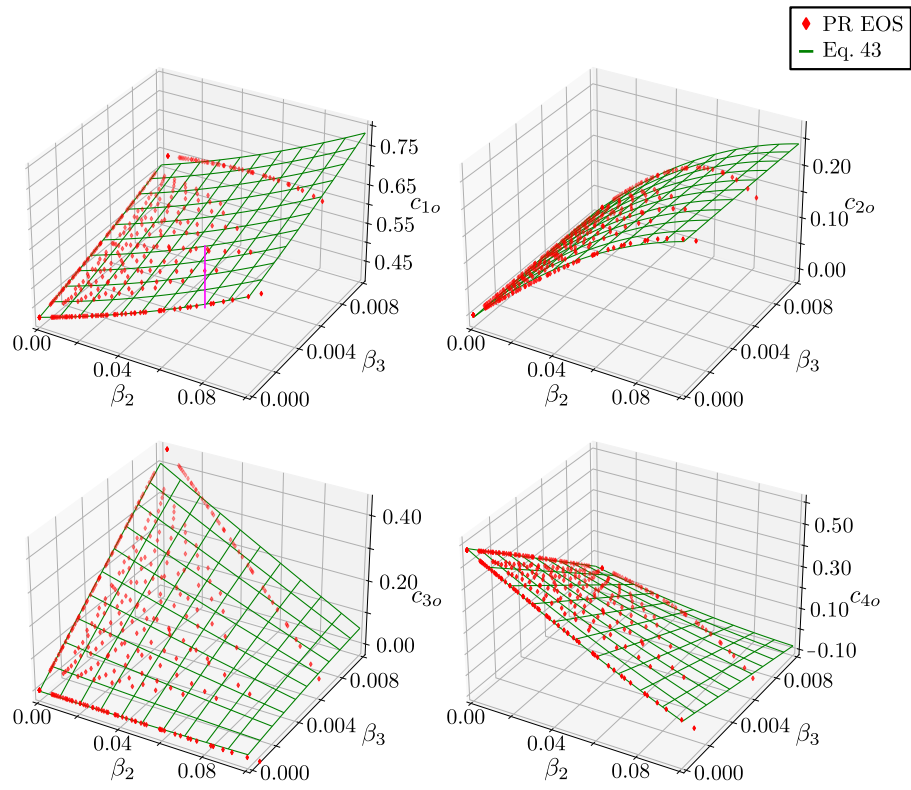


Figure 2: Adjusted equilibrium volumetric composition surface (Equation 43) for oil phase

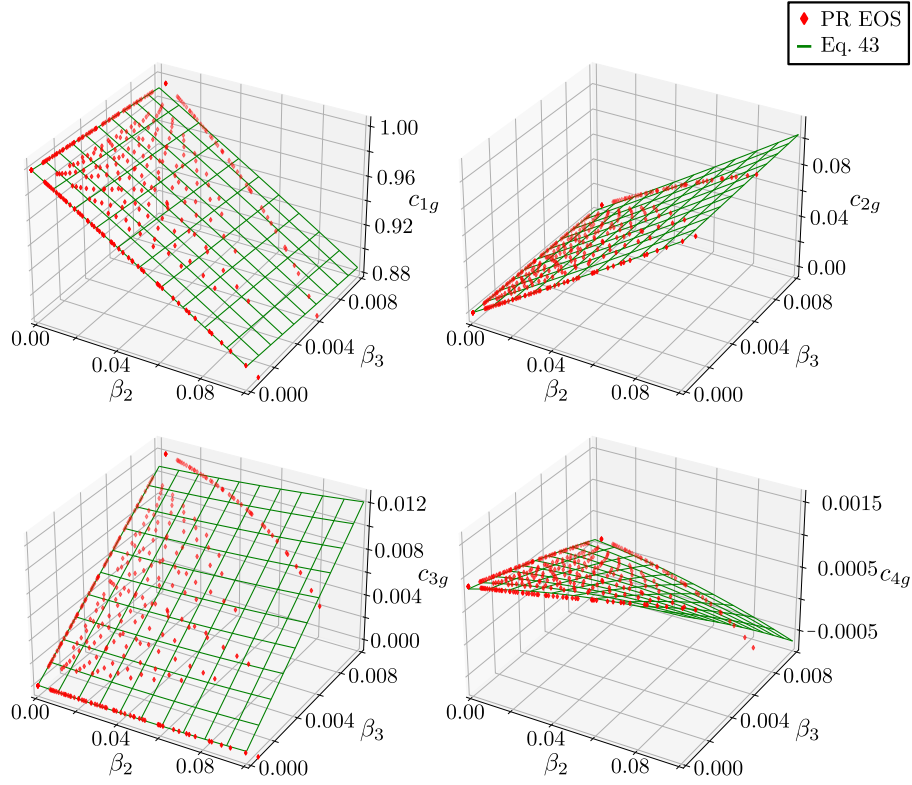


Figure 3: Adjusted equilibrium volumetric composition surface (Equation 43) for gas phase

#### 4.3. Solution of the Thermodynamic Auxiliary System

Once we adjusted analytical expressions for  $\vec{\alpha}$  we can write the analytical solutions for the thermodynamic auxiliary system by direct application of the solutions described in Section 3. The volumetric composition of the original oil in-situ and the injected gas is showed in Table 3 as the calculated  $\vec{\beta}$  for each composition. We are using  $J$  and  $I$  to express the injection and initial compositions in the charts showed in this section.

Table 3: Initial oil and injected gas volumetric compositions

	$C_1$	$C_3$	$C_6$	$C_{10}$	$\beta_2$	$\beta_3$
Oil	0.2897	0.1180	0.3146	0.2777	$2.3158 \times 10^{-2}$	$6.1089 \times 10^{-3}$
Gas	0.9897	0.0091	0.0012	0.0000	$9.0753 \times 10^{-3}$	$1.2512 \times 10^{-3}$

The eigenvalues and the integral curves (Equations 35 and 36) are showed in Figures 4 and 5, while the Hugoniot locus for initial and injection points is showed in Figure 6. It can be noted that there is no combination of rarefaction paths that connects  $J$  and  $I$  points. Thus, the solution for this condition is a shock from  $\vec{\beta}_J$  to the intermediate  $\vec{\beta}_A$  point ( $S_{\beta^1}$ ), followed by a shock from  $\vec{\beta}_A$  to the initial point  $\vec{\beta}_I$  ( $S_{\beta^2}$ ), showed in Figure 7.

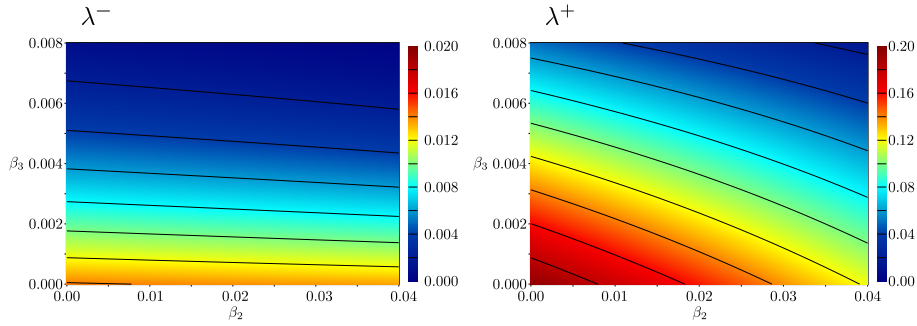


Figure 4: Slow and fast eigenvalues ( $\lambda^-$  and  $\lambda^+$ ) for the thermodynamic auxiliary system

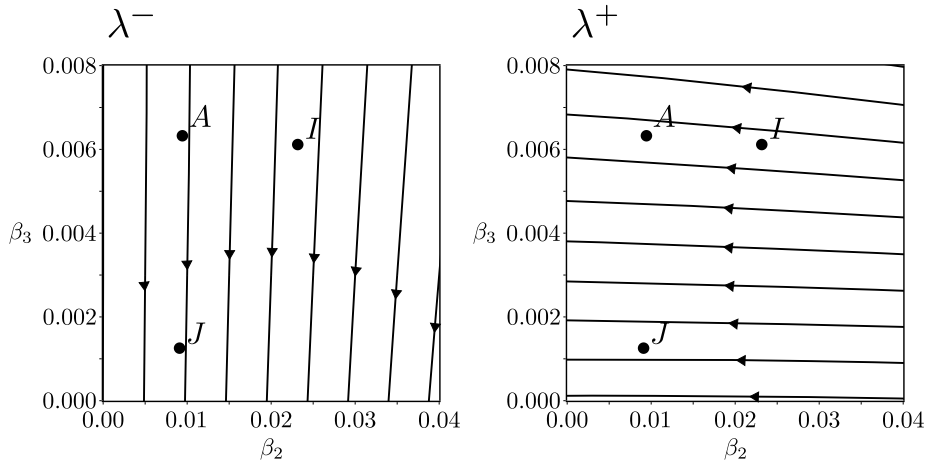


Figure 5: Slow and fast integral curves ( $\lambda^-$  and  $\lambda^+$ ) for the thermodynamic auxiliary system. The arrows point toward the eigenvalue increase direction

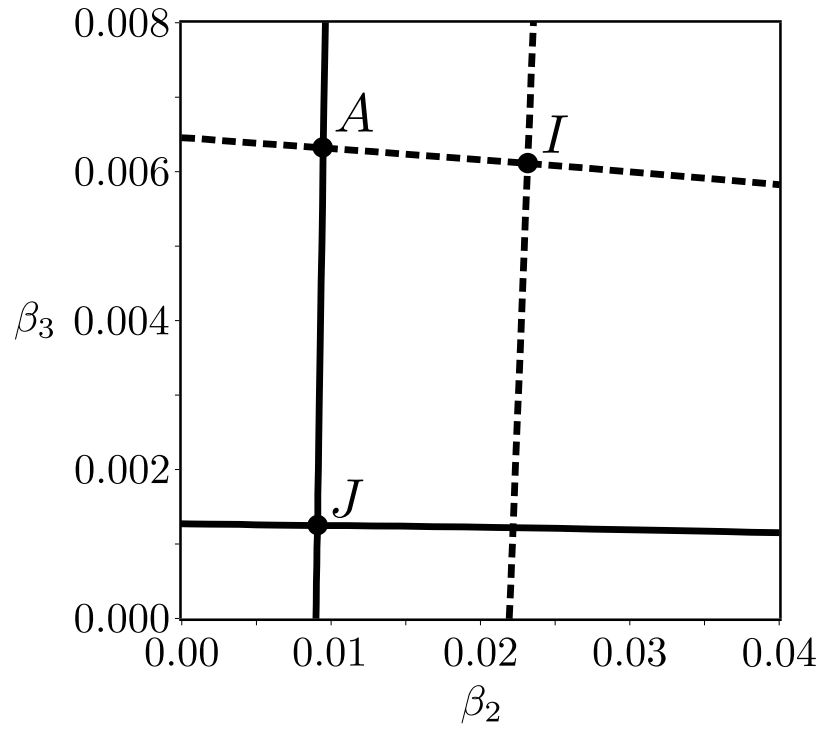


Figure 6: Hugoniot locus for injection (solid) and initial (dashed) conditions in auxiliary system

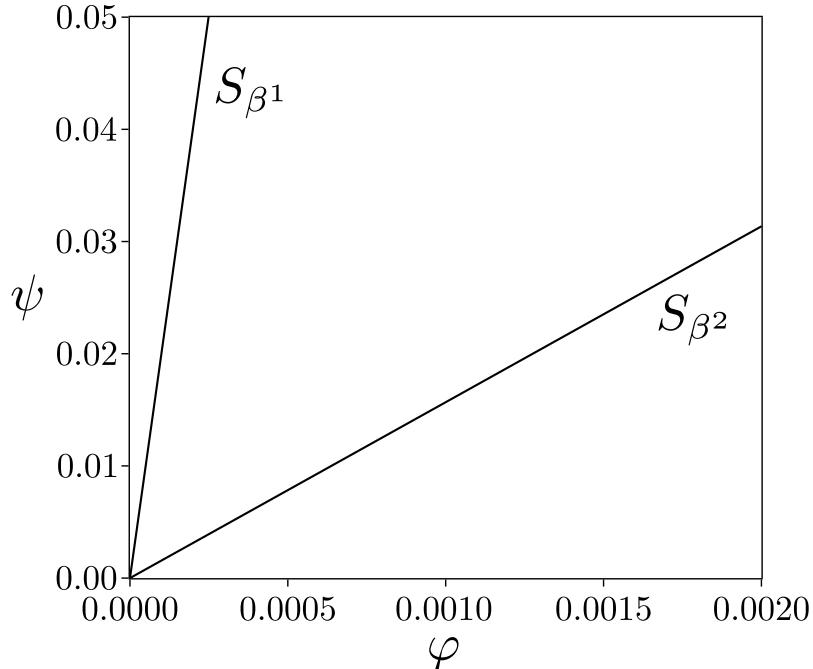


Figure 7: Characteristic diagram for  $\vec{\beta}$  solution in the auxiliary system

## 5. Solution of MWAG Problem

In the last section we solved the thermodynamic equilibrium in the  $(\varphi, \psi)$  space. In this section we will describe the complete solution of the miscible WAG problem, including both hydrodynamic and thermodynamic systems. The methodology applied here is similar of the immiscible solution, where we first build the analytical solutions for each WAG cycle without consider the wave interaction and after we solve each interaction as it is a new Riemann problem centered in the interaction point.

All solution profiles presented in this section were compared with numerical simulations using the first order, implicit, upwind method (LeVeque et al., 2002). The linear porous medium was discretized using 100,000 cells uniformly spaced, in order to decrease numerical diffusion effects.

### 5.1. Hydrodynamic Solution: Wave Positioning

We solved three injection steps to identify the key aspects of the MWAG solution (Table 4). The inlet condition is how the reservoir is saturated at the

moment that the next step starts in  $x_D = 0$  position, where for the first step is the same of the initial condition. The system starts with the linear porous medium completely saturated with oil at irreducible water saturation  $S_{wi}$ . The first step we inject pure water in the rock ( $f_w = 1$ ) saturating the inlet face with water and residual oil saturation for water ( $S_{or}^w$ ). After this, in the second step, we inject pure gas with composition showed in Table 3 ( $f_g = 1$ ) that saturates the inlet face with water and irreducible water. For the third step, we repeat the water injection, but now we could achieve 100% of water saturation, because the gas in the last step completely remove the oil in this face. Next steps boundary conditions are simple repetitions of steps 2 and 3 where, because of the miscibility effect, only the water saturation changes.

Table 4: Boundary and inlet face conditions considered in the MWAG solution

Step	$t_D$	Boundary Condition	Inlet Condition
		$B_C = (S_w, C_n, \beta_2, \beta_3)$	$I_C = (S_w, C_n, \beta_2, \beta_3)$
Water	0.00	$(1 - S_{or}^w, C_n^I, \beta_2^I, \beta_3^I)$	$(S_{wi}, C_n^I, \beta_2^I, \beta_3^I)$
Gas	0.10	$(S_{wi}, C_n^J, \beta_2^J, \beta_3^J)$	$(1 - S_{or}^w, C_n^I, \beta_2^I, \beta_3^I)$
Water	0.20	$(1.0, C_n^J, \beta_2^J, \beta_3^J)$	$(S_{wi}, C_n^J, \beta_2^J, \beta_3^J)$

The rock-fluid interaction is described using relative permeability curves. For the two-phase interaction, we are using the Corey's model (Corey et al., 1956) with parameters showed in Table 5 (Figure 8):

$$\begin{cases} k_{rw} = k_{rw}^{S_{or}^w} (S_{nw})^{n_w} \\ k_{ro}^{w|g} = k_{ro}^{S_{wi}} (S_{no})^{n_o^{w|g}} \\ k_{rg} = k_{rg}^{S_{or}^g} (S_{ng})^{n_g} \end{cases} \quad (45)$$

where  $S_{nw}$ ,  $S_{no}$  and  $S_{ng}$  are the normalized water, oil and gas saturations:

$$\begin{cases} S_{nw} = \frac{S_w - S_{wi}}{1 - S_{wi} - S_{om}}, & S_w \in [S_{wi}, 1 - S_{om}] \\ S_{no} = \frac{S_o - S_{om}}{1 - S_{wi} - S_{om}}, & S_o \in [S_{om}, 1 - S_{wi}] \\ S_{ng} = \frac{S_g}{1 - S_{wi} - S_{om}}, & S_g \in [0, 1 - S_{wi} - S_{om}] \end{cases} \quad (46)$$

in which  $S_{om} = \min(S_{or}^w, S_{or}^g)$  is the minimum residual oil by immiscible processes. The two-phase curves are converted to three-phase relative permeability curves by the modified Stone I model (Stone, 1970; Aziz and Settari, 1979):

$$\begin{cases} k_{rw} = k_{rw}(S_{nw}) \\ k_{ro} = k_{ro}(S_{nw}, S_{no}, S_{ng}) = \frac{S_{no}}{k_{ro}^{S_{wi}}} \left( \frac{k_{ro}^w}{1-S_{nw}} \right) \left( \frac{k_{ro}^g}{1-S_{ng}} \right) \\ k_{rg} = k_{rg}(S_{ng}) \end{cases} \quad (47)$$

Table 5: Relative permeability Corey's parameters

Waterflooding	Gasflooding
$S_{wi} = 0.20$	$S_{wi} = 0.20$
$k_{ro}^{S_{wi}} = 0.80$	$k_{ro}^{S_{wi}} = 0.80$
$S_{or}^w = 0.40$	$S_{or}^g = 0.20$
$k_{rw}^{S_{or}^w} = 0.30$	$k_{rg}^{S_{or}^g} = 0.70$
$n_w = 2.20$	$n_g = 2.40$
$n_o^w = 2.00$	$n_o^g = 1.80$

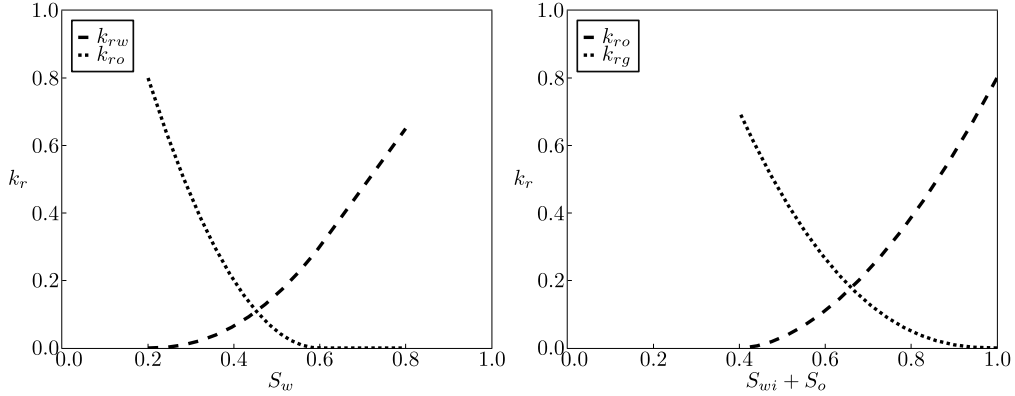


Figure 8: Two-phase relative permeability curves with parameters showed in Table 5

### 5.1.1. First Step: Water Injection

For the first water step, the solution is described by the traditional Buckley-Leverett equations, that can be analyzed in the  $f_w$  diagram (9). The tangent express the traditional Buckley-Leverett shock that has the same velocity of the last rarefaction. Note that the injection point in the initial oil composition curve ( $f_w = 1$ ) happens when  $S_w = 1 - S_{or}^w$ , showing that the first water step has a low efficiency letting a huge portion of oil in

the reservoir when compared with the same curve in the injected gas composition. The Figure 10 shows the solution in the characteristic diagram, where solid lines represent shocks and dashed lines rarefactions, while the Figure 11 shows the solution profile when  $t_D = 0.1$ , where it can be noted that the  $\vec{\beta}$  values does not change in this first step.

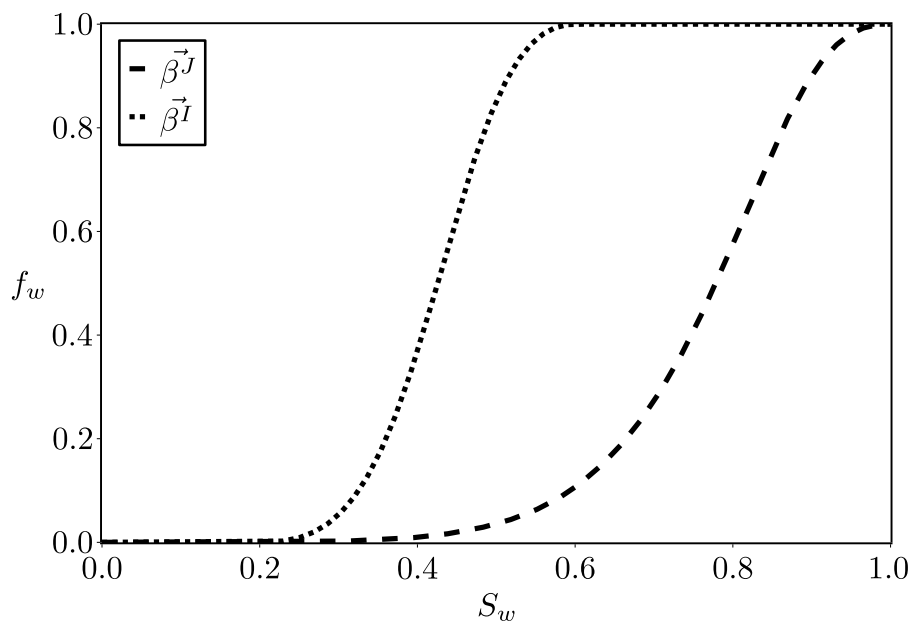


Figure 9: Water fractional flow in initial oil composition (dotted) and injection gas composition (dashed)

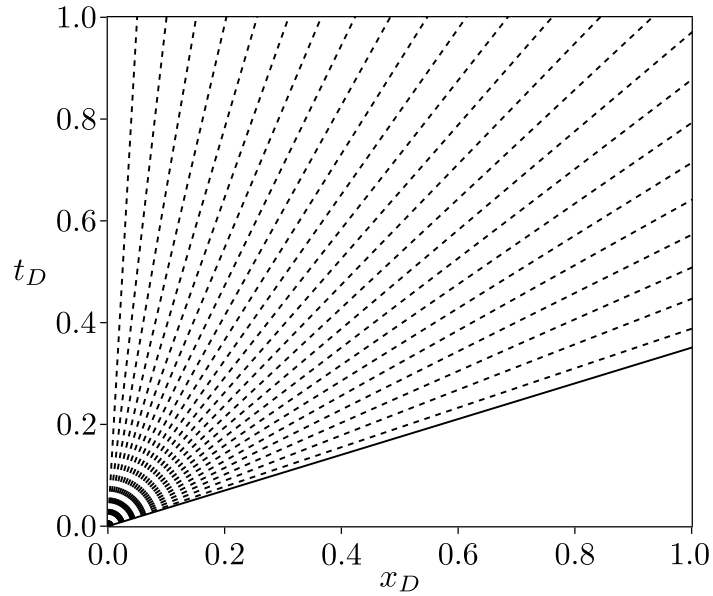


Figure 10: Characteristic diagram for the first water injection step without consider wave interactions

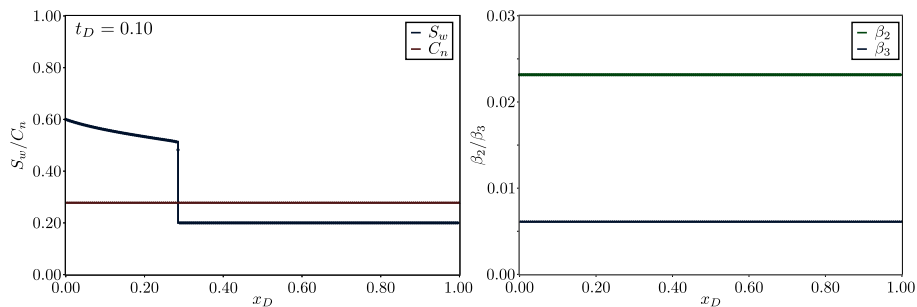


Figure 11:  $(S_w, C_n, \beta_2, \beta_3)$  solution profile for  $t_D = 0.10$  for the first water injection step without consider wave interactions, compared with numerical solution

### 5.1.2. Second Step: Gas Injection

Because the injected gas exchanges mass with the original oil, the thermodynamic interactions must obey the speed of the characteristics solved in the auxiliary system (7). Once we have already calculated the  $\vec{\beta}$  in the  $(\varphi, \psi)$  plane, we can construct the  $F_n$  diagram (Figure 12) for any water saturation. By analogy of the two-phase miscible solution, when the  $F_n$  curve for

injection  $\vec{\beta}$  values (red) is in the right of the  $F_n$  curve for the initial  $\vec{\beta}$  values (green), then the  $\vec{\beta}$  transition will end with a right composite wave, otherwise the solution will start with a left composite wave. Thus, for the parameters we are using, the easiest way to describe the gas injection solution is from  $I$  to  $J$  point.

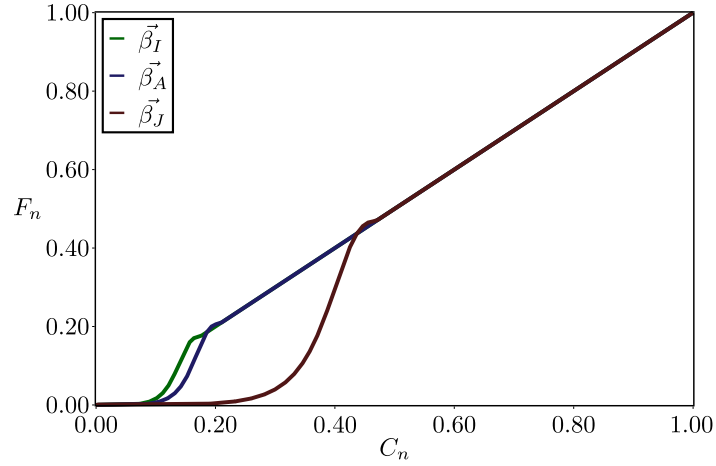


Figure 12:  $F_n$  versus  $C_n$  chart for initial ( $\vec{\beta}_I$ ), intermediate ( $\vec{\beta}_A$ ) and injection ( $\vec{\beta}_J$ ) tie-lines

Considering the initial composition  $\vec{\beta}_I$  we construct the constant  $\vec{\beta}$  rarefactions (Equation 40) by analyzing the eigenvalues in  $(x_D, t_D)$  domain (Figures 13 and 14). By analyzing those maps we can make three important conclusions: 1) there is no rarefaction curve that enters or leaves the three-phase saturation region ( $C_n < 0.17$ ); 2) the speed in  $I$  point is null, obligating the solution end with a shock and 3) there is an elliptic region in the map where the eigenvalues of System 40 are not real and the rarefaction curves does not enter in this zone (marked with gray).

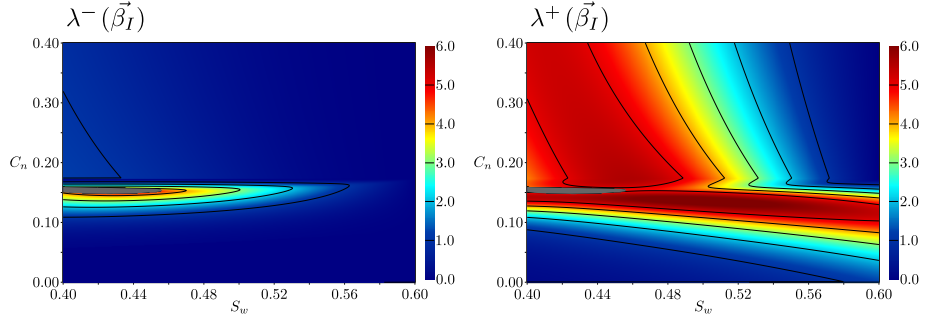


Figure 13: Slow and fast eigenvalues for constant  $\vec{\beta}_I$  values in  $(x_D, t_D)$  domain, with the elliptic region marked in gray

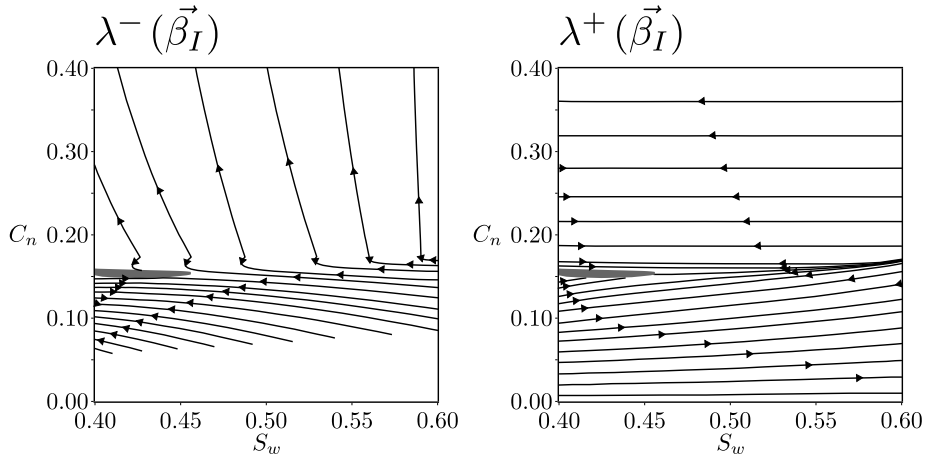


Figure 14: Slow and fast rarefaction curves for constant  $\vec{\beta}_I$  values in  $(x_D, t_D)$  domain, with the elliptic region marked in gray

As we determined that the solution must finish with a shock we must plot the Hugoniot locus for the inlet face point  $(\mathcal{H}(I))$ , showed in Figure 15. This horizontal line means that the solution must end with a Buckley-Leverett left composite shock, where the eigenvalues of the left condition has the same value of the shock speed ( $S_I$  shock in Figure 16).

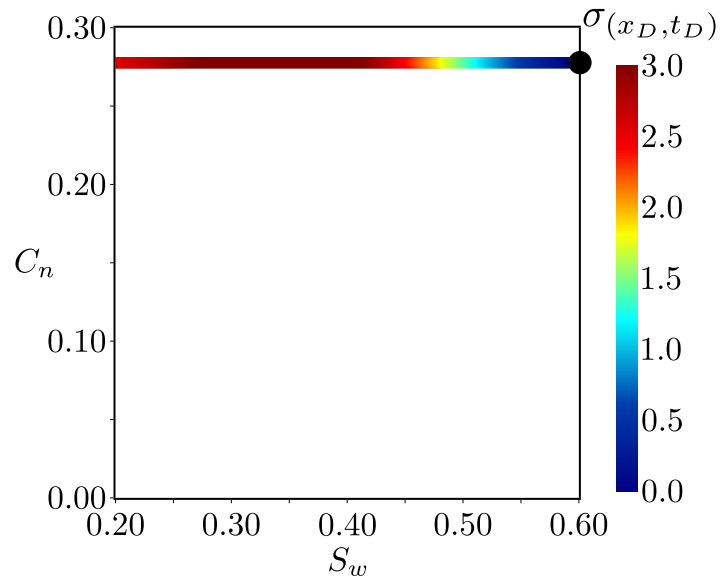


Figure 15: Hugoniot locus for  $I$  point ( $\mathcal{H}(I)$ ) for initial tie-line ( $\vec{\beta}_I$ ) in  $(x_D, t_D)$  domain

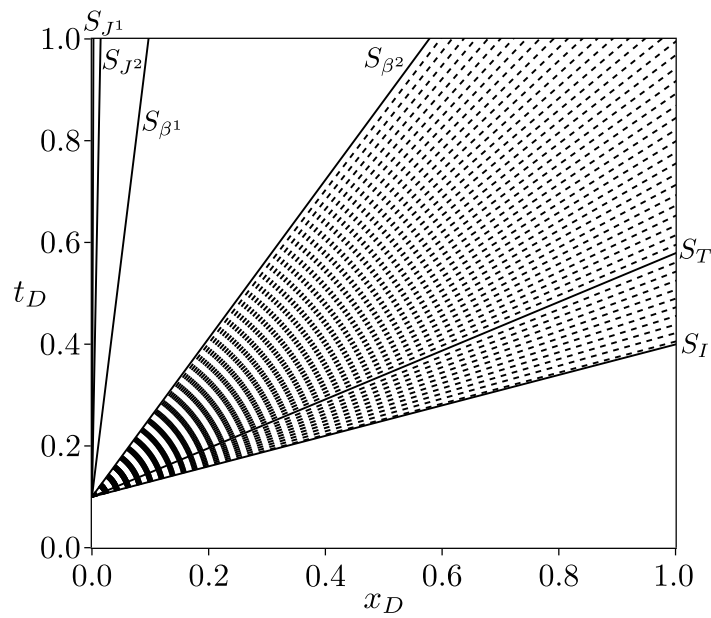


Figure 16: Characteristic diagram for the second step injection solution without consider the wave interactions

The next step to construct the gas solution is determine the point along  $\mathcal{H}(I)$  locus that leaves the three-phase saturation zone. If we construct a Hugoniot locus for the points in this locus for  $S_{wi} < S_w < 1 - S_{or}^w$ , we conclude that for each locus there is at least one point where the left fast eigenvalue is the same of the shock speed (marked with triangles in Figure 17). However, exists a particular point where the shock velocity is equal both left and right fast eigenvalues, creating a stable solution called transitional shock wave ( $S_T$  in Figure 16), that is the shock that leaves the three-phase saturation zone.

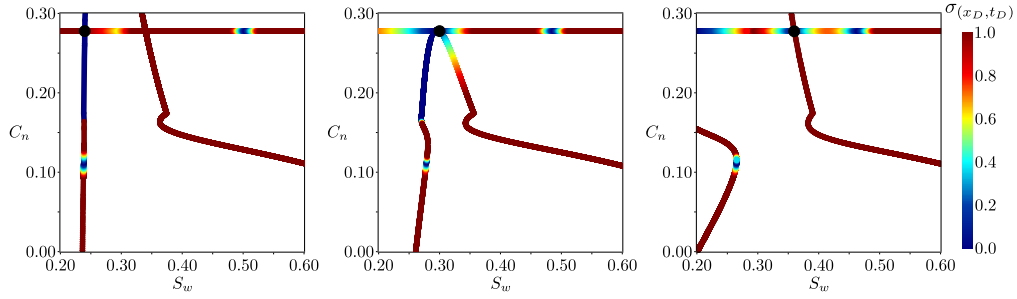


Figure 17: Hugoniot locus for different points along  $\mathcal{H}(I)$  curve for initial tie-line ( $\vec{\beta}_I$ ) in  $(x_D, t_D)$  domain

Once we entered in the three-phase saturation region, the solution is found by following the fast integral curve until the rarefaction velocity be the same of the second  $\vec{\beta}$  shock in  $(\varphi, \psi)$  domain ( $S_{\beta^2}$ ). The same procedure applies to the first  $\vec{\beta}$  shock, by direct conversion ( $S_{\beta^1}$ ), where the left shock side is entirely in the injection tie-line ( $S_{\beta^1}^L$  in Figure 18). Analyzing the Hugoniot locus  $\mathcal{H}(S_{\beta^1}^L)$  we can see that the solution connects to the injection point by a partial shock to  $J^2$  followed to a shock  $J$  ( $S_{J^1}$  and  $S_{J^2}$  in Figure 16). The Figures 19 and 20 show the solution and saturation profiles for  $t_D = 0.15$ . It can be noted that the tie-line variables ( $\vec{\beta}$ ) only change in the  $S_{\beta^1}$  and  $S_{\beta^2}$  shocks, remaining constant in the other points, while the gas injection front completely miscibilizes the oil in the inlet face, saturating the porous medium with only water and gas at this point.

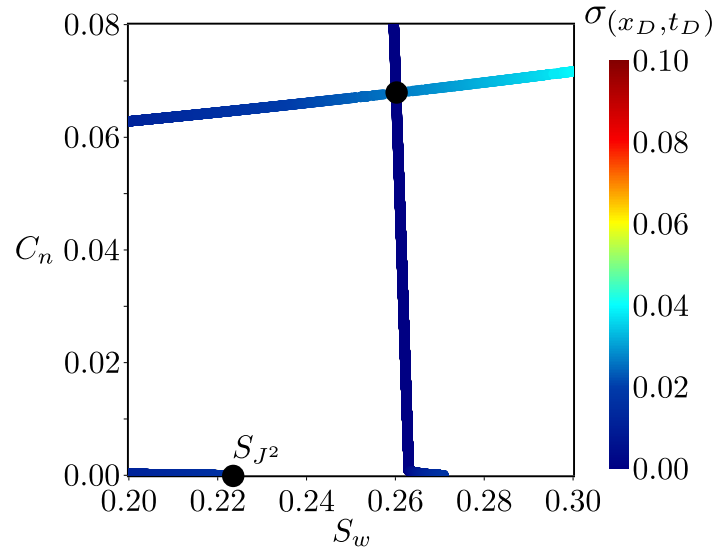


Figure 18: Hugoniot locus  $\mathcal{H}(S_{\beta^1}^L)$  in the injection tie-line ( $\vec{\beta}_I$ ) in  $(x_D, t_D)$  domain

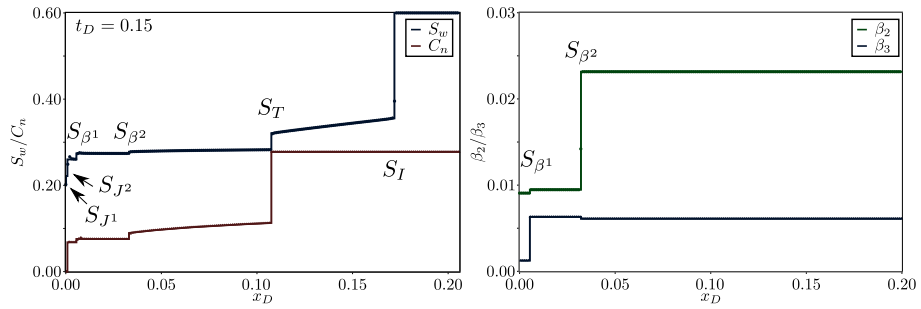


Figure 19:  $(S_w, C_n, \beta_2, \beta_3)$  solution profile for  $t_D = 0.15$  in the gas injection step without consider wave interactions, compared with numerical solution

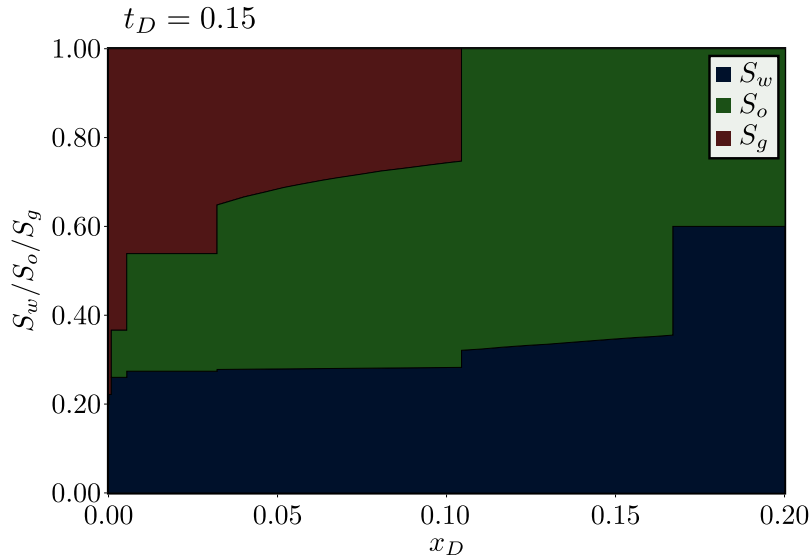


Figure 20: Saturation profile for  $t_D = 0.15$  in the gas injection step without consider wave interactions

### 5.1.3. Third Step: Water Injection

For the next water injection step, the oil was completely removed from the inlet face by the gas injection. Thus, the injection point for  $f_w = 1$  is the inlet face completely saturated with water ( $S_w = 1$ ). The solution without consider wave interactions for this step is the conventional Buckley-Leverett composite shock, that can be analyzed in the traditional fractional flow diagram (9). If we construct the solution profile for this injection step (Figure 21) we can note that the  $\beta$  and  $C_n$  profiles are constant and equal to the injection gas tie-line. That is the reason why the next steps that we are not treating are just repetitions of steps 2 and 3.

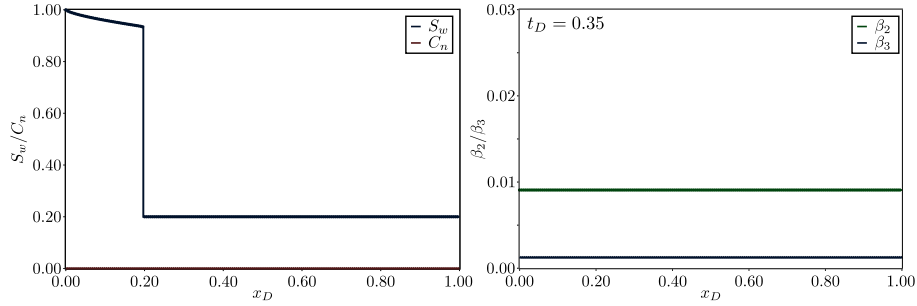


Figure 21:  $(S_w, C_n, \beta_2, \beta_3)$  solution profile for  $t_D = 0.35$  for the third injection step without consider wave interactions, compared with numerical solution

After we solve the injection steps we can position each of them in the characteristic diagram and start the wave interaction solution procedure (Figure 22). We always solve the interactions following the time that they occur, in order to respect the causality principle.

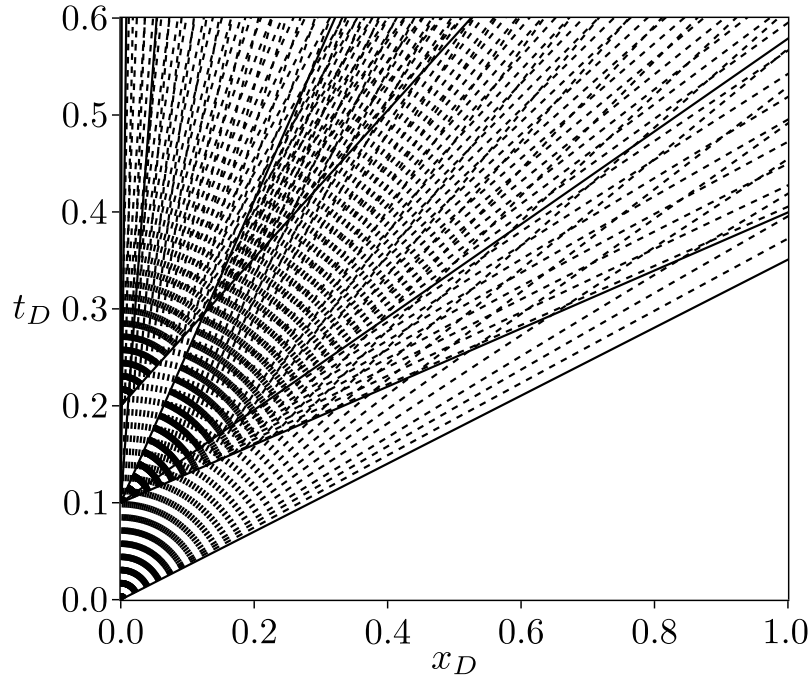


Figure 22: Characteristic diagram for the third three injection steps, without consider wave interactions

### 5.2. MWAG Solution: Wave Interactions

We now present the MWAG solution after solving the wave interactions (23). We use here the same procedure and nomenclature for immiscible solutions where each crossing wave in the characteristic diagram is treated as a new Riemann problem. To facilitate the comprehension, the interactions were divided in three main groups.

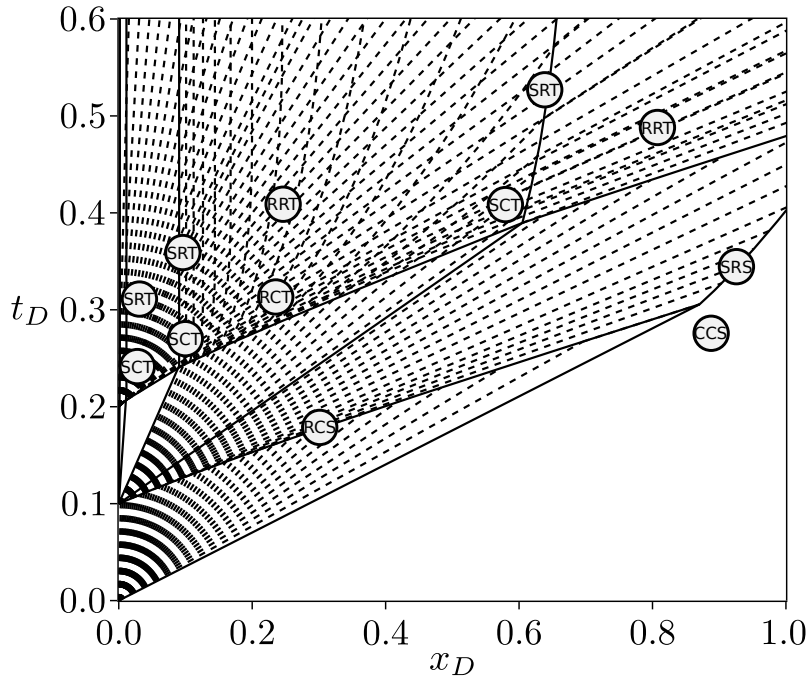


Figure 23: Characteristic diagram for the miscible WAG problem after three injection steps

#### 5.2.1. Group 01 - Water/Gas Interactions

These interactions appears by the interaction of the first water and the second gas steps (Figure 24). The rarefactions of the water cycle interacts with the last composite shock from the gas cycle (Shock  $S_I$  in Figure 16), where the rarefactions and the shock superimposes their waves accelerating the shock of the composite wave (RCS interaction). This speed increasing decompresses the  $S_I$  composite fan, opening space for appearing new rarefactions as the interactions evolves. The Figure 25 shows two solution profiles for different times, showing how this interaction affects the solution. It can

be noted that this is an interaction of two different water banks, where the bank behind is faster and is superimposing with the slow one and the others properties remain constant.

At some time the shock that defines both water bank will reach each other, generating the Composite-Composite Superposition interaction  $((x_D, t_D) \approx (0.85, 0.31))$  point in Figure 24). The two composite waves superimposes and a resulting shock continues traveling in the domain (solution profile showed in Figure 31). This shock interacts with the rarefactions of the gas injection cycle, reducing its speed by a Shock-Rarefaction Superposition.

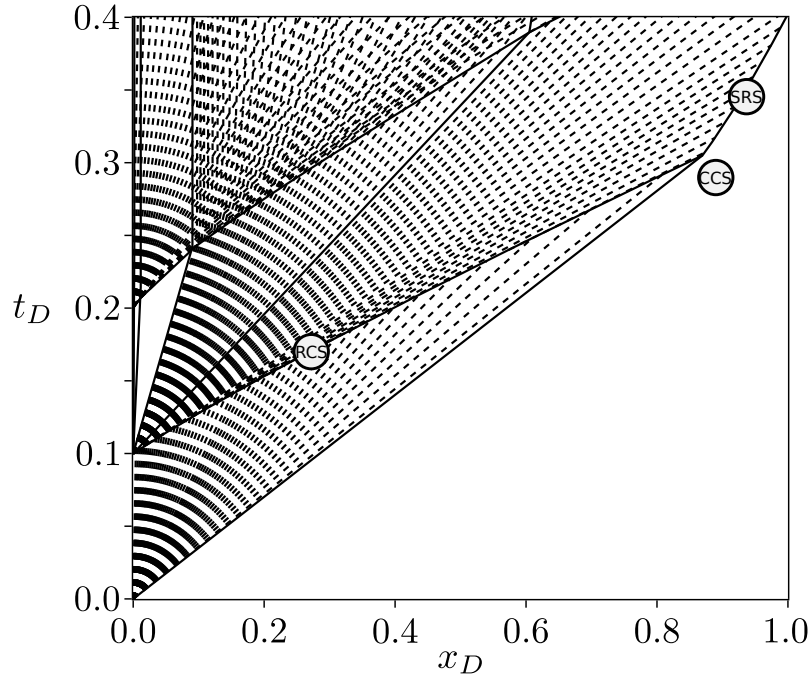


Figure 24: Group 01 characteristic diagram for the miscible WAG problem after three injection steps

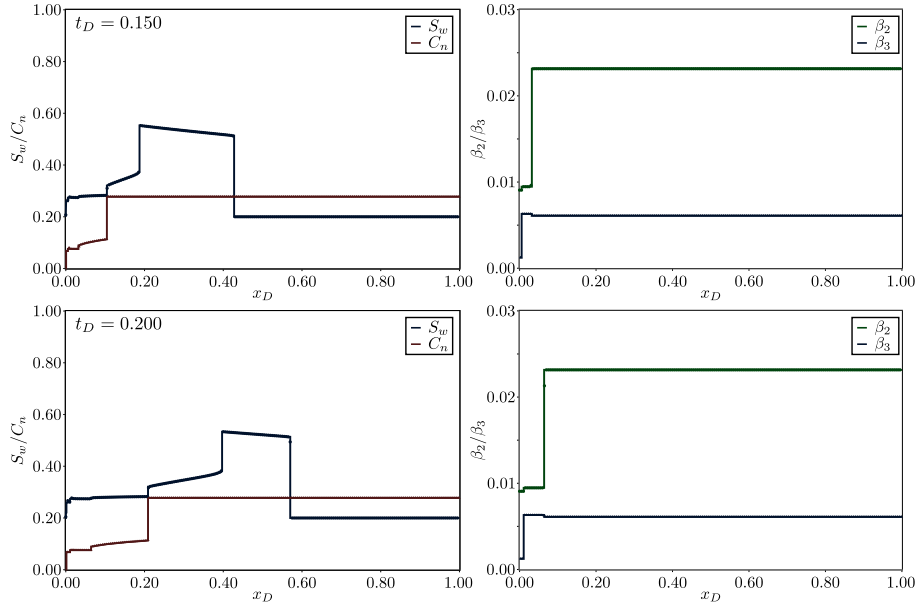


Figure 25:  $(S_w, C_n, \beta_2, \beta_3)$  solution profile for  $t_D = 0.150$  and  $t_D = 0.200$ , compared with numerical solution

### 5.2.2. Group 02 - Initial Gas/Water Interactions

The second group is formed by the interaction of the first waves in the gas step with the posterior water injection step (Figure 26). First the  $S_{J1}$  shock (Figure 16) superimposes with the water composite wave (SCS interaction). Then, there are two similar Shock-Composite Transmissions between shocks  $S_{J2}$  and  $S_{\beta1}$  and the water composite wave. In both cases the water wave decompresses, releasing new rarefactions in the solution.

The solution profiles for these initial interactions are showed in Figure 27. Note that the transmitted shocks interacts with the water rarefactions (Shock-Rarefaction Transmissions) reducing its speed until the shock velocity become almost null (vertical lines). At this point the water injection almost not changes the fluid saturation, remaining a residual oil saturation that will be removed only in the next gas injection step. The Figure 28 shows the saturation profile for  $t_D = 0.205$  and  $t_D = 0.208$ , showing the presence of the residual oil bank after the water injection step.

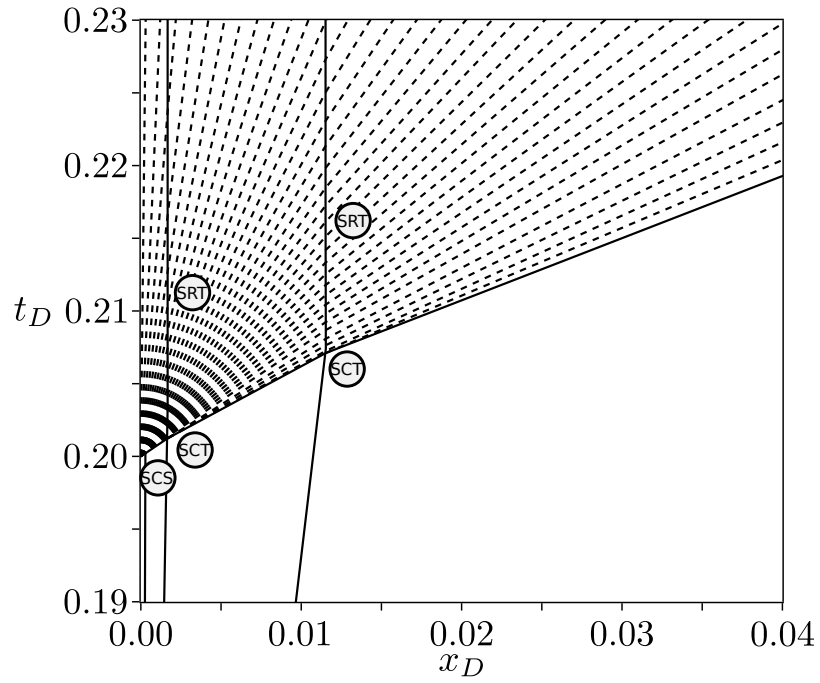


Figure 26: Group 02 characteristic diagram for the miscible WAG problem after three injection steps

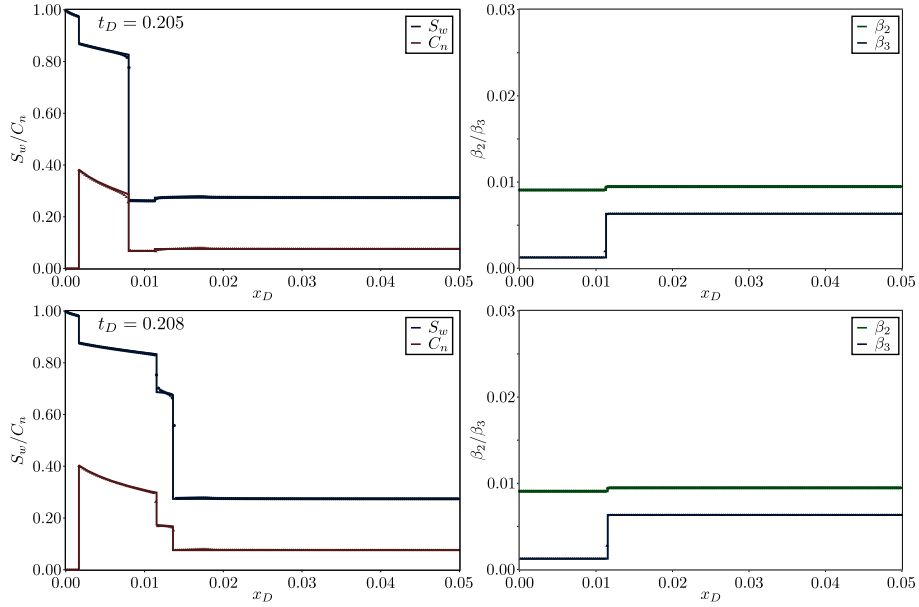


Figure 27:  $(S_w, C_n, \beta_2, \beta_3)$  solution profile for  $t_D = 0.205$  and  $t_D = 0.208$ , compared with numerical solution

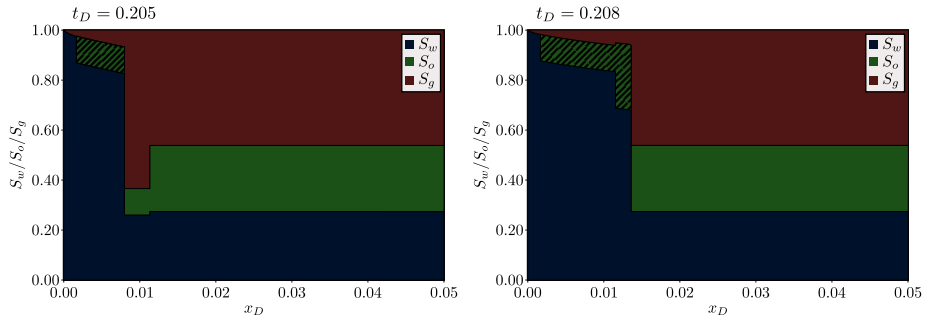


Figure 28: Saturation profile for  $t_D = 0.205$  and  $t_D = 0.208$  showing the residual oil saturation bank (dashed area) after a water injection step

### 5.2.3. Group 03 - Later Gas/Water Interactions

This group occurs after the SCT interaction between the  $S_{\beta^1}$  shock and the water composite wave (Figure 29). The rarefaction fan after  $S_{\beta^1}$  transmits over the water composite wave in a Rarefaction-Composite Transmission and interacts with the rarefactions of the water injection step (RRT transmission). If we analyze the solution profile for  $t_D = 0.230$  and  $t_D = 0.250$  (Figure 30) we

can see that after the  $S_{\beta 1}$  SCT interaction ( $(x_D, t_D) \approx (0.10, 0.24)$ ) it forms two shocks: one faster for RCT interaction and one slow for the SRT. Due to the rarefaction interactions (SRT and RRT) the transmitted characteristic waves become increasingly vertical until the speed becomes null, indicating the presence of the residual oil.

At some point the water composite wave will reach the transitional shock wave ( $S_T$  in Figure 16) creating the same SCT/SRT/RRT pattern, as showed in Figures 32 and 33. There are the creation of a slow shock that interacts with the water rarefactions (SRT) and a fast shock that interacts with the rarefactions in the gas step before. An interesting result occurs after the SCT interaction where after the water front the gas dissolves in the oil phase and the system becomes saturated with water and an oil that has a different composition of the original oil in reservoir.

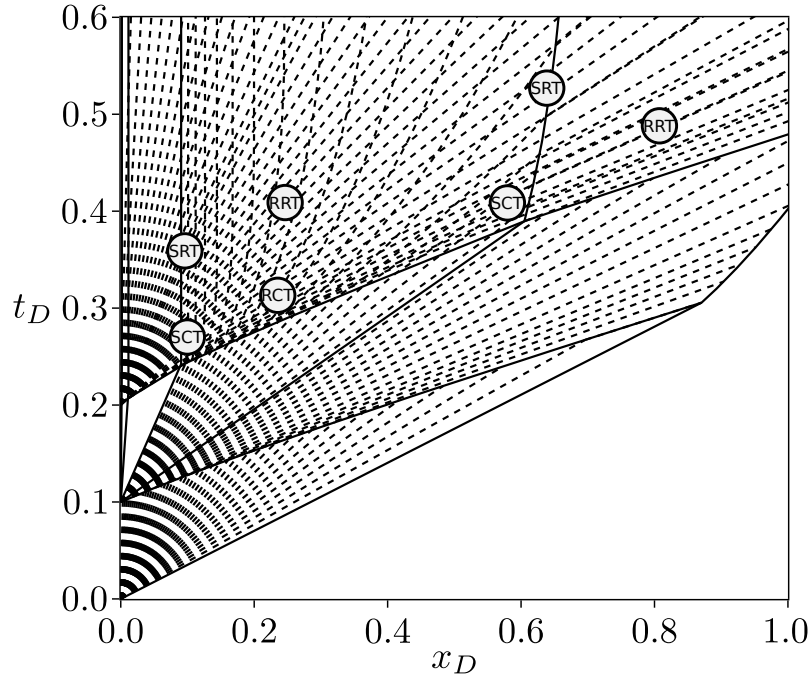


Figure 29: Group 03 characteristic diagram for the miscible WAG problem after three injection steps

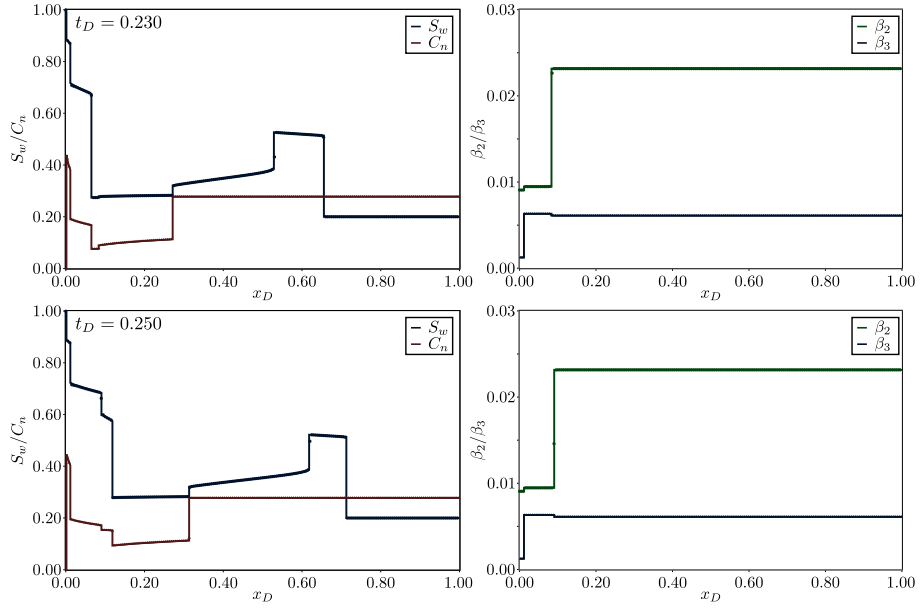


Figure 30:  $(S_w, C_n, \beta_2, \beta_3)$  solution profile for  $t_D = 0.230$  and  $t_D = 0.250$ , compared with numerical solution

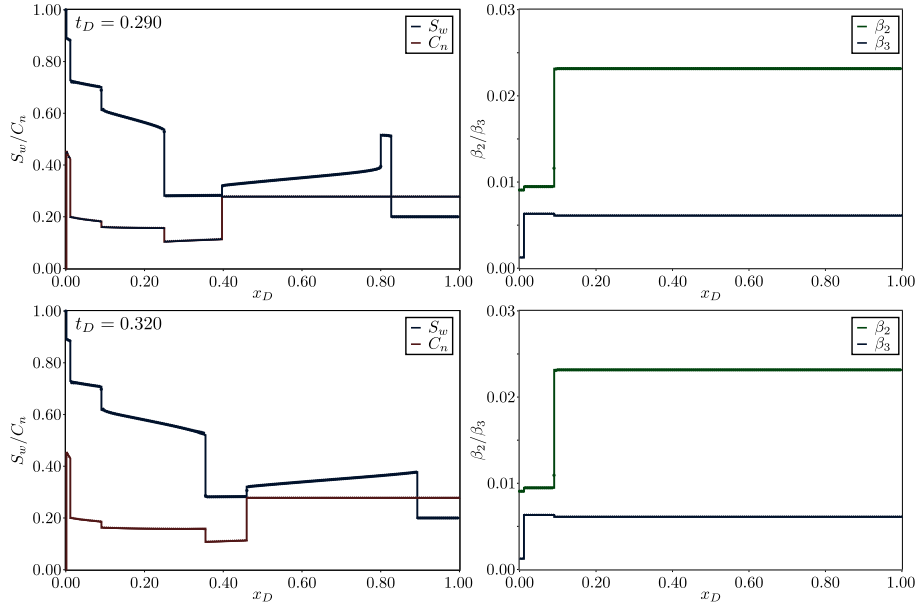


Figure 31:  $(S_w, C_n, \beta_2, \beta_3)$  solution profile for  $t_D = 0.290$  and  $t_D = 0.320$ , compared with numerical solution

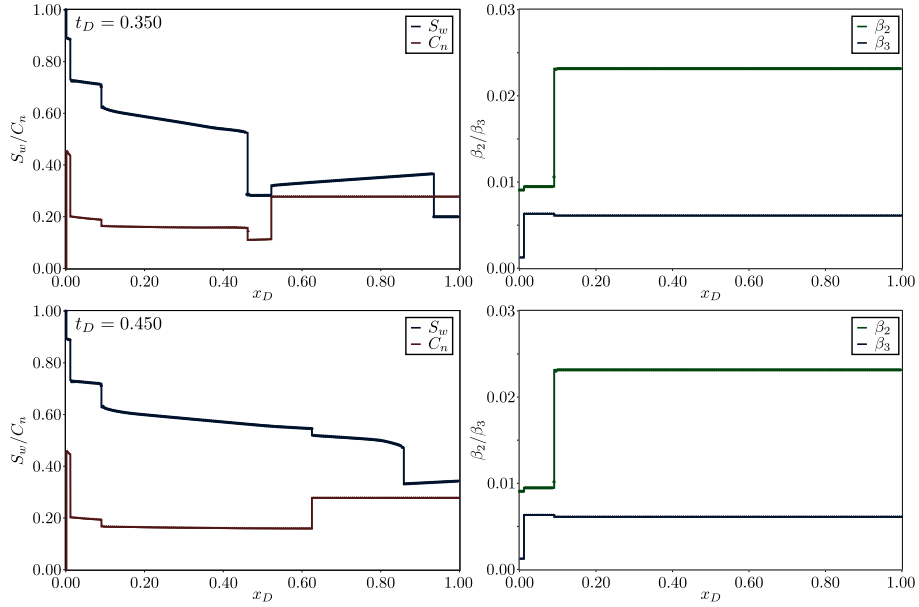


Figure 32:  $(S_w, C_n, \beta_2, \beta_3)$  solution profile for  $t_D = 0.350$  and  $t_D = 0.450$ , compared with numerical solution

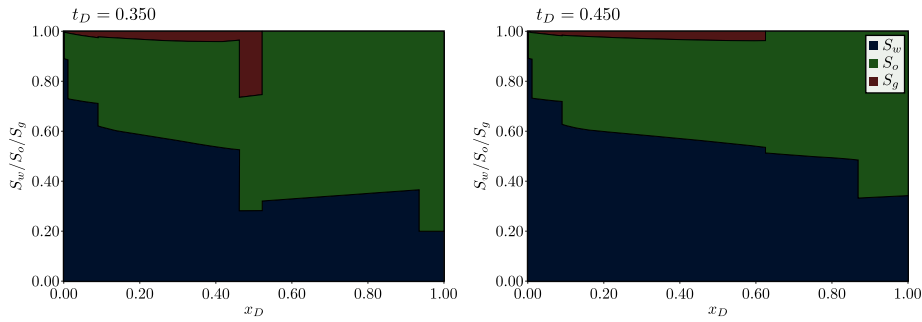


Figure 33: Saturation profile for  $t_D = 0.350$  and  $t_D = 0.450$

## 6. Conclusions

This work presents a new mathematical model for the miscible water alternating gas (MWAG) injection scheme in linear porous media. In this formulation, oil and gas exchanges mass while water is treated as an immiscible phase. As showed, this approach is useful because allowed the application of

the splitting technique, and the MWAG problem can be described and solved for any number of components.

Hydrodynamic and thermodynamic equations are decoupled by the splitting technique generating different hyperbolic partial differential equation systems, that are solved separately. Then, the time variable boundary condition problem for WAG cycles are solved by the wave interaction technique, where each interaction is treated as a new Riemann problem. The solutions described in this paper are compared with numerical schemes showing the accuracy of the method. Note that this formulation approaches to the used in commercial reservoir simulators, where the water is treated as an immiscible phase, and the analytical solution described in this paper can provide a new understanding about physical phenomena involved in WAG enhanced oil recovery.

### **Acknowledgements**

This study was financed in part by the Coordenação de Aperfeiçoamento de Pessoal de Nível Superior - Brasil (CAPES) - Finance Code 001. Alvaro Peres acknowledges the Universidade Estadual do Norte Fluminense (UENF) for financial support.

### **References**

- Afzali, S., Rezaei, N., Zendehboudi, S., 2018. A comprehensive review on enhanced oil recovery by water alternating gas (WAG) injection. *Fuel* 227, 218–246. URL: <https://doi.org/10.1016/j.fuel.2018.04.015>, doi:10.1016/j.fuel.2018.04.015.
- Andrade, P., de Souza, A., Furtado, F., Marchesin, D., 2018. Three-phase fluid displacements in a porous medium. *Journal of Hyperbolic Differential Equations* 15, 731–753. doi:10.1142/s0219891618500236.
- Andrade, P.L., de Souza, A.J., Furtado, F., Marchesin, D., 2016. Oil displacement by water and gas in a porous medium: the riemann problem. *Bulletin of the Brazilian Mathematical Society, New Series* 47, 77–90. doi:10.1007/s00574-016-0123-4.
- Azevedo, A.V., de Souza, A.J., Furtado, F., Marchesin, D., 2014. Uniqueness of the riemann solution for three-phase flow in a porous medium. *SIAM Journal on Applied Mathematics* 74, 1967–1997. doi:10.1137/140954623.

- Azevedo, A.V., de Souza, A.J., Furtado, F., Marchesin, D., Plohr, B., 2009. The solution by the wave curve method of three-phase flow in virgin reservoirs. *Transport in Porous Media* 83, 99–125. doi:10.1007/s11242-009-9508-9.
- Aziz, K., Settari, A., 1979. Petroleum reservoir simulation. Applied Science Publishers.
- Barros, W.Q., Pires, A.P., Peres, A.M., 2021. Analytical solution for one-dimensional three-phase incompressible flow in porous media for concave relative permeability curves. *International Journal of Non-Linear Mechanics* 137, 103792. URL: <https://doi.org/10.1016/j.ijnonlinmec.2021.103792>, doi:10.1016/j.ijnonlinmec.2021.103792.
- Bedrikovetsky, P., Shapiro, A., Pires, A., 2004. New analytical solutions for 1-d multicomponent gas injection problems, in: Abu Dhabi International Conference and Exhibition, Society of Petroleum Engineers. URL: <https://doi.org/10.2118/88760-ms>, doi:10.2118/88760-ms.
- Buckley, S., Leverett, M., 1942. Mechanism of fluid displacement in sands. *Transactions of the AIME* 146, 107–116. URL: <https://doi.org/10.2118/942107-g>, doi:10.2118/942107-g.
- Castañeda, P., Abreu, E., Furtado, F., Marchesin, D., 2016. On a universal structure for immiscible three-phase flow in virgin reservoirs. *Computational Geosciences* 20, 171–185. doi:10.1007/s10596-016-9556-5.
- Christensen, J., Stenby, E., Skauge, A., 2001. Review of WAG field experience. *SPE Reservoir Evaluation & Engineering* 4, 97–106. URL: <https://doi.org/10.2118/71203-pa>, doi:10.2118/71203-pa.
- Corey, A., Rathjens, C., Henderson, J., Wyllie, M., 1956. Three-phase relative permeability. *Journal of Petroleum Technology* 8, 63–65. URL: <https://doi.org/10.2118/737-g>, doi:10.2118/737-g.
- Dumoré, J.M., Hagoort, J., Risseuw, A.S., 1984. An analytical model for one-dimensional, three-component condensing and vaporizing gas drives. *Society of Petroleum Engineers Journal* 24, 169–179. URL: <https://doi.org/10.2118/10069-pa>, doi:10.2118/10069-pa.

- Dutra, T.A., Pires, A.P., Bedrikovetsky, P.G., 2009. A new splitting scheme and existence of elliptic region for gasflood modeling. *SPE Journal* SPE 107886.
- Fayers, F., Sheldon, J., 1959. The effect of capillary pressure and gravity on two-phase fluid flow in a porous medium. *Transactions of the AIME* 216, 147–155. doi:10.2118/1089-g.
- Guerrero, L.F.L., Marchesin, D., 2020. Diffusive riemann solutions for 3-phase flow in porous media, in: *Brazilian Society of Computational and Applied Mathematics, SBMAC*. doi:10.5540/03.2020.007.01.0372.
- Guzmán, R.E., Fayers, F.J., 1997a. Mathematical properties of three-phase flow equations. *SPE Journal* 2, 291–300. doi:10.2118/35154-pa.
- Guzmán, R.E., Fayers, F.J., 1997b. Solutions to the three-phase buckley-leverett problem. *SPE Journal* 2, 301–311. doi:10.2118/35156-pa.
- Hirasaki, G.J., 1981. Application of the theory of multicomponent, multiphase displacement to three-component, two-phase surfactant flooding. *Society of Petroleum Engineers Journal* 21, 191–204. URL: <https://doi.org/10.2118/8373-pa>, doi:10.2118/8373-pa.
- Holtz, M.H., 2016. Immiscible water alternating gas (IWAG) EOR: Current state of the art, in: *SPE Improved Oil Recovery Conference*, Society of Petroleum Engineers. URL: <https://doi.org/10.2118/179604-ms>, doi:10.2118/179604-ms.
- Isaacson, E.L., Marchesin, D., Plohr, B.J., 1990. Transitional waves for conservation laws. *SIAM Journal on Mathematical Analysis* 21, 837–866. doi:10.1137/0521047.
- Isaacson, E.L., Marchesin, D., Plohr, B.J., Temple, J.B., 1992. Multiphase flow models with singular riemann problems. *Matemática Aplicada Computacional* 11, 147–166.
- Jackson, M.D., Blunt, M.J., 2002. Elliptic regions and stable solutions for three-phase flow in porous media. *Transport in Porous Media* 48, 249–269. doi:10.1023/a:1015726412625.

- Johns, R., Orr, F., 1996. Miscible gas displacement of multicomponent oils. *SPE Journal* 1, 39–50. URL: <https://doi.org/10.2118/30798-pa>, doi:10.2118/30798-pa.
- Johns, R.T., Dindoruk, B., Orr, F.M., 1993. Analytical theory of combined condensing/vaporizing gas drives. *SPE Advanced Technology Series* 1, 7–16. URL: <https://doi.org/10.2118/24112-pa>, doi:10.2118/24112-pa.
- LaForce, T., Jessen, K., 2010. Analytical and numerical investigation of multicomponent multiphase WAG displacements. *Computational Geosciences* 14, 745–754. URL: <https://doi.org/10.1007/s10596-010-9185-3>, doi:10.1007/s10596-010-9185-3.
- LaForce, T., Jessen, K., Orr, F.M., 2006. Analytical solutions for compositional three-phase four-component displacements, in: *SPE Annual Technical Conference and Exhibition*, SPE. URL: <https://doi.org/10.2118/102777-ms>, doi:10.2118/102777-ms.
- LaForce, T., Johns, R.T., 2005. Composition routes for three-phase partially miscible flow in ternary systems. *SPE Journal* 10, 161–174. URL: <https://doi.org/10.2118/89438-pa>, doi:10.2118/89438-pa.
- Lax, P.D., 1957. Hyperbolic systems of conservation laws II. *Communications on Pure and Applied Mathematics* 10, 537–566. doi:10.1002/cpa.3160100406.
- LeVeque, R., J, L., Crighton, D., 2002. *Finite Volume Methods for Hyperbolic Problems*. Cambridge Texts in Applied Mathematics, Cambridge University Press.
- Leverett, M., 1939. Flow of oil-water mixtures through unconsolidated sands. *Transactions of the AIME* 132, 149–171. URL: <https://doi.org/10.2118/939149-g>, doi:10.2118/939149-g.
- Liu, T.P., 1974. The riemann problem for general 2x2 conservation laws. *Transactions of the American Mathematical Society* 199, 89. doi:10.2307/1996875.
- Liu, T.P., 1975. The riemann problem for general systems of conservation laws. *Journal of Differential Equations* 18, 218–234. doi:10.1016/0022-0396(75)90091-1.

- Marchesin, D., Mailybaev, A.A., 2006. Dual-family viscous shock waves in n conservation laws with application to multi-phase flow in porous media. *Archive for Rational Mechanics and Analysis* 182, 1–24. doi:10.1007/s00205-005-0419-9.
- Marchesin, D., Plohr, B.J., 2001. Wave structure in WAG recovery. *SPE Journal* 6, 209–219. doi:10.2118/71314-pa.
- Monroe, W.W., Silva, M.K., Larsen, L.L., Orr, F.M., 1990. Composition paths in four-component systems: Effect of dissolved methane on 1d c02 flood performance. *SPE Reservoir Engineering* 5, 423–432. URL: <https://doi.org/10.2118/16712-pa>, doi:10.2118/16712-pa.
- Orr Jr., F.M., 2007. *Theory of Gas Injection Processes*. Tie-Line Publications, Copenhagen, Denmark.
- Pires, A.P., Bedrikovetsky, P.G., Shapiro, A.A., 2006. A splitting technique for analytical modelling of two-phase multicomponent flow in porous media. *Journal of Petroleum Science and Engineering* 51, 54–67. doi:10.1016/j.petrol.2005.11.009.
- Robinson, D., Peng, D., 1978. The Characterization of the Heptanes and Heavier Fractions for the GPA Peng-Robinson Programs. volume RR-28 of *Research report (Gas Processors Association)*. Gas Processors Association.
- Sanchez, N.L., 1999. Management of water alternating gas (WAG) injection projects, in: *Latin American and Caribbean Petroleum Engineering Conference*, Society of Petroleum Engineers. URL: <https://doi.org/10.2118/53714-ms>, doi:10.2118/53714-ms.
- Shahverdi, H., Sohrabi, M., 2013. An improved three-phase relative permeability and hysteresis model for the simulation of a water-alternating-gas injection. *SPE Journal* 18, 841–850. URL: <https://doi.org/10.2118/152218-pa>, doi:10.2118/152218-pa.
- Shahverdi, H., Sohrabi, M., Fatemi, M., Jamiolahmady, M., 2011. Three-phase relative permeability and hysteresis effect during WAG process in mixed wet and low IFT systems. *Journal of Petroleum Science and Engineering* 78, 732–739. URL: <https://doi.org/10.1016/j.petrol.2011.08.010>, doi:10.1016/j.petrol.2011.08.010.

- Shearer, M., Trangenstein, J.A., 1989. Loss of real characteristics for models of three-phase flow in a porous medium. *Transport in Porous Media* 4. doi:10.1007/bf00179533.
- Sheldon, J., Cardwell, W., 1959. One-dimensional, incompressible, noncapillary, two-phase fluid flow in a porous medium. *Transactions of the AIME* 216, 290–296. doi:10.2118/978-g.
- Stone, H., 1970. Probability model for estimating three-phase relative permeability. *Journal of Petroleum Technology* 22, 214–218. URL: <https://doi.org/10.2118/2116-pa>, doi:10.2118/2116-pa.
- Tai-Ping, L., 2007. *Hyperbolic and Viscous Conservation Laws*. CBMS-NSF Regional Conference Series in Applied Mathematics, Siam.
- Wachmann, C., 1964. A mathematical theory for the displacement of oil and water by alcohol. *Society of Petroleum Engineers Journal* 4, 250–266. URL: <https://doi.org/10.2118/879-pa>, doi:10.2118/879-pa.
- Welge, H.J., 1952. A simplified method for computing oil recovery by gas or water drive. *Journal of Petroleum Technology* 4, 91–98. doi:10.2118/124-g.

## 8 *Conclusions*

This thesis presents the results obtained along a four year doctoral research about the mathematical and physical aspects of the Water Alternating Gas EOR method. First the simultaneous three-phase immiscible flow in porous medium was modeled and a new solution for concave relative permeability curves was published. Then it was evaluated how step variable boundary conditions affects the analytical solution, and an application to injectivity well tests was developed.

After that, the immiscible WAG problem was solved using the wave interaction theory to handle the interactions between different characteristics caused by the variable boundary condition. Finally a new mathematical formulation was developed for the miscible WAG problem where the split technique was applied to decouple the hydrodynamic and thermodynamic parts of the original problem. Suggestion for further research includes:

- Development of a simultaneous immiscible three-phase flow solution for mixed concave and convex relative permeability curves;
- Develop a well-test pressure solution applied for an injectivity test after WAG cycles;
- Analyze the influence of the stable orbits of the associated vanishing viscosity problem in both WAG and MWAG solutions;
- Develop the miscible WAG solution considering injected gas slugs with different compositions.

## ***Bibliography***

- AFZALI, S.; REZAEI, N.; ZENDEHBOUDI, S. A comprehensive review on enhanced oil recovery by water alternating gas (WAG) injection. *Fuel*, Elsevier BV, v. 227, p. 218–246, sep 2018. Disponível em: <<https://doi.org/10.1016/j.fuel.2018.04.015>>.
- AWAN, A.; TEIGLAND, R.; KLEPPE, J. A survey of north sea enhanced-oil-recovery projects initiated during the years 1975 to 2005. *SPE Reservoir Evaluation and Engineering*, SPE 99546, p. 497 – 512, 2008.
- BAKER, L. E. Three-phase relative permeability correlations. *Enhanced Oil Recovery Symposium, Tulsa*, p. 539–554, 1988.
- BEDRIKOVETSKY, P. A new mathematical model for EOR displacements honouring oil ganglia. *SPE Annual Technical Conference and Exhibition*, SPE 38892, p. 513–528, 1997.
- BEDRIKOVETSKY, P.; SHAPIRO, A.; PIRES, A. New analytical solutions for 1-d multicomponent gas injection problems. In: *Abu Dhabi International Conference and Exhibition*. Society of Petroleum Engineers, 2004. Disponível em: <<https://doi.org/10.2118/88760-ms>>.
- BEDRIKOVETSKY, P. G.; MARCHESIN, D.; BALLIN, P. Mathematical theory for two phase displacement with hysteresis (with application to WAG injection). *5th European Conference on the Mathematics of Oil Recovery*, 1996.
- BELL, J. B.; TRANGENSTEIN, J. A.; SHUBIN, G. R. Conservation laws of mixed type describing three-phase flow in porous media. *SIAM Journal on Applied Mathematics*, Society for Industrial & Applied Mathematics (SIAM), v. 46, n. 6, p. 1000–1017, dec 1986. Disponível em: <<https://doi.org/10.1137/0146059>>.
- BUCKLEY, S.; LEVERETT, M. Mechanism of fluid displacement in sands. *Transactions of the AIME*, Society of Petroleum Engineers (SPE), v. 146, n. 01, p. 107–116, dec 1942. Disponível em: <<https://doi.org/10.2118/942107-g>>.
- CHRISTENSEN, J.; STENBY, E.; SKAUGE, A. Review of WAG field experience. *SPE Reservoir Evaluation & Engineering*, Society of Petroleum Engineers (SPE), v. 4, n. 02, p. 97–106, apr 2001. Disponível em: <<https://doi.org/10.2118/71203-pa>>.
- COREY, A.; RATHJENS, C.; HENDERSON, J.; WYLLIE, M. Three-phase relative permeability. *Journal of Petroleum Technology*, Society of Petroleum Engineers (SPE), v. 8, n. 11, p. 63–65, nov 1956. Disponível em: <<https://doi.org/10.2118/737-g>>.
- DELSHAD, M.; POPE, G. Comparison of the three-phase oil relative permeability models. *Transport in Porous Media*, Springer Science and Business Media LLC, v. 4, n. 1, feb 1989. Disponível em: <<https://doi.org/10.1007/bf00134742>>.

DINDORUK, B. *Analytical Theory of Multiphase, Multicomponent Displacement in Porous Media*. Tese (Doutorado) — Stanford University, 1992.

GUZMÁN, R. E.; FAYERS, F. J. Mathematical properties of three-phase flow equations. *SPE Journal*, SPE 35154, p. 291–300, 1997.

GUZMÁN, R. E.; FAYERS, F. J. Solution to the three-phase buckley-leverett problem. *SPE journal*, SPE 35156, p. 301–311, 1997.

HOLDEN, L. On the strict hyperbolicity of the buckley–leverett equations for three-phase flow in a porous medium. *SIAM Journal on Applied Mathematics*, Society for Industrial & Applied Mathematics (SIAM), v. 50, n. 3, p. 667–682, jun 1990. Disponível em: <<https://doi.org/10.1137/0150039>>.

HOLTZ, M. H. Immiscible water alternating gas (IWAG) EOR: Current state of the art. In: *SPE Improved Oil Recovery Conference*. Society of Petroleum Engineers, 2016. Disponível em: <<https://doi.org/10.2118/179604-ms>>.

JACKSON, M. D.; BLUNT, M. J. Elliptic regions and stable solutions for three-phase flow in porous media. *Transport in Porous Media*, v. 48, p. 249–269, 2002.

JOHNS, R.; ORR, F. Miscible gas displacement of multicomponent oils. *SPE Journal*, Society of Petroleum Engineers (SPE), v. 1, n. 01, p. 39–50, mar 1996. Disponível em: <<https://doi.org/10.2118/30798-pa>>.

JUANES, R. Determination of the wave structure of the three-phase flow riemann problem. *Transport in Porous Media*, v. 60, p. 135–139, 2005.

JUANES, R.; PATZEK, T. W. Relative permeabilities in co-current three-phase displacements with gravity. *Society of Petroleum Engineers*, SPE-83445, 2003.

JUANES, R.; PATZEK, T. W. Analytical solution to the riemann problem of three-phase flow in porous media. *Transport in Porous Media*, v. 55, p. 47–70, 2004.

JUANES, R.; PATZEK, T. W. Relative permeabilities for strictly hyperbolic models of three-phase flow in porous media. *Transport in Porous Media*, v. 57, p. 125–152, 2004.

JUANES, R.; PATZEK, T. W. Three-phase displacement theory: An improved description of relative permeabilities. *Society of Petroleum Engineers*, SPE-88973, 2004.

KATS, F. M. V.; DUIJN, C. J. V. A mathematical model for hysteretic two-phase flow in porous media. *Transport in Porous Media*, v. 43, p. 239–263, 2001.

MAMANI, B. L. *Solução Analítica Unidimensional da Injeção Alternada de Água e Gás*. Dissertação (Mestrado) — Universidade Estadual Norte Fluminense, 2016.

MARCHESIN, D.; PLOHR, B. J. Wave structure in WAG recovery. *SPE Journal*, Society of Petroleum Engineers (SPE), v. 6, n. 02, p. 209–219, jun 2001. Disponível em: <<https://doi.org/10.2118/71314-pa>>.

NADESON, G.; ANUA, N. A. B.; SINGHAL, A.; IBRAHIM, R. B. Water-alternating-gas (WAG) pilot implementation, a first EOR development project in dulang field, offshore peninsular malaysia. In: *SPE Asia Pacific Oil and Gas Conference and Exhibition*. Society of Petroleum Engineers, 2004. Disponível em: <<https://doi.org/10.2118-/88499-ms>>.

PANDA, M.; NOTTINGHAM, D.; LENIG, D. Systematic surveillance techniques for a large WAG flood. *SPE Oil and Gas India Conference and Exhibition*, SPE 127563, p. 1–23, 2010.

PLOHR, B.; MARCHESIN, D.; BEDRIKOVETSKY, P.; ALTOÉ, J. E.; SOUZA, A. J. de. Hysteresis in three-phase porous media flow. *8th European Conference on the Mathematics of Oil Recovery*, 2002.

ROGERS, J. D.; GRIGG, R. B. A literature analysis of the WAG injectivity abnormalities in the CO<sub>2</sub> process. *SPE Reservoir Evaluation and Engineering*, SPE 73830, p. 375–386, 2001.

SHAHVERDI, H. *Characterization of Three-Phase Flow and WAG Injection in Oil Reservoirs*. Tese (Doutorado) — Heriot-Watt University, 2012.

SHEARER, M.; TRANGENSTEIN, J. A. Loss of real characteristics for models of three-phase flow in a porous medium. *Transport in Porous Media*, v. 4, p. 499–525, 1989.

STONE, H. L. Probability model for estimating three-phase relative permeability. *Journal of Petroleum Technology*, v. 249, p. 214–218, 1970.

YANG, D.; CUI, H.; ZHANG, Q.; LI, L.; WU, Z. Tracer technology for water-alternating-gas miscible flooding in pubei oil field. *2000 SPE/AAPG Western Regional Meeting*, 2000.

ZAHOOR, M. K.; DERAHMAN, M. N.; YUNAN, M. H. WAG process design - an updated review. *Brazilian Journal of Petroleum and Gas*, v. 5, p. 109–121, 2011.